PERMAFROST AND PERIGLACIAL PROCESSES
Permafrost and Periglac. Process. **26**: 208–288 (2015)
Published online in Wiley Online Library
(wileyonlinelibrary.com) DOI: 10.1002/ppp.1843

Palaeoenvironmental Interpretation of Yedoma Silt (Ice Complex) Deposition as Cold-Climate Loess, Duvanny Yar, Northeast Siberia

Julian B. Murton,[1]* *Tomasz Goslar,*[2,3] *Mary E. Edwards,*[4,5] *Mark D. Bateman,*[6] *Petr P. Danilov,*[7] *Grigoriy N. Savvinov,*[7] *Stanislav V. Gubin,*[8] *Bassam Ghaleb,*[9] *James Haile,*[10,11] *Mikhail Kanevskiy,*[12] *Anatoly V. Lozhkin,*[13] *Alexei V. Lupachev,*[8,14] *Della K. Murton,*[15] *Yuri Shur,*[12] *Alexei Tikhonov,*[16] *Alla C. Vasil'chuk,*[17] *Yurij K. Vasil'chuk*[17,18] *and Stephen A. Wolfe*[19]

[1] Permafrost Laboratory, Department of Geography, University of Sussex, Brighton, UK
[2] Adam Mickiewicz University, Faculty of Physics, Poznan, Poland
[3] Poznan Radiocarbon Laboratory, Poznań Science and Technology Park, Poznan, Poland
[4] School of Geography, University of Southampton, Southampton, UK
[5] Alaska Quaternary Center, College of Natural Science and Mathematics, University of Alaska-Fairbanks, Fairbanks, AK, USA
[6] Department of Geography, University of Sheffield, Sheffield, UK
[7] Science Research Institute of Applied Ecology of the North of North-East Federal University, Yakutsk, Russia
[8] Institute of Physicochemical and Biological Problems in Soil Sciences, Russian Academy of Sciences, Moscow, Russia
[9] GEOTOP-UQAM-McGILL, Université du Québec à Montréal, Montreal, QC, Canada
[10] School of Biological Sciences, Murdoch University, Murdoch, WA, Australia
[11] Centre for Geogenetics, Natural History Museum of Denmark, University of Copenhagen, Copenhagen, Denmark
[12] Institute of Northern Engineering, University of Alaska Fairbanks, Fairbanks, AK, USA
[13] North East Interdisciplinary Science Research Institute, Far East Branch Russian Academy of Sciences, Magadan, Russia
[14] Institute of the Earth Cryosphere, Siberian Branch, Russian Academy of Sciences, Tyumen, Russia
[15] Department of Geography, University of Cambridge, Cambridge, UK
[16] Zoological Institute, Russian Academy of Sciences, Universitetskaya nab.1, Saint-Petersburg, Russia
[17] Faculty of Geography, Lomonosov Moscow State University, Moscow, Russia
[18] Faculty of Geology, Lomonosov Moscow State University, Moscow, Russia
[19] Geological Survey of Canada, Natural Resources Canada, Ottawa, ON, Canada

ABSTRACT

Uncertainty about the geological processes that deposited syngenetically frozen ice-rich silt (*yedoma*) across hundreds of thousands of square kilometres in central and northern Siberia fundamentally limits our understanding of the Pleistocene geology and palaeoecology of western Beringia, the sedimentary processes that led to sequestration of hundreds of Pg of carbon within permafrost and whether yedoma provides a globally significant record of ice-age atmospheric conditions or just regional floodplain activity. Here, we test the hypotheses of aeolian versus waterlain deposition of yedoma silt, elucidate the palaeoenvironmental conditions during deposition and develop a conceptual model of silt deposition to clarify understanding of yedoma formation in northern circumpolar regions during the Late Pleistocene. This is based on a field study in 2009 of the Russian stratotype of the 'Yedoma Suite', at Duvanny Yar, in the lower Kolyma River, northern Yakutia, supplemented by observations that we have collected there and at other sites in the Kolyma Lowland since the 1970s. We reconstruct a cold-climate loess region in northern Siberia that forms part of a vast Late Pleistocene permafrost zone extending from northwest Europe across northern Asia to northwest North America, and that was characterised by intense aeolian activity.

Five litho- and cryostratigraphic units are identified in yedoma remnant 7E at Duvanny Yar, in ascending stratigraphic order: (1) massive silt, (2) peat, (3) stratified silt, (4) yedoma silt and (5) near-surface silt. The yedoma silt of unit 4 dominates the stratigraphy and is at least 34 m thick. It is characterised by horizontal to gently undulating subtle colour bands but typically lacks primary sedimentary stratification. Texturally, the yedoma silt has mean values of 65 ± 7 per cent silt, 15 ± 8 per cent sand and 21 ± 4 per cent clay. Particle size distributions are bi- to polymodal, with a primary mode of about 41 μm (coarse silt) and subsidiary modes are 0.3–0.7 μm (very fine clay to fine clay), 3–5 μm (coarse clay to very fine silt), 8–16 μm (fine silt) and 150–350 μm (fine sand to medium sand). Semidecomposed fine plant material is abundant and fine *in-situ* roots are pervasive. Syngenetic ice wedges, cryostructures and microcryostructures record

* Correspondence to: J. B. Murton, Permafrost Laboratory, Department of Geography, University of Sussex, Brighton BN1 9QJ, UK.
E-mail: j.b.murton@sussex.ac.uk

Received 3 December 2013
Revised 30 January 2015
Accepted 24 February 2015

syngenetic freezing of the silt. An age model for silt deposition is constructed from 47 pre-Holocene accelerator mass spectrometry (AMS) ^{14}C ages, mostly from *in-situ* roots and from three optically stimulated luminescence (OSL) ages of quartz sand grains. The ^{14}C ages indicate that silt deposition extends from 19 000 ± 300 cal BP to 50 000 cal BP or beyond. The OSL ages range from 21.2 ± 1.9 ka near the top of the yedoma to 48.6 ± 2.9 ka near the bottom, broadly consistent with the ^{14}C age model.

Most of the yedoma silt in unit 4 at Duvanny Yar constitutes *cryopedolith* (sediment that has experienced incipient pedogenesis along with syngenetic freezing). Mineralised and humified organic remains dispersed within cryopedolith indicate incipient soil formation, but distinct soil horizons are absent. Five buried palaeosols and palaeosol 'complexes' are identified within cryopedolith on the basis of sedimentary and geochemical properties. Magnetic susceptibility, organic content, elemental concentrations and ratios tend to deviate from average values of these parameters at five levels in unit 4. The cryopedolith-palaeosol sequence accreted incrementally upwards on a vegetated palaeo-land surface with a relief of at least several metres, preserving syngenetic ground ice in the aggrading permafrost. Pollen spectra dated to between about 17 000 and 25 000 ^{14}C BP characteristically have frequencies of 20–60 per cent tree/shrub pollen (mainly *Betula* and *Pinus*) and 20–60 per cent graminoids, predominantly Poaceae, plus forbs, whereas spectra dated to about 30 000–33 000 ^{14}C BP have lower values of woody taxa (about 10%) and are dominated by graminoids (mainly Poaceae), forbs (particularly Caryophyllaceae and Asteraceae) and *Selaginella rupestris*. The latter are more typical of Last Glacial Maximum (LGM) samples reported elsewhere in Siberia, and the unusually high arboreal pollen values in the LGM yedoma at Duvanny Yar are attributed to long-distance transport of pollen.

Three hypotheses concerning the processes and environmental conditions of yedoma silt deposition at Duvanny Yar are tested. The *alluvial-lacustrine* hypothesis and the *polygenetic* hypothesis are both discounted on sedimentary, palaeoenvironmental, geocryological and palaeoecological grounds. The *loessal* hypothesis provides the only reasonable explanation to account for the bulk of the unit 4 yedoma silt at this site. Supporting the loessal interpretation are sedimentological and geocryological similarities between the Duvanny Yar loess-palaeosol sequence and cold-climate loesses in central and northern Alaska, the Klondike (Yukon), western and central Siberia and northwest Europe. Differences between loess at Duvanny Yar and that in western and central Siberia and northwest Europe include the persistence of permafrost and the abundance of ground ice and fine *in-situ* roots within the yedoma. Modern analogues of cold-climate loess deposition are envisaged at a local scale in cold, humid climates where local entrainment and deposition of loess are generally restricted to large alluvial valleys containing rivers that are glacially sourced or drain areas containing Late Pleistocene glacial deposits, and thus glacially ground silt. The Duvanny Yar yedoma shares sedimentological and geocryological features with yedoma interpreted as ice-rich loess or reworked loess facies at Itkillik (northern Alaska) and in the central Yakutian lowland, and with yedoma in the Laptev Sea region and the New Siberian Archipelago. It is therefore suggested that many lowland yedoma sections across Beringia are primarily of aeolian origin (or consist of reworked aeolian sediments), although other depositional processes (e.g. alluvial and colluvial) may account for some yedoma sequences in river valleys and mountains.

A conceptual model of yedoma silt deposition at Duvanny Yar as cold-climate loess in Marine Isotope Stage (MIS) 3 and MIS 2 envisages summer or autumn as the main season of loess deposition. In summer, the land surface was snow-free, unfrozen and relatively dry, making it vulnerable to deflation. Graminoids, forbs and biological soil crust communities trapped and stabilised windblown sediments. Loess accretion resulted from semicontinuous deposition of fine background particles and episodic, discrete dust storms that deposited coarse silt. Winter was characterised by deep thermal contraction cracking beneath thin and dusty snow covers, and snow and frozen ground restricted deflation and sediment trapping by dead grasses. Sources of loess at Duvanny Yar potentially include: (1) sediments and weathered bedrock on uplands to the east, south and southwest of the Kolyma Lowland; (2) alluvium deposited by rivers draining these uplands; and (3) sediments exposed in the Khallerchin tundra to the north and on the emergent continental shelf of the East Siberian Sea. Glacially sourced tributaries of the palaeo-Kolyma River contributed glacially ground silt into channel and/or floodplain deposits, and some of these were probably reworked by wind and deposited as loess in the Kolyma Lowland.

The palaeoenvironmental reconstruction of the sedimentary sequence at Duvanny Yar is traced from MIS 6 to the late Holocene. It includes thermokarst activity associated with alas lake development in the Kazantsevo interglacial (MIS 5e), loess accumulation, pedogenesis and syngenetic permafrost development, possibly commencing in the Zyryan glacial (70 000–55 000 cal BP) and extending through the Karginsky interstadial (55 000–25 000 cal BP) and Sartan glacial (25 000–15 000 cal BP), cessation of yedoma silt deposition during the Lateglacial, renewed thermokarst activity in the early Holocene, and permafrost aggradation in the mid to late Holocene.

Beringian coastlands from northeast Yakutia through the north Alaskan Coastal Plain to the Tuktoyaktuk Coastlands (Canada) were characterised by extensive aeolian activity (deflation, loess, sand dunes, sand sheets, sand wedges) during MIS 2. Siberian and Canadian high-pressure cells coupled with a strengthened Aleutian low-pressure cell would have created enhanced pressure gradient-driven winds sufficient to entrain sediment on a regional scale. Summer winds are thought to have deflated sediment exposed on the East Siberian Sea shelf and deposited silt as a distal aeolian facies to the south. Additionally, stronger localised winds created by local downslope gravity flows (katabatic winds) may have entrained

sediment. Local katabatic winds in summer may have transported silt generally northwards towards the Kolyma Lowland, particularly during times of extended upland glaciation in the North Anyuy Range to the east during the Zyryan (MIS 4) period, whereas winter winds carried limited amounts of silt generally southwards as a result of pressure gradient forces. The Duvanny Yar yedoma is part of a subcontinental-scale region of Late Pleistocene cold-climate loess. One end member, exemplified by the yedoma at Duvanny Yar, was loess rich in syngenetic ground ice (Beringian yedoma). The other, exemplified by loess in northwest Europe, was ice-poor and subject to complete permafrost degradation at the end of the last ice age. These end members reflect a distinction between enduring cold continuous permafrost conditions leading to stacked ice-rich transition zones and large syngenetic ice wedges in much of Beringia versus conditions oscillating between cold permafrost, warm permafrost and seasonal frost, leading to repeated permafrost thaw and small ice-wedge pseudomorphs in northwest Europe. Copyright © 2015 John Wiley & Sons, Ltd.

KEY WORDS: aeolian; Beringia; cryostructures; depositional processes; ice wedges; Kolyma; loess; palaeosols; permafrost; pollen; radiocarbon dating; silt; sand; yedoma

INTRODUCTION

Syngenetically frozen silt underlies hundreds of thousands of square kilometres of lowlands in central and northeastern Siberia, significant areas of central and northern Alaska and the Klondike region of Yukon, Canada – all part of the unglaciated Pleistocene subcontinent of Beringia (Hopkins *et al.*, 1982). Figure 1 indicates the main regions where frozen silt is widespread to scattered, although its detailed distribution, at least in Siberia, is more complex and less extensive than the generalised regions shown in Figure 1A (Grosse *et al.*, 2013). The silt forms a distinctive stratigraphic unit 3–80 m thick that is rich in ground ice and organic carbon, and blankets many Beringian lowlands and foothills (Romanovskii, 1993; Sher, 1997; Zimov *et al.*, 2006a, 2006b; Gubin and Veremeeva, 2010; Schirrmeister *et al.*, 2011a, 2011b, 2013). The unit has been intensively studied for several decades in Siberia, where it is

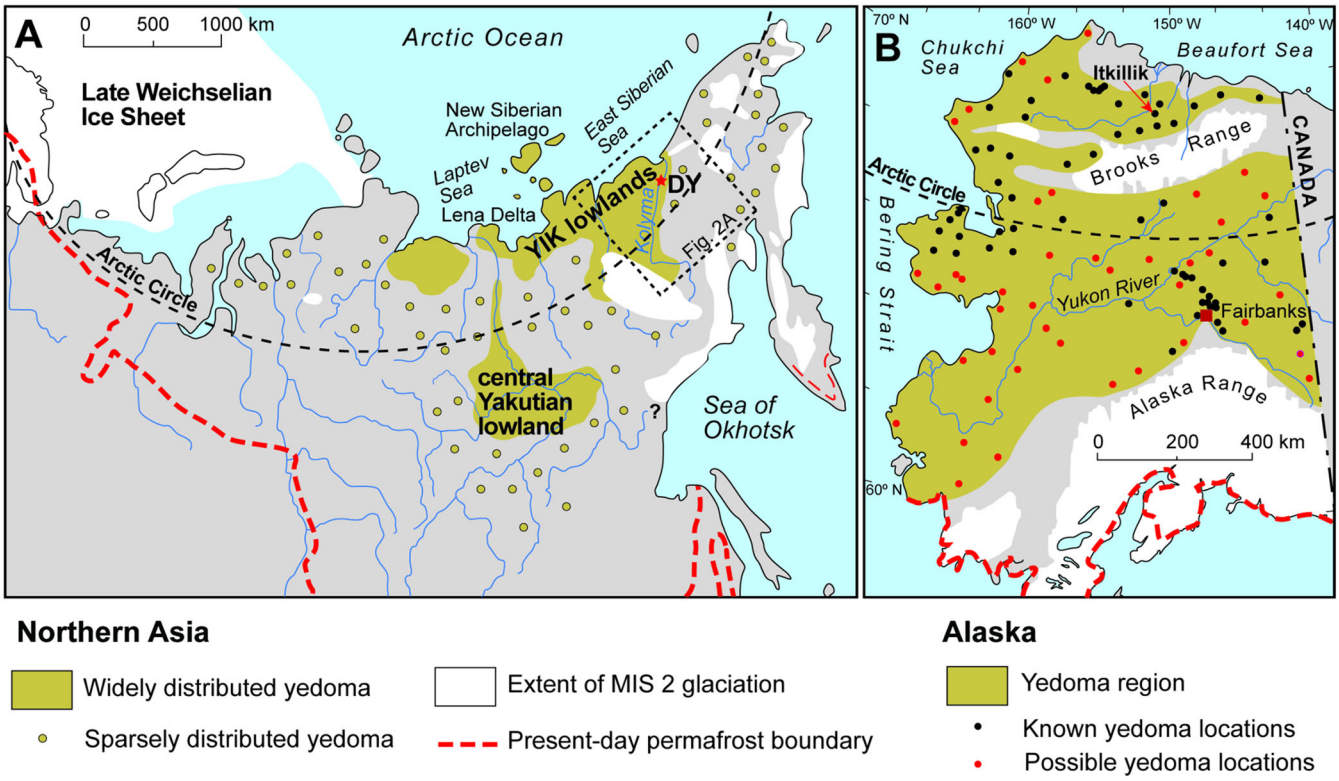

Figure 1 General distribution of yedoma deposits in (A) Siberia (yedoma distribution modified from Romanovskii, 1993; Konishchev, 2009) and (B) Alaska. Modified from Kanevskiy *et al.* (2011) and references therein. Glaciated areas in (A) are approximated from Brigham-Grette *et al.* (2004), Elias and Brigham-Grette (2013) and Ehlers *et al.* (2013). The question mark in (A) indicates uncertainty about the glacial limit. Permafrost limit in Alaska modified from Jorgenson *et al.* (2008). DY = Duvanny Yar; YIK lowlands = Yana-Indigirka-Kolyma lowlands; MIS = Marine Isotope Stage. This figure is available in colour online at wileyonlinelibrary.com/journal/ppp

known by the translated Russian term 'Ice Complex', although the Russian term 'Yedoma' (Kaplina, 1981; Murzaev, 1984; Tomirdiaro, 1982, 1986; Sher, 1997) is now used more often than 'Ice Complex' in both the Russian and North American literature (Kanevskiy *et al*., 2011). We adopt this modern usage of *yedoma*, defined as

> 'encompassing distinctive ice-rich silts and silty sand penetrated by large ice wedges, resulting from sedimentation and syngenetic freezing, and driven by certain climatic and environmental conditions during the late Pleistocene.' (Schirrmeister *et al*., 2013, p. 542)

Yedoma preserves an exceptional terrestrial sedimentary record of Late Pleistocene environmental history. Cold permafrost conditions during yedoma accumulation limited oxidation of organic material, preserving remains of the former steppe-tundra ecosystem (Yurtsev, 1981; Sher, 1997; Guthrie, 2006), including plant roots, mammal bones and carcasses, pollen, insect remains, plant macrofossils, fossil rodent burrows, soil DNA and microbial communities immobilised on the surface of ancient seeds (Stakhov *et al*., 2008; Boeskorov *et al*., 2011; Zazula *et al*., 2011; Willerslev *et al*., 2014). Regeneration of whole fertile plants from 30 000-year-old fruit tissue preserved in Siberian yedoma demonstrates the important role for such permafrost as a depository for an ancient gene pool (Yashina *et al*., 2012). The organic material within yedoma accumulated through incremental sedimentation and syngenetic permafrost growth over thousands of years. However, different interpretations of yedoma persist between researchers in eastern and western Beringia (Brigham-Grette, 2001). The differences are fundamental to understanding the geology and palaeoecology of Beringia, the sedimentary processes that led to sequestration of hundreds of Pg of carbon (Zimov *et al*., 2006a; Schirrmeister *et al*., 2011a; Kuhry *et al*., 2013) and whether yedoma provides a globally significant record of ice-age atmospheric conditions or just regional floodplain activity.

The differences concern the prominence given to aeolian deposition of silt (Schirrmeister *et al*., 2013; Muhs, 2013a). Researchers in Alaska and Yukon (eastern Beringia) initially attributed silt deposition to several processes, including aeolian, weathering, fluvial, lacustrine and estuarine or their interaction (Taber, 1943). But following T. L. Péwé's (1955) convincing advocacy of aeolian deposition, North American researchers have accepted a predominantly aeolian origin, while acknowledging that some reworking has occurred by processes such as snowmelt or overland flow, particularly on hillslopes and valley bottoms (Péwé, 1975a; Carter, 1988; Muhs *et al*., 2008). Collectively, these silt- and silty sand-dominated sediments are described in the North American literature as 'loessal' (Sanborn *et al*., 2006; Froese *et al*., 2009), and incremental deposition of loess under full-glacial conditions is hypothesised to have been a key factor in maintaining a highly productive soil and Beringian ecosystem that supported a large Pleistocene megafauna (Schweger, 1992, 1997). By contrast, many researchers working in northeast Siberia (western Beringia) and the adjacent Siberian lowlands to the west (Figure 1A) continue to favour a diversity of hypotheses for silt deposition, including alluvial, colluvial, lacustrine, deltaic, cryogenic-aeolian, nival and polygenetic processes (reviewed in Péwé and Journaux, 1983; Schirrmeister *et al*., 2011b, 2013; Kanevskiy *et al*., 2011), despite strong geological arguments that the silts are primarily windblown (Hopkins, 1982; Tomirdiaro, 1980, 1982; Péwé and Journaux, 1983; Astakhov, 2014). Until the depositional processes are identified, the palaeoenvironmental significance of yedoma will remain uncertain and obscure its huge potential insights into Late Pleistocene atmospheric or ground surface conditions. To resolve these differences, an essential step is to re-evaluate the depositional processes and chronology at a key Siberian yedoma site.

The yedoma-type site is at Duvanny Yar, in the Kolyma Lowland of northeast Yakutia, Siberia (Figure 1A). Its upper Late Pleistocene horizon is the Russian stratotype of the 'Yedoma Suite' (Sher *et al*., 1979; Kaplina, 1981, 1986; Y. K. Vasil'chuk, 2006; Zanina *et al*., 2011), where $\leq$ 50 m of silt and ice form the most complete and thickest-known section through yedoma in the Kolyma Lowland (Kaplina *et al*., 1978). Despite more than 50 years of research at Duvanny Yar, active debate continues about the processes of silt deposition (Y. K. Vasil'chuk, 2006; Wetterich *et al*., 2011a; Strauss *et al*., 2012a), and ^{14}C ages from the yedoma have led to conflicting age models of Kaplina (1986), Tomirdiaro and Chyornen'kiy (1987), Y. K. Vasil'chuk (1992, 2006) and Gubin (1999), the timescales of which commence in the early to late periods of Marine Isotope Stage (MIS) 3 and extend through MIS 2.

Our aims are to: (1) test the hypotheses of aeolian versus waterlain deposition of yedoma silt at Duvanny Yar; (2) elucidate the palaeoenvironmental conditions at the time of deposition; and (3) develop a conceptual model of silt deposition to clarify understanding of yedoma formation during the Late Pleistocene. To achieve these aims, our specific objectives are to: (1) report field observations on the sedimentary sequence, litho- and cryostratigraphy of the yedoma and adjacent stratigraphic units; (2) describe the micromorphological features, sediment properties (particle size, carbonate content, organic content, magnetic susceptibility and major element and trace element composition) and pollen spectra from the yedoma; (3) establish an age model with radiocarbon dating, mostly of *in-situ* roots, supplemented by OSL dating of sand; and (4) compare, using the same laboratory protocol, the sediment properties of yedoma at Duvanny Yar with those of yedoma in the lower Itkillik River of northern Alaska. The Itkillik yedoma is regarded as similar to that at Duvanny Yar (Kanevskiy *et al*., 2011), its silt interpreted as loess (Carter, 1988) and assigned to the north Alaskan loess belt (Muhs, 2013a, Figure 15a). Preliminary findings on the Duvanny Yar yedoma were reported by J. B. Murton *et al*. (2010, 2013), and the cryostratigraphy of the Itkillik yedoma was described by Kanevskiy *et al*. (2011) and Strauss *et al*. (2012b). To elucidate the processes and environmental context of silt deposition, we evaluate an extensive body of Russian literature and compare the Duvanny Yar silt with cold-climate loesses in Eurasia and North America.

REGIONAL SETTING OF THE KOLYMA LOWLAND

Introduction

The Kolyma Lowland forms the easternmost segment of the northeast Siberian coastal plain – comprising the Yana, Indigirka and Kolyma lowlands – to the south of the East Siberian Sea (Figure 1A). It is drained by the northward-flowing Kolyma River, the sixth largest river flowing into the Arctic Ocean. The lowland is bordered by the North Anyuy Range to the east, the Yukagir Plateau to the south, the Alazeya Plateau to the southwest and the Ulakhan-Sis Ridge to the northwest (Figure 2A; Shahgedanova *et al.*, 2002). Tectonically, the lowland is part of the Pacific fold belt and straddles two late Mesozoic volcanic belts, the Late Cretaceous Okhotsk-Chukotka belt to the south and the Svyatonos-Chukotka belt to the north (Koronovsky, 2002). The lowland is thought to have remained unglaciated throughout the Quaternary, whereas some

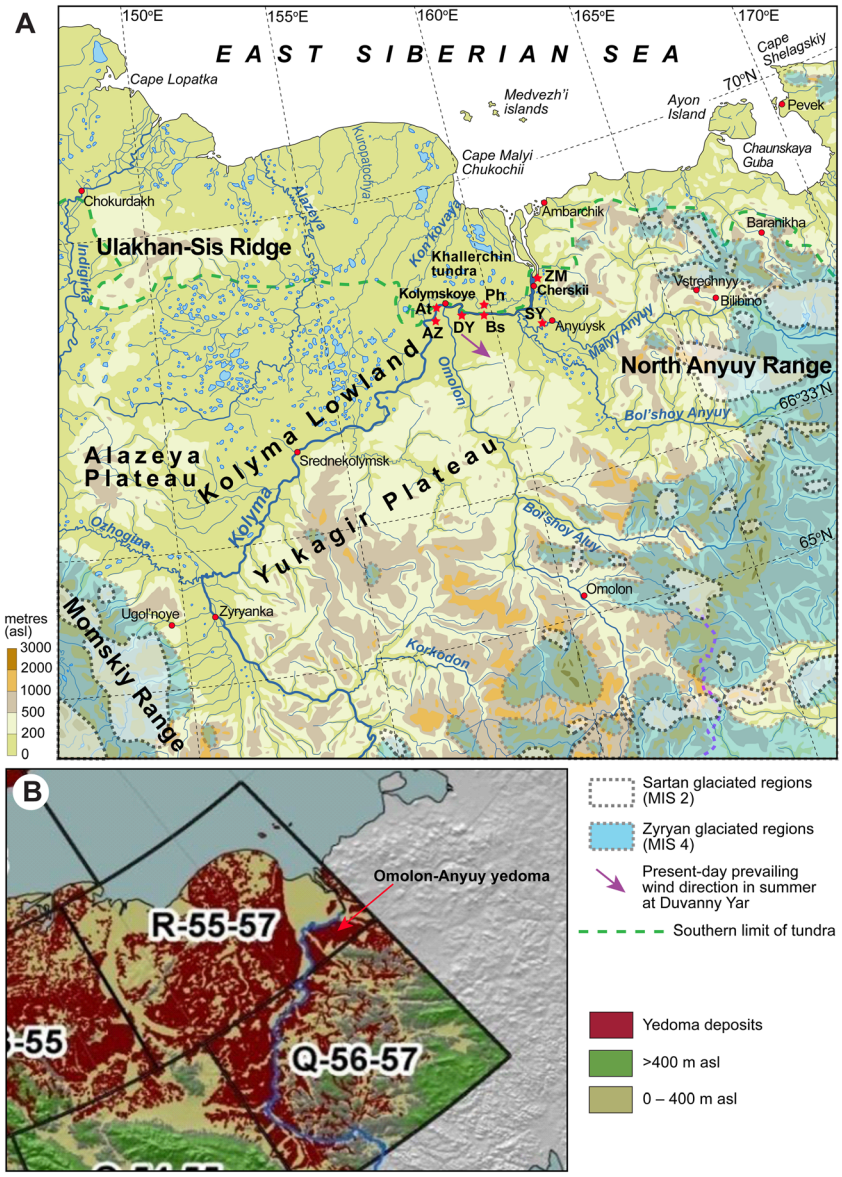

Figure 2 (A) Physiographic setting of the Kolyma Lowland and surrounding uplands of northeast Yakutia, Chukotka and Kamchatka. A yedoma surface (Figure 3A) is at an elevation of about 50 m asl at Duvanny Yar (DY), and rises to about 100 m asl to the south of Duvanny Yar. Inset into the yedoma surface is a fluvial terrace (At = Alyoshkina terrace) surface at 15–20 m asl, whose stratigraphy is exposed at Alyoshkina Zaimka (AZ). The terrace extends north of the Kolyma River and underlies the Khallerchin tundra. The generalised southern limit of tundra is modified from the CAVM Team (2003). Glaciated areas during the Zyryan glaciation (MIS 4) and Sartan glaciation (MIS 2) are based on Glushkova (2011). Other yedoma sites discussed in the text: Bs = Bison; Ph = Plakhinskii Yar; SY = Stanchikovsky Yar; ZM = Zelyony Mys. (B) Distribution of yedoma deposits within the Kolyma Lowland and adjacent areas. Source: Grosse *et al.* (2013). MIS = Marine Isotope Stage. This figure is available in colour online at wileyonlinelibrary.com/journal/ppp

surrounding uplands were glaciated to limited extents, as discussed below.

Yedoma

Yedoma is widespread in the Kolyma Lowland (Figure 2B). Its southern limit in this region stretches along the margins of river floodplains, where they abut the front of adjacent uplands (Lupachev and Gubin, 2012; Grosse *et al*., 2013). Such yedoma is metres to tens of metres thick and underlies a flattish 'yedoma surface' (i.e. the depositional land surface that formed along the top of the yedoma) that was subsequently modified by thermokarst activity (Sher *et al*., 1979; Veremeeva and Gubin, 2008, 2009). The yedoma surface is well developed between the Omolon and Bol'shoy Anyuy rivers (Figure 2B), where it is termed the Omolon-Anyuy yedoma (>1000 km^2; Y. K. Vasil'chuk *et al*., 2001a). The surface descends from > 100 m asl in the south to about 35–50 m asl in the north, at Duvanny Yar (Sher *et al*., 1979). Other important yedoma exposures in the Kolyma Lowland include Bison, Plakhinskii Yar, Stanchikovsky Yar and Zelyony Mys (Figure 2A; Rybakova, 1990; Y. K. Vasil'chuk *et al*., 2003; A. C. Vasil'chuk and Y. K. Vasil'chuk, 2008).

Yedoma also occurs in some low mountainous areas south and west of the Kolyma Lowland. Sections through basal slope deposits in intermontane basins near the settlements of Utinoe and Sinegor'ye in the Upper Kolyma River basin of the western Magadan region also contain syngenetic ice wedges > 20 m high (Y. K. Vasil'chuk and A. C. Vasil'chuk, 1998). The host sediments, which include coarse clastic rock debris of colluvial origin, are much coarser grained than the yedoma near the lower Kolyma River.

Topography

The topography of the Kolyma Lowland comprises a number of accumulation levels (Sher *et al*., 1979), that is, land surfaces formed by sediment aggradation. The highest (watershed) level forms a plain known as the Omolon-Anyuy yedoma surface (Figure 2B), discussed previously. The plain is underlain by yedoma and deposits of Middle and Early Pleistocene age (Gubin and Zanina, 2013, 2014). Collectively, these deposits overlie a bedrock surface that dips significantly to the north-northwest. We have previously observed nearly the same stratification of yedoma and palaeosols beneath the high level of the Omolon-Anyuy yedoma surface as that beneath the relatively lower levels at Malyi Chukochii Cape and the Kuropatochya River (Figure 2A). Thus, the origin of the levels clearly relates in part to the underlying bedrock surface, which dips to the north-northwest: the Early and Middle Pleistocene deposits and the yedoma above them inherit this relief. The present study examines the stratigraphy beneath the Omolon-Anyuy yedoma surface at Duvanny Yar.

A second surface, inset into the yedoma surface, comprises the 15–20 m high Alyoshkina terrace together with the highest surface of the Khallerchin tundra (Figure 2A). The Alyoshkina terrace is at a lower elevation than the yedoma surface and is underlain by relatively ice-poor silty sands ('Alyoshkin Suite') whose stratigraphy has been described from the right bank of the Kolyma River, at Alyoshkina Zaimka (Sher *et al*., 1979, Figure 22), about 25 km west of Duvanny Yar (Figure 2A). Arkhangelov (1977) also described the Alyoshkin Suite, distinguishing its sediments from those of the yedoma. The terrace is thought to correspond to the 15–20 m high surface in the southern region of the Khallerchin tundra and with remnants of this sandy surface at a similar elevation on the left bank of the Kon'kovaya River, on the northwest margin of the Khallerchin tundra (Sher *et al*., 1979).

The Khallerchin tundra lies mostly to the north of the east-west aligned reach of the lower Kolyma River, east of Kolymskoye, extending over 120 km north to the Kon'kovaya River and falling in elevation towards the coast (Figure 2A). It is underlain by ice-poor sand and forms a generally waterlogged landscape inset with abundant lakes (Fyodorov-Davydov *et al*., 2003). Within the Khallerchin tundra, a 2 m to 5 m high terrace forms a coastal strip that extends > 30 km inland, and an 8 m to 12 m high surface forms the dominant part to the south, rising farther south to the 15 m to 20 m high Alyoshkina terrace. According to Sher *et al*. (1979), the Khallerchin tundra has been interpreted as: (1) a marine terrace, (2) an alluvial plain that forms the lowest terrace above the modern floodplain of the Kolyma River, (3) a thermokarst plain developed by thaw subsidence in the Omolon-Anyuy yedoma surface and (4) an ancient deflation region contemporaneous with the yedoma surface to the south of the Kolyma River. Alternatively, it may represent an aeolian dune tract formed on the surface of a braided floodplain of the Kolyma River (Hopkins, 1982).

The floodplain of the meandering lower Kolyma River is inset into the Alyoshkina terrace near Alyoshkina Zaimka and, with its tributaries, feeds into the Kolyma's delta plain, an area of about 3000 km^2 north of Cherskii (Figure 2A). The floodplain is low-lying and almost flat, dotted with numerous lakes.

Present-day Climate

The present-day climate of the Kolyma Lowland is strongly continental, even though the region is near the Arctic Ocean. The winter climate is dominated by a secondary high-pressure centre of the Siberian high, which develops over the Yana-Indigirka-Kolyma basins between October and March, controlling winter temperatures and seasonal precipitation patterns (Shahgedanova *et al*., 2002). Regional climate data are sparse. For Kolymskoye, about 20 km northwest of Duvanny Yar (Figure 2A), Sher *et al*. (1979) reported the average temperature of the coldest month (January) as -34.8°C, and that in the warmest month (July)

as 10.9°C, resulting in an annual monthly temperature range of 45.7°C. The mean annual air temperature (MAAT) at Kolymskoye is -13.4°C, and the mean annual precipitation (MAP) 229 mm. For comparison with more recent data (1986–2004), values of the MAAT of about -14°C and the MAP of ≤ 200 mm or less are interpolated by Park *et al.* (2008) from the observational data-sets of the Baseline Meteorological Data in Siberia Version 4.1 (Suzuki *et al.*, 2007), and a MAAT value of -10.8°C and a MAP of 224 mm are given for 1980–2007 data from Cherskii (Davydov *et al.*, 2008). Precipitation occurs mainly as rain in summer. Snow cover persists from the end of September until the end of May and is thickest in late April. The average thickness of snow cover in Kolymskoye village is 0.45 m, while for treeless areas in the Kolyma Lowland it is no more than 0.25 m (Sher *et al.*, 1979).

Modern climate conditions at Duvanny Yar are generally not favourable for aeolian transport of silts. Although data on wind velocity and direction as well as aeolian sediment transport have not been systematically measured at Duvanny Yar, we make several observations based on many years' field experience of working there. Prevailing winds are from the northwest during summer, with an average wind speed of about 4–6 m s^{-1}. Probably on account of the often windy summer conditions, one of the possible meanings of the toponym 'Duvanny' is 'windy'. Occasionally, summer winds are subparallel to the Kolyma floodplain valley, blowing either eastward or westward, depending on current cyclonic activity. Winds coming from inland (from the south) tend to be dry and transport silt and fine sand, whereas winds coming from the sea tend to be damp and therefore do not transport sediment. Dry, stable winds from the south that come from the Pacific region are quite rare at Duvanny Yar, occurring two or three times each summer; such winds, we speculate, may transport sediments within the upper catchments of the Kolyma River tributaries in the mountain chains along the southeast border of the Kolyma Lowland (Figure 2A). During winter, the Siberian high-pressure system prevails over the whole region, producing calm conditions or gentle easterly winds (1–3 m s^{-1}).

Vegetation and Soils

The vegetation of the Kolyma Lowland grades northward from open forest through forest-tundra to tundra. The northern limit of forest-tundra is located at Duvanny Yar, where the vegetation is open forest composed of larch (*Larix dahurica*) with a shrub understorey of birch (*Betula*), willow (*Salix* spp.) and Labrador tea (*Rhododendron* spp.; Smith *et al.*, 1995). To the north, tundra vegetation forms an 80–100 km wide strip near the Arctic Ocean coast, and – where developed on yedoma surfaces – tends to be grassy, and dominated by forbs rather than sedges and mosses (Smith *et al.*, 1995).

Soil development is controlled by soil moisture, surface organic layer thickness, landscape position and permafrost (Smith *et al.*, 1995). Permafrost-affected soils in the region can be termed Cryosols or Gelisols. Moister soils tend to be churned by cryoturbation, which cycles organic material downward into the mineral profile, largely determining the organic carbon content in the uppermost B horizons. Cryoturbation is active in soils beneath the forested upland yedoma surface, disrupting soil horizons, incorporating organic matter and contributing to a hummocky surface topography, as found on the upland yedoma surface at Duvanny Yar. Hummock development may also be influenced by vegetation growth and organic matter accumulation (Shur *et al.*, 2008). Such soils have a surface organic layer that is thickest in hummock troughs. Beneath the organic layer are silty mineral horizons with a grey-brown colour (10YR 3/2 m) — indicating little oxidative weathering — that contain redoximorphic features (soil mottles) in the active layer, which indicate at least periodic saturation.

Drier yedoma soils are developed beneath grassy, forb-dominated tundra near the coast. In such soils, cryoturbation is minor and hummock formation is weak. These tundra soils have a well-developed and continuous 50–100 mm thick A horizon more characteristic of temperate grasslands than of tundra, and most organic matter is well decomposed. The B horizon of the tundra soils is well drained, enriched with plant roots, largely lacks signs of gleyisation, has a moderately developed postcryogenic structure and, rarely, contains weakly expressed features indicative of cryoturbation. Further details on soils developed on yedoma in northern Yakutia are given in Fyodorov-Davydov *et al.* (2003), Gubin and Lupachev (2008), Gubin and Veremeeva (2010) and Lupachev and Gubin (2012).

Peat formation in the Kolyma Lowland tends to be limited to the wettest areas, for example, in alases (i.e. large depressions produced by thaw of very ice-rich permafrost). No extensive areas on yedoma remnants were observed by Smith *et al.* (1995) with peat thicker than 40 cm, a common thickness criterion for classifying soils as 'Histosols' (IUSS Working Group WRB, 2006), although peat within alases can reach thicknesses of several metres.

Permafrost, Ground Ice and Active Layer Thickness

Permafrost in the Kolyma Lowland is continuous, except in taliks (a layer or body of unfrozen ground within a permafrost region) beneath large river channels or lakes. Permafrost thickness is 500–650 m, and the mean temperature of permafrost varies from -3°C to -11°C (Davydov *et al.*, 2008). Mean annual ground temperatures are about -6°C to -10°C beneath tundra of the left-hand bank of the Kolyma River, and about -4°C to -8°C beneath open forest, where snow cover thicker than that on the tundra better insulates the ground from cold winter air temperatures (Sher *et al.*, 1979).

Ground ice in the yedoma consists of pore, segregated and wedge ice. Pore and segregated ice in the silt at Duvanny Yar commonly have combined gravimetric (i.e. mass of ice as a % of mass of dry soil) ice contents of about 40–75 per cent

(Wetterich *et al*., 2011a, Figure 2.6). Syngenetic wedge ice confers additional volumetric ice contents of 30–70 per cent for the silts of the coastal lowland of Yakutia (Kaplina *et al*., 1978). At Duvanny Yar, syngenetic ice wedges ≤ 4–4.5 m wide and ≤ 20–40 m high divide the silts into mineral blocks (Kaplina, 1986; Y. K. Vasil'chuk, 2006) 3–12 m in diameter. Primary, secondary and, locally, tertiary networks of polygonal wedge ice have been reported at Duvanny Yar (Kaplina *et al*., 1978). Holocene ice-wedge growth, either active or recent, is indicated in the floors of some drained thaw lake basins by the occurrence of low-centred polygons (Smith *et al*., 1995), and also by a polygonal crack network marked by vegetation in troughs in a gravelly island in the Kolyma River that we observed in 2009 near the study site.

A transition zone occurs in the uppermost horizon of permafrost, separating the top of the Pleistocene permafrost from the base of the modern active layer. The transition zone consists of (1) an *intermediate layer* (about 1–1.5 m thick) whose base marks the maximum depth of thaw at some time in the past, overlain by (2) a *transient layer* that thaws during the warmest and more recent conditions (Shur, 1988a, 1988b; Shur *et al*., 2005; Lupachev and Gubin, 2008). The intermediate layer is very ice-rich, with a mean volumetric soil moisture content of 55 per cent (compared to a mean value of 25% for the active layer; Davydov *et al*., 2008) and is characterised by ataxitic, lenticular-layered and lenticular-reticulate cryostructures. The equation used to calculate these values in Davydov *et al*. (2008), however, is not correct, and we regard these values as very low for any ice-rich soil; we would expect volumetric ice contents typically of about 70–80 per cent for the intermediate layer and about 30–40 per cent for the active layer.

The timing and environmental conditions associated with the maximum depth of thaw (marked by the bottom of the intermediate layer) after yedoma accumulation had ceased are disputed. According to Davydov *et al*. (2008), the upper 0.1–2.0 m of yedoma thawed during the Holocene Climatic Optimum (9600–6300 ^{14}C BP for northeast Siberia), before refreezing. However, Shur (1988a) has studied numerous exposures of yedoma at placer gold mines in Kular (northern Yakutia) and observed no differences in the levels of the bottom of the intermediate layer above ice wedges and adjacent polygonal ground. Such uniformity, he suggested, would not be possible if the active-layer thickness (ALT) had increased during the Holocene, because numerous observations by this author have showed that increases in ALT always have deeper impacts on ice wedges than on soil inside adjacent polygons. Shur (1988a) concluded that the active layer at the end of the Late Pleistocene was thicker than that during the Holocene Climatic Optimum. He attributed this to the accumulation of organic matter on the soil surface during the Pleistocene to Holocene transition, when steppe ecosystems with low thermal insulation properties in summer were replaced by tundra vegetation with a thick organic layer and high thermal insulation properties. According to Lozhkin (1976), cold and dry conditions in the Late Pleistocene were replaced by cold and wet conditions that preceded the Holocene Climate Optimum by 2000 years; this provided enough time for ecosystems to adjust to warmer climatic conditions. In line with this, Shur (1988a) has suggested that the possible increase in ALT during the Holocene Climatic Optimum did not reach the bottom of the intermediate layer attained at the end of the Pleistocene. Shur *et al*. (2011) showed that ALT depends more on local factors than on regional ones, and that ALT is always greater in present-day Arctic regions with cold climatic conditions and a thin organic layer than in areas of discontinuous permafrost with a thick organic layer. Therefore, the proposition that 'the warmer the climate, the thicker the active layer' is not always applicable. After organic matter accumulated on the soil surface during the Holocene, a decrease in ALT led to the formation of the ice-rich intermediate layer. Shur (1988a) termed this formation process *quasi-syngenetic*, which is similar to the term *syngenetic* in relation to permafrost aggradation, but occurs without accumulation of new sediment on the ground surface.

ALT in the Kolyma Lowland in the present day rarely exceeds 1 m, with minimal depths of about 0.2 m beneath some peaty soils. At Duvanny Yar, ALTs of about 0.3–0.4 m were reported for peaty deposits in alases, about 0.4–0.5 m for earth hummocks developed on the upland yedoma surface and about 0.8 m for the active silty floodplain of the Kolyma River (Smith *et al*., 1995, Figure 4). For grassy coastal tundra developed on yedoma, the absence of mosses allows soils to warm more during summer, resulting in deeper active layers (>0.5 m) than those beneath open forest. ALTs beneath hummocky tundra soils in the Kolyma Lowland do not exceed 1 m and are generally about 0.6–0.8 m under the hummocks and ≤ 0.4 m beneath the surrounding peaty troughs (Lupachev and Gubin, 2012). Dry sands thaw two to three times more deeply in summer than the moist yedoma loams (Fyodorov-Davydov *et al*., 2003). No trends in ALT were reported by Fyodorov-Davydov *et al*. (2003) for sandy tundra soils at Ahmelo Lake between 1989 and 2002. In contrast, an increase in ALT by ≤ 40 per cent (relative to the long-term mean value) was measured at seven sites in the northern taiga of the Kolyma Lowland between 2001 and 2005 (Davydov *et al*., 2008); the increased ALT resulted in thaw of the transition zone, which at some sites degraded completely, allowing thaw to extend into the underlying permafrost. ALTs on both the tundra and taiga soils strongly correlate with mean summer air temperatures.

Kolyma River

The modern Kolyma River discharges about 100–132 km^3 yr^{-1} of water into the Arctic Ocean, mostly fed by spring snowmelt and summer rainfall (Majhi and Yang, 2008; Griffin *et al*., 2011). Using Landsat imagery obtained on 4 October 2013 of the Kolyma Lowland, we observe that the Kolyma River generally has a meandering form, with some anabranching developed in the main river and in some tributaries. The alluvial channel belt between Duvanny Yar and

Cherskii (Figure 2A) is approximately 10 to 20 km wide, and contains abundant abandoned meander point bars, numerous abandoned channels, and myriad ponds and lakes up to several kilometres in maximum dimension.

The streamflow characteristics of the lower Kolyma River at Kolymskoye, between 1978 and 2000, indicate that the monthly mean discharge tends to be low from November to April (18–47 m^3 s^{-1}) and high from May to June (178–754 m^3 s^{-1}; Majhi and Yang, 2008). Peak flows in June (1490 m^3 s^{-1}), during the snowmelt season, are approximately 80 times greater than the lowest flows in April. We estimate that the peak river level can rise about 5–6 m above winter level near Duvanny Yar and Cherskii. The floods transport abundant organic detritus, including tree trunks, some of which is deposited as a distinctive 'trash layer' of logs protruding from the river banks several metres above late-summer river level at Duvanny Yar. The floods also contribute abundant suspended sediment to the floodplain, a large proportion of it being silt eroded from yedoma deposits. We have measured sediment deposition rates of about 1 mm yr^{-1} (in June) in sediment pots emplaced in the floodplain near Cherskii during the 1980s and 1990s; of this material (n = 5), about 85 per cent was in the silt fraction and the total organic carbon content was 1.1–1.3 per cent. A significant amount of silt there was also deposited on grasses, tussocks, and leaves and branches of shrubs, from where it was later washed down to the ground surface by rains. Such material can be redistributed *within* the river valley by dry winds blowing across sandy bars or beaches during periods of low river level.

Late Quaternary History of Northeast Siberia (Western Beringia)

Western Beringia extended from the Verkhoyansk Mountains in the west to the Bering and Chukchi Sea coasts in the east (Elias and Brigham-Grette, 2013, Figure 1). The Kolyma Lowland is located centrally in the north of western Beringia. The Lena Delta region to the west of the Verkhoyansk Range is included in the following review because yedoma there provides a valuable source of palaeoenvironmental information (Astakhov, 2014). The main time divisions of the Late Pleistocene in western Beringia comprise: (1) the Kazantsevo interglacial (MIS 5e), (2) the Zyryan glaciation (MIS 4), (3) the Karginsky interstadial (MIS 3) and (4) the Sartan glaciation (MIS 2) (Table 1). Late Pleistocene events in Beringia are reviewed by Elias and Brigham-Grette (2013) and vegetation history by Lozhkin and Anderson (2013a). The palaeoenvironmental history of western Beringia during MIS 3 and MIS 2 is discussed by Brigham-Grette *et al*. (2004).

Kazantsevo Interglacial: 130 000–70 000 cal BP (MIS 5). During peak last interglacial (LIG) conditions of MIS 5e, eustatic sea level was about 6–7 m higher than present across Beringia, and terrestrial climates were generally warmer (Brigham-Grette, 2001; Elias and Brigham-Grette, 2013). Thermokarst activity occurred in areas of ice-rich permafrost. Mean January air temperatures, reconstructed from $\delta^{18}O$ values in syngenetic ground ice in the lower Kolyma and adjacent regions, were 2°C warmer than present (Nikolayev and Mikhalev, 1995). Mean July air temperatures, reconstructed from pollen data on Bol'shoy Lyakhovsky Island, are thought to have been at least 4–5°C higher than those today during the MIS 5e climatic optimum (Andreev *et al*., 2011).

Treeline advanced significantly in northeast Siberia during the last interglaciation, with the larch-stone pine (*Pinus pumila*) forest limit perhaps 600 km north and east of its current position, and tree-birch (*Betula* spp.) similarly displaced. In interior forests, spruce (*Picea obovata*) was mixed with larch (Lozhkin and Anderson, 1995). The major extension of forests north and east is compatible with the above estimates of summer air temperature about 4°C higher than that at present. At Lake El'gygytgyn in Chukotka (Lozhkin and Anderson, 2013b), the record indicates a two-stage interglacial vegetation progression, initially with larch, birch and alder (*Alnus* spp.) and subsequently with a high abundance of stone pine; the increase in stone pine probably reflects a shift to a warmer, moister winter climate with deeper snow cover.

Zyryan Glacial Conditions: 70 000–55 000 cal BP (MIS 4). During Pleistocene glacial periods – when the present area of the Kolyma Lowland was several hundred kilometres inland from the Arctic Ocean due to lowered sea levels – the climate was more continental than that at present and probably more continental than in any other part of Beringia (Zanina *et al*., 2011). Increased continentality, rather than decreased air temperatures, was arguably the most important difference between the Late Pleistocene and modern climates in western Beringia (Alfimov and Berman, 2001). Exposure of the Bering Land Bridge and nearby continental shelves cut off circulation between the Arctic and Pacific

Table 1 The main divisions of the Late Pleistocene in Beringia.

Division	Russian spelling	Marine Isotope Stage	Age (cal BP)
Sartan glaciation	Сартанское оледенение	2	25 000–15 500
Karginsky interstadial	Каргинский интерстадиал	3	55 000–25 000
Zyryan glaciation	Зырянское оледенение	4	70 000–55 000
Kazantsevo interglacial	Казанцевское межледниковье	5	130 000–70 000

Modified from Velichko and Spasskaya (2002, table 2.1), Lozhkin and Anderson (2011) and Elias and Brigham-Grette (2013, table 1).

oceans, and reduced moisture advection from the North Pacific (Elias and Brigham-Grette, 2013). As a result, Zyryan (MIS 4) glaciers in northeast Asia were restricted largely to mountain ranges, and eastern Siberian lowlands remained ice-free. Mountain glaciers developed in the North Anyuy Range to the east of the Kolyma Lowland, the Yukagir Plateau to the south and the Momskiy Range to the southwest (Figure 2A). Glacial meltwater discharged into tributaries of the palaeo-Kolyma River. Mean winter air temperatures inferred from $\delta^{18}O$ values in ground ice in the Lena Delta region were lowest in the last cold stage at about 60 000–55 000 BP, prior to a long stable period of cold winter temperatures from 50 000 BP to 24 000 BP (Meyer *et al*., 2002a).

Karginsky Interstadial: 55 000–25 000 cal BP (MIS 3).

MIS 3 vegetation and climate, at least during summer, varied spatially and temporally between northern and southern parts of western Beringia (Lozhkin and Anderson, 2011). Although the exact timing and number of climate and vegetation changes are uncertain, some general patterns are apparent, particularly after about 40 000 ^{14}C BP, when sequences are more firmly dated. Two warm periods and two cool and dry periods during the Karginsky interstadial have been identified in northeast Siberia (Anderson and Lozhkin, 2001). The warm periods – when summer climates in western Beringia were probably as warm or nearly as warm as those at present – were 39 000–33 000 ^{14}C BP and 30 000–26 000 ^{14}C BP. Both resulted in the development of *Larix* forests – of almost interglacial character and approximating their present-day range – in the Yana-Indigirka-Kolyma lowlands. The timing of maximum summer warmth and forest development in this region is placed by Anderson and Lozhkin (2001) and Brigham-Grette *et al*. (2004) between about 39 000 ^{14}C BP and 33 000 ^{14}C BP, coinciding with a peak in June insolation at 60°N at about 35 000 cal BP. A radiocarbon age of 34 410 ± 770 ^{14}C BP was obtained from wood within sphagnum peat overlying lacustrine silts, from Stanchikovsky Yar (Rybakova, 1990); the peat is thought to have accumulated within a larch-birch forest. A phase of thermokarst activity during the Karginsky interstadial is indicated by lake (alas) development.

The climatic optimum during MIS 3 in the Laptev Sea region is also placed in the 40 000–32 000 BP interval, based on numerous bioindicators, excluding insects (Andreev *et al*., 2011). However, insect faunas dated to about 45 000 ^{14}C BP and 35 000 ^{14}C BP from the lower Kolyma region are thought to indicate summer air temperatures 1.0–4.5°C warmer than present, representing a possible July temperature range of 12.0–15.5°C (Alfimov *et al*., 2003). Two cool and dry periods identified in western Beringia were 45 000–39 000 ^{14}C BP and 33 000–30 000 ^{14}C BP, the latter coinciding with the replacement of forest by herbaceous vegetation (Anderson and Lozhkin, 2001). Given the uncertainties of dating materials of such age, this alignment of climate patterns between different proxies is quite reasonable. Interestingly, Brigham-Grette *et al*. (2004, p. 32) noted that the variable climates in western Beringia during MIS 3 are 'reminiscent of fluctuations described from the North Atlantic sector.' Valley glaciers are thought to have retreated from their maximum extent in MIS 4 as a result of ameliorating conditions in MIS 3, sometime after about 60 000 BP (Brigham-Grette *et al*., 2004). Retreat rates are unknown. The MIS 3–2 transition at about 27 000–26 000 BP is marked in western Beringia by a shift from warm/moist to severely cool-dry climates (Anderson and Lozhkin, 2001).

Sartan Glacial Conditions: 25 000–15 500 cal BP (MIS 2).

In the Paleoclimate Modeling Intercomparison Project simulations of the Last Glacial Maximum (LGM) (Braconnot *et al*., 2007), the northern extra tropics were particularly cold. Strong cooling occurred across northern Siberia as a result of changes in the stationary wave pattern; cooling in eastern Siberia was about -5°C. The whole of Eurasia was drier than present. Western Beringia lay downwind of ice sheets in Scandinavia and northern Eurasia, which depleted much of the moisture from the westerly winds, and the Siberian high was likely intensified (Guthrie, 2001). As a result, cold, arid conditions dominated western Beringia, and this is supported by geological and biological data (Brigham-Grette *et al*., 2004; cf. Kienast *et al*., 2005).

Extremely continental and arid climatic conditions, with colder winters and warmer summers than present, are inferred for the period from 60 000 ^{14}C BP until the end of MIS 2, based on plant macrofossils in yedoma near the Lena Delta (Kienast *et al*., 2005). The former occurrence of *Kobresia* meadows and Arctic pioneer communities suggests that snow cover was thin or lacking and that winters were colder than present. Limited snow cover promoted ground cooling, thermal contraction cracking and ice-wedge growth. Late Pleistocene mean winter air temperatures 9–15°C colder than those of the Holocene have been reconstructed from $\delta^{18}O$ values in Kolymian ice wedges (Nikolayev and Mikhalev, 1995). These authors inferred similar temperature changes for MIS 2, 4 and 6 in Yakutia from $\delta^{18}O$ values in pore ice and segregated ice formed syngenetically during permafrost aggradation, with LGM mean January air temperatures 10–14°C colder and mean cold season temperatures 8–13°C colder than those at present. A Pacific moisture source for winter precipitation during the LGM is consistent with low deuterium excess values in wedge ice at Duvanny Yar (Strauss, 2010) and in yedoma on Big Lyakhovsky Island, in the eastern Laptev Sea (Meyer *et al*., 2002b). Pollen and stable isotope ice-wedge data from permafrost in the east Siberian Arctic suggest that the coldest and driest climatic conditions during the Sartan glaciation occurred about 24 000–18 000 BP (Wetterich *et al*., 2011b). Summer air temperatures reconstructed from insect fauna in sediments dated to 17 000–16 000 ^{14}C BP and 14 000–13 000 ^{14}C BP from the Kolyma Lowland were 12.0–13.6°C, which represents

a warming of 1.0–2.5°C above present-day conditions (Alfimov *et al*., 2003).

The extent of mountain glaciers during the Sartan glaciation in northeast Asia is thought to have been about one-half to one-third of that during the Zyryan glaciation (Glushkova, 2011). Figure 2A shows the different glacial limits identified in the uplands that border the east, south and southwest of the Kolyma Lowland. Less extensive Sartan glaciation is attributed by Glushkova (2011) to an eastward rise in snowline, which left low mountains in the east below the level of snow accumulation, whereas in the west, the decrease in the snow accumulation area was limited. Another factor that probably reduced the extent of Sartan glaciation was a reduced moisture supply during MIS 2, when ice sheets in Scandinavia and northern Eurasia reached their maximum size. During the LGM, glaciation was limited to valleys and cirques in some mountain ranges of western Beringia, with ice reaching its maximum extent between 24 000 ^{14}C BP and 17 000 ^{14}C BP (27 000–20 000 cal BP; Elias and Brigham-Grette, 2013). To the west and southwest of the Kolyma Lowland in the Cherskii, Suntar-Kyatar and Verkhoyansk ranges, the extent of Sartan glaciation is thought to have been not much smaller than that of the Zyryan glaciation, although the extent of Sartan glaciation in the Verkhoyansk Mountains is debated (Glushkova, 2011).

The exact nature of the largely treeless vegetation during the Sartan glaciation is still debated, as each approach (palynology, plant macrofossils, mammalian palaeoecology and vegetation modelling) has different strengths. On the one hand, a vast 'mammoth steppe' has been reconstructed as a low herbaceous sward dominated by grasses, xerophilous sedges, forbs and sages suitable for grazing by bison, horse and woolly mammoth (Guthrie, 2001). Alternatively, a mosaic of tundra (rather than steppe) types – graminoid-forb tundra, prostrate dwarf shrub tundra dominated by willows, and, in places, dwarf shrub tundra – has been inferred from some palaeovegetation reconstructions and vegetation simulations based on palaeoclimate model output (Bigelow *et al*., 2003; Kaplan *et al*., 2003; Brigham-Grette *et al*., 2004; Lozhkin and Anderson, 2013a). There is little evidence of regional differentiation of vegetation across western Beringia in MIS 2. Pollen assemblages dated to MIS 2 from the Laptev Sea region are similarly dominated by grass with some sedge and *Artemisia* (Andreev *et al*., 2011). At Stanchikovsky Yar on the Malyy Anyuy River, near Anyuysk, about 110 km east-southeast of Duvanny Yar (Figure 2A; Rybakova, 1990), the vegetation reconstructed during the Sartan glaciation was dominated by herbaceous plants, especially grasses, wormwood (*Artemisia* sp.) and saxifrages, as well as significant amounts of mosses.

Lateglacial Transition: 15 500–11 700 cal BP (MIS 2).

The start of the Lateglacial transition at about 13 000 ^{14}C BP (15 500 cal BP) marked a shift across western Beringia from cold and dry environmental conditions to those that were warmer and wetter. Increased relative humidity and precipitation, and a growing oceanic influence contributed to a major reorganisation of vegetation. Regional thermokarst activity occurred during to the glacial-to-interglacial transition (Rybakova, 1990), and the landscape experienced widespread paludification.

Substantial vegetation and climate changes during the Allerød Interstadial and Younger Dryas Stadial in the Laptev Sea region have been reconstructed, based largely on pollen records (Andreev *et al*., 2011). During the Allerød (13 000 –11 000 ^{14}C BP), shrubby tundra vegetation, with *Salix* spp. and *Betula* spp. in protected places, was widespread inland from the Laptev Sea. Summer air temperatures reached 8–12°C (≤4°C higher than present), and annual precipitation was similar to that at present. Yedoma development at Duvanny Yar is thought to have ceased at or slightly before the beginning of the Allerød (Y. K. Vasil'chuk, 2005). Younger Dryas (11 000–10 300 ^{14}C BP) cooling is inferred from major decreases of shrub and tree pollen in comparison to the Allerød record. The Younger Dryas vegetation in the Laptev Sea region is reconstructed as open tundra and steppe-like habitats, based on grass- and sedge-dominated pollen spectra and low pollen concentrations.

Holocene: 11 700 cal BP to the Present (MIS 1).

In the early Holocene (10 300–7700 ^{14}C BP), shrubs reestablished and shrub tundra developed widely. *Larix* was also present at and beyond its northern limits by the beginning of the Holocene (Binney *et al*., 2009). Summer air temperatures in the Laptev Sea region were ≤ 4°C higher than those at present, and precipitation was higher than present (Andreev *et al*., 2011). During the middle and late Holocene, shrubs gradually disappeared from coastal regions around the Laptev Sea, resulting in grass tundra, with dwarf birches in protected areas. *P. pumila* increased in the mid-Holocene (about 8000 ^{14}C BP), reflecting an increase in winter snow (Brubaker *et al*., 2005). Warmer-than-modern summer air temperatures persisted until about 3700 ^{14}C BP to 3300 ^{14}C BP, inferred from high values of *Betula nana* in pollen records, and the continuance of *Larix* north of its present range (Binney *et al*., 2009), after which environmental conditions were similar to those at present (Andreev *et al*., 2011).

In summary, the Kolyma Lowland has undergone significant climatic shifts in moisture and temperature during the Late Pleistocene and contains a thick sedimentary record of gradual aggradation that is preserved in permafrost that has apparently never thawed.

DUVANNY YAR

Field Site

Our main field site (68°, 37′, 51.1″N; 159°, 09′, 06.8″E) is located in a retrogressive thaw slump at Duvanny Yar, on the right bank of the lower Kolyma River, in northeast

Yakutia (Figure 2A). The slump is one of several slumps, intermittently active, that expose up to 50 m of frozen and partially thawed yedoma along a 10 to 12 km long section of river bank. Amongst the exposures, Sher *et al*. (1979) distinguished eight remnants (1E–8E) of the yedoma surface, inset by four alases and three thermo-erosional valleys (Figure 3A). The eight remnants form a broad arch-like landform that declines in elevation from about 50 m above river level (arl) in its centre to about 35 m arl on its eastern and western margins. Beneath the arch (Figure 3A, B), the stratigraphy reported by Kaplina *et al*. (1978) and Sher *et al*. (1979) more or less mirrors the yedoma surface and comprises four main horizons, with the oldest horizon exposed in the centre to heights of several metres above river level (Figure 3A).

The studied slump provided the most complete and accessible series of adjacent stratigraphic sections exposed in 2009 beneath the yedoma surface. The slump is located near the centre of remnant 7E, about 700 m east of a thermo-erosional valley (Figure 3A). The sections examined extend from bluffs a few metres above river level through thermokarst mounds (baydzherakhs) 1 m to 5 m high in the slump floor to the headwall above. At the top of the headwall, the yedoma surface is about 39 m arl (Figure 3C).

Previous Research on Duvanny Yar Yedoma

The exposures at Duvanny Yar have a long history of study since the 1950s (Popov, 1953; Arkhangelov *et al*., 1979; Sher *et al*., 1979; Konishchev, 1983; Rosenbaum and Pirumova, 1983; Tomirdiaro and Chyornen'kiy, 1987; Y. K. Vasil'chuk, 1992, 2006, 2013; Strauss, 2010; Wetterich *et al*., 2011a; Zanina *et al*., 2011; Strauss *et al*., 2012a). The most detailed stratigraphic and sedimentological study of the silts is by Kaplina *et al*. (1978), summarised in Sher *et al*. (1979).

The stratigraphy identified by Kaplina *et al*. (1978) and Sher *et al*. (1979) comprises four horizons (Figure 3A), from the base upwards: (H1) *bluish-grey silts* interpreted as lacustrine taberal sediments (i.e. sediments that have thawed beneath a former lake and then refrozen after lake drainage); (H2) *heterogeneous sediments* consisting mainly of bluish-grey clayey silts beneath peat, and interpreted as a transitional sequence from lacustrine through to peat bog to alluvial sediments; (H3) *yedoma*, dominated by silts, with subordinate sands and loams, interpreted as floodplain and channel alluvial deposits; and (H4) *veneer deposits* of ice-rich silt attributed to deep thaw of the top of the yedoma followed by upward permafrost aggradation. Table 2 summarises the sediments, organic material and ground ice identified by Kaplina *et al*. (1978) and Sher *et al*. (1979).

^{14}C ages obtained from yedoma sampled in different exposures at Duvanny Yar and using different types of organic material range from non-finite ages (several metres above the river level) to 13 080 ± 140 ^{14}C BP (from the top of the yedoma) (Table S1 in Supporting Information). Kaplina (1986) suggested that the lower 10 m of the dated deposits are older than 50 000–40 000 ^{14}C BP. The ages have usually provided no consistent age-height patterns (Figure 4). Such variability has been attributed to the presence of allochthonous (reworked) organic material in the dated samples and particularly to reworking associated with the domed surface on which the yedoma silt accumulated. As a result, the most recent chronology of yedoma deposition – proposed by Y. K. Vasil'chuk (2006) – is based on the youngest ages obtained for given horizons (Figure 4; Table S2). The rationale and evidence for this, and for reworking of organic material from the basal dome, are set out in Appendix S1. Based on the youngest ages, the lower 25–30 m of yedoma are thought to date from 40 000–35 000 ^{14}C BP, and the upper part of the yedoma is dated at 30 000–13 000 ^{14}C BP. Further discussion of the existing ^{14}C geochronology of the Duvanny Yar sedimentary sequence is given in Appendix S1 and Tables S1–S4. Information on palaeotemperatures derived from the stable isotope record of ground ice at Duvanny Yar and adjacent sites from MIS 4–2 is given in Appendix S2, Figures S1 and S2 and Tables S5 and S6. Information on pollen spectra from ice wedges at this site is given in Appendix S3, and Figures S3 and S4.

METHODS

Sections and Sampling

Sedimentary sections in and near the thaw slump were examined to determine the litho- and cryostratigraphy of the yedoma deposits and the sediments above and beneath them. Eighteen sections were logged sedimentologically to refine these observations and interpret the origin of the sediments based on field evidence, prior to collecting samples for sediment and pollen analysis, and for dating. Cryostratigraphic descriptions follow those of J. B. Murton (2013a).

Stratigraphic sections were examined at 16 locations through yedoma deposits and the overlying transition zone and modern active layer. Section locations relative to Sher *et al*.'s (1979) schematic stratigraphic diagram of the Duvanny Yar exposures are shown on Figure 3A. Individual sections were about 0.5 to 3.0 m high, four to some tens of metres apart and formed a transect that extended from directly above a thermo-erosional niche cut by the river up to the yedoma surface at the top of the slump headwall (Figure 3C). Their relative vertical positions and heights above river level in early August 2009 were measured with a tape measure and abney level. The 16 sections (2–14, 20, 21, 23) were combined into a composite stratigraphic section through the yedoma (hereafter termed 'section CY') that spans a height from 3.5 m arl to 38.6 m arl (Figure 5). Heights above river level are relative to an arbitrary datum (1 m arl) marked by a break of slope between the top of the river beach and the base of the river bluff. Wedge ice volume in the steep upper headwall was approximated by measuring the proportion of wedge ice and yedoma silt

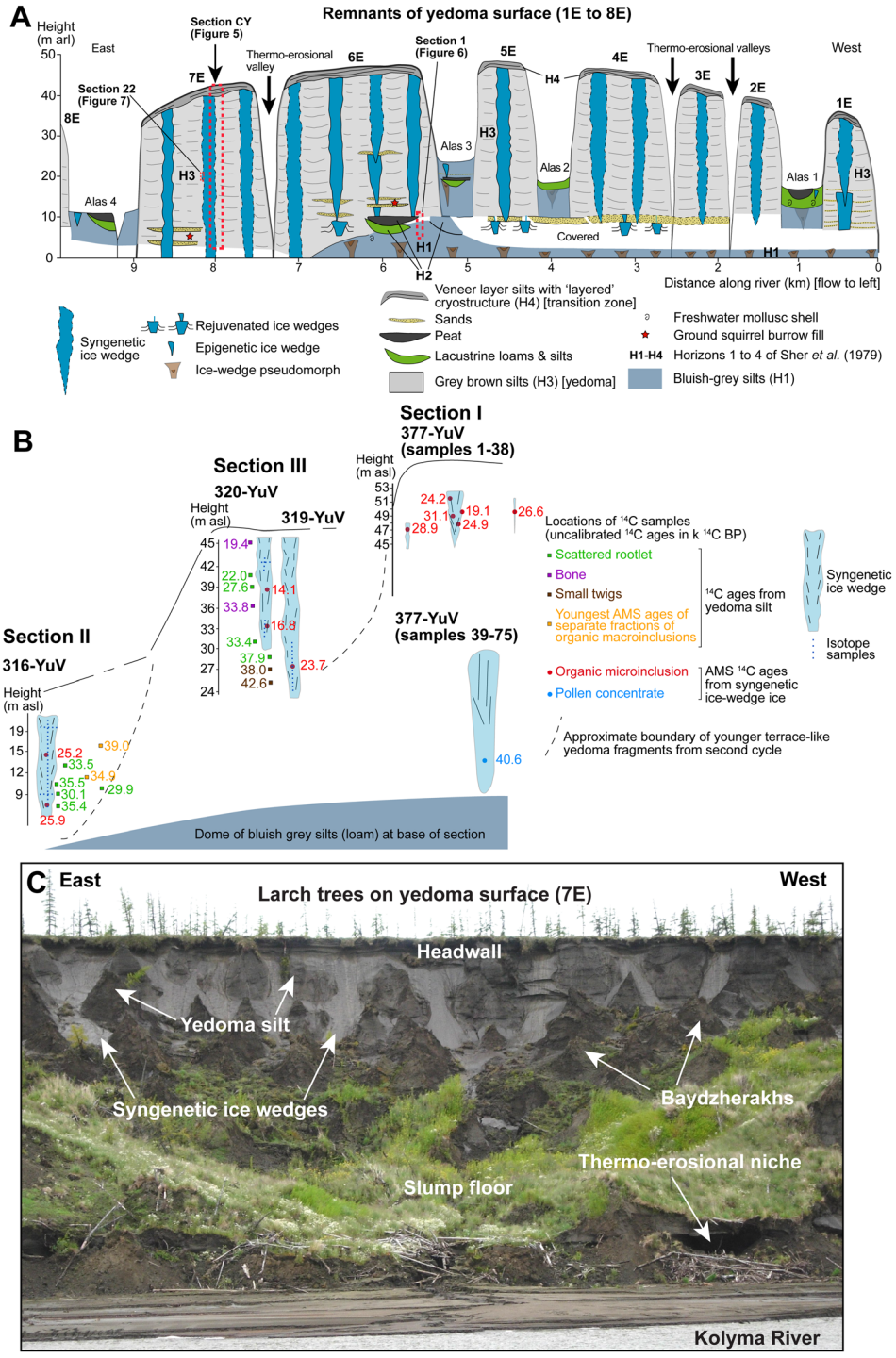

Figure 3 Stratigraphy of yedoma deposits at Duvanny Yar. (A) Relief and schematic stratigraphy of the Duvanny Yar exposures (modified from Sher *et al.*, 1979, Figure 14), showing location of sections CY, 1 and 22 (red dashed rectangles). The view is looking south, and so east is on the left. 1E–8E indicate remnants of the yedoma surface distinguished by Sher *et al.* (1979). (B) Yedoma sections I–III of different height, age and structure (modified from Y. K. Vasil'chuk, 2013). Section I is located at approximately either 4.5 or 5.5 km on (A) and was sampled in 1999; sections II and III are located at approximately 8.5 and 6.0 km, respectively, on (A) and were sampled in 1985. 316-YuV, 319-YuV, 320-YuV and 377-YuV denote ice wedges sampled for ^{14}C dating and/or stable isotope analysis (Tables S3-S6). Values in colour are ^{14}C ages (k ^{14}C BP). (C) Thaw slump headwall exposing large syngenetic ice wedges that penetrate yedoma silt. Melting of polygonal ice wedges has left conical thermokarst mounds of yedoma silt (baydzherakhs) upstanding on the headwall and slump floor. The top of the headwall is about 39 m above the Kolmya River, and underlies larch trees in the forest-tundra on the upland yedoma surface. The composite stratigraphic section through the yedoma (section CY; Figure 5) was established from this location. Photographed in 2009, looking south. arl = Above river level. This figure is available in colour online at wileyonlinelibrary.com/journal/ppp

Table 2 Summary of stratigraphic units, sediment, organic material and ground-ice characteristics of sections at Duvanny Yar identified by Kaplina *et al*. (1978) and Sher *et al*. (1979).

Stratigraphic unit[a]	Sediment	Organic material	Ground ice[b]	Interpretation
H4: Veneer deposits (0.7–1.2 m; ≤4 m in 'basins')	Grey-brown silts similar to those in yedoma	*In-situ* grass roots Peat clumps and wood fragments in lower part of 'basins' Pollen dominated by trees and shrubs	Extremely high ice content expressed as 'bands' with ataxitic Cs separated by reticulate or layered Cs Thaw unconformity along base truncates tops of ice wedges in yedoma	Warmer climate than previously with recent-type vegetation Deep seasonal thaw (early stage of thermokarst) of the top of the yedoma followed by upward freezing from permafrost; and/or solifluction
H3: Yedoma (40–50 m[c])	Grey-brown silts; uniform; texturally similar to unit H1	*In-situ* grass roots Banding records varying amount of organic matter	Alternating massive and lenticular Cs	Banded silts deposited on floodplain, with peat accumulating in occasional low-centred polygons
Upper subunit (≤30 m)	Alternating dark- and light-coloured horizontal bands (3–50 cm thick) Horizontal laminae 1-2 mm thick Local lenticular wavy bedding Occasional cross-lamination	Lenses of very dark poorly decomposed organic remains (grass roots, moss) Pollen dominated by herbs, particularly Caryophyllaceae; almost no tree pollen Spores dominated by *Selaginella sibirica* Cryoxeric insect remains Tundra bog macroflora Mammal bones dominated by large herbivores	Primary syngenetic ice wedges (1.3–2 m wide, 8–12 m apart); Secondary ice wedges (0.3–0.5 m wide, 4–6 m apart, 30–40 m high); Tertiary ice wedges (0.1–0.3 m wide, 2–2.3 m apart), uncommon, mostly incomplete polygonal network	Banding indicates varying degree of soil processes Exceptionally severe geocryological and climatic (ultracontinental) conditions indicated by ice wedges[d] Rapid sedimentation during several tens of millennia allowed syngenetic ice wedges 30-40 m high to develop Rapid freezing and incorporation of moisture Treeless tundra-steppe with abundant Gramineae and *Artemisia* sp. on interfluves (pollen and insects) versus swampy areas in river valley (macroflora)
Lower subunit (5–10 m)	Interbedded sands and silts: Sand fine to medium grained or silty, yellow to grey (0.2–3 m thick); lamination indistinct to clear; horizontal, wavy or cross-laminated; Fine gravel; Dispersed pebbles (≤1.5 cm diameter) in medium sand, including clayey intraclasts; Silts horizontally laminated	Finely divided plant detritus in sand (including very small branches); *in-situ* grass roots abundant in silts Lenses of dark brown peaty silts (0.3–0.5 m thick) Infilled ground squirrel burrows lined with grass stems in silt layers Two pollen units with tree and shrub species separated by unit dominated by non-woody plants (Gramineae, sedges, *Artemisia* sp.) Mammal bones dominated by large herbivores	Very ice-rich sands (75–85% gravimetric ice content); massive, reticulate layered, lenticular Cs 'Bands' with ataxitic, lentic. or layered Cs (80–100% gravimetric ice content) Primary syngenetic ice wedges (2–4 m wide, 9–10 m apart) with tops truncated by thaw; Secondary ice wedges (0.15–0.4 m wide, 3 m apart)	Alluvial deposits of channel and floodplain types High floodplain with inundated polygons Density and width of ice wedges are greater than those in present floodplain of the Kolyma River Two phases of expansion of open larch-birch forests separated by tundra-steppe vegetation

(Continues)

Table 2 (Continued)

Stratigraphic unit[a]	Sediment	Organic material	Ground ice[b]	Interpretation
H2: Heterogeneous sediments (≤6 m) *Upper subunit*	Peat (≤1.6 m thick)	Interbedded peat and silt, overlying sedge peat (0.4–0.5 m), overlying moss peat (0.3–0.4 m), overlying wood peat (0.4–0.5 m) with branches and roots of shrubs, birch and larch wood Tree and shrub pollen more abundant than in H1; tundra and steppe insect remains		Change from boggy to alluvial conditions Peat bog with vegetation similar to present-day vegetation of Duvanny Yar area Sparse larch forest with dwarf Siberian pine, alder thickets, dwarf birches and willows (cf. present-day vegetation at Duvanny Yar)
Lower subunit	Bluish-grey clayey silts (cf. H1)			Lacustrine deposits
H1: Bluish-grey silts (≥9 m)	Massive silts, locally with indistinct horizontal bedding; texturally homogeneous silt	Scattered fragments of mosses and grass roots; herbaceous plant pollen dominant (mostly Gramineae and *Artemisia* sp.); spores dominated by *S. sibirica*; freshwater mollusc remains (e.g. *Valvata confusa*); horse bones Tundra and steppe insect remains	Ice wedge pseudomorphs 6–9 m apart Reticulate to lenticular/ layered to massive Cs with depth in upper 1 m	Taberal sediments (i.e. thawed and consolidated; former ice wedges and segregated ice have melted) Epigenetic freezing Lacustrine sediments Treeless tundra-steppe vegetation Cold and dry climate

[a]See Figure 3A; thickness in metres.
[b]Cryostructures are interpreted from descriptions given.
[c]Estimated exposed thickness above river level.
[d]Primary ice-wedge network attributed to yearly cracking; secondary network cracked less frequently and tertiary wedges cracked only in particularly severe winters. Primary wedges are similar to those in the high floodplain of the Kolyma Lowland; secondary wedges are similar to those in yedoma in the tundra zone, where snow is blown off and mean annual ground temperature is ≤ −9°C; tertiary wedges have no known modern analogue. Cs = Cryostructure.

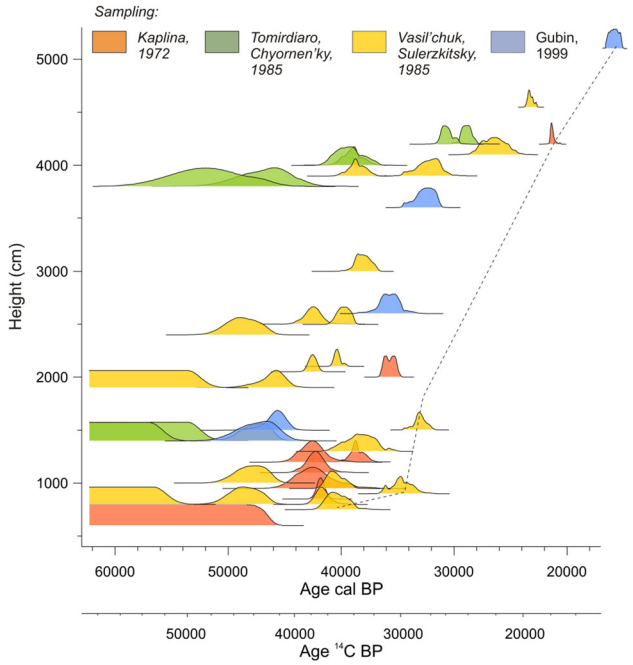

Figure 4 Calibrated ^{14}C ages obtained by different authors for different types of organic material collected from the yedoma at Duvanny Yar (Table S1). Because of the large scatter, ^{14}C ages of organic microinclusions and alkali extracts (Table S3) are not shown. The very youngest ages obtained for given horizons, on which the chronology proposed by Y. K. Vasil'chuk (2006) was based (Table S2), are connected with a dashed line. Age-height relationships are not directly comparable between different ^{14}C age series because sampling was carried out in different exposures of yedoma. This figure is available in colour online at wileyonlinelibrary.com/journal/ppp

along horizontal traverses at depths of about 5 m and 10 m across Figure 3C.

Two additional sections (1 and 22) were also examined for stratigraphic purposes, and their locations are indicated in Figure 3A. Section 1 exposed peat and silt stratigraphically beneath the yedoma, and was located about 2.5 km west of section CY and about 4.5–11.5 m arl. The section was traced discontinuously along a lateral distance of about 200 m of river bluff and logged in two locations, designated section 1A (Figure 6A) and section 1B (Figure 6B). Section 22 exposed an involuted organic layer about 19.8 m arl in the headwall of a small thaw slump about 150 m east of section CY (Figure 7).

Systematic sampling of frozen sediment was carried out at sections CY and 1 using a portable hand-held drill to obtain three adjacent horizontal cores about 6.5 cm diameter and ≤ about 8 cm long of frozen yedoma silt. The vertical sampling spacing in each section was typically 0.5 m (Figure 5). Gaps in the vertical sequence of samples occur between 9 and 11 m arl and between 15 and 16.8 m arl due to the discontinuous exposure of the yedoma.

Micromorphological Analysis

Micromorphological analysis of thin sections from the yedoma silt was carried out in order to identify any small-scale primary sedimentary structures, deformation structures, traces of microcryostructures, organic material and pedogenic features. Four undisturbed and vertically oriented samples of recently thawed yedoma silt were collected in 9–10 cm diameter tins. Two samples were collected from the upper part of the yedoma (29.3 m arl) and two from the lower part (6.5 m arl) (Figure 5).

Impregnated thin sections of the samples were prepared in the Thin Section Laboratory of the British Geological Survey. The samples were oven-dried at 40°C and impregnated with resin. After the resin had set, the outer 1 cm of each sample was sawn off and discarded to ensure that there were no edge effects. Because of the tightly packed nature of the silt, it was necessary to re-impregnate the cut surface several times before a consolidated and representative surface could be established. The next stage was to lap a flat surface on the chips with a suspension of 15 µm aluminium oxide powder in water. It was this lapped surface which was bonded to the glass slide with epoxy resin. When set, the bulk of the chip was cut off using a diamond-tipped saw, and further material was removed in a grinding process down to a thickness of 100 µm. Automated lapping machines reduced this to about 40 µm, and then the thin sections were hand finished. Subsequent polishing was achieved using diamond compound of various grades from 1 to 15 µm.

Thin sections were scanned at 2400 dots per inch on an Epson Perfection 4990 photo scanner (Long Beach, CA, USA) in the Micromorphology Centre, Queen Mary University of London. Photomicrographs of thin sections, under plane light, were taken with a Leica M420 microscope (Heerbrugg, Switzerland). All images are in correct vertical orientation.

Sediment Analysis

One batch of sediment cores collected from sections CY and 1 was shipped frozen to the University of Sussex for analysis. Physical and chemical analyses of 82 sediment samples were carried out to characterise the sediment properties, compare them with data from a sedimentary sequence at Itkillik and elsewhere, and elucidate the depositional processes. The sediment cores were thawed in the laboratory, prior to determining their water content as a percentage of dry soil weight (gravimetric water content). Estimates of sediment volumetric ice content were calculated from the measured gravimetric ice contents. Munsell colours of moist sediment were determined before the sediments were oven-dried at 40°C. Samples were gently disaggregated with mortar and pestle, and subsampled for sediment analysis.

Organic content and calcium carbonate content were estimated by loss on ignition. This method was used to identify semiquantitative changes in these parameters rather than precise values appropriate for carbon budgets. Organic content was determined by burning 1 g of sediment in a furnace for 4 h at 550°C, and $CaCO_3$ content was determined by

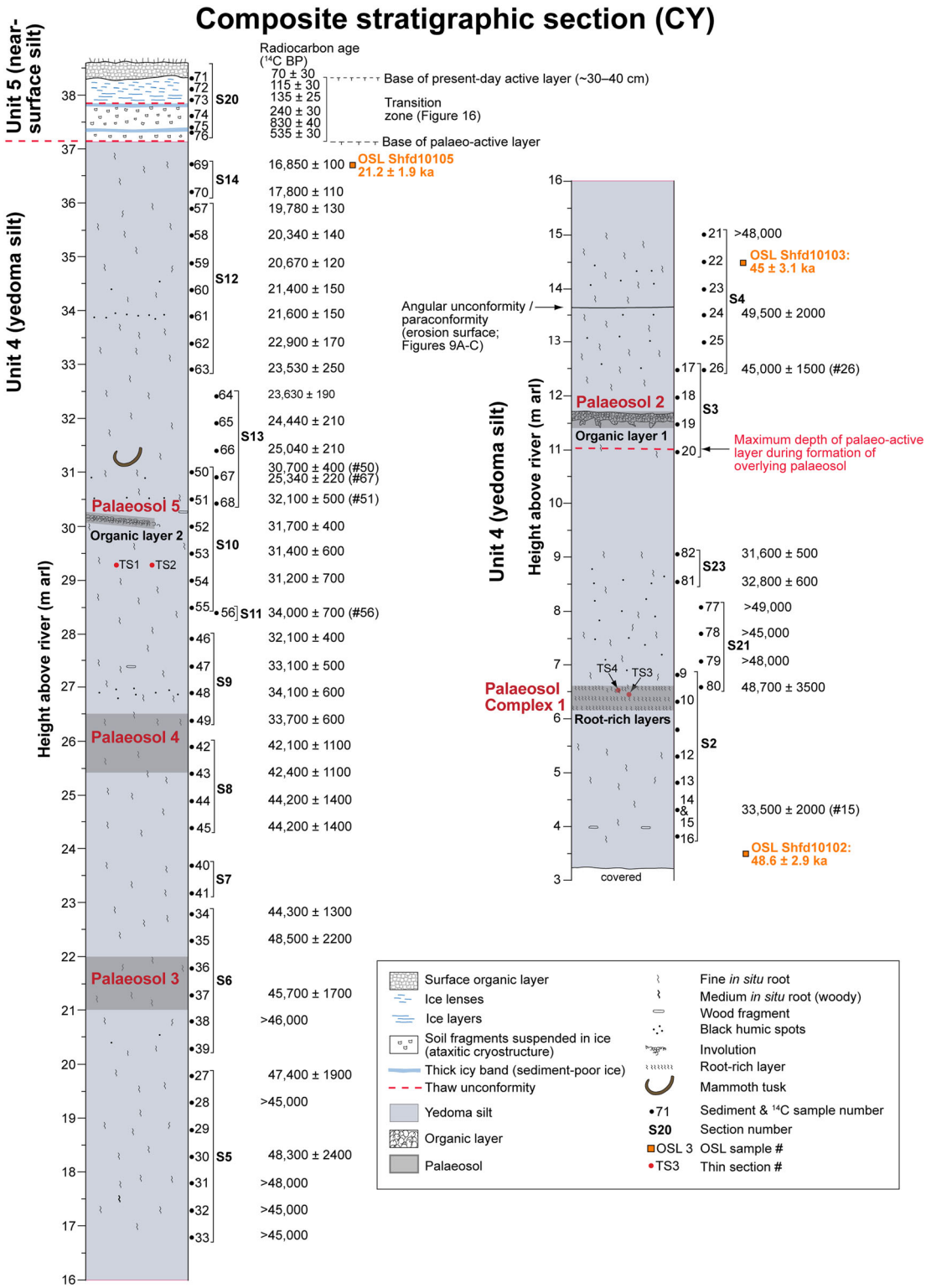

Figure 5 Composite stratigraphic section (section CY) examined in 2009 at Duvanny Yar, showing relative vertical position of the 16 individual sections through units 4 (yedoma silt) and 5 (near-surface silt). Sample locations indicated. S2 to S23 indicate individual section numbers within the composite section CY. arl = Above river level. This figure is available in colour online at wileyonlinelibrary.com/journal/ppp

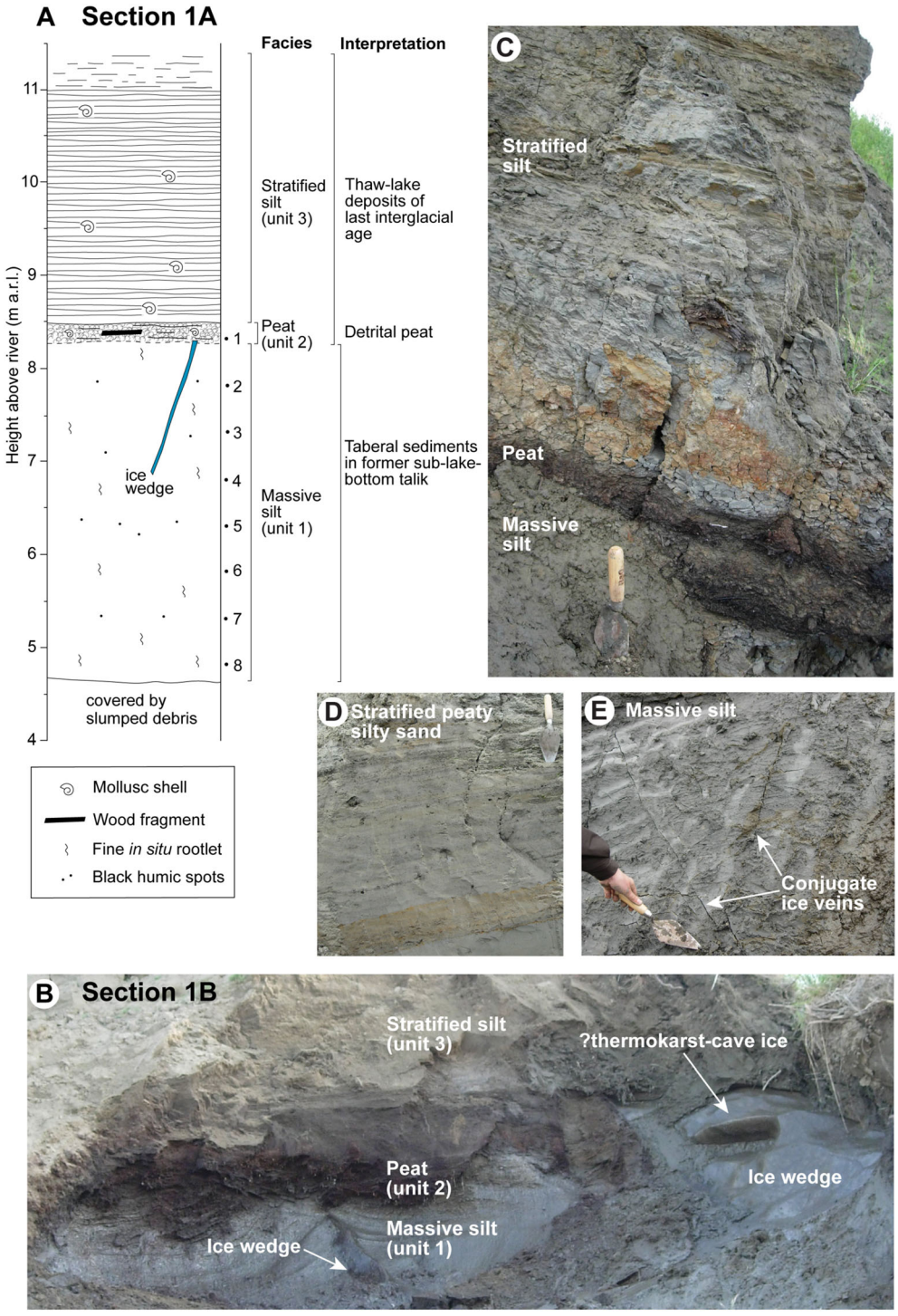

Figure 6 Silt and peat of units 1 to 3 (stratigraphically beneath yedoma silt of unit 4), section 1. (A) Sedimentary log of section 1A, showing facies and their interpretation. (B) Peat between silt units at subsection 1B, about 150 m east of section 1A. Two ice wedges are visible in the massive silt beneath the peat. Ice tentatively interpreted as thermokarst-cave ice is seen above the top of the large wedge, and two higher lens-like bodies (not shown) were subsequently exposed above this ice. The section is about 3 m high. (C) Stratified silt (thaw lake deposits) above peat and massive silt, section 1A. Trowel for scale. (D) Stratified peaty silty sand, section 1A. Trowel for scale. (E) Massive silt (taberal sediments) with conjugate ice veins melting out, section 1A. Trowel for scale. arl = Above river level. This figure is available in colour online at wileyonlinelibrary.com/journal/ppp

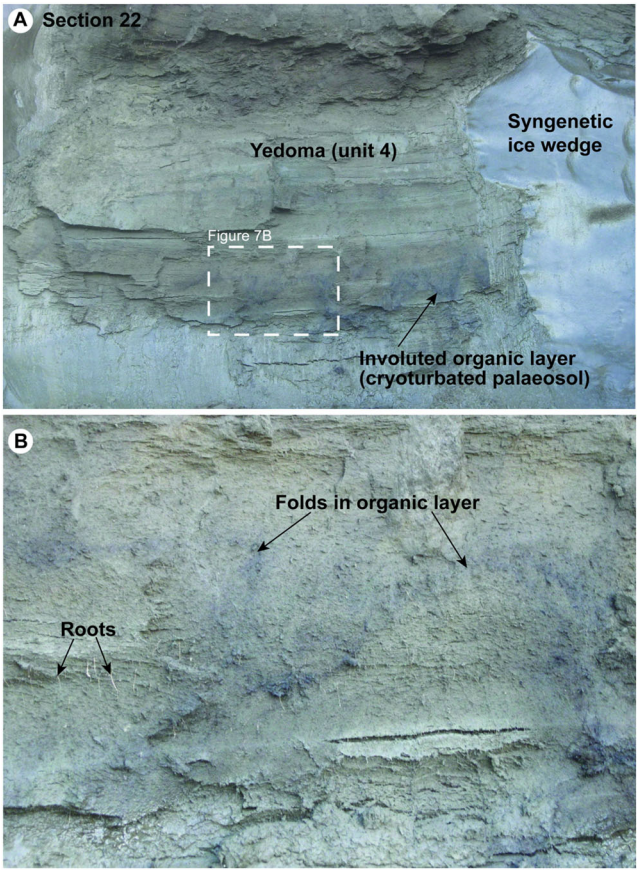

Figure 7 (A) Involuted organic layer (cryoturbated palaeosol) 19.8 m arl in yedoma of unit 4 exposed in the headwall of a small thaw slump, section 22. The section is about 2.5 m high. (B) Close-up of indistinct dark streaks and folds in the organic layer, with a relief of about 20–30 cm. Abundant roots are visible in both the organic layer and the yedoma above and below it. Horizontal fissures mark sites of thawing ice lenses. The section is about 0.5 m high. arl = Above river level. This figure is available in colour online at wileyonlinelibrary.com/journal/ppp

burning the same sample for an additional 4 h at 950°C (modified from Gale and Hoare, 1991, pp. 262–264).

Prior to particle-size analysis and magnetic susceptibility measurement, the samples were pre-treated to remove organic matter and carbonates. As some organic material (e.g. roots) in yedoma is quite resistant to oxidation (G. Schwamborn, personal communication, 2009), larger pieces of organic detritus were first removed with a dry brush, before adding 20 ml of 1M HCl to 20 g of sediment to dissolve the carbonates. Ten millilitres of 35 per cent H_2O_2 were added to oxidise the organic matter, and the supernatant liquid was pipetted off after fine sediment had settled from suspension and the liquid was clear. This procedure was repeated until all organic matter was oxidised. The inorganic clastic residue was then oven-dried at 40°C and gently disaggregated with mortar and pestle.

Particle size was determined by laser diffraction, pipette analysis and dry sieving. A HORIBA Partica LA-950 Laser Scattering Particle Size Distribution Analyzer (Irvine, CA, USA) was used to carry out the majority of the analyses because laser sizers are excellent for accurate sizing of equant particles, coarse silt and sand (i.e. particles exceeding about 30 μm) and for rapid analysis of large numbers of samples (cf. Strauss *et al*., 2012a). Because laser diffraction methods may record some platy particles of coarse clay and fine silt (due to their large projected area) as equant particles of medium to coarse silt and therefore contaminate the size distribution up to about 30 μm (Konert and Vandenberghe, 1997; McCave and Hall, 2006; McCave *et al*., 2006), laser diffraction methods often underestimate the clay fraction (Hao *et al*., 2008). To minimise this underestimation, the HORIBA LA-950 uses Mie correction theory to take account of the flatter particles smaller than 20–25 μm. In order to check the validity of the laser diffraction measurements of the < 30 μm fraction in our samples, we also carried out pipette analysis and sieving of sediment samples from the same stratigraphic unit of yedoma at Duvanny Yar. Each dried sample was placed on a watch glass and 2 per cent $(NaPO_3)_6$ added to form a paste. The paste was added incrementally into the particle-size analyser until it was within the analytical obscuration limits. Samples were run out of sequence to minimise the effects of machine drift. Each subsample was run usually three to four times and the percentages of clay (<5.5 μm; see Konert and Vandenberghe, 1997), silt (5.5–63 μm) and sand (>63 μm) and the ratio of medium-grained and coarse-grained silt (16–44 μm) to fine-grained and very fine-grained silt (5.5–16 μm), which is termed the U-ratio (Vandenberghe *et al*., 1985), were calculated. These values were averaged to obtain the mean values of clay, silt, sand and the U-ratio, after discounting any values that were anomalously high or low. Mean values of particle size, skewness and kurtosis were not calculated because the bi- to polymodal particle-size distributions of most sediment samples indicated that such values were not informative (see Vandenberghe, 2013). Pipette analysis and dry sieving were conducted using standard methods (Klute, 1986; Vadyunina and Korchagina, 1986). Samples were sieved air-dry, and then coarse fragments of plant detritus were physically removed. Fine earth material (<1 mm) was subjected to the pipette analysis with no preliminary physical or chemical treatment.

Magnetic susceptibility of the sediment was measured with a Bartington MS2B Dual Frequency Sensor (Witney, UK). The results are reported as low-frequency volume-specific magnetic susceptibility (κ) in x 10^{-5} SI units (Gale and Hoare, 1991, pp. 201–229). To check the reproducibility of the κ values, the same samples were analysed in two laboratories (universities of Sussex and Southampton) with two different Bartington MS2B Dual Frequency Sensors.

The same methods (excluding pipette analysis and dry sieving) were applied by the same operator to 54 samples of yedoma silt from the Itkillik River (Alaska), and the results were compared with those from Duvanny Yar. The pH of sediment samples from the yedoma at Duvanny Yar was determined by the slurry potentiometric method using a combined electrode with a ratio of 'soil: solution' of 1:2.5 (Arinushkina, 1970; Vorobyov, 1998).

Geochemical Analysis

Major element and trace element concentrations from 82 sediment samples were analysed by x-ray fluorescence (XRF) in order to (1) identify buried soils, (2) determine the degree of chemical weathering of the yedoma silt, (3) establish if the sediment source(s) changed over time and (4) compare the results with data from loess from central Yakutia. Identification of buried soils – to validate field observations and establish if additional unidentified soils are present – was determined from the total phosphorus content (expressed as P_2O_5). The rationale for using P_2O_5 is that 'high-low-high' depth functions, which record surface enrichment and subsurface depletion of phosphorus by pedogenic processes, indicate buried soils within loess profiles (Muhs *et al*., 2003). Weathering effects were evaluated from the ratios of mobile elements (Na, Si, Ca, Mg, K) to immobile elements (Ti, Zr), which provide proxies for the degree of chemical weathering of detrital silt minerals such as those found in loess (Muhs *et al*., 2008). Sediment source changes were determined from Ti/Zr ratios, as both elements are chemically immobile in most near-surface environments and so are unlikely to be lost through diagenesis, weathering and soil formation (Muhs *et al*., 2003). Potential source regions of the silt are considered broadly, although determination of specific sediment sources is beyond the scope of this study.

The samples were ground to a fine powder in an agate planetary mill, and the finely ground raw powder was compressed into pellets using a 25-tonnes Herzog HT40 hydraulic press. Three samples (GAU2163-1, GAU2163-4 and GAU2163-9) were taken to validate the major element data obtained on pellets. These samples were mixed with lithium tetraborate flux in a platinum-gold dish and fused at 1100°C for 15 min before casting as a glass disk in a Pt-Au dish. The sample:flux ratio was 10:1. The samples were measured at the National Oceanography Centre, Southampton, using a Philips Magix-Pro wavelength dispersive XRF spectrometer 4kW Rh end-window x-ray tube. XRF precision for trace elements is typically in the range 2–5 per cent for elements that are greater than three times the detection limit.

Dating

Radiocarbon.

A second batch of sediment cores was thawed at Cherskii, and organic matter (mainly *in-situ* roots) collected by wet sieving in preparation for radiocarbon dating. Fifty-three samples of organic material from 11 sections along the composite section CY were dated to establish an age model for section CY. The ^{14}C samples were treated with 1M HCl (80°C, > 1 h), 0.1M NaOH (room temperature) and 0.25M HCl (80°C, 1 h), then combusted at 900°C with CuO and Ag, and the obtained CO_2 was reduced to solid carbon, using H_2 and hot Fe (600°C) as a catalyst. ^{14}C was then analysed with the 'Compact Carbon AMS' spectrometer at the Adam Mickiewicz University in Poznan (Goslar *et al*., 2004). Almost all samples were large enough to allow for standard precision of AMS ^{14}C measurement (i.e. for AMS > 1 mg of carbon was available). Only in four samples were < 1 mgC measured, and only in one sample (#15), was the small mass of the sample appreciably affected the precision of ^{14}C dating. The ^{14}C ages obtained were used to construct an age-depth model. ^{14}C ages of individual samples were first calibrated using Intcal09 (Reimer *et al*., 2009), and the modelling was performed with the free-shape algorithm (Goslar *et al*., 2009), designed to build age-depth lines as smoothly as possible, while keeping calendar dates of ^{14}C-dated levels in reasonable agreement with the calibrated ^{14}C ages.

Optically Stimulated Luminescence (OSL).

Three samples of yedoma silt were collected for OSL dating in order to compare the OSL and ^{14}C chronologies, and, potentially, to extend the chronology back beyond the limits of radiocarbon. OSL samples were collected in opaque tubes from freshly exposed sediment and transported to the University of Sheffield Luminescence Laboratory in light-proof plastic bags.

Elemental concentrations of uranium, thorium, potassium and rubidium (analysed with inductively coupled plasma mass spectroscopy and inductively coupled optical emission spectroscopy) were, when combined with a calculated cosmogenic contribution based on the algorithm of Prescott and Hutton (1994), used to establish sample dose rates. Dose rates were suitably attenuated for sample grain size and palaeomoisture content, which, given the site's history of aggrading permafrost, was taken to be the same as present-day values (Table 3). To establish the dose stored within each sample since burial (i.e. the palaeodose), each sample was prepared following the procedure outlined in Bateman and Catt (1996) to extract cleaned quartz grains 90–180 μm in diameter, although where the amount of material permitted, this was further reduced to 90–125 μm in diameter.

OSL measurements were made at the small-aliquot (5 mm diameter) and single-grain level. Between 800 and 1400 single grains and 24 small aliquots per sample were measured. All OSL palaeodose (De) measurements, irrespective of level, were made on an automated TL-DA-15 Risø Reader (Roskilde, Denmark) (see Bateman and Murton, 2006; Bateman *et al*., 2010, for details). De values were derived using a single-aliquot regeneration (SAR) protocol (Murray and Wintle, 2003) with a pre-heat determined experimentally of 180°C for 10 s. For the single-aliquot measurements, De values were only accepted where the recycling ratio was 1 ± 0.1 of unity, recuperation was < 5 per cent, the naturally acquired OSL was significantly above background and the SAR regeneration points could be adequately fitted by a growth curve. As the OSL signal-to-noise ratio for single grains is much lower, the same criteria were applied, except the recycling ratio was relaxed to 1 ± 0.2 of unity (Bateman *et al*., 2010).

Once De outliers were excluded (those falling outside two standard deviations of the mean), at the single-aliquot level both samples Shfd10102 and Shfd10105 had a

Table 3 OSL-related data for samples from section CY, Duvanny Yar.

Sample code	Depth from surface (m)	Water content (%)	K (%)	U (ppm)	Th (ppm)	Cosmic dose rate (μGy a^{-1})	Total dose rate (Gy ka^{-1})	D_e (Gy)	n	OD (%)[a]	Age (ka)
Small-aliquot OSL ages											
Shfd10105	1.9	59	1.9	2.41	8.3	0.163 ± 0.008	1.299 ± 0.063	27.59 ± 2.12	13	53 (21)	21.2 ± 1.9
Shfd10103	24.1	45	1.8	2.49	8.6	0.022 ± 0.001	1.595 ± 0.085	71.79 ± 3.25	19	22 (22)	45.0 ± 3.1
Shfd10102	35.1	47	1.9	2.12	7.1	0.012 ± 0.001	1.424 ± 0.079	69.2 ± 1.3	20	11 (7)	48.6 ± 2.9
Single-grain OSL ages											
Shfd10105	1.9	59	1.9	2.41	8.3	0.163 ± 0.008	1.299 ± 0.063	41.92 ± 4.35	6	43	32.3 ± 3.7
Shfd10103	24.1	45	1.8	2.49	8.6	0.022 ± 0.001	1.595 ± 0.085	89.09 ± 9.37	7	24	55.8 ± 6.6
Shfd10102	35.1	47	1.9	2.12	7.1	0.012 ± 0.001	1.424 ± 0.079	81.58 ± 2.9	33	80	57.3 ± 3.9

[a]OD in parenthesis reflects over dispersion once outliers were excluded. K = potassium; U = uranium; Th = thorium; De = palaeodose; OD = over dispersion.

relatively low over-dispersion and the replicates were normally distributed around the mean (Table 3); thus, the final De values used for age calculations were based on the central age model calculations of Galbraith and Green (1990). For sample Shfd10103, whose De distribution appeared slightly bi-modal, the De used for final age calculation is based on the dominant De component as extracted by the finite mixture model of Roberts *et al*. (2000). With the single-grain measurements, sample sensitivity to dose was low, and so relatively few grains met the quality assurance criteria described previously and resultant De distributions were non-normal (Table 3). As a result, for samples Shfd10102 and Shfd10105 the De values used for final age calculation are based on the dominant De component as extracted by the finite mixture model of Roberts *et al*. (2000). For sample Shfd 10103, whose De distribution was more unimodal, the final De value used for age calculation was based on the central age model calculations.

Pollen Analysis

Pollen was extracted from 10 g of sediment from the horizontal cores used for sediment analyses. We used standard methods for organic-poor sediments as described by the PALE Steering Committee (1994). Pollen was counted at the North East Interdisciplinary Science Research Institute. Loess-derived material yields pollen inconsistently (Edwards, 1997); some samples were functionally barren, whereas others yielded pollen sums (terrestrial pollen only) of 50 to > 400 grains. Added exotic markers were used to estimate the pollen/exotic ratio, to indicate concentration per unit volume of silt. We counted representative samples from sections 1 and CY. Pollen diagrams were created using TILIA software (Grimm, 2004). Samples are plotted by their depth below the top of the section. They are not numerically zoned; rather, the chronological/stratigraphic units described for the sections are used to identify stages in the pollen record. Pollen spectra were subject to ordination (using PC-ORD; McCune and Mefford, 2011) in order to clarify compositional differences among groups of samples classified by age/stratigraphic position (Appendix S4).

RESULTS

Stratigraphy and Sedimentology

The litho- and cryostratigraphy examined in 2009 were divided into five units, in ascending stratigraphic order: (1) massive silt, (2) peat, (3) stratified silt, (4) yedoma silt and (5) near-surface silt (Figs. 5 and 6). Their stratigraphic, sedimentary, organic matter and ground-ice characteristics, and their inferred correlations with the stratigraphy reported in Sher *et al*. (1979) are detailed in Table 4 and summarised below.

Unit 1: Massive Silt.

Unit 1 consists of massive silt at least 3.5 m thick exposed near the base of the river bluff in section 1, where its upper contact is at 8.3 m arl (Figure 6). The colour varies between 2.5Y 3/1 (very dark grey) and 2.5Y 4/2 (dark greyish brown). The silt appears massive and contains abundant, fine *in-situ* roots. Ice wedges within unit 1 include small (10 cm wide, 1.5 m high; Figure 6A) and large (≥1 m wide, ≥ 1.5 m high) types (Figure 6B). An irregular/trapezoidal reticulate cryostructure, conjugate ice veins (Figure 6E) and decimetre-thick lens-like ice bodies (Figure 6B) are also present. The gravimetric water content has a mean value (n = 7) of 36.0 per cent, ranging from 29.9 per cent to 50.9 per cent (Figure 8A).

Texturally, unit 1 contains on average (n = 7) 65 ± 3 per cent silt, 18 ± 3 per cent sand and 18 ± 4 per cent clay. The ratio of medium-grained and coarse-grained silt (16–44 μm) to fine-grained and very fine-grained silt (5.5–16 μm) – the U-ratio – has a mean value of 2.9 ± 0.8 (Figure 8A). Particle-size distributions in unit 1 are polymodal (Figure 8B). The primary mode averages 36.4 μm (range: 32.0–48.0 μm; coarse silt). A secondary mode occurs between 0.3 and 0.6 μm (very fine clay to fine clay, i.e. 'ultra fine' fraction), and a tertiary mode commonly occurs between 3 and 4 μm (coarse clay to very fine silt). Overall, the summary values and particle-size distributions are relatively uniform with height through unit 1 (Figure 8). Magnetic susceptibility (κ) values average 54.7 x 10^{-5} SI units (range: 36.5–72.2 x 10^{-5} SI units; Figure 8A). They are uniform with height

Table 4 Stratigraphic units, lithological, organic material and ground-ice characteristics of sections examined during the 2009 study at Duvanny Yar, and their interpretation.

Stratigraphic unit[a]	Lithology	Organic material	Ground ice	Interpretation
5. Near-surface silt (1.9–2.0 m) [H4]		Organic layer: fibrous, woody and non-woody roots abundant, mossy at top; brown in upper part, blacker with depth; hummocky surface	Organic-matrix Cs below frost table	Present-day active layer (0.3–0.4 m thick)
	Silt; 2.5Y 3/2 (very dark greyish brown); texturally similar to unit 4	*In-situ* roots abundant	0.30–0.75 m depth: lenticular and lentic./bedded Cs, ice-rich silt, above thaw unc.	Transient layer (0.45 m)[b]
	Silt; 2.5Y 3/1 (very dark grey) to 2.5Y 3/2 (very dark greyish brown); texturally similar to unit 4	*In-situ* roots abundant	0.75–1.9 m depth: ataxitic Cs, sediment-rich ice and sediment-poor ice (about 3–40% sediment by vol.), latter forms two distinctive icy bands; basal thaw unc., horizontal to gently undulating	Intermed. layer (1.15 m)[b] Basal thaw unc. = base of end Pleistocene or early Holocene palaeo-active layer
4. Yedoma silt (>34 m)	Silt; bands commonly 1–20 cm thick marked by slight colour variations between 2.5Y 3/1 (very dark grey) and 2.5Y 3/2 (very dark greyish brown); distinct to indistinct, horiz. to gently undulating, parallel, internally massive	Fine *in-situ* rootlets pervasive, typically <1 mm diameter, few to several cm long, some form horiz. root-rich layers (6.2–6.6 m arl) Woody roots (2 mm diam., few cm long)	Syngenetic ice wedges, grey, max. height ≥24 m, max. width few metres, shoulders, raised tops, irregular width; narrow raised tops, grey, >1 m high, few cm to few tens of cm wide, variable width, often with shoulders Epigenetic ice wedges, grey, few metres high, ≤ about 1 m wide, downward taper	Loess containing five palaeosols
[Upper subunit of H3]	Massive homogeneous silt; occasionally faintly stratified with horiz., parallel strata few millimetres to 10 cm thick	Wood fragments ≤ 1 cm diameter, few cm long at 4 m, 27.4 and 30.3 m arl	Bedded and lentic. (horiz. to inclined, <1 mm to few mm thick) Cs abundant, locally irregular/foliated reticulate Cs or	Syngenetic permafrost
	Angular unconformity about 13.7 m arl truncates gently dipping bands and grades laterally into paraconformity	Organic layers: layer 1 (20 cm thick), involuted base, 20–30 cm involution relief, 11.7 m arl, cf. involuted organic layer at 19.8 m arl; layer 2 (15 cm thick), sharp planar to gently undulating base, laterally discontin., 29.7 m arl	lentic. and irreg./foliated reticul. transit. with ataxitic Cs; Cs in bands, horiz. to subhoriz., few cm to tens of cm thick Massive Cs common (i.e. Cs not visible in field) Ice veins, small, locally present	Erosional surface (angular unc.)
		Black humic spots, equant, few mm diam., dispersed Mammoth tusk *in-situ*	Thaw uncs form shoulders to ice wedges and discontinuities between Cs	Base of palaeo-active layers (thaw uncs)
3. Stratified silt (>2.5 m) [H2]	Silt, grey; well stratified, strata few millimetres to 1 cm thick, slightly wavy parallel, horiz. to subhoriz. Lower contact sharp to gradational, undulating	Wood fragments abundant, scattered mollusc shells, white, fragmented, include gastropods		Lacustrine sediments deposited in a thaw lake within an alas

(*Continues*)

Table 4 (Continued)

Stratigraphic unit[a]	Lithology	Organic material	Ground ice	Interpretation
2. Peat (0.2–0.8 m) [H2]	Two end members: (1) *Stratified peaty silty sand*, strata horiz. to subhoriz., planar to slightly wavy parallel few millimetres to 2 cm thick, containing detrital peaty lenses and laminae, wood fragments and vivianite; orange-brown mottles; overlies 10 cm thick sand bed	(2) *Massive to stratified peat*, 2.5Y 2.5/1 (black), strata several millimetres to 2 cm thick, horiz. to subhoriz., planar to slightly wavy parallel; wood fragments (≤6 cm diam., ≥20 cm long); leaves, stems and fibrous plant material abundant; *Betula papyrifera* bark well preserved; mollusc shells abundant; vivianite common; lower contact sharp to gradational with unit 1	Lentic. and irregular/foliated reticulate Cs in siltier units; organic-matrix Cs in peat Top of ice wedge (≥1 m wide, ≥1.5 m high) extends up into peat	'Trash layer' deposited on bottom of thaw lake Detrital plant material derived from vegetation beside lake
1. Massive silt (≥3.5 m) [H1]	Silt, 2.5Y 3/1 (very dark grey) and 2.5Y 4/2 (dark greyish brown), locally mottled orange brown; massive	Fine *in-situ* rootlets pervasive Black humic spots 1 to few centimetres diameter	Ice wedges, narrow (10 cm wide, 1.5 m high) to wide (≥1 m wide, ≥1.5 m high); Irreg./trapezoidal retic. Cs; conjug. ice veins three lens-like ice bodies, decimetres thick, > 0.5 m wide, near top of unit	Taberal sediments thawed in former sublake-bottom talik then refroze epigenetically Thermokarst-cave ice

[a]Thickness in metres; correlations with horizons 1 to 4 (H1-H4) of Kaplina et al. (1978) and Sher et al. (1979); see Table 2. Lower part of horizon 3 (interbedded sands and silts) not observed in present study. [b]Collectively, the transient layer and the intermediate layer form the transition zone (1.6 m thick), which represents a refrozen palaeo-active layer. Cs = Cryostructure; conjug. = conjugate; lentic. = lenticular; retic. = reticulate; transit. = transitional; thaw unc. = thaw unconformity; arl = above river level.

between 4.85 and 6.85 m arl, dropping to a minimum value at 7.35 m arl before rising to a maximum at 7.85 m arl (Figure 8A). Organic content averages 3.3 per cent (range: 1.8–4.2%), and carbonate content averages 2.2 per cent (range: 1.3–2.8%); both are relatively uniform with height.

Unit 2: Peat.

Unit 2 is a peat layer 0.2–0.8 m thick that forms a prominent stratigraphic marker horizon about 8.5 m arl, traced discontinuously along a lateral distance of > 150 m of yedoma remnant 6E (Figure 3A). Its colour is 2.5Y 2.5/1 (black). Two end-member facies are identified: (1) massive to stratified peat, containing abundant detrital plant material and mollusc shells (Figure 6B, C); and (2) stratified peaty silty sand, with well-developed parallel strata a few millimetres to 2 cm thick and containing lenses and layers of detrital peat (Figure 6D). Wood fragments are common in both facies. Cryostructures include organic matrix, lenticular and irregular/foliated reticulate, and the top of one large ice wedge was observed to extend up into the peat. A single measurement of gravimetric water content of 116.7 per cent indicates the ice-rich nature of this unit (Figure 8A).The lower contact of the peat facies varies from sharp to gradational with unit 1. The sedimentary properties of the single sample of unit 2 are similar to those of unit 1, except for the higher organic content (16.7%; Figure 8). The sample contains 64 per cent silt, 21 per cent sand and 15 per cent clay, and has a U-ratio of 3.4. The magnetic susceptibility value is 38.7 x 10^{-5} SI units and the carbonate content is 1.4 per cent.

Unit 3: Stratified Silt.

Unit 3 is stratified silt at least 2.5 m thick. The colour is dark grey, with some orange-brown mottling near the base (Figure 6B–D). Well-developed strata are horizontal to subhorizontal, and planar to slightly wavy parallel (Figure 6C). Wood fragments and mollusc shells are abundant. The lower contact is sharp to gradational, and undulating. No sedimentary properties were determined in the laboratory on unit 3, although field examination indicated that the particle size was similar to that in units 1, 2, 4 and 5.

Unit 4: Yedoma Silt.

Unit 4 (yedoma silt) is at least 34 m thick and dominates the stratigraphy exposed at Duvanny Yar (Figs. 3, 5, 7, 9 and 10). Banding characterises freshly exposed sections of yedoma. The bands are defined by subtle colour variations between 2.5Y 3/1 (very dark grey) and 2.5Y 3/2 (very dark greyish brown). The bands are commonly 1–20 cm thick (maximum about 1 m), horizontal to gently undulating, parallel and internally massive (Figs. 9A–C and 10A). Their colour is determined by the quantity and type of plant detritus (ratio of grass, sedge and moss remnants; and the above ground and below ground plant material), the trend and depth of its humification and mineralisation, and the quantity and thickness of organic coatings on mineral particles.

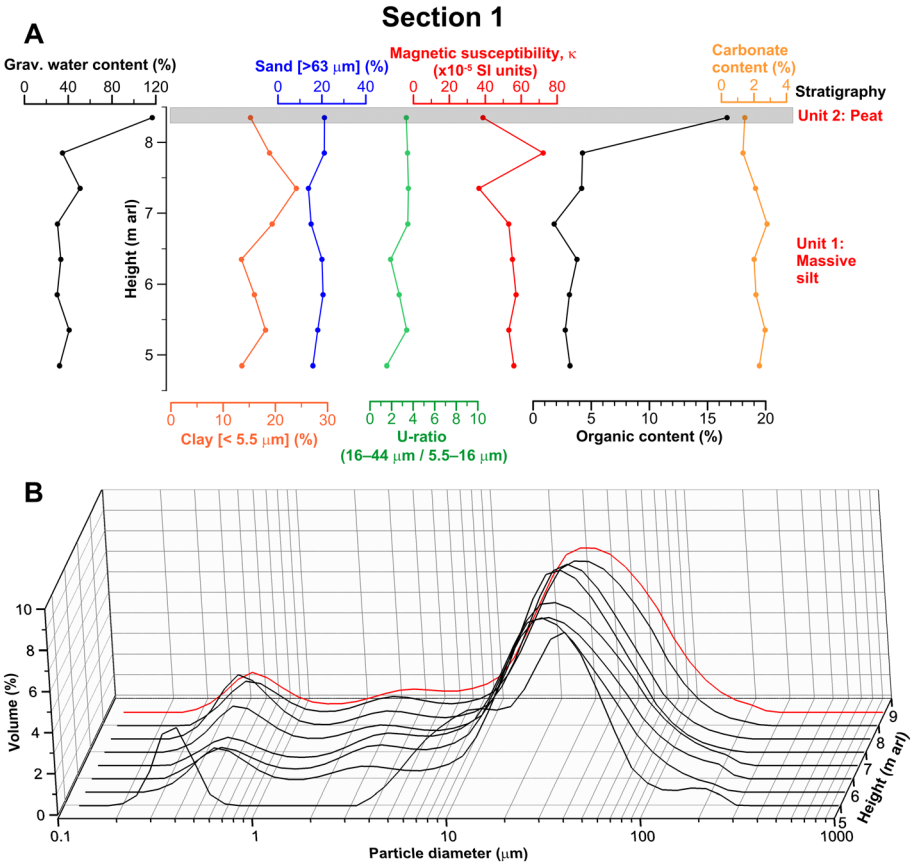

Figure 8 (A) Sedimentary properties and (B) particle-size distributions plotted against height through section 1, Duvanny Yar. In (B), the red line indicates unit 2 (peat), and black lines indicate unit 1 (massive silt). arl = Above river level. This figure is available in colour online at wileyonlinelibrary.com/journal/ppp

Lighter-coloured bands characteristically contain thin and short roots attributed to grasses (Figure 11A). Thin sections reveal that the plant detritus is mostly discoloured, and the mineral particles have rare and thin iron-humus coatings (Figure 11B, C). In contrast, darker-coloured bands characteristically contain long and flattened roots (Figure 11D) attributed to sedge-dominated communities and more moss detritus than the lighter-colour bands. Thin sections indicate that the darker-coloured bands also show strong features of humification and oxidation, and mineral particles tend to be covered with thick and dark iron-humus coatings (Figure 11E, F). Different coloured bands have nearly the same organic carbon content (±0.3%), particle size (Figure 12), mineralogical composition and degree of weathering. An angular unconformity at about 13.7 m arl in section 3 truncates gently dipping bands of yedoma silt (Figure 9A, B). The unconformity grades laterally over a few metres into a paraconformity (i.e. where bands above and below the unconformity are parallel, and no erosional surface is evident; Figure 9C).

Organic material in unit 4 is mainly semidecomposed fine plant detritus (cf. Lupachev and Gubin, 2012). Fine *in-situ* roots are pervasive (Figs. 7B, 10C and 11), and some larger woody roots and wood fragments are present. Three root-rich layers, each several centimetres thick, occur between 6.2 and 6.6 m arl. The highest and most prominent one contains organic-rich lenses and streaks, woody roots and involutions. More prominent still are two organic layers that form stratigraphic marker horizons. Organic layer 1 is about 0.2 m thick and at an elevation of about 11.7 m arl in section 3 (Figs. 5 and 9A, D, E); a similar organic layer is present in section 22 (Figure 7) at an elevation of 19.8 m arl, although it is not known if this correlates with organic layer 1. Both are involuted, with an involution relief of 20–30 cm. Organic layer 2 is 15 cm thick and at an elevation of 30.2 m arl (Figure 10A). Unlike organic layer 1, it has a sharp planar base (i.e. it lacks involutions) and is laterally discontinuous. This layer had an apparent dip of several degrees to the east, dropping in elevation from about 30.2 to 29.7 m arl along a horizontal distance of several metres. Bones of mammoth, horse and bison are abundant along the river bank, presumably eroded from unit 4. A mammoth tusk was found *in situ* within yedoma of unit 4 at 31.3 m arl (Figure 10B).

In terms of primary sedimentary structures, the great majority of the yedoma silt examined in unit 4 is unstratified and very uniform in appearance (Figure 10B, C). As a result, the colour bands described previously are generally internally massive and are not related to primary sedimentary stratification. Occasionally, however, faint stratification

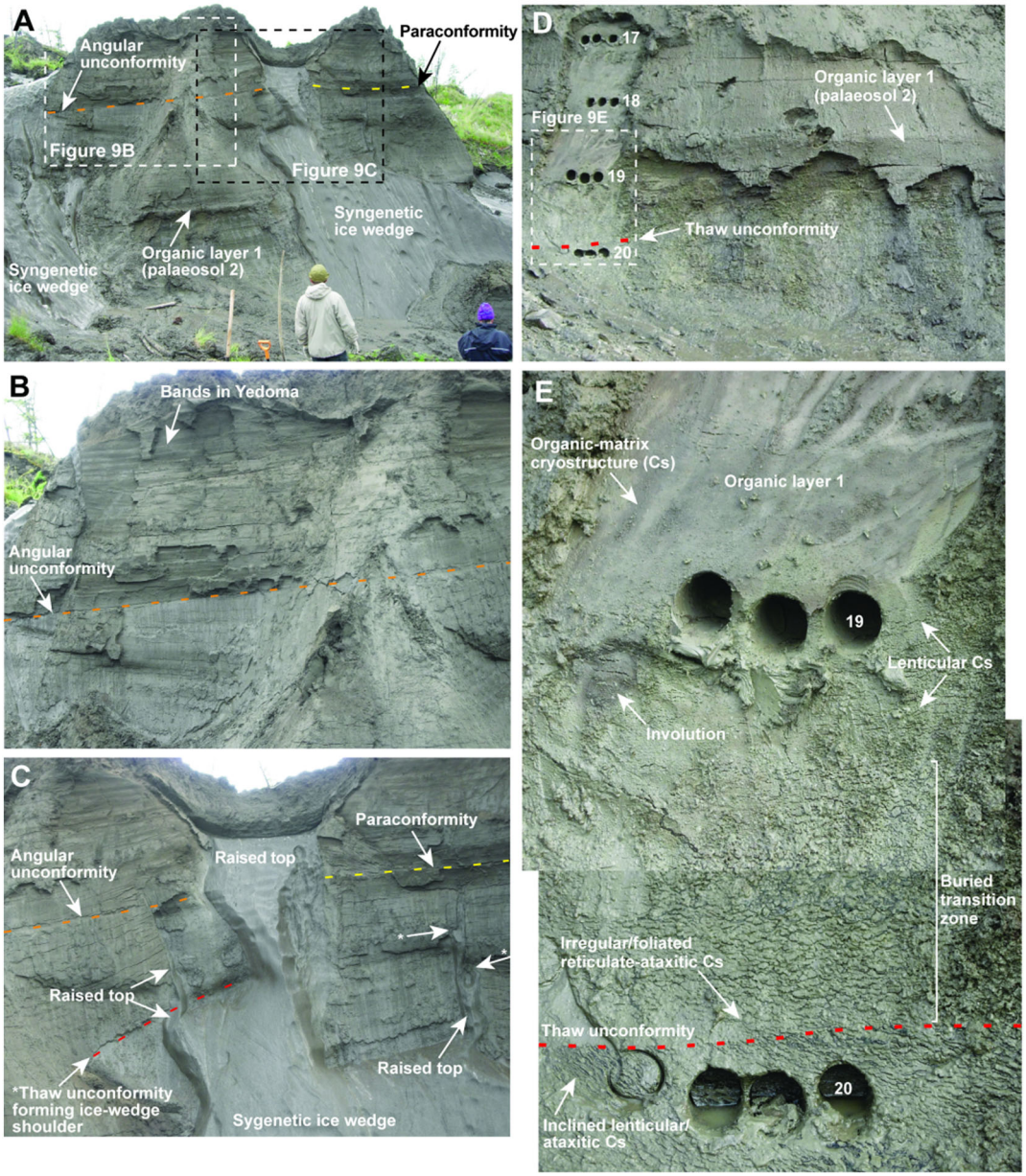

Figure 9 Sedimentary and ground-ice characteristics of yedoma of unit 4, section 3. (A) Organic layer 1 (palaeosol 2) about 11.7 m arl, syngenetic ice wedges and angular unconformity. Persons for scale. (B) Angular unconformity truncating bands and thin ice layers in underlying yedoma. Lighter- and darker-coloured bands in yedoma are horizontal to gently dipping and vary from distinct to indistinct. (C) Raised top of large syngenetic ice wedge, with two adjacent small syngenetic ice wedges extending above the same wedge but to lower stratigraphic horizons than the highest raised top (upper centre). The small syngenetic ice wedge on the left crosses a thaw unconformity that forms a prominent shoulder to the large syngenetic wedge, and is therefore younger than the unconformity. Two small shoulders are marked by * on the small syngenetic wedge on the right (see Figure 13C). (D) Organic layer 1 and location of drill holes (6.5 cm diameter) for sediment samples 17–20. The section is located several metres to the left of the left margin of (A) and shows the same organic layer 1. (E) Close-up of organic layer 1 showing involutions, cryostructures and a thaw unconformity that delineate a buried and refrozen palaeo-active layer associated with palaeosol development. The cryostructure in this thawing section of the organic layer is largely organic matrix and not visible here, whereas the cryostructure of the underlying yedoma grades downwards from lenticular to transitional between irregular/foliated reticulate and ataxitic. The latter is underlain by a thaw unconformity that truncates a cryostructure transitional between inclined lenticular and ataxitic. The unconformity is thought to have developed at the base of the active layer associated with the formation of the overlying palaeosol 2, prior to refreezing of the active layer and development of the ice-rich, buried transition zone. The horizontal line one-third of the way up the image is an artefact of joining two photographs together. Cs = Cryostructure; arl = above river level. Orange dashed line marks an angular unconformity; yellow dashed line marks a paraconformity; red dashed line marks a thaw unconformity. This figure is available in colour online at wileyonlinelibrary.com/journal/ppp

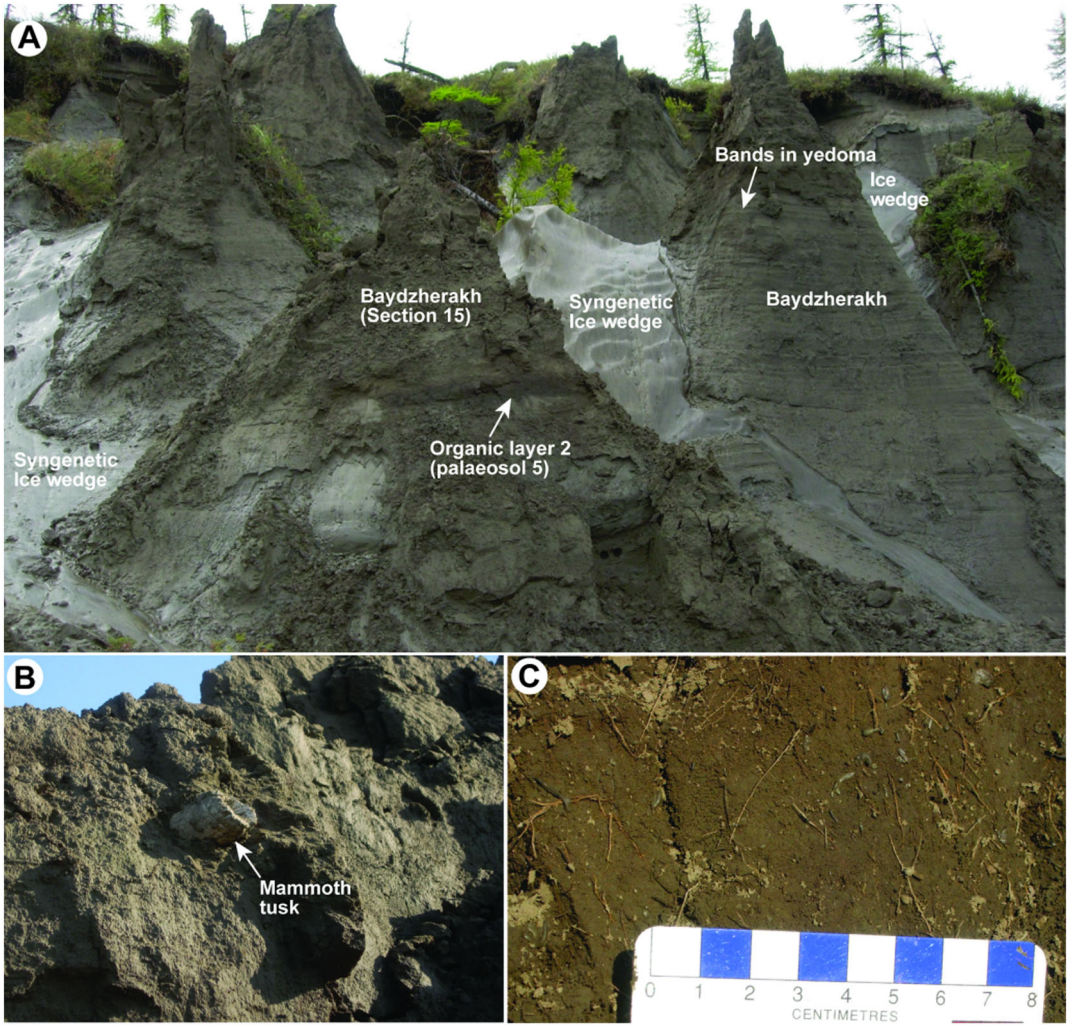

Figure 10 Yedoma (unit 4) characteristics continued. (A) Organic layer 2 (15 cm thick) with sharp planar base. The organic layer disappears in the left part of the baydzherakh. Bands in yedoma silt are visible on the baydzherakh to the right of section 15. (B) Mammoth tusk protruding from thawing yedoma silt. Note massive appearance of the host yedoma silt, lacking any visible field evidence of sedimentary stratification. (C) Fine *in-situ* roots in thawed, massive yedoma silt, section 8. This figure is available in colour online at wileyonlinelibrary.com/journal/ppp

is locally apparent in some silt, and is indicated by horizontal, parallel strata a few millimetres to about 10 cm thick.

Two types of ice wedges are distinguished in unit 4 (Figure 13). *Syngenetic wedges* have maximum heights of at least 34 m and maximum true widths (orthogonal to axial planes) of a few metres (Figs. 3 and 13A). The width of individual wedges commonly varies with depth, but not systematically. Widths may vary abruptly, where marked by prominent shoulders beneath a thaw unconformity (Figs. 9C and 13B), or gradually. The wedges form a large polygonal network superimposed on the yedoma silt, deforming the adjacent sediment. Some syngenetic wedges have narrow raised tops $>$ 1 m high and true maximum widths of a few centimetres to about 20 cm or more, with small shoulders (Figs. 9C and 13C). *Epigenetic ice wedges* up to a few metres high and up to about 1 m in true maximum width are superimposed on the upper several metres of yedoma silt, penetrating down through the overlying transition zone (Figure 13A). The ice examined, from syngenetic wedges, was grey and contained minor amounts of disseminated silt.

Cryostructures in unit 4 comprise lenticular, layered and irregular/foliated reticulate types, some transitional with ataxitic ones (i.e. where sediment aggregates are suspended in ice). Many ice lenses and layers are $<$ 1 mm to a few millimetres thick and difficult to see with the naked eye, such that the silt appears almost to lack a cryostructure. Such barely visible cryostructures (i.e. microcryostructures) are the most typical of yedoma and include several types: microporphyritic, microlenticular, microbraided and microataxitic (Kanevskiy *et al.*, 2011, Figure 4). Cryostructures in unit 4 are commonly arranged in horizontal to subhorizontal bands a few centimetres to tens of centimetres thick. Occasionally, distinct ice layers up to several centimetres thick (‘ice belts’ in the Russian

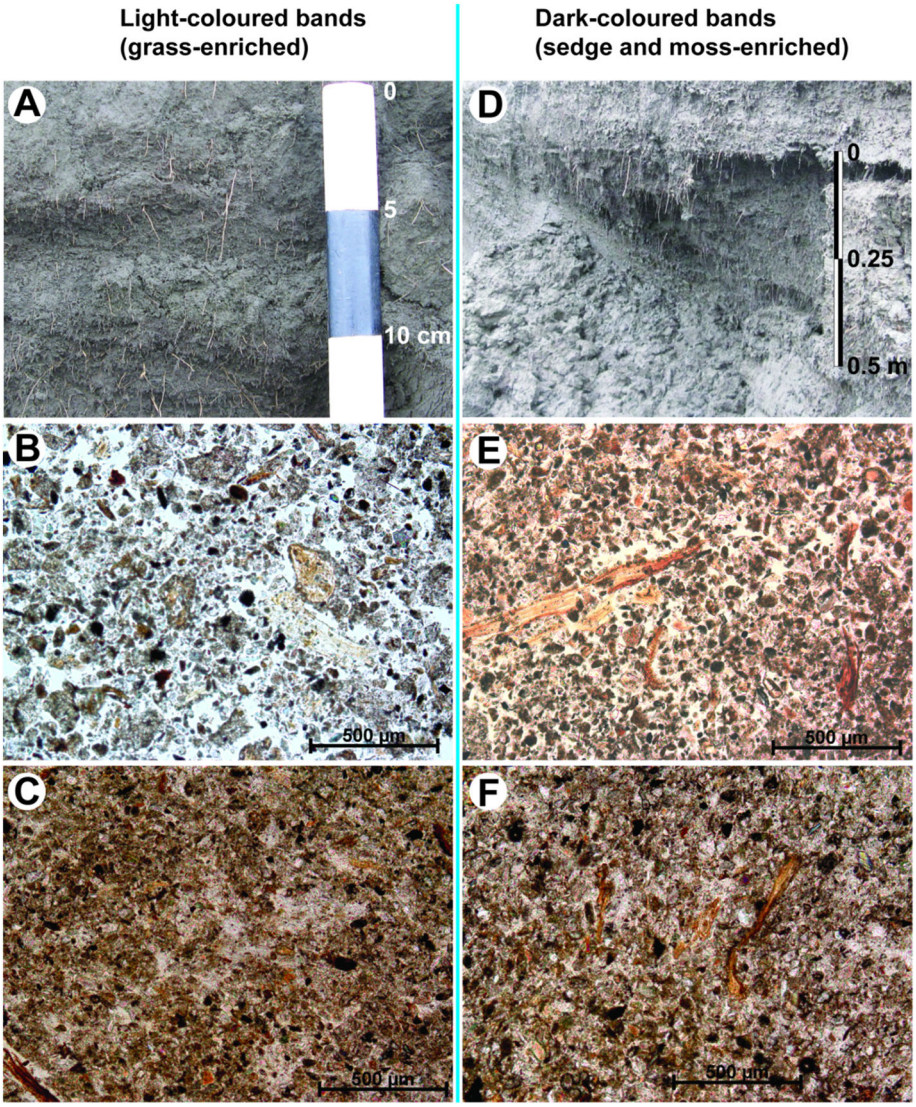

Figure 11 (A–C) Light-coloured bands and (D–F) dark-coloured bands in yedoma silt within remnant 7E at Duvanny Yar. (A) Grass roots. (B) Light-coloured band containing grass-moss detritus and dominantly with thin organic coatings, 7.25 m depth in yedoma of Sartan age (DY_CHGS-1979_PK-4). (C) Light-coloured band containing fine detritus and few organic coatings, 30 m depth in yedoma of Karginsky age (DY_CHGS-1990_R-512). (D) Sedge roots. (E) Dark-coloured band containing sedge-grass detritus and abundant thick organic coatings, 7.30 m depth in yedoma of Sartan age (DY_CHGS-1979_PK-4). (F) Dark-coloured band containing coarse detritus and many organic coatings, 32 m depth in yedoma of Karginsky age (DY_CHGS-1990_R-512). (B), (C), (E) and (F) are in unpolarised light. This figure is available in colour online at wileyonlinelibrary.com/journal/ppp

permafrost literature) and small ice veins are present. The measured gravimetric water content of the silt averages 49.1 per cent (n = 68), ranging from 30.5 to 91.6 per cent (Figure 14A). The calculated volumetric ice content averages 58 per cent and ranges from 50 to 74 per cent. Wedge ice volumes at depths of about 5 m and 10 m in Figure 3C are about 50 and 40 per cent, respectively, indicating that the upper 8 m of unit 4 contains about 45 per cent wedge ice by volume and 55 per cent yedoma silt. The total ice volume of the upper 8 m is therefore about 77 per cent. Thaw unconformities form shoulders to syngenetic ice wedges (Figure 9C) and sharp discontinuities between cryostructures (Figure 9E).

Texturally, the yedoma silt of unit 4 has mean values (n = 68) of 65 ± 7 per cent silt, 15 ± 8 per cent sand and 21 ± 4 per cent clay (Figure 14A). The mean U-ratio is 3.3 ± 1.8. Particle-size distributions are bi- to polymodal, most with three or four modes (Figure 15A). The primary mode averages 40.9 µm (coarse silt; range: 17.7–82.7 µm). Subsidiary modes occur at about 0.3–0.7 µm (very fine clay to fine clay), 3–5 µm (coarse clay to very fine silt), 8–16 µm (fine silt) and 150–350 µm (fine sand to medium sand). Overall, the particle-size distributions and summary values are relatively uniform with height through unit 4, with some exceptions (Figures 14 A and 15 A). Higher-than-average clay contents are associated with organic layers 1 and 2, some

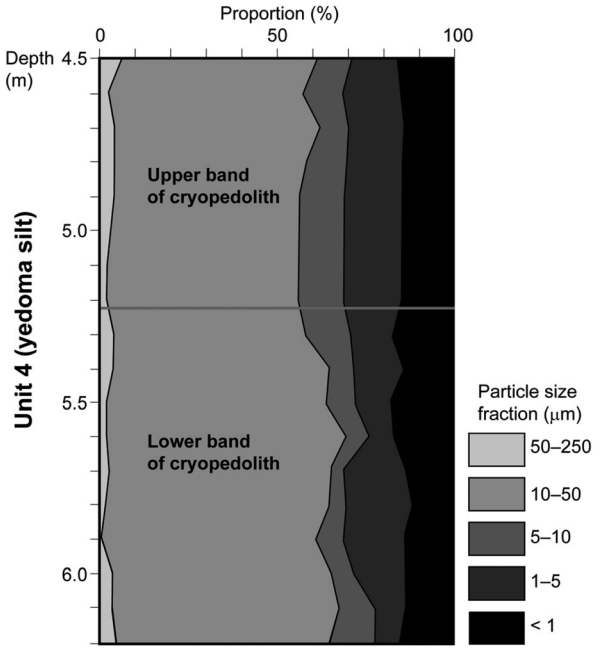

Figure 12 Particle-size fractions in two bands of cryopedolith at a depth of 4.5 to 6.2 m below the ground surface in yedoma silt of unit 4, of Sartan (MIS 2) age in remnant 7E, Duvanny Yar. Fractions measured by pipette and sieve analysis. Vertical sampling interval = 10 cm. MIS = Marine Isotope Stage.

root-rich layers, and occur at heights of about 23 and 26 m arl (Figure 14 A). Coarser-than-average yedoma silt occurs at heights of 4.3 m arl (median = 50 μm; 38% sand) and 12.5 m arl (median = 75 μm; 63% sand). Magnetic susceptibility values for yedoma silt in unit 4 average 52.6 x 10^{-5} SI units, and range from 30.4 to 98.9 x 10^{-5} SI units (Figure 14A). Lower-than-average values (about 30–40 x 10^{-5} SI units) cluster around organic layers 1 and 2 and the three root-rich layers. Organic contents in unit 4 average 4.4 per cent, and range from 1.9 to 9.5 per cent (Figure 14A). Higher-than-average values of about 6–8 per cent occur in organic layers 1 and 2, and in the three root-rich layers. Two additional peaks in organic content (8.0 and 9.5%) occur at heights of 21.3 and 25.4 m arl. Carbonate contents from unit 4 average 2.1 per cent (range: 1.2–3.5%) and are fairly uniform with height (Figure 14A). pH values (n = 62) determined on the silt in unit 4 average 8.1 (range: 6.8–9.0).

Unit 5: Near-surface Silt.

Unit 5 forms a near-surface horizon of silt, 1.9 m thick, that overlies a prominent thaw unconformity and is capped by an organic layer beneath the forest tundra (Figure 16). Texturally, unit 5 is slightly enriched in clay and depleted in silt relative to much of the underlying yedoma in unit 4. Unit 5 has mean values (n = 6) of 58 ± 4 per cent silt, 18 ± 4 per cent sand and 24 ± 4 per cent clay (Figure 14A). The mean U-ratio is 2.2 ± 0.8. Particle-size distributions in unit 5 (red lines in Figure 15A) in the silt are similar to those in unit 4 (black lines in Figure 15A). Magnetic

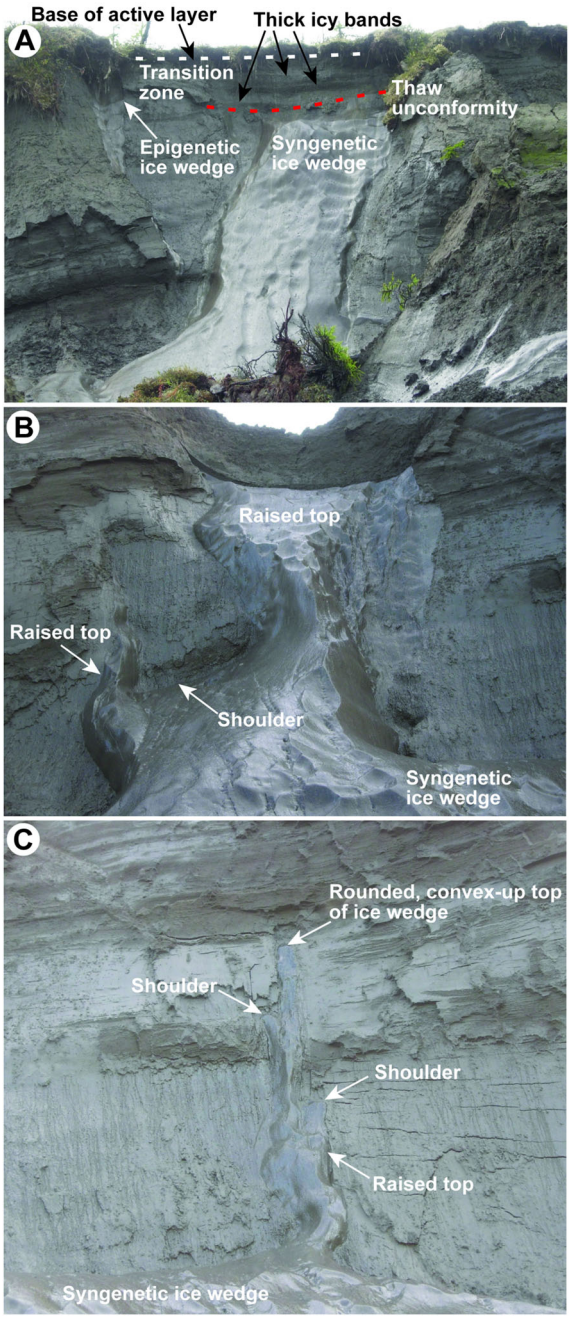

Figure 13 Ice-wedge types in yedoma silt of unit 4 and overlying near-surface silt of unit 5, Duvanny Yar. (A) Large syngenetic wedge with its top truncated by a thaw unconformity (marked by red dashed line) at the base of the transition zone (base of unit 5 near-surface silt). Base of the modern active layer (about 25–30 cm depth) is indicated by white dashed line. Small epigenetic wedge about 1 m wide at the top extends down through the transition zone (unit 5) and into underlying yedoma silt (unit 4). (B) Large syngenetic ice wedge with prominent shoulder and raised top in unit 4, section 3. Small syngenetic ice wedge on the left extends about 1 m above the shoulder of the large wedge. Note that the small wedge becomes thicker with depth and penetrates the large wedge. (C) Small syngenetic wedge about 1 m high with two shoulders and rounded convex-up top, section 3. Base of wedge extends down into the large syngenetic wedge. Location of (B) and (C) is shown in Figure 9A and C. This figure is available in colour online at wileyonlinelibrary.com/journal/ppp

susceptibility values average 20.7 x 10^{-5} SI units, and range from 16.0 to 29.1 x 10^{-5} SI units (Figure 14A). They are less than those in unit 4. Organic contents average 6.3 per cent and range from 2.5 to 14.9 per cent (Figure 14A). The highest value is in the ice-rich silt just beneath the active layer (sample 71 in Figure 16). Carbonate contents average 1.6 per cent (range: 1.1–2.3%), and reach a minimum value in sample 71.

Two cryostratigraphic layers are identified in unit 5: (1) the present-day active layer and, beneath it, (2) the transition zone. The active layer is estimated to be about 0.3–0.4 m thick in the fibrous organic layer developed beneath the forest-tundra surface (Figures 13A and 16). At the time of examination (3 August 2009), about 1 month before the active layer typically reaches its maximum depth in northern Yakutia (Lupachev and Gubin, 2012), the frost table was at a depth of 22 cm.

The transition zone contains two layers (Figure 16). An upper layer (about 0.30–0.75 m depth) of ice-rich silt is characterised by a lenticular cryostructure that grades down (as the ice content increases) into a cryostructure transitional between lenticular and layered. Gravimetric ice contents of 98.9, 67.9 and 89.0 per cent were measured on samples from the upper layer (Figure 14A). The lower, more ice-rich half of this layer (about 0.55–0.75 m depth) may be a secondary intermediate layer formed as a result of partial thawing and refreezing of the original (primary) intermediate layer (e.g. after a forest fire). It is uncertain, however, if the upper, less ice-rich half (about 0.30–0.55 m depth) represents the upper half of a secondary intermediate layer or a transient layer, although the ice content is rather high for a transient layer. A thaw unconformity at the base of the ice-rich silt (0.75 m depth) indicates a former position of the permafrost table (Figure 16B, D).

Beneath this unconformity is an extremely ice-rich primary *intermediate layer* (about 0.75–1.9 m depth). This contains bands of sediment-poor ice and sediment-rich ice 10–30 cm thick and is characterised by an ataxitic cryostructure combined with thick ice belts (Figure 16D, E). The thick icy bands commonly form two to three distinctive marker horizons that are more or less parallel to the ground surface and that protrude from the thawing face above unit 4 and beneath the active layer (Figures 3 and 13A). Gravimetric ice contents of 69.3, 108.0 and 88.8 per cent were measured on samples from the intermediate layer (Figure 14A), but these do not include samples of the most ice-rich material. The base of the intermediate layer is a thaw unconformity, and is clearest where it truncates the tops of large syngenetic ice wedges (Figure 13A). As noted previously, small epigenetic ice wedges extend downward through the transition zone, across the basal thaw unconformity and into the underlying yedoma silt of unit 4 (Figure 13A). The exact depth of the tops of such wedges is unknown.

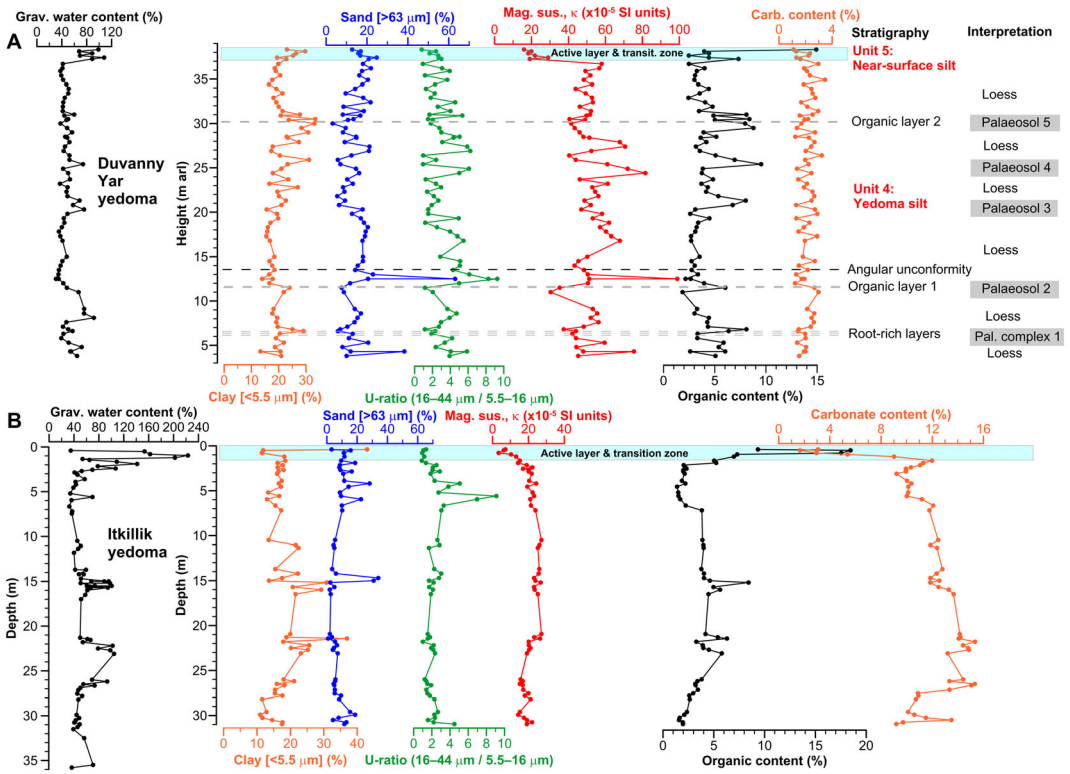

Figure 14 Sedimentary properties of yedoma silt of unit 4 plotted (A) against height for section CY, Duvanny Yar, and (B) against depth below the ground surface for the Itkillik River. In (A) the stratigraphy and interpretation are given on the right. arl = Above river level. This figure is available in colour online at wileyonlinelibrary.com/journal/ppp

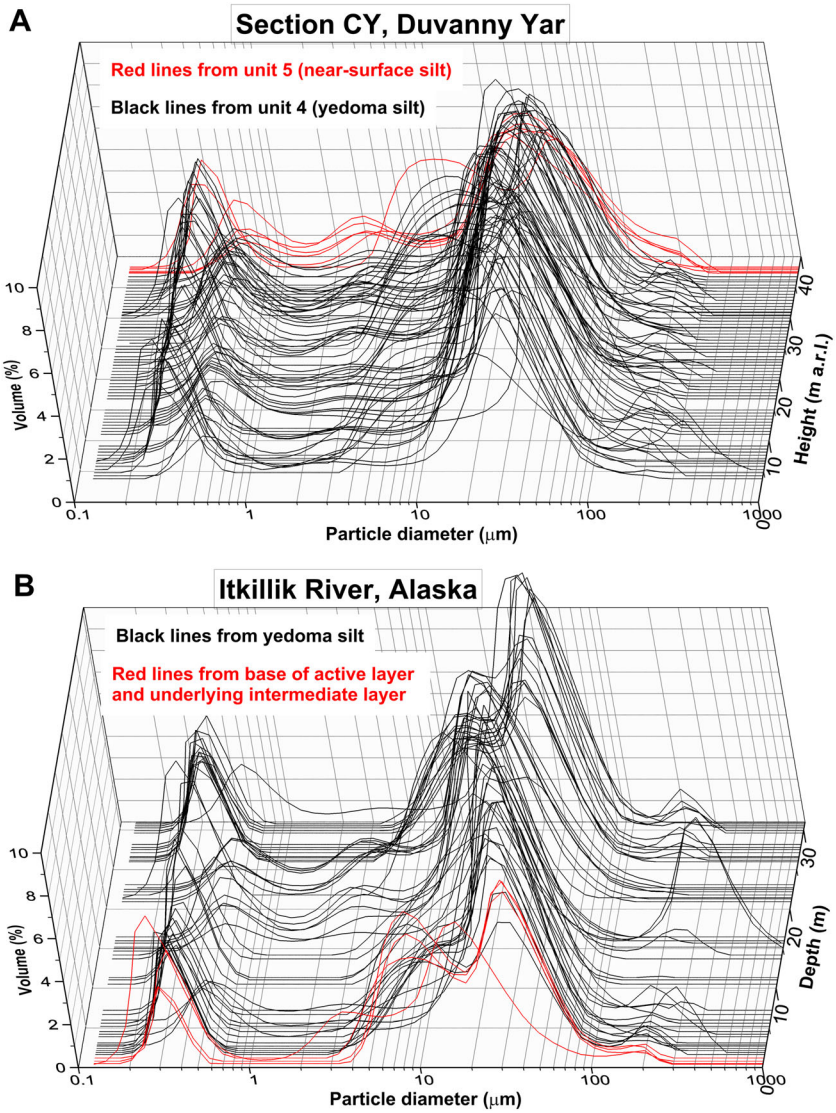

Figure 15 Particle-size distributions (PSDs) of yedoma silt of unit 4 plotted (A) against height above river level (arl) for Duvanny Yar and (B) against depth below the ground surface for the Itkillik River. In (A) PSDs are for samples 9–14, 16–54 and 56–82 from section CY. Red lines are from samples 71–76 in unit 5 (near-surface silt); black lines are from unit 4 (yedoma silt). In (B) PSDs are for samples 1–3, 5–9 and 11–54. The red line at the shallowest depth indicates a sample from the base of the active layer, and the others indicate samples from the underlying intermediate layer. The black lines are for samples from underlying yedoma silt of units 3 and 4 (see Table 6). This figure is available in colour online at wileyonlinelibrary.com/journal/ppp

Micromorphology

Scanned thin sections and photomicrographs of recently thawed yedoma silt from unit 4 indicate that the silt is unstratified but contains a variety of former microcryostructures, organic material, aggregates and deformation structures. Primary sedimentary structures were not observed in any thin sections. Instead, the silt is unstratified (Figures 11B, C, E, F, 17A, 18A and 19A), and sometimes texturally heterogeneous (Figure 20B).

Former microcryostructures include pore, lenticular and reticulate types. Pore microcryostructures (microporphyritic) are identified where pores (white) of irregular size and shape intersperse silt particles, aggregates and organic material (Figure 17B, C). Such pores previously contained ice cement, accounting for the solid, frozen nature of unit 4 beneath the recently thawed veneer of silt. Lenticular microcryostructure is widespread in the thin section shown in Figure 18B, where a platy microstructure comprises horizontal plates of silt separated by planar to wavy voids (white) that mark the positions of former ice lenses. If the silt has not consolidated much since thaw, then the ice lenses were a few tens to a few hundreds of micrometres thick. Higher in the thin section, the microcryostructure becomes transitional between lenticular and a three-dimensional (reticulate) network of ice lenses and veins (Figure 18C). A fully

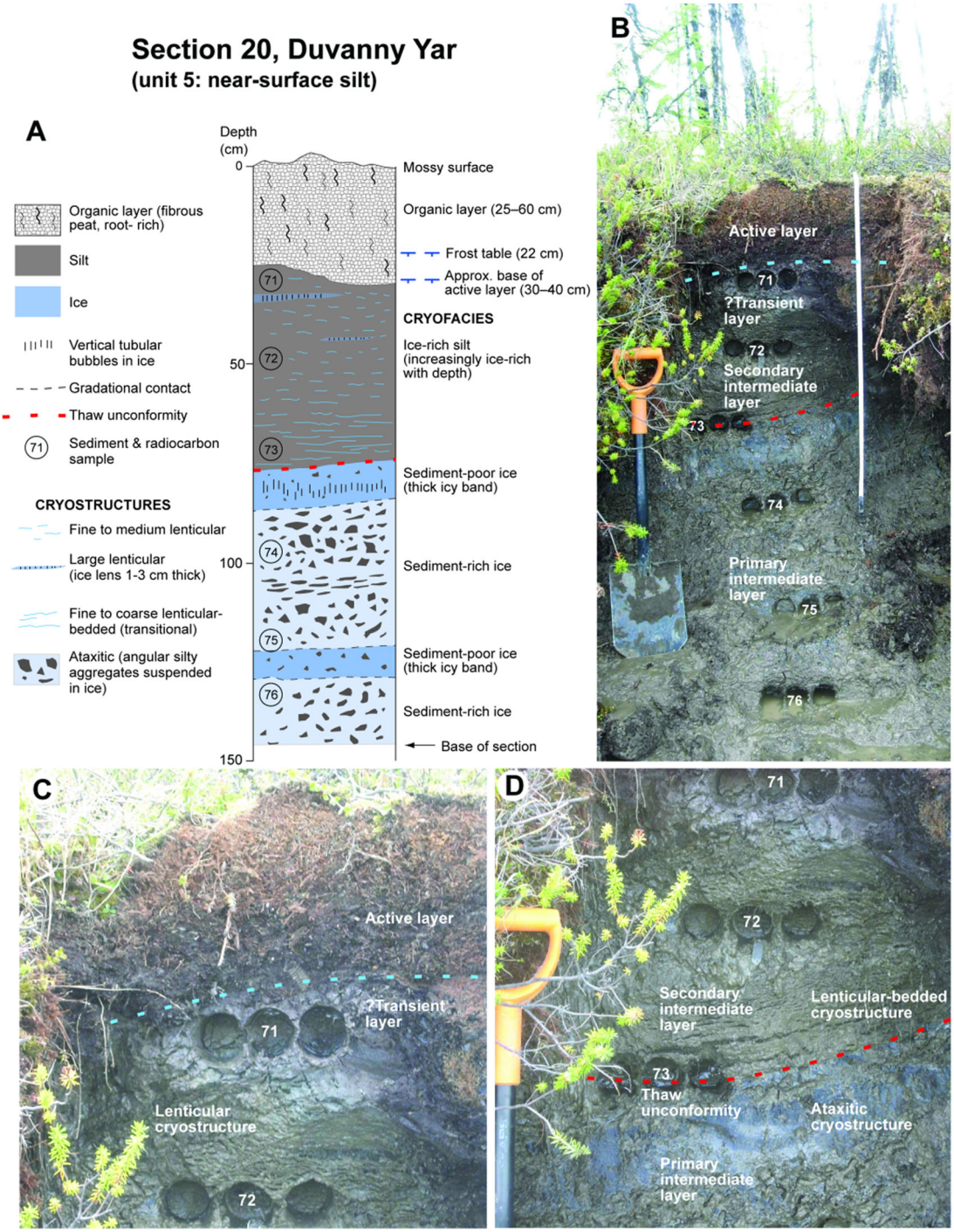

Figure 16 Vertical sections through the modern active layer and underlying transition zone in section 20 (A to D) and nearby at Duvanny Yar (E). The transition zone comprises (1) a layer of ice-rich silt (secondary intermediate layer, possibly with overlying transient layer) that overlies (2) a primary intermediate layer of layered sediment-poor ice and sediment-rich ice. A thaw unconformity (dashed red line) separates the primary and secondary intermediate layers, marking the maximum depth of thaw prior to the development of the modern active layer. The base of the transition zone is not visible in this section and is estimated to lie at about 1.9 m depth, based on observations from adjacent sections. (A) Cryostratigraphic log. The frost table (22 cm depth) was measured on 3 August 2009. (B) Cryostratigraphy of the active layer (with estimated base marked by the dashed blue line), transient layer and intermediate layer. (C) Close-up photograph of the active layer and upper part of transient layer, showing lenticular cryostructure in the latter. (D) Close-up photograph of thaw unconformity between the secondary intermediate layer and underlying and more ice-rich primary intermediate layer. The unconformity is marked by an abrupt change from a transitional lenticular-layered cryostructure to an ataxitic cryostructure. (E) Modern intermediate layer at 0.45–1.15 m depth observed in 1994 at Duvanny Yar. Ataxitic cryostructure within thick ice belts from 0.5 to 0.95 m depth. Ten centimetre intervals marked on scale.

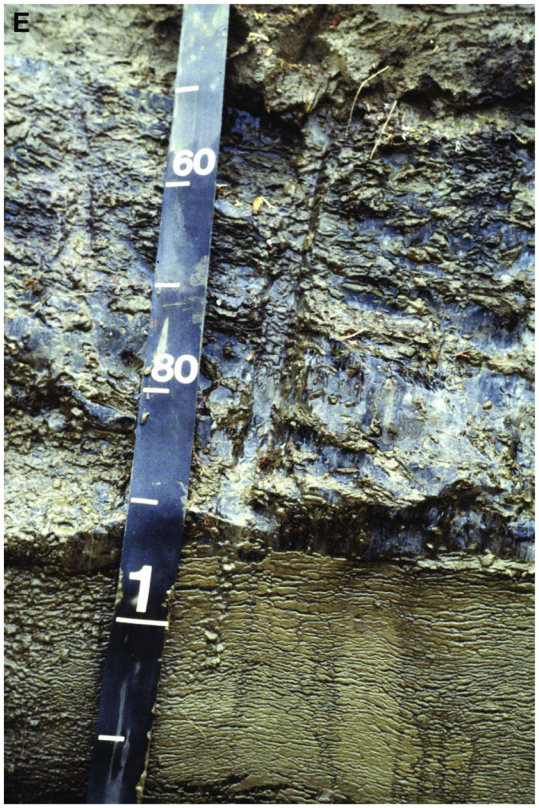

Figure 16 (Continued)

developed reticulate microcryostructure characterises thin section 3 (Figure 19). Again, the dominant structural element is a horizontal to subhorizontal platy microstructure (microbraided). Remnants of a more irregular reticulate microcryostructure, transitional to a pore microcryostructure, occur in thin section 4, where a former network of ice lenses and veins encased sediment aggregates (Figure 20D).

Organic material is common in all four thin sections. Fine roots tend to be vertically oriented to steeply dipping, and cross-cut platy microstructures (Figures 18B and 19A, B). Roots are commonly partially decomposed and narrower than the elongate voids which they occupy; prior to thaw, much of this void space was probably filled with ice sheaths around the roots, because the root-occupied voids are contiguous with horizontal voids between the platy microstructure (Figure 19B). Mineralised and humified organic remains are dispersed throughout the host mineral particles, varying in size, shape and concentration (Figures 17–20). Organic-rich patches appear as dark areas of thin-section scans (Figures 17A, 19A and 20B). They are particularly well developed in the involuted organic lens in thin section 4 (Figure 20A, B), where roots and other plant materials are abundant (Figure 20C).

Aggregates of silt to sand size are abundant in the thin sections (Figures 17B, 18C and 20D, E), as reported by Zanina *et al*. (2011, Figure 10). Such mixtures of mineral particles and mineralised and humified organic remains vary in shape (from equant to elongate) and roundness (from rounded to subangular). Some aggregates are clearly defined by surrounding voids (Figure 20D) that mark an irregular reticulate microcryostructure.

Deformation structures comprise microfolds, a chaotic microstructure and sediment intrusions. Folds are well developed in the involuted organic lens (Figure 20A), whose microstructure is shown in Figure 20B. Microfolds are marked by elongate roots within the lens (Figure 20C). Near the microfolds is a chaotic microstructure of fragmented and irregularly oriented organic material and sediment aggregates. Additionally, the irregular distribution of darker-coloured material with finer aggregates (about 0.1–1 mm; Figure 20B, E) and lighter-coloured material with coarser aggregates (about 0.3–2 mm; Figure 20D) suggests small-scale intrusion of one into the other. Deformation is also indicated by the reticulate microcryostructure in Figure 19A, where the elongate pores show broad and open anticlines and synclines across the thin section, consistent with differential frost heave and/or thaw consolidation (i.e. cryoturbation).

Elemental Concentrations and Ratios

P_2O_5 concentrations in yedoma silt show several substantial and abrupt departures from average values (n = 68) with height through unit 4 (Figure 21A). P_2O_5 concentrations average 0.207 ± 0.021 per cent. Higher-than-average values are associated with organic layers 1 (0.217%) and 2 (≤0.248%), and both higher- and lower-than-average values occur within and beneath the three root-rich layers. Additionally, two abrupt increases in P_2O_5 concentrations occur at heights of 20.8–21.3 arl (0.236–0.268%) and 25.4–25.9 m arl (0.236–0.266%), the former with a depleted value beneath it (0.183% at 20.3 m arl). Above unit 4, a distinct 'high-low-high' depth function is apparent in unit 5 (Figure 21A). Beneath unit 4, P_2O_5 concentrations in unit 1 (massive silt) from section 1 average (n = 7) 0.197 ± 0.010 per cent, and are quite variable with depth (Figure 21B). A single P_2O_5 value from unit 2 (peat) is 0.176 per cent (Figure 21B).

Mobile-to-immobile element ratios tend to covary in unit 4 (Figure 21A). This covariation is strongest between Na_2/TiO_2 and SiO_2/TiO_2, and to lesser or more variable degrees by MgO/TiO_2 and K_2O/TiO_2, and least with CaO/TiO_2. Five prominent decreases in some or all of these ratios are apparent at stratigraphic levels associated with: (1) organic layer 2, (2) a level about 26 m arl, (3) a level about 21 m arl, (4) organic layer 1 and, to some extent, with (5) the three root-rich layers. CaO/TiO_2 ratios are relatively low and show less distinct fluctuations. All apart from the SiO_2/TiO_2 ratio drop substantially in unit 5, and even this ratio drops distinctly in the highest sample. In units 1 and 2 of section 1, all five of these ratios are of similar magnitude to those in unit 4.

Immobile element ratios Ti/Zr in unit 4 average 29.8 and range from 23.6 to 35.8 (Figure 21A). They tend to show an

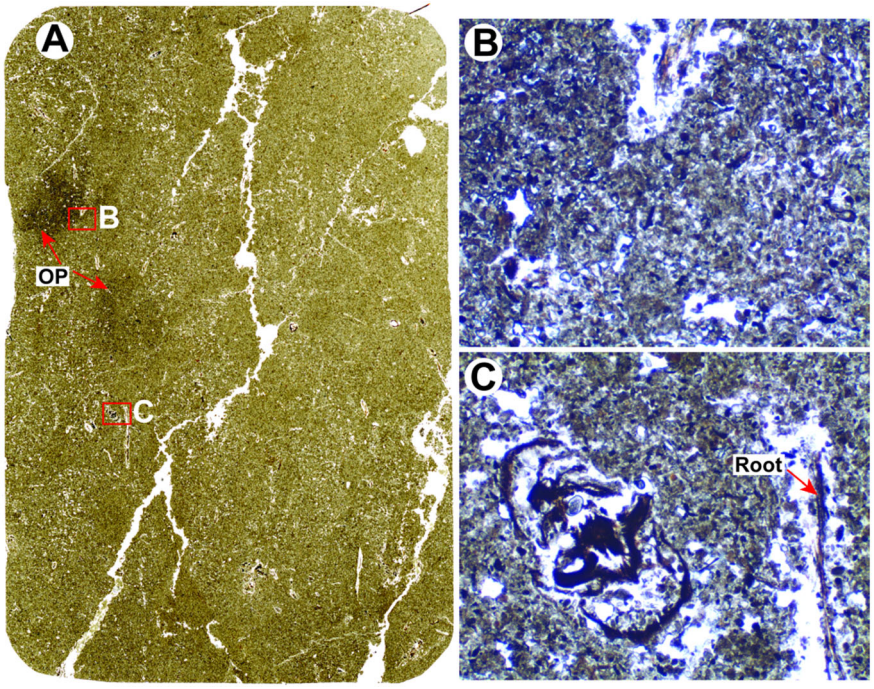

Figure 17 Microstructures in cryopedolith within yedoma silt of unit 4, thin section 1, 29.3 m arl. (A) Organic-rich patches (OP) occur within otherwise massive yedoma. (B) Mineralised and humified organic remains (black and brown) are dispersed throughout the host mineral particles. Many of the organic and mineral particles are clustered as sediment aggregates. (C) Partially decomposed root and adjacent organic material. Scanned thin section in (A) is 45 mm wide x 68 mm high, in correct vertical orientation; photomicrograph frame widths in (B) and (C) are 2.6 mm. arl = Above river level. This figure is available in colour online at wileyonlinelibrary.com/journal/ppp

anti-phase relation with the mobile-to-immobile element ratios and an in-phase relation with clay contents. For example, prominent increases in Ti/Zr ratios occur around organic layers 1 and 2, as well as heights of about 21 and 26 m arl, and in unit 5. Ti/Zr ratios in unit 1 from section 1 average 30.1 (range: 28.2–31.6), and a single value from unit 2 is 29.3 (Figure 21B), all similar to those in unit 4.

Major element concentrations in unit 4 generally differ from those reported by Péwé and Journaux (1983, table 6) for silty permafrost deposits (loess) in central Yakutia (Figure 22). MgO values at Duvanny Yar are higher (average = 2.33 ± 0.28%) than those in central Yakutia (average = 0.99 ± 0.17%; n = 12), whereas CaO values from Duvanny Yar are lower (average = 1.40 ± 0.33%) than those from central Yakutia (average = 5.20 ± 1.24%; Figure 22A). Duvanny Yar yedoma contains only slightly less K_2O (average = 2.36 ± 0.06%) and Na_2O (average = 2.03 ± 0.12%) than central Yakutian loess (averages of 2.87 ± 0.17% and 2.26 ± 0.25%, respectively; Figure 22B), and both values from Duvanny Yar are very close to average upper crustal values. SiO_2 values are similar in both regions (Duvanny Yar average = 62.4 ± 1.2%; central Yakutia average = 62.0 ± 3.4%), although Al_2O_3 values are higher at Duvanny Yar (average = 13.7 ± 0.3%) than those from central Yakutia (average = 11.9 ± 0.6%; Figure 22C). Finally, Fe_2O_3 values at Duvanny Yar average 5.6 ± 0.4 per cent, compared with an average of 4.5 ± 1.0 per cent in central Yakutia (Figure 22D).

Geochronology

Radiocarbon Ages.

The ^{14}C ages obtained from yedoma silt of unit 4 at Duvanny Yar range from > 49 000 ^{14}C BP to 16 850 ± 100 ^{14}C BP, and those from near-surface silt of unit 5 range from 830 ± 40 ^{14}C BP to 70 ± 30 ^{14}C BP (Figures 5 and 23; Table 5). ^{14}C ages of *in-situ* roots are thought to indicate the age of their transition into the frozen state (cf. Gubin and Lupachev, 2008), as permafrost aggraded upward into the silt. These ages are younger than the age of silt deposition, and to assess the magnitude of the age shift, we dated several samples of *in-situ* roots from the transition zone within the near-surface silt of unit 5 (Figure 24). Interestingly, none of the four samples collected 30–100 cm below the present-day ground surface revealed a modern ^{14}C age, suggesting that in this section, modern roots have not penetrated more than 30 cm below the surface. The age-height models developed from ^{14}C ages of these roots may be smoothly extrapolated towards AD 2009 (year of sample collection) on the modern land surface, indicating that the sampled roots did not introduce significant bias in dating of this silt. The inversion of ^{14}C ages between samples from 37.41 and 37.27 m arl might relate to reworking material of the upper sample, but could also indicate that the sample at 37.41 m arl contained some deeper (and thus relatively younger in terms of ^{14}C) roots than those collected for the other samples. Being unable to resolve this dilemma, we may say only that

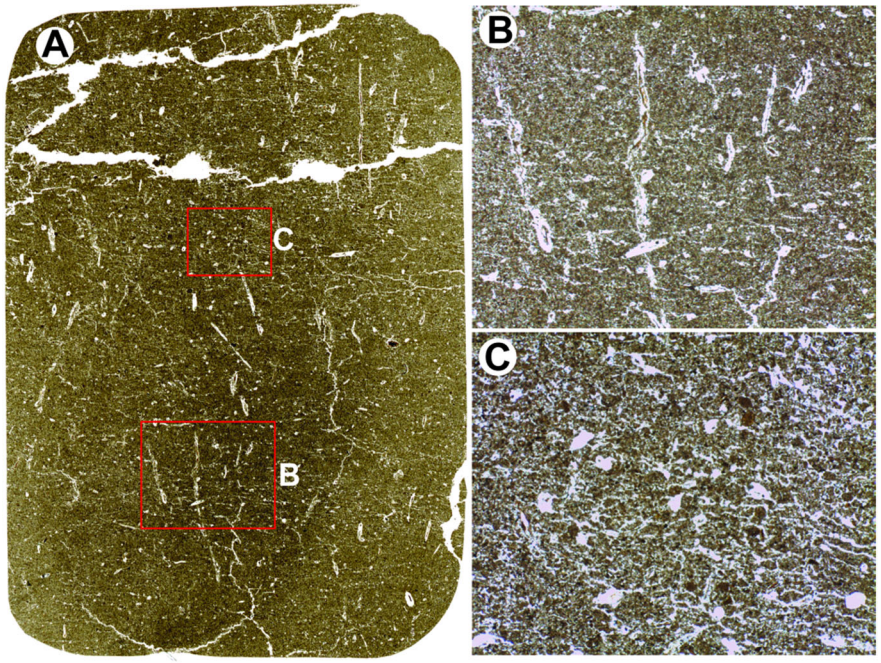

Figure 18 Microstructures in cryopedolith within yedoma silt of unit 4, thin section 2, 29.3 m arl. (A) Massive silt traversed by abundant roots and with dark brown central patch enriched in fine humified organic remains. (B) Former lenticular microcryostructure, where a platy microstructure comprises horizontal plates of sediment separated by planar to wavy voids (white) that mark the sites of former micro-ice lenses. Several vertical to steeply dipping roots penetrate the sediment. (C) Former microcryostructure transitional between lenticular and reticulate, with location of former micro-ice lenses and veins indicated by elongate white pores. Sediment aggregates are abundant. Scanned thin section in (A) is 46 mm wide x 65 mm high, in correct vertical orientation; photomicrograph frame widths in (B) and (C) are 13.1 mm and 8.3 mm, respectively. arl = Above river level. This figure is available in colour online at wileyonlinelibrary.com/journal/ppp

both age-height models shown in Figure 24 (orange and blue) are possible. Although this ambiguity decreases the accuracy of the combined age-height model, the introduced uncertainty is not large relative to the analytical uncertainty of ^{14}C dating of very old (>20 000 ^{14}C BP) samples. Thus, within analytical error, we consider that ^{14}C ages from *in-situ* roots provide a close approximation of the depositional age of pre-Holocene silt.

OSL Ages.

OSL ages from unit 4 are based from the year of measurement, with one standard deviation error (Table 3). Given the small numbers of grains measured for the single-grain ages, the OSL ages are considered as approximate rather than definitive. They show a consistent relative relationship to each other, which is comparable to that of the small-aliquot ages. The relatively good reproducibility without skewing of the small-aliquot data is interpreted to indicate that all sampled sediments were exposed to sunlight prior to burial and thus the ages should reflect true burial ages without any antecedent signal. If the sediment had been partially bleached, then the single-grain data would have shown younger age components reflecting grains that had been fully bleached. Such younger age components are lacking from the single-grain data. Given this, the better signal-to-noise ratio of small aliquots and the more representative sample size measured (due to the fact that each small aliquot contained about 1600 grains), only small-aliquot ages are used in the following discussions. The three OSL ages increase in age with depth, from 21.2 ± 1.9 ka near the top of unit 4 to 48.6 ± 2.9 ka near the bottom (Figure 5). The upper sample fits very well with the calibrated radiocarbon ages for the same stratigraphic level (Figure 23).

Palaeovegetation

Present-day pollen spectra from moss polsters in the lower Kolyma region (see Appendix S4 and Figure S5) are dominated by woody taxa (60–80%): *Pinus*, *Larix*, *Betula*, *Alnus* (includes *Duschekia* and *Alnaster*), but they also have a moderate component of Poaceae, Cyperaceae and herbs, these being more dominant in the tundra. The dominance of pollen of coniferous trees, woody trees/shrubs and Ericales can be considered diagnostic of interglacial forest pollen spectra in the region.

The pollen spectra from units 1 and 2 are shown in Figure 25. The three lower samples, corresponding to the massive silt of unit 1, are characterised by Poaceae and forbs. In contrast, the highest sample, from the peat of unit 2, is dominated by *Pinus* (haploxylon group) at a high value (about 75%) seldom seen in Holocene records, together with lesser amounts of *Betula* and *Alnus*. The peaty deposit is dominated by woody detritus and brown (aquatic) moss remains.

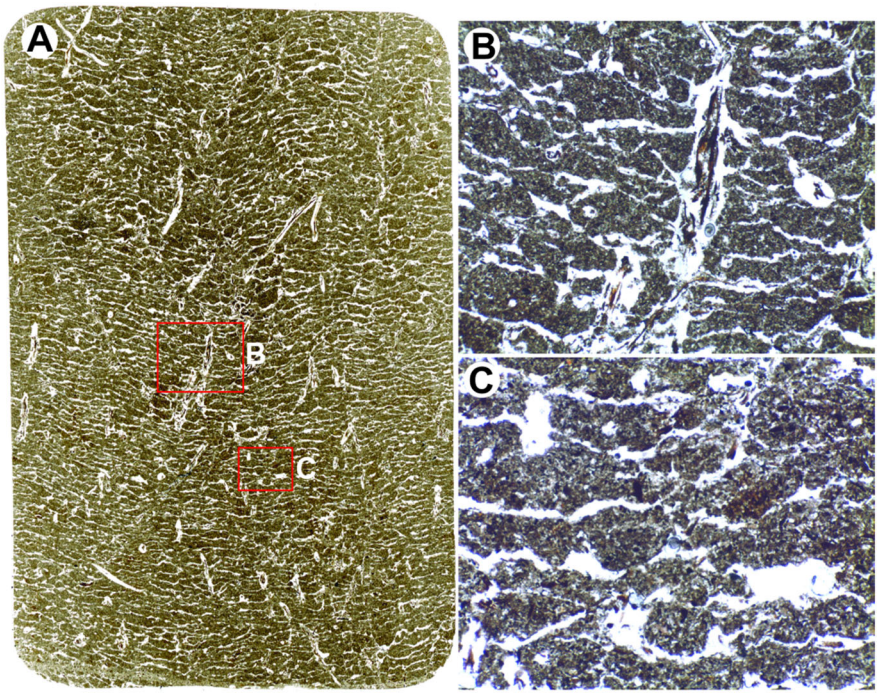

Figure 19 Microstructures in cryopedolith within yedoma silt of unit 4, thin section 3, 6.5 m arl. (A) Former reticulate microcryostructure, with a dominant structural element of horizontal to subhorizontal platy microstructure. Elongate pores (white) show broad and open anticlines and synclines across the thin section that are attributed to differential frost heave. (B) Partially decomposed roots surrounded by sheath-like vertical voids continuous with horizontal voids between a platy microstructure. (C) Former reticulate microcryostructure. Scanned thin section in (A) is 44 mm wide x 67 mm high, in correct vertical orientation; photomicrograph frame widths in (B) and (C) are 8.3 mm and 5.2 mm, respectively. arl = Above river level. This figure is available in colour online at wileyonlinelibrary.com/journal/ppp

Pollen spectra from units 4 and 5 are shown in Figure 26. Four zones are defined by sedimentary changes and/or dating unconformities and palaeosols shown in Figure 5 and discussed below. Zones D to B are from unit 4, and zone A from unit 5.

Zone D is the lowermost unit (about 5–26 m arl). Samples in the lower part of this zone vary in composition, with the main variation reflecting the ratio of woody taxa (*Pinus*, *Larix*, *Betula* and *Alnus*) to Poaceae. Most forb taxa in these samples are represented by sporadic occurrences, but Caryophyllaceae and Asteraceae appear in nearly all samples. Other more commonly occurring taxa include Chenopodiaceae, Ranunculaceae, Saxifragaceae and Brassicaceae. *Artemisia* occurs in only trace amounts in most samples.

In zone C (about 26–33 m arl), which lies above the unconformity at palaeosol 4 (Figure 5) and corresponds to the period just prior to the LGM, samples have low values of woody taxa (about 10%) and are dominated by graminoids (mainly Poaceae), forbs (particularly Caryophyllaceae and Asteraceae) and *Selaginella rupestris*. *Larix* is present in small amounts.

Zone B (about 33–37 m arl) dates to the LGM (discussed below). Samples are characterised by a variable range of frequencies of tree/shrub pollen (20–60%: mainly *Betula* and *Pinus*, with low amounts of *Salix* and *Alnus*, but lacking *Larix*) and graminoids (20–60%: predominantly Poaceae, plus forbs). Total frequencies for woody taxa and graminoids tend to be reciprocal and dominate the pollen sum. *S. rupestris* values are about 10–40 per cent. Spores of Polypodiales and Lycopodiales are consistently present.

The two Holocene samples (zone A) are dominated by *Betula*, Ericales and *Sphagnum*, with lower amounts of Poaceae and Cyperaceae (10–20%). *Pinus* values are relatively low (about 10%).

For comparison of fossil and modern samples, an ordination (detrended correspondence analysis; see Appendix S4) of the samples is presented (Figure S6). The ordination shows the Holocene samples (zone A) nested within all modern samples from the lower Kolyma region, and this group of samples is separated from all other samples. LGM samples, those attributed to MIS 6, and other samples from zones B–D are intermixed, and no zone is distinct from the others. Thus, there is only a weak stratigraphic signal in the pollen record: interglacial samples can be distinguished from non-interglacial samples, but the different stages of the last glacial cycle are not distinct.

Itkillik Yedoma

Introduction.

The Itkillik yedoma was sampled at 69°34′ N, 150°52′ W, at the boundary of the Arctic Coastal Plain and the

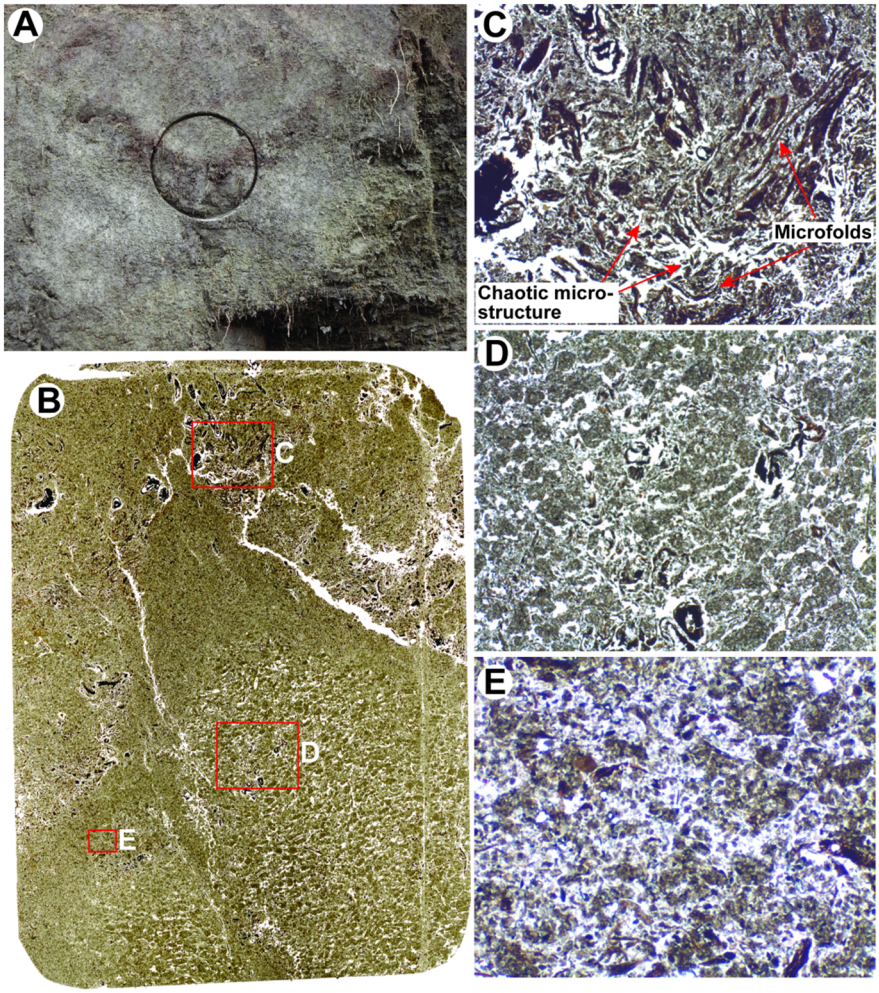

Figure 20 Microstructures in palaeosol complex 1 within yedoma silt of unit 4, thin section 4, 6.5 m arl. (A) Upper of three root-rich layers, showing involuted organic-rich lens (palaeosol) in the centre and numerous *in-situ* roots, the larger ones (upper right) woody. Imprinted circle (9 cm diameter) marks the location of the sediment sample from which thin section 4 (B) was obtained. (B) Organic-rich silt within involuted lens, showing locally high concentrations of organic material (dark brown) and textural heterogeneity attributed to cryoturbation. (C) Root-rich silt containing (1) microfolds that are picked out by elongate roots and (2) a chaotic microstructure of fragmented and irregularly oriented organic material and aggregates. (D) Aggregates of about 0.3–2 mm maximum dimension surrounded by an irregular pore network (white) that represents a former microcryostructure transitional between irregular reticulate and pore. (E) Aggregates of about 0.1–1 mm maximum dimension and interspersed particles of mineral and humic material. The former microcryostructure is pore, indicated by the irregular pore network. Scanned thin section in (B) is 47 mm wide x 64 mm high, in correct vertical orientation. Photomicrograph frame widths in (C), (D) and (E) are 8.3, 8.3 and 2.6 mm, respectively. arl = Above river level. This figure is available in colour online at wileyonlinelibrary.com/journal/ppp

Arctic Foothills of northern Alaska (Figure 1B). Erosion by the Itkillik River had exposed in 2007 and 2011 a section ≤ 34 m high and about 400 m long through fresh, undisturbed yedoma (Figure 27; Kanevskiy *et al*., 2011). The exposure is part of a large remnant of a continuous, relatively flat yedoma plain. Two similar exposures within the same remnant were studied by Carter (1988), and preliminary findings of permafrost studies at the present study site in 2012 are reported by Strauss *et al*. (2012b).

The cryostratigraphy at Itkillik comprises seven units, in ascending order: (7) silt with short ice wedges underlain by gravel at a depth of approximately 1.5 m below the water level, (6) buried intermediate layer, (5) buried peat, (4) yedoma silt with thick ice wedges, (3) yedoma silt with thin ice wedges, (2) intermediate layer and (1) transient and active layers (Table 6; Kanevskiy *et al*., 2011). The yedoma silt of units 3 and 4 is generally uniform, with occasional indistinct subhorizontal laminae. Bands within the yedoma relate mainly to cryogenic structures (e.g. ice belts) rather than primary sedimentary features. The yedoma is dominated by relatively ice-poor sediments with microcryostructures interspersed by ice-rich 'belt' cryostructures (≤10 mm thick) that consist of abundant short and thin ice lenses or continuous ice layers. Large syngenetic ice wedges occur within the yedoma, with the largest wedges (≤9 m wide) in the lower part (unit 4).

Radiocarbon ages from twigs and fine-grained organic material in the yedoma range from 14 300 ± 50 ^{14}C BP at

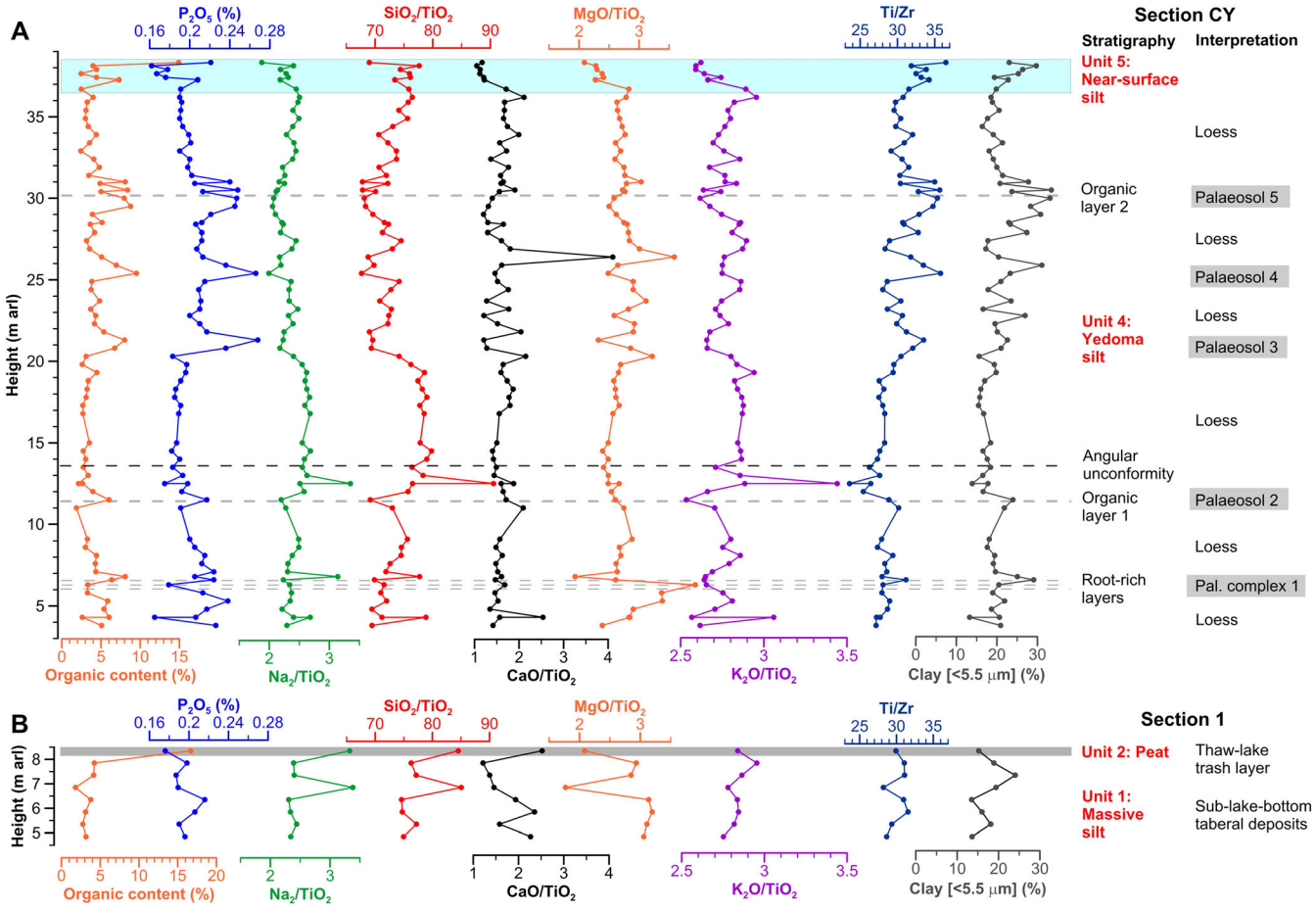

Figure 21 Organic content, elemental concentrations of phosphorus (expressed as P_2O_5), ratios of mobile elements (Na, Si, Ca, Mg, K) to immobile element Ti, ratios between immobile elements Ti and Zr, and clay content as a function of height for (A) section CY and (B) section 1, Duvanny Yar. arl = Above river level. This figure is available in colour online at wileyonlinelibrary.com/journal/ppp

3.0 m depth to 41 700 ± 460 ^{14}C BP at 23.0 m depth (Table 6), suggesting a Middle Wisconsin (MIS 3) to Late Wisconsin (MIS 2) age for yedoma deposition. However, three age inversions occur, and the anomalously young age of 15 500 ± 65 ^{14}C BP from twigs at 28.0 m depth is regarded as probably invalid by Kanevskiy *et al.* (2011). A non-finite age of > 48 000 ^{14}C BP at 30.9 m depth was obtained from the buried peat (Table 6).

Sediment Properties.

The yedoma silt at Itkillik contains on average (n = 48) 72 ± 7 per cent silt, 9 ± 7 per cent sand and 18 ± 5 per cent clay (Figure 14B). The mean U-ratio is 2.5 ± 1.4. Particle-size distributions are bi- to polymodal, most with three or four modes (Figure 15B). The primary mode averages 40.0 μm (coarse silt) and ranges from 15.9 to 179 μm (medium silt to fine sand); the value of 179 μm is anomalously high, the next highest value being 48.4 μm (coarse silt). Between 11 and 23 m depth, the size of the primary mode is generally 24–37 μm, finer than that above and below it (about 40–44 μm). Subsidiary modes occur at 0.3–0.6 μm (very fine clay to fine clay), 3–5 μm (coarse clay to very fine silt), 10–16 μm (fine silt) and 100–400 μm (fine sand to medium sand). The fine silt mode is often indicated as a distinct 'shoulder' on the fine-grained flank of the primary mode. Magnetic susceptibility values in the yedoma silt average 21.0 x 10^{-5} SI units (range: 14.2–27.3 x 10^{-5} SI units; Figure 14B). Organic contents average 3.4 per cent (range: 1.4–8.4%), with above-average organic contents of 8.4 and 6.3 per cent at 15.2 and 21.5 m depths, respectively, and the lowest values (few %) in the lower several metres and the upper few metres (Figure 14B). Carbonate contents average 12.1 per cent (range: 9.2–15.3%) and decline gradually upward through the profile from about 15 per cent at a depth of 26 m to about 10 per cent at a depth of 2.5 m.

The transition zone and basal part of the active layer contain on average (n = 4) 68 ± 10 per cent silt, 10 ± 5 per cent sand and 21 ± 15 per cent clay, and have a mean U-ratio of 1.1 ± 0.2 (Figure 14B). The largest clay content (43%) was determined from the shallowest sample (0.4 m depth), in the

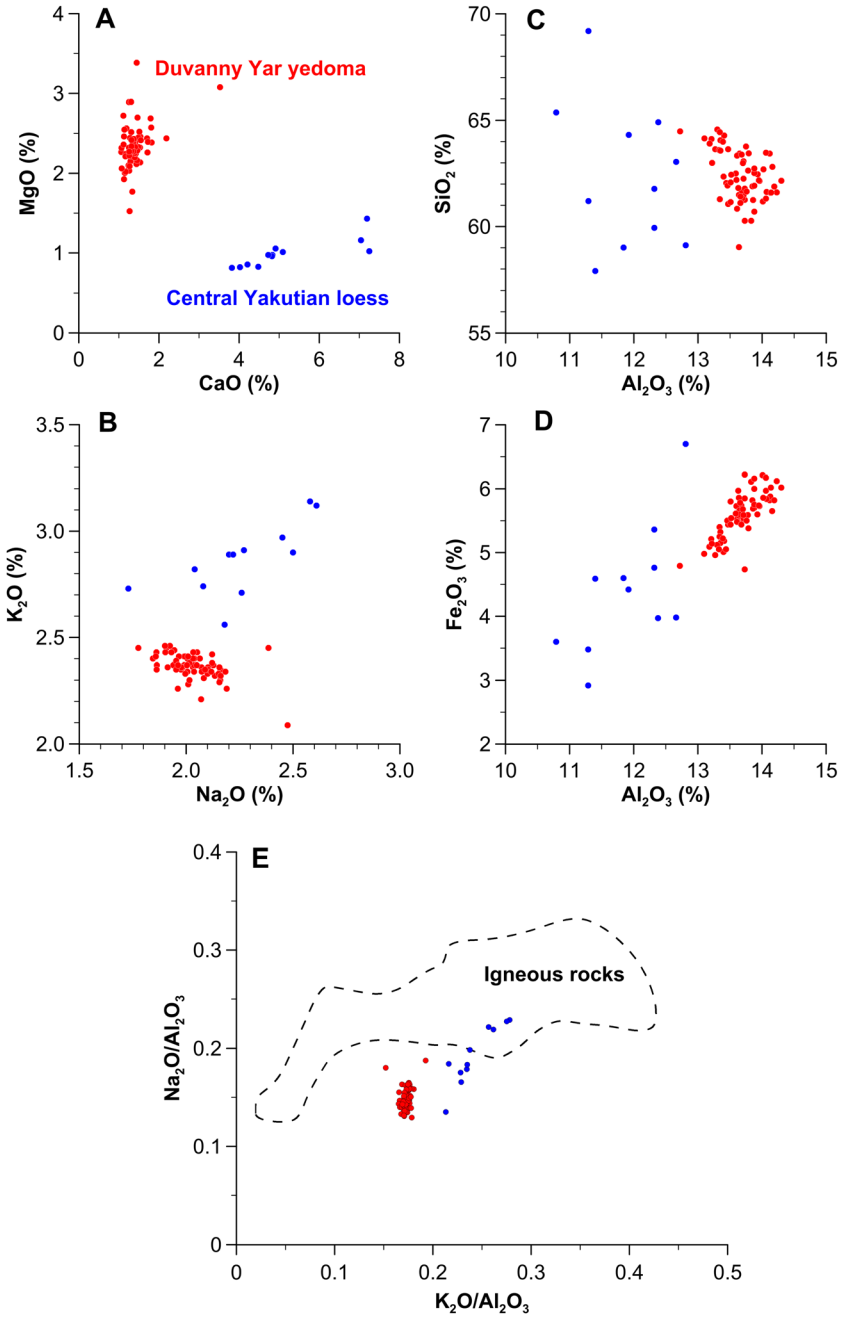

Figure 22 Major element concentrations from Duvanny Yar yedoma silt of unit 4, section CY (red circles) compared to loess samples from central Yakutia (blue circles). (A) MgO vs. CaO; (B) K_2O vs. Na_2O; (C) SiO_2 vs. Al_2O_3; (D) Fe_2O_3 vs. Al_2O_3; and (E) Na_2O/Al_2O_3 vs. K_2O/Al_2O_3. Dashed line in (E) indicates field occupied by unaltered igneous rocks (from Muhs and Budahn, 2006, Figure 5; compiled from Garrels and MacKenzie, 1971). Central Yakutian loess data from Péwé and Journaux (1983, table 6). This figure is available in colour online at wileyonlinelibrary.com/journal/ppp

modern soil within the active layer. Magnetic susceptibility values (average 8.0 x 10^{-5} SI units; range: 3.4–13.2 x 10^{-5} SI units) and carbonate contents (average = 4.45%; range 1.7–9.0%) are generally lower in the transition zone and active layer than in the underlying yedoma silt, and organic contents (average = 11.9%; range: 7–18.5%) are generally higher (Figure 14B).

INTERPRETATION AND DISCUSSION

Correlations and Depositional Processes

The stratigraphic units observed in the present study can be correlated with those previously recorded and interpreted in terms of their depositional processes.

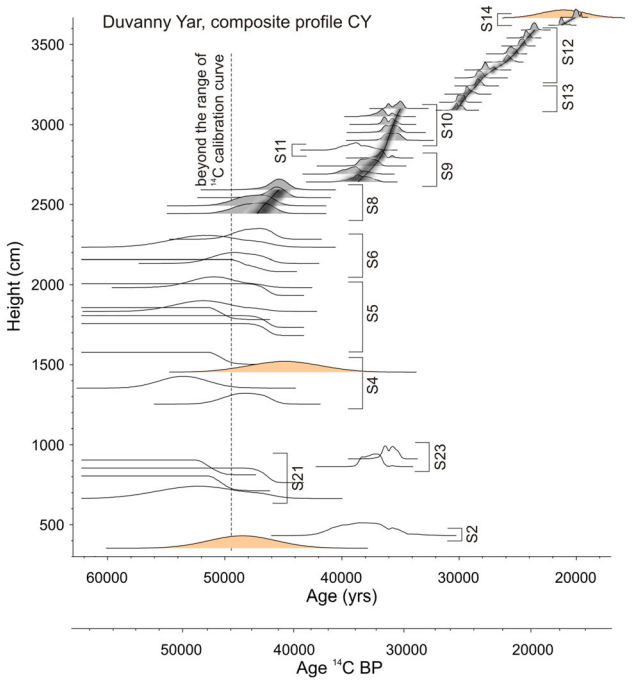

Figure 23 Age-height models of yedoma silt of unit 4 in the composite section CY at Duvanny Yar plotted on a scale that is common to both the ^{14}C and OSL ages (upper horizontal axis: age (yrs)). Uncalibrated ^{14}C ages are shown on the lower horizontal axis (age (^{14}C BP)). Grey-filled silhouettes represent probability distributions of individual calibrated ^{14}C ages used in the models, while unfilled silhouettes represent calibrated ages not used in the models. The OSL ages are shown by light brown-filled silhouettes, and correspond to ages of 21.2 ± 1.9 ka in section 14, 45.0 ± 3.1 ka in section 4 and 48.6 ± 2.9 ka below section 2. The best-fit models and model uncertainties are displayed by black lines and grey-scale shadows. S2 to S23 indicate individual section numbers within the composite section CY. This figure is available in colour online at wileyonlinelibrary.com/journal/ppp

Unit 1: Massive Silt.

Unit 1 is correlated with the bluish-grey silts (horizon 1) of the Sher *et al*. (1979) stratigraphy (Figure 3A; Table 2). The depositional history of the massive silt is not known. Possibly, the silt represents an old yedoma deposit, given its massive appearance, textural similarity to the yedoma silt of unit 4 and pollen assemblage characterised by Poaceae and forbs. It is clear that unit 1 underlies sediments attributed to deposition in a thaw lake (units 2 and 3; see below) and at that time they would have been within a talik and so unfrozen. Subsequently, the unit has refrozen, allowing post-thaw ground ice to develop within it. Thus, we support Sher *et al*.'*s* (1979) interpretation that unit 1 comprises taberal sediment that thawed in a former sublake talik and then refroze epigenetically. We interpret decimetre-thick lens-like ice bodies (Figure 6B) as thermokarst-cave ice, which indicates subsequent underground thermal erosion of ice wedges and refreezing of water in cavities.

Unit 2: Peat.

Unit 2 correlates broadly with peat identified in horizon 2 of the Sher *et al*. (1979) stratigraphy, indicated on Figure 3A by the peat lens several metres above river level near 6 km (Table 2). Precise correlation is uncertain, however, because the peat in our unit 2 directly overlies our unit 1, rather than being separated from it by a lower subunit of bluish-grey clayey silts reported by Sher *et al*. This uncertainty may reflect changing exposures from year to year and/or stratigraphic differences between remnants 7E (our study) and 6E (peat lens in Figure 3A).

A detrital origin of the peat is indicated by the abundant detrital plant material (including large wood fragments) and by the primary sedimentary structures indicative of sorting and sedimentation in unit 2. Thus, we discount the peat bog

Table 5 ^{14}C and OSL ages of samples from the outcrop at Duvanny Yar analysed in the present study.

Unit	Section	Sample number (mg C)	Altitude above river (m)	Poz-	^{14}C (BP) or **OSL (ka)**
5 (near-surface silt)	20	71	38.315	32565	70 ± 30
	20	72	38.115	32567	115±30
	20	73	37.885	32568	135±25
	20	74	37.635	32569	240±30
	20	75 (0.5)	37.405	32570	830±40
	20	76	37.265	32625	535±30
4 (yedoma silt)	14	69	36.7	32563	16 850±100
		Shfd10105	**36.65**		**21.2±1.9**
	14	70	36.2	32564	17 800±110
	12	57	35.9	32457	19 780±130
	12	58	35.4	32458	20340±140
	12	59	34.9	32490	20670±120
	12	60	34.4	32554	21400±150
	12	61	33.9	32555	21600±150
	12	62	33.4	32557	22900±170
	12	63	32.9	32558	23530±250
	13	64	32.4	32559	23630±190
	13	65	31.9	32560	24440±210

(*Continues*)

Table 5 (Continued)

Unit	Section	Sample number (mg C)	Altitude above river (m)	Poz-	^{14}C (BP) or **OSL (ka)**
	13	66	31.4	32561	25040±210
	13	67	30.9	32562	25340±220
	10	50	31	32417	30700±400
	10	51	30.5	32418	32100±500
	10	52	30	32419	31700±400
	10	53	29.5	32454	31400±600
	10	54 (0.7)	29	32455	31200±700
	11	56	28.4	32456	34000±700
	9	46	27.9	32487	32100±400
	9	47	27.4	32489	33100±500
	9	48	26.9	32415	34100±600
	9	49	26.4	32416	33700±600
	8	42	25.9	32483	42100±1100
	8	43	25.4	32484	42400±1100
	8	44	24.9	32485	44200±1400
	8	45	24.4	32486	44200±1400
	6	34	22.8	32376	44300±1300
	6	35	22.3	32377	48500±2200
	6	37	21.3	32378	45700±1700
	6	38	20.8	32302	>46000
	5	27	19.8	32369	47400±1900
	5	28	19.3	32370	>45000
	5	30	18.3	32371	48300±2400
	5	31	17.8	32373	>48000
	5	32	17.3	32374	>45000
	5	33	16.8	32375	>45000
	4	21	15	32301	>48000
		Shfd10103	**14.5**		**45±3.1**
	4	24	13.5	32232	49500±2000
	4	26	12.5	32368	45000±1500
	21	77	8.1	32626	>49000
	21	78	7.6	32627	>45000
	21	79	7.1	32628	>48000
	21	80	6.6	32629	48700±3500
	23	82 (0.7)	9.1	32631	31600±500
	23	81	8.6	32630	32800±600
	2	15 (0.4)	4.3	32300	33500±2000
		Shfd10102	**3.5**		**48.6±2.9**

Fifty-three ^{14}C ages, three OSL ages; all ^{14}C samples consisted of *in-situ* roots, except 71 (black peaty material). Poz- = Poznan laboratory number. Bold values indicate OSL data and ages.

interpretation of Kaplina *et al*. (1978) for section 1. Instead, we interpret unit 2 as a 'trash layer' that grades from detrital peat to stratified peaty silt, with the dominant plant material (woody detritus and aquatic moss remains) derived from vegetation in and around the lake. Wave and current action probably redeposited the plant material across the lake bottom, as well as sorting the silt into horizontal to subhorizontal layers and lenses. The similar particle size to that in the underlying unit 1 (Figure 8) is consistent with reworking of silt from that unit. Similar trash layers are common in the basal sedimentary sequences of thermokarst lakes in Alaska and northwest Canada (e.g. McCulloch and Hopkins, 1966; Hopkins and Kidd, 1988; Burn and Smith, 1990; J. B. Murton, 1996a) and in exposures along rivers in northeast Siberia (summarised in Anderson and Lozhkin, 2002).

Unit 3: Stratified Silt.

Unit 3 correlates broadly with the lower subunit of lacustrine loams and silts identified in horizon 2 of the Sher *et al*. (1979) stratigraphy (Figure 3A). However, we observed the silt in remnant 7E to *overlie* peat (Figure 6A–C), in contrast to the silt indicated by Sher *et al*. in remnant 6E near 6 km on Figure 3A, which underlies peat (Table 2).

We interpret unit 3 as lacustrine sediments deposited in an alas (thaw lake), consistent with the interpretation of Kaplina *et al*. (1978). The well-stratified unit, characterised by horizontal to subhorizontal parallel strata, is very similar to deposits that we have observed beneath drained alas lake basins in the Kolyma Lowland (Figure 28) and to well-stratified deposits beneath many drained thermokarst lake basins in Canada, Alaska, and elsewhere in

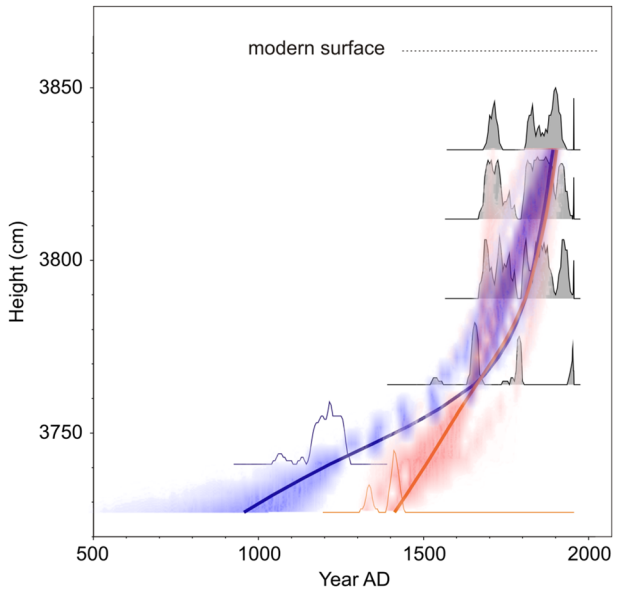

Figure 24 ^{14}C ages and age-height models through the near-surface silt of unit 5 of the composite section at Duvanny Yar. Grey-filled silhouettes represent probability distributions of individual calibrated ^{14}C ages used in both models. Calibrated ages used in one model only are shown with thin blue and orange lines. The best-fit models are shown with thick (blue or orange) lines, and uncertainties of the models are represented by blue and orange shadows. This figure is available in colour online at wileyonlinelibrary.com/journal/ppp

Siberia (J. B. Murton, 1996a; Kienast *et al.*, 2011, Figure 3). The type of stratification, abundant wood fragments and similar particle size to the underlying units are attributed to wave and current action in shallow water. Identification of the mollusc taxa, however, is needed to confirm this interpretation.

Unit 4: Yedoma Silt.

Unit 4 correlates with the upper subunit of grey-brown silts of horizon 3 in the Sher *et al.* (1979) stratigraphy (Figure 3A; Table 2). Our interpretation of yedoma silt deposition is set out below, after we have evaluated the associated palaeoenvironmental conditions and age model.

Unit 5: Near-surface Silt.

Unit 5 correlates with the veneer layer silts of horizon 4 of the Sher *et al.* (1979) stratigraphy (Figure 3A; Table 2). Geocryologically, unit 5 is a transition zone that represents a refrozen palaeo-active layer, the basal thaw unconformity of which marks a maximum thaw depth at some point in time after yedoma accumulation had ceased. Maximum thaw may have occurred during the early Holocene Climatic Optimum (Kaplina, 1981), although increased soil moisture and surface moss accumulation even in a warmer climate might lead to active-layer thinning. Alternatively, the maximum thaw may have occurred at the end of the Late Pleistocene, as discussed previously. The mineral silt within unit 5 therefore represents sediment that thawed from the underlying yedoma, prior to refreezing. Some colluvial silt in unit 5 at section 20 may have been deposited during or after the time of maximum thaw; this colluvial interpretation is based on the gently dipping cryostratigraphic features at this section (Figure 16), the location on the gently sloping margin of the yedoma exposures at Duvanny Yar (Figure 3A), and the six young ^{14}C ages of between 830 ± 40 ^{14}C BP and 70 ± 30 ^{14}C BP obtained mostly on *in-situ* roots within the transition zone (Figures 5 and 24). The present-day active layer, together with the underlying transition zone, corresponds to the recent *soil-permafrost complex* developed on yedoma beneath relatively flat surfaces in the coastal lowlands of northern Yakutia (Gubin and Lupachev, 2008).

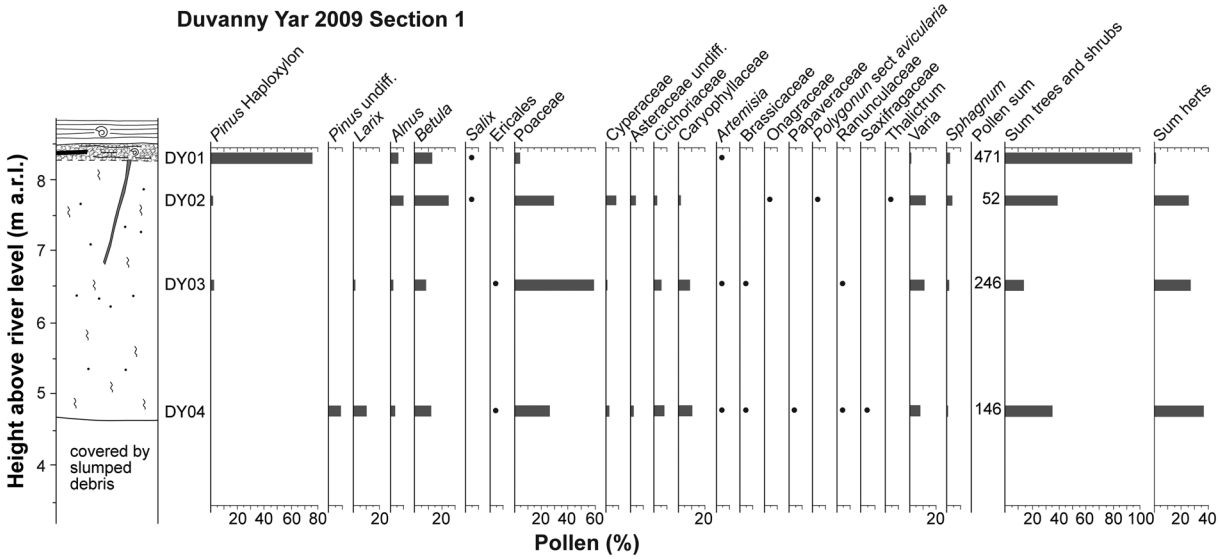

Figure 25 Pollen spectra from units 1 (massive silt; samples DY04 to DY02) and 2 (peat; sample DY01), section 1, Duvanny Yar. arl = Above river level.

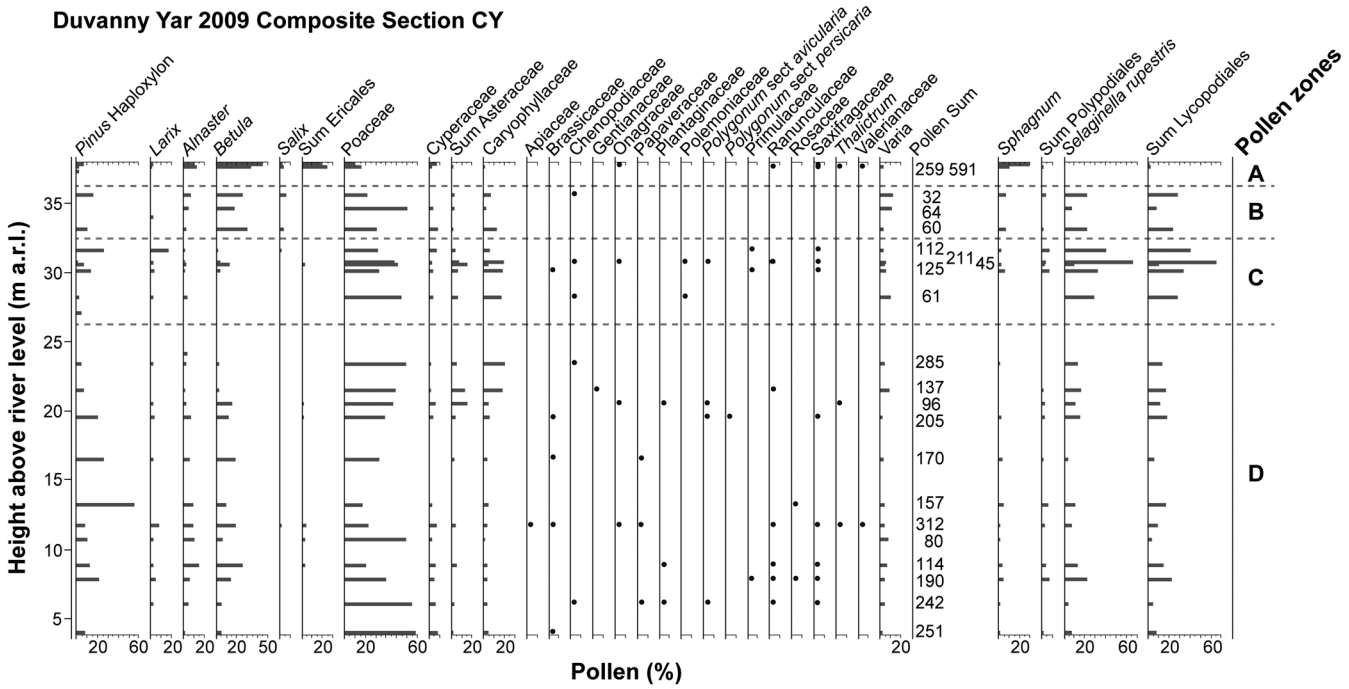

Figure 26 Pollen spectra from units 4 (yedoma silt) and 5 (near-surface silt), section CY, Duvanny Yar. Pollen zones are defined by sedimentary changes and/or dating unconformities. Zone D lies between about 5 and 26 m arl. Zone C (about 26–33 m arl) lies above an unconformity at palaeosol 4 and corresponds to the period just prior to the LGM. Zone B (about 33–37 m arl) dates to the LGM. Zone A comprises the two Holocene samples and aligns with unit 5. arl = Above river level; LGM = Last Glacial Maximum.

Age Model for Duvanny Yar Yedoma

Radiocarbon dating provides the main chronological framework for developing an age model for the yedoma silt in unit 4, supplemented by OSL dating.

Radiocarbon Dating.

Age-height models of the yedoma silt of unit 4 were built similarly to that for unit 5. One difference is that for ^{14}C ages older than 46 400 ^{14}C BP (before a calendar date of 50 500 BP), a ^{14}C calibration curve is not available, and so we assume that before 50 000 yr BP, differences between calendar and ^{14}C ages are constant and the same as at the oldest end of Intcal09. Thus, calendar dates of the oldest ^{14}C samples are regarded as very provisional; fortunately, this drawback affects few samples. Model calculations incorporated OSL ages.

Unlike previous ^{14}C dating attempts at Duvanny Yar (Figure 4), ^{14}C ages obtained in the present study revealed almost perfect stratigraphical order (Figure 23), pointing to rather continuous silt deposition in unit 4, with only a few discontinuities (at heights of 25.9–26.4 m arl, around 31 m arl and of 35.9–36.2 m arl). Significantly, these discontinuities coincide with boundaries between sections (8–9, 10–13 and 12–14, respectively), and the discontinuities at 25.9–26.4 m arl and around 31 m arl also coincide with the position of palaeosols 4 and 5 (Figure 5). By contrast, within individual sections, the age-height relations are quite smooth, strongly suggesting rather continuous sedimentation at heights of 12.5–25.9 m arl (over the sections 4, 5, 6 and 8), 26.4–31.0 m arl (sections 9, 11 and 10) and 30.9–35.9 m arl (sections 13 and 12). Because of the discontinuities between some sections, the age-height model was constructed in separate parts. The age difference between the upper sample in section 12 (at 35.9 m arl) and the lower one in section 14 (at 36.2 m arl) was not large (Figure 23), and one would be able to build a continuous model over sections 13, 12 and 14. However, the approach of making separate, independent models is considered to be more conservative and therefore more reliable.

In section 14, the model was based on two ^{14}C ages and one OSL age, and the latter is consistent with the former. The section accumulated between about 20 000 ± 300 and 19 000 ± 300 cal BP (16 500–18 000 ^{14}C BP), its average accumulation rate being similar to that in the underlying sections. In sections 13–12, all 11 ^{14}C ages formed a highly consistent series, indicating that these sections accumulated between about 30 200 ± 500 and 23 500 ± 400 cal BP (about 26 500–19 500 ^{14}C BP), and the accumulation rate was relatively constant during this period. Consistency of all ^{14}C ages in the series suggests a quasi-constant accumulation rate and that the samples did not contain any reworked organic material. This is a unique case, not revealed in the previous attempts of dating the yedoma silt at Duvanny Yar. One reason for this could be our focus on dating of *in-situ* roots. Ordinarily, ^{14}C dating studies

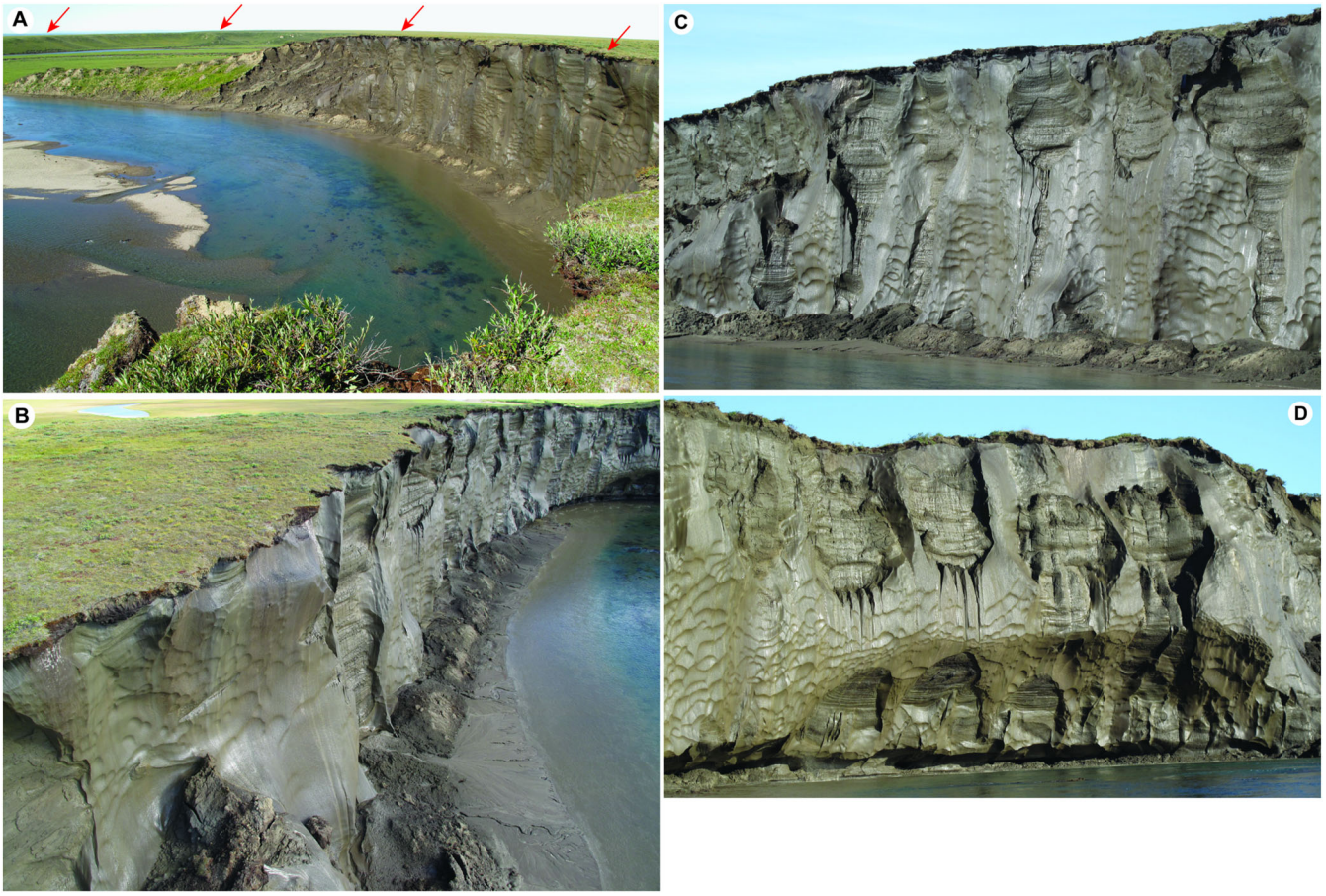

Figure 27 Yedoma silt with large syngenetic ice wedges exposed in the 34 m high bank of the Itkillik River, northern Alaska (August 2011). Note the relatively flat yedoma plain in (A) indicated by arrows. (B) to (D) show large syngenetic ice wedges (with scalloped surfaces) penetrating yedoma silt of units 3 and 4 in Table 6. Note bands within the yedoma silt. This figure is available in colour online at wileyonlinelibrary.com/journal/ppp

avoid sampling roots because they can contain ^{14}C signatures from plants living higher up in the soil profile. However, as argued previously, in permafrost profiles such as this, the transport distance is short, making the effect insignificant within analytical error. Moreover, roots buried within ground are less susceptible to redeposition compared with plant remains originally deposited on the ground surface.

Another consistent series of ^{14}C ages was obtained from nine samples in sections 9 and 10, indicating that this silt accumulated between about 39 000 ± 800 and 35 000 ± 500 cal BP (35 000–30 000 ^{14}C BP). The single-dated sample from section 11 that is somewhat offset from the series might result from (1) laboratory error of dating this sample, (2) reworked material present in this sample, or (3) contemporaneous layers of silt situated at different heights in different sections of the composite profile. That last effect is clearly demonstrated by the apparent inversion of ^{14}C ages at 30.9 m arl (section 13: 25 340 ± 220 ^{14}C BP) and 31.0 m arl (section 10: 30 700 ± 400 ^{14}C BP). In case of severe inversion, one usually claims that one or both of the ages is not representative and should be rejected. However, the ages of both samples fit the age-height models of the sections that they belong to. Thus, we conclude that the oldest silt of section 13 (about 30.9 m arl) started to accumulate about 4000 years after the youngest silt of 10 (about 31.0 m arl). This altitudinal shift between sections might reflect an originally undulating relief of the palaeo-land surface or perhaps post depositional slumping of frozen sediment. The occurrence of palaeosol 5 at approximately this level seems consistent with a period of a few thousand years of little or no silt deposition and hence soil formation during this missing part of the age model, from about 35 000 ± 500 to 30 200 ± 500 cal BP.

The oldest discontinuity in the profile is documented around 26 m arl (between sections 8 and 9), and its coincidence with palaeosol 4 again suggests a period of little or no silt accumulation, allowing limited soil formation to take place. Below it, all 17 samples from sections 4, 5, 6 and 8 (between 12.5 and 25.9 m arl) appeared older than 40 000 ^{14}C BP, and some of them gave non-finite ages (e.g. $>$ 46 000 ^{14}C BP). Despite large uncertainty, most of the finite ^{14}C ages revealed stratigraphical order. One

Table 6 Cryostratigraphic units, sediments, organic material and ^{14}C ages, ground ice and interpretation of the Itkillik exposure, northern Alaska (based on Kanevskiy *et al.*, 2011, and studies in 2011 and 2012).

Cryostratigraphic unit[a]	Sediment	Organic material and ^{14}C ages	Ground ice	Interpretation
1. Active and transient layers (0.5–1.0 m)	Organic-rich silt with some clay and very fine sand; grey-brown	Moss and peat (0.04–0.4 m thick) above mineral soil	Reticulate Cs with prominent vertical ice veins at contact between active layer and underlying transient layer 35–55% gravimetric ice content in transient layer	Modern active layer above transient layer that occasionally thaws
2. Intermediate layer (average 0.5 m; ≤1.08 m)	Organic-rich silt with some clay and very fine sand; yellow-grey	Peat inclusions 5,320 ± 35 ^{14}C BP @ 0.7 m depth 8,610 ± 35 ^{14}C BP @ 1.3 m depth (both on peat)	Ataxitic Cs, soil inclusions 3 x 8 mm to 10 x 30 mm 148% average gravimetric ice content (range: 54–233%) Ice wedges up to 2 m wide, up to 4 m high (penetrate in unit 3), white, clean	
3. Yedoma silt with thin ice wedges (11.5–12.5 m)	Silt; yellow-grey to uniform grey Lamination, subhorizontal, indistinct, occasional	Inclusions of poorly decomposed rootlets and twigs, small and rare 14 300 ± 50 ^{14}C BP @ 3.0 m depth 16 550 ± 75 ^{14}C BP @ 4.0 m depth 29 300 ± 200 ^{14}C BP @ 11.0 m depth (all on twigs)	33–142% gravimetric ice content Microbraided, microlenticular, microporphyritic Cs; ataxitic Cs in upper 1 m Ice veins, vertical to inclined ≤8 mm wide, isolated Syngenetic ice wedges (3–5 m wide at top), yellowish-grey (due to silt inclusions), some of them taper downward to 1–2 m wide, spaced 7–10 m apart; shoulders along sides (i.e. ragged lateral margins)	Windblown silt (loess) Shoulders of ice wedges indicate periods of slower sedimentation
4. Yedoma silt with thick ice wedges (13–15 m)	Silt, uniform; grey, brownish-grey or yellowish-grey Lamination, subhorizontal, indistinct, occasional	Inclusions of organic material, rootlets and twigs 26 300 ± 130 ^{14}C BP @ 15.0 m depth 23 900 ± 110 ^{14}C BP @ 16.0 m depth 41 700 ± 460 ^{14}C BP @ 23.0 m depth 15 500 ± 65 ^{14}C BP @ 28.0 m depth[b] (on twigs, except for fine-grained organic material @ 23 m depth)	41–104% gravimetric ice content (higher water contents in unit 4 silt relative to unit 3) Microporphyritic, microbraided, microataxitic, microlenticular Cs; several ice layers (*belts*) 2–10 mm thick, spaced 10–100 mm apart; ice lenses, wavy, inclined at 20–70°; ice veins, ≤2 mm wide, subvertical Syngenetic ice wedges (≤ 9 m wide, width fairly constant with depth), shoulders along sides Bodies of thermokarst-cave ice 0.4–3 m wide, 0.1–1 m thick	Windblown silt (loess) Major climatic shift to dry and cold period with aeolian activity

(*Continues*)

Table 6 (Continued)

Cryostratigraphic unit[a]	Sediment	Organic material and ^{14}C ages	Ground ice	Interpretation
5. Buried peat (2–3.5 m)	Organic silt with medium-grained sand grades upward into peat or occurs between two layers of peat	Peat; dark brown >48 000 ^{14}C BP @ 30.9 m depth (on peat)	Ice wedges from unit 4 penetrate through peat	Warmer and wetter conditions than unit 4
6. Buried intermediate layer (1 m)	Organic-rich silt	Peat inclusions	Ataxitic Cs with numerous ice belts ≤50–70 mm thick Ice wedges from unit 4 penetrate through buried intermediate layer	Period of slower sedimentation or changing climatic or environmental conditions
7. Silt with short ice wedges (≥2.7 m), underlain by gravel at depth of approximately 1.5 m below water level	Silt, similar to units 3 and 4	>47 500 ^{14}C BP @ 31.8 m depth (on fine-grained organic material, from the thermokarst-cave ice)	Ice wedges from unit 4 penetrate through silt to the depth of more than 1 m below the water level Buried ice wedges <0.7 m wide, 2.5–3.0 m high Bodies of thermokarst-cave ice	

[a]Thickness in metres.
[b]Age regarded as probably invalid. Cs = Cryostructure.

Figure 28 Stratified alas lake silts, Cherskii Dump site. (A) Horizontal to subhorizontal undulating to planar parallel strata. (B) Close-up photograph of well-developed lamination. Trowel for scale in both photographs. This figure is available in colour online at wileyonlinelibrary.com/journal/ppp

exception is the age at 22.3 m arl, older than the ages of three underlying samples. The second one is an inversion of ^{14}C ages between 12.5 and 13.5 m arl. Taking into account that the younger age (at 12.5 m arl) is concordant with the OSL age at 14.5 m arl, whereas the older one (at 13.5 m arl) is not, one could suggest that the samples collected from 22.3 and 13.5 m arl might contain reworked material, and that the silt in sections 4–8 accumulated between 50 000 ± 2000 cal BP and 45 400 ± 700 cal BP. This seems to allow extrapolation below 8.1 m arl, where one finite ^{14}C age in section 21, and the concordant OSL age at 3.5 m arl suggest that the silt also accumulated around 50 000 ± 4000 cal BP. However, as indicated by Pigati *et al.* (2007), ^{14}C dating near the limit of the method is very tricky, since extremely little modern carbon turns infinite radiocarbon ages into apparently finite ones. Therefore, we must admit that in the sections where infinite and finite ^{14}C ages appear alternately (sections 2 and 4–6), the silt may have been deposited well before 50 000 cal BP, although such

an interpretation is not supported by the two OSL ages of 45.0 ± 3.1 ka and 48.6 ± 2.9 plotted on Figure 23. Further investigations of potential contamination by older or younger carbon are required.

Previous attempts of ^{14}C dating the yedoma at Duvanny Yar (e.g. Kaplina, 1986; Tomirdiaro and Chyornen'kiy, 1987; Gubin, 1999; Y. K. Vasil'chuk, 2006), performed on different profiles from different outcrops (Table S1), have provided stratigraphically consistent age series in the upper parts of the profiles (Figure 4), with the ages monotonically increasing back to about 36 000–38 000 cal BP (about 31 000–33 000 ^{14}C BP). But in the lower parts, the age-height pattern appears confusing, with ^{14}C ages at roughly the same heights covering extremely wide intervals (from about 31 000 to > 50 000 ^{14}C BP). Based on this, and on the ages from microinclusions and alkali extracts (Table S4), Y. K. Vasil'chuk (2006) concluded that most of the dated material has been reworked, and proposed that the most representative ages for silt deposition were the youngest ^{14}C ages obtained in each horizon (Table S2; dashed line in Figure 4). Alternatively, the large scatter of ^{14}C ages in the lower parts of the yedoma could also result from contamination by silt that has slumped from higher elevations.

OSL Dating.

Briant and Bateman (2009) reported ^{14}C age underestimations where old (>35 ka) ^{14}C ages from fluvial deposits in eastern England were compared with OSL ages. Although contamination from older carbon potentially is high in permafrost regions (where organic decomposition is limited and older carbon can be recycled and frozen), radiocarbon ages obtained in the present study appear concordant with the independently derived luminescence ages, which are based on the sediments themselves. Moreover, the moisture content of the silt at Duvanny Yar has probably varied little in comparison to that at many non-permafrost sites because the silt became frozen in the aggrading permafrost. Given this concordance, one could claim for rapid sediment aggradation between 3 and 26 m arl between approximately 50 and 44 ka (Figure 23). However, as argued previously, we cannot exclude the possibility that the silt in the lower part of the profile (below 24 m arl) was deposited before 50 ka.

Substrate and Palaeo-land Surface during Yedoma Silt Deposition

To elucidate the processes that deposited yedoma silt at Duvanny Yar, we first evaluate the substrate and palaeo-land surface associated with unit 4.

Cryopedoliths.

Cryopedoliths constitute most of the yedoma silt in unit 4 at Duvanny Yar and indicate that pedogenesis was a key postdepositional process. Cryopedoliths comprise sediments that have experienced incipient pedogenesis along with syngenetic freezing. They have properties that reflect pedogenic processes but lack well-expressed buried soil profiles (Gubin, 1994, 2002). Cryopedoliths that formed during MIS 4 and MIS 2 have very similar morphological and chemical properties and contain no known buried epigenic soils (i.e. soils that developed on a land surface that was not subject to deposition of soil-forming material). Several boreholes drilled at Duvanny Yar by D. Gilichinsky revealed – during drilling and sampling of cores for microbiological purposes – that MIS 4 deposits contain no significant organic layers or soil-like bodies to the depth of 15–20 m below the water level of the Kolyma River at the locations drilled (D. Gilichinsky, personal communication, 2009); we note, however, that the datum is not constant, and we report LIG deposits (unit 2) above river level (Table 4).

Colour bands within the cryopedolith are thought to reflect the structure of plant cover, its productivity and trends of mineralisation, and humification of plant remnants in the upper horizons of synlithogenic soils. Cryopedolith within the active-layer soil profiles, however, must have thawed each summer probably for hundreds of years before incremental accumulation of silt allowed perennial freezing of organic matter within permafrost. Prior to freezing in permafrost, changes of the organic matter may have taken place in significantly different bioclimatic conditions that are specific for the upper band of accumulated material, as confirmed by the penetration of plant roots through two or more differently coloured layers.

Cryostructures (Table 4) and microcryostructures (Figures 17–19), with characteristic banding of lenticular and bedded types, are typical of syngenetic permafrost (French and Shur, 2010; Kanevskiy *et al*., 2011) and record progressive stacking and amalgamation of palaeotransient layers superimposed on each other following silt accumulation and permafrost aggradation. *In-situ* fine roots are pervasive in cryopedoliths (Figures 17C, 18 and 19A, B) and are interpreted to indicate a vegetated land surface on which the silt accumulated. Mineralised and humified organic remains are dispersed within cryopedoliths (Figures 17A, 18A and 19A), indicating incipient soil formation, but distinct soil horizons are absent.

Preservation of organic matter is determined by (1) low temperatures of the active layer in relict cryosynlithogenic soils, (2) low metabolic activity of microorganisms and (3) rapid incorporation of the material into aggrading permafrost. Organic carbon in cryopedoliths occurs mostly as fine, dispersed detritus of mosses, shrubs and herbs. A minor part occurs as humic and fulvic acids, root remains, seeds, spores and pollen. The relatively high soil organic carbon (SOC) content (0.6–2.4% by weight) of cryopedoliths is one of their main diagnostic features.

Significant differences in SOC have previously been obtained between MIS 2 and MIS 3 cryopedoliths examined at other sections at Duvanny Yar (Gubin, 1994, 2002; Zanina *et al*., 2011). The upper 25 m of cryopedoliths (MIS 2) contain about 0.6–1.4 per cent SOC (n = 60), whereas the underlying material of MIS 3 cryopedoliths contains 0.8–2.4 per cent SOC (n = 80). Buried epigenic

soils contain 1.8–4.0 per cent SOC (n = 30). The SOC content of cryopedolith layers can vary spatially by ± 10 per cent of total organic carbon content. These spatial differences are expressed more strongly in MIS 3 cryopedoliths than in MIS 2 ones.

Palaeosols and Chemical Weathering.

Pilot studies of palaeosols at Duvanny Yar conducted by S. V. Gubin (1984) described four buried palaeosols and a thick layer of allochthonous peat (equivalent to palaeosol 3 in Figure 5). In the present study, five buried palaeosols and palaeosol 'complexes' are identified between the cryopedolith materials in unit 4 of section CY (Figures 5, 14A, 20 and 21A), and one palaeosol in section 22 (Figure 7). Their stratigraphic expression varies, with only three palaeosols identified in the field, as organic layers (1 and 2) or root-rich layers (Figures 5 and 20A). From oldest to youngest, the palaeosols are identified as follows. Palaeosol 'complex' 1 is identified from the three root-rich layers between 6.2 and 6.6 m arl (Figure 5); the term *complex* denotes the close vertical stacking of three thin individual palaeosols. Of these, only the uppermost is involuted, at both macro- and microscale (Figure 20A–C). Palaeosol 2 (11.7 m arl) is the most obvious palaeosol observed, on account of (1) its expression as an organic layer that forms a stratigraphic marker, (2) involutions within it and (3) a thaw unconformity beneath it that is interpreted to mark the maximum ALT when the soil underlay the land surface (Figure 9A, D, E). Characteristics (1) and (2) also apply to the unnumbered palaeosol in section 22 (Figure 7).

Palaeosols 3 and 4 are identified from their sediment properties alone, which they share with the field-identified palaeosols 1, 2 and 5 and with the modern soil (Figs. 14A and 21A). Palaeosol 3, at about 21–22 m arl, has elevated organic contents and slightly depressed magnetic susceptibility values (Figure 14A), as well as elevated phosphorus and lower mobile-to-immobile element ratios (Na_2/TiO_2, SiO_2/TiO_2, MgO/TiO_2, K_2O/TiO_2) (Figure 21A). Elevated organic contents are expected when input of mineral silt declines, allowing build-up of plant material in a soil profile. Depressed magnetic susceptibility values are attributed to a reduced supply of coarse-grained magnetic minerals during soil-forming episodes, similar to the lower magnetic susceptibility signal of palaeosols in loess from central Alaska (Begét, 2001) and western and central Siberia (Chlachula, 2003). Elevated phosphorus values are attributed to surface enrichment by pedogenic processes (Muhs *et al*., 2003), and depressed mobile-to-immobile element ratios to chemical weathering of detrital silt particles and loss of mobile elements, as also found in central Alaskan loess (Muhs *et al*., 2008). Palaeosol 4 (about 25.4–26.5 m arl) also exhibits all four of these characteristics, as do some of the samples from the transition zone in unit 5 above the yedoma, where the drop in magnetic susceptibility values attributed to Holocene pedogenesis is particularly striking. The other field-identified palaeosols share these characteristics, but they also show elevated clay concentrations (see palaeosols 5 and 2, and palaeosol complex 1 in Figure 14A) that we attribute to a higher degree of pedogenesis (and hence field expression) than that associated with palaeosols 3 and 4. Palaeosol 5 (30.2 m arl) is more subtle than palaeosols 3 and 4, being a thinner, laterally discontinuous organic layer (2) and lacking involutions (Figure 10A). All five palaeosols, as well as the modern soil, show some elevated Ti/Zr ratios and clay contents (Figure 21A). Higher Ti/Zr ratios are often expected in palaeosols because Ti tends to be enriched in clay minerals, and Zr is found only in zircon, which usually occurs in the coarse silt or sand-sized fraction.

Collectively, the five palaeosols in unit 4 vary from weakly developed (incipient; 3 and 4) to moderately developed (in order of development: 1, 5 and 2). Such variability may reflect: (1) cold-climate conditions with limited soil development and chemical weathering; (2) variations in the rate of supply of mineral particles during soil formation (cf. Höfle *et al*., 2000; Kemp, 2001; Sanborn *et al*., 2006); (3) discontinuous grass cover, which also slowed soil formation because less organic material was available for pedogenesis, especially on higher ground; and (4) variable spans of time during which the palaeosols developed. We hypothesise that soils were best developed and most organic-rich in depressions, where more vegetation grew. We speculate that high-resolution vertical sampling may identify additional palaeosols. Correlations of the palaeosols in unit 4 of section CY with those identified previously at Duvanny Yar and Stanchikovsky Yar are discussed in Appendix S5, and the palaeosols are illustrated in Figures S7 and S8.

Cryopedolith formation and pedogenesis extended across much of the land surface. But the resulting features (e.g. soil profiles, detritus, roots) are preserved only in the yedoma silt between the ice wedges, particularly in the central parts of the silt columns (Gubin, 2002; Gubin and Lupachev, 2012). Vertical and horizontal growth of ice wedges repeatedly erased and renewed this surface, with the result that there are no clear data on soils above them. Significantly, the buried soils at Duvanny Yar change their structure and properties along the several kilometres of the exposure, even grading into the material of other deposits.

ALT during formation of palaeosol 2 was probably similar to that of the present day. If the thaw unconformity beneath palaeosol 2 developed when the palaeo-land surface was at or above the top of the organic layer shown in Figure 9D and E, then the apparent ALT recorded by the unconformity is about 0.7 m. The original ALT was significantly less, because the value of 0.7 m includes the volume of ground ice now contained in the underlying buried transition zone, which we estimate to have subsequently raised the palaeo-land surface by about 0.3 m or more, indicating an original ALT of about 0.4 m, similar to the present-day ALT.

Infilled Rodent Burrows.

Infilled rodent burrows within cryopedoliths at Duvanny Yar (Zanina *et al*., 2011) provide palaeoenvironmental information about contemporaneous vegetation, drainage

and palaeo-ALTs. Subhorizontal galleries (3–5 cm in diameter) are filled with excrement, and processed moss and herbs occur in the uppermost horizons of palaeosols 3 and 4 (Figure 5). Vertical burrow systems of different age in allochthonous peat (palaeosol 3) suggest that peat accumulation was interrupted by long periods with a stable surface.

Abundant seeds, detritus, hair, insects and excrement have been found within buried rodent burrows in cryopedolith deposits of MIS 3 age (Lopatina and Zanina, 2006; Gubin *et al*., 2011; Yashina *et al*., 2012). The radiocarbon age of the organic material is 28 000–32 000 yr BP. Analysis of the store chamber material shows that it can contain 600 000–800 000 seeds of more than 80 species and indicates the complex structure of plant communities that existed when the cryopedoliths formed during MIS 3. Pioneer communities and mosses are dominant in this structure. Because of the relatively rapid burial and freezing of burrows, their organic infill tends to be well preserved. Indeed, a number of viable plants have been grown *in vitro* and a few plants of *Silene stenophylla* Ledeb. (Caryophyllaceae) were even brought to flowering and fruiting and they set viable seeds (Yashina *et al*., 2012). Similar burrow fills of *Urocitellus parryii* were analysed from cryopedoliths of other regions of north Yakutia. This Arctic species of ground squirrel occupies well-drained lake, river and sea banks with steppe-like and pioneer vegetation communities.

The gallery structure of buried burrows is simpler than that of modern ones. In the former, the store chamber – containing seeds – lies above the bottom of the palaeo-active layer and often is connected to the palaeo-land surface by a single tunnel. The palaeo-land surface itself is identified by a thin layer of cryopedolith enriched in rodent excrement. Burrow exits have no clear expression in former microrelief.

Palaeo-ALTs of about 60–80 cm for MIS 3 cryopedoliths have been inferred from the base of store chambers relative to the palaeo-land surface (Zanina, 2005). The cryopedoliths contain less ice than the relatively ice-rich active layers and transient layers associated with buried epigenic soils. Thus, the values of 60–80 cm for cryopedolith ALTs will not change significantly as a result of soil thaw. Such values are similar to modern ALTs in the Duvanny Yar region. But compared with modern active layers, the palaeo-active layers associated with the cryopedoliths formed beneath a thinner near-surface organic horizon, within drier soils and were probably associated with lower permafrost temperatures resulting from substantially colder winters.

Vegetation.

The pollen samples placed in MIS 2–4 are not readily distinguishable into subgroups (Appendix S4), though samples dating to the LGM (zone B in Figure 26) are notable for an absence of *Larix*. Low arboreal pollen values and high values of Poaceae, forbs and *S. rupestris* in samples dating from about 30 000 ^{14}C BP to about 33 000 ^{14}C BP indicate cold and/or dry conditions similar to those from the LGM or indeed to other LGM samples described from northeast Siberia (Anderson and Lozhkin, 2001). However, *Larix* pollen is present in these older samples. Further variation is evident in the lower part of the main section. Between about 12 and 22 m arl, three samples show higher values of *Pinus* (haploxylon) and lower values of Poaceae.

It is likely that woody taxa survived the LGM in favourable sites in Siberia (Binney *et al*., 2009; Werner *et al*., 2010). *Larix* pollen is poorly distributed and easily damaged, and its occurrence is conventionally taken to indicate the nearby presence of the taxon. *Betula* pollen is more readily transported and better preserved. Although it may represent local plants, it could also reflect the regional occurrence of *Betula* in favourable sites (such as the Kolyma River valley). Relatively high arboreal pollen values, particularly those of *Pinus*, can also reflect long-distance transport (LDT) of pollen, which may vary depending upon sediment accumulation rates and atmospheric conditions. To assess whether the arboreal pollen values are largely a function of overall low pollen presence in the sediments, we checked whether the percentage of *Pinus* was correlated with the pollen sum, as would be the case if there were a bias due to low counts, or with the pollen exotic ratio, which reflects pollen concentration. Neither test was significant ($r^2 = 0.019$ and 0.055, respectively).

The explanation may be linked to the processes of yedoma silt deposition, assuming a contribution from both local and LDT pollen. When material accreted rapidly (as during the LGM, according to the age model), silt would have been trapped by the vegetation cover, which was probably largely non-woody, as most forb pollen (which is entomophilous) is produced in low amounts and not transported far. However, the windy conditions likely enhanced LDT of arboreal pollen from other regions. Conversely, during periods of relative quiescence and little or no silt deposition, the pollen spectra reflected predominantly local vegetation, which, for most periods, would still have had a large component of non-arboreal (herb) taxa. If this interpretation is correct, pollen values are partly a function of climate, but the arboreal/non-arboreal pollen ratio cannot be directly interpreted as reflecting favourable or less favourable conditions for woody plant growth (i.e. periods of climate amelioration). We conclude that during much of the Karginsky interstadial it was possible for *Larix* to persist in the region, and that the ground surface at Duvanny Yar was seldom bare during deposition of yedoma silt, being dominated by grasses and forbs. Given the ample evidence of an herbivorous megafauna (Sher *et al*., 2005), even during the LGM, this interpretation appears reasonable. Such vegetation as well as the ground squirrel requirements for well-drained substrates, all co-existing while silt aggraded incrementally on the land surface, indicate that silt deposition occurred under subaerial conditions. For further discussion of pollen spectra origin and characteristics, see Appendix S4.

Permafrost and Ground Ice.

Permafrost existed continuously during deposition of yedoma silt at Duvanny Yar, experiencing only small-scale

thermokarst and thermo-erosional events unrelated to climate change. Continuity is inferred from cryostructures (Figures 17–19) and large syngenetic ice wedges extending vertically through unit 4. The wedges grew syngenetically upwards as incremental silt deposition resulted in a rising permafrost table. Although thaw truncation of some wedges is indicated by their shoulders (Figure 9C), preservation of wedge ice indicates that thaw depth was limited, only truncating the tops of the wedges along the base of the contemporary palaeo-active layer. Preservation of syngenetic ground ice in unit 4 and the apparent absence of thaw modification structures (J. B. Murton and French, 1993) allow us to discount permafrost thaw other than that associated with active-layer fluctuations. No evidence was observed for talik formation as might develop beneath deep lakes or river channels, except for the inferred taberal sediments of unit 1 (Table 4), which signifies that there has been no significant subsidence of the yedoma profile in section CY in the past.

Cryoturbation within palaeo-active layers was limited or absent during silt accumulation, and significant only during certain soil-forming episodes. Evidence for cryoturbation in unit 4 is limited to involuted organic layers, which include folds with a relief of $\leq$ 20–30 cm (Figures 7, 9E and 20A). The involutions, however, contrast with the sharp planar base of organic layer 2 (palaeosol 5) and the horizontal to gently undulating banding and, occasionally, the sedimentary stratification in the cryopedolith. Such limited cryoturbation is consistent with rapid sediment accumulation (limiting the time for cryoturbation) and/or a relatively dry palaeo-active layer (limiting the moisture supply for ice segregation). Although cryoturbation appears to have been minimal during silt accumulation, the growth of large syngenetic ice wedges added volume to the substrate incrementally, resulting in vertical extension and some lateral deformation of the silt. The volume of silt also increased due to accumulation of segregated ice within it.

Palaeo-land Surface Relief.

An undulating palaeo-land surface with a relief of several metres or more is indicated by the variable elevations of palaeosols identified by Zanina *et al*. (2011) along several kilometres of exposures at Duvanny Yar. The elevation ranges recorded for three Late Karginsky palaeosols are 5, 10 and 2 m. Such variation is consistent with Y. K. Vasil'chuk's (2005) findings that bed elevation varies by several metres in different stratigraphic sections and with our own observations that show palaeosol 5 to gently dip and range in elevation by about 0.5 m across a lateral distance of several metres.

Deformation of the ground surface resulted from ice-wedge growth, which added a volume of approximately 45 per cent to the upper 8 m of unit 4. Such added volume of wedge ice must be accommodated by deformation of the wedges and/or lateral or upward displacement of adjoining ground (Leffingwell, 1915). In addition, ice wedges may gradually rise through adjoining ground (Black, 1974, 1983) because of (1) density differences (the wedge ice is less dense than the surrounding silt) and (2) summer expansion of permafrost on either side of ice wedges (which laterally compresses wedges) (Mackay, 1990). Gradual rise of ice wedges occurs during formation of low-centred polygons.

In conclusion, the silt accumulated as a mantle or drape across an undulating land surface rather than a flat and horizontal plain underlain by a layercake stratigraphy. This argument for deposition as a sedimentary drape also applies at the overall scale of the Duvanny Yar sections, where both the base and the top of the yedoma are convex-upward (Figure 3A; Y. K. Vasil'chuk, 2005; Sher *et al*., 1979; Wetterich *et al*., 2011a), rising in the centre of the 12 km long sections by several metres or more. The elevation ranges of the undulating palaeo-land surface at Duvanny Yar, however, were probably insufficient to favour widespread and frequent hillslope erosion and reworking of silt, unlike in Late Pleistocene silty regions with well-developed gulley or valley networks (see, for example, Vreeken and Mücher, 1981; Vreeken, 1984).

Erosion during Syngenetic Permafrost Formation.

At least one episode of erosion interrupted silt accumulation in unit 4. Syndepositional erosion of silt is indicated by the angular unconformity (erosion surface) about 13.7 m arl, which truncates at low angle some colour bands in the underlying silt (Figures 5 and 9A–C). The silt above and below the unconformity is texturally similar (Figure 14A), with no evidence of any coarse lag above it. Erosion may have occurred by running water or, possibly, by wind (deflation), probably in summer, when the silt surface was unfrozen. Deflation of silt during winter, however, cannot be excluded, as this process can occur in present-day cold-climate regions, as indicated by blowouts in western Greenland (Dijkmans and Törnqvist, 1991).

Sediments of the Alyoshkin Suite.

Sediments of the Alyoshkin Suite are contemporaneous with the final stages of yedoma silt deposition at Duvanny Yar. The sediments underlie the 15–20 m high Alyoshkina terrace at Alyoshkina Zaimka (Figure 2A) and are interpreted by Sher *et al*. (1979) as channel and floodplain deposits. The putative channel deposits, however, differ significantly from the yedoma silt in section CY: (1) they are generally coarser grained, comprising silty sand and fine- and medium-grained sand; (2) they include both well-developed horizontal stratification and cross-stratification, with the steepest foresets dipping at $>$ 30°; (3) unconformities within the sands are obvious and numerous (Sher *et al*., 1979, Figure 22); (4) sand wedges and composite (ice-silt/sand) wedges are present within them; and (5) the maximum sizes of the wedges (about 5 m high and 2.5–3.5 m wide) are distinctly smaller than those of the large syngenetic wedges in the yedoma. Hopkins (1982) interpreted these sediments as aeolian dune sand, which we believe better explains their contained: (1) foresets, at or near the angle of repose of the sand; (2) sand, ice and

composite wedges at several levels, with the sand wedges and composite wedges probably comprising aeolian sand (J. B. Murton *et al*., 2000); (3) unabraded and articulated bison skeleton observed by Hopkins; and (4) roots. The sandy deposits at Alyoshkina Zaimka appear similar to those of the Late Pleistocene Kittigazuit Formation in western Arctic Canada. The latter was originally interpreted as deltaic in origin (Mackay, 1963, p. 21; Rampton, 1988), but re-interpreted by Hopkins (1982) and Vincent (1989) as aeolian dune sand, an interpretation later supported by detailed sedimentological studies (Dallimore *et al*., 1997; Bateman and J. B. Murton, 2006; J. B. Murton *et al*., 2007).

The floodplain deposits of Sher *et al*. (1979) – which occur mainly in the lower part of the Alyoshkina Zaimka section – comprise silts and silty sands containing abundant grass roots and stems, and ice wedges as wide as 2 m. Radiocarbon ages of 15 000 ± 200 ^{14}C BP and 14 980 ± 100 ^{14}C BP from roots and grass stems in these deposits 1.5–2.0 m above the flood level of the Kolyma River (Sher *et al*., 1979) suggest that deposition occurred during the latter part of MIS 2. Significantly, this is the same time as yedoma accumulated at Duvanny Yar, where the ice-wedge complex in the yedoma is thought to have ceased forming about 14 000–13 000 ^{14}C BP, at an elevation of about 50 m arl. This is based on dating of the host yedoma and of organic inclusions within ice-wedge ice (Y. K. Vasil'chuk *et al*., 2001a; Y. K. Vasil'chuk, 2005), including radiocarbon ages of 13 080 ± 140 ^{14}C BP obtained from soil about 51 m arl (Gubin, 1999, in Y. K. Vasil'chuk *et al*., 2001a) and 13 500 ± 160 ^{14}C BP obtained from a palaeosol at the top of the yedoma (Zanina *et al*., 2011).

Depositional Processes of Yedoma Silt

Deposition of the > 34 m thick sequence of yedoma silt in unit 4 at Duvanny Yar (with its ubiquitous fine roots, > 30 m high syngenetic ice wedges, buried palaeosols and age spanning an interval from before about 50 000 to after 20 000 cal BP) requires subaerial conditions, permafrost and silt deposition persisting for tens of thousands of years. In light of these conditions, we evaluate the three main hypotheses concerning the processes and environmental conditions of yedoma silt deposition.

Alluvial-lacustrine Hypothesis.

The first hypothesis that interpreted yedoma silt primarily as floodplain alluvium was proposed by Popov (1953, 1973), and most Russian permafrost scientists have supported it (reviewed in Péwé and Journaux, 1983). Sher *et al*. (1979) interpreted the yedoma silt of the Kolyma Lowland as alluvium deposited on the floodplain of the palaeo-Kolyma River (Table 2). Channel alluvium was thought to be restricted mainly to the lower part of the yedoma exposure at Duvanny Yar and was inferred from sand facies (≤25 m arl), some of which are cross-bedded (Sher *et al*., 1979, Figure 18). In addition, overbank floodplain alluvium, possibly with some channel bar deposits, was thought to make up the bulk of the grey-brown silts of horizon 3 (Figure 3A; Kaplina *et al*., 1978); unfortunately, Figure 3A, modified from Sher *et al*. (1979, Figure 14), does not identify the putative channel bar deposits. Arkhangelov *et al*. (1979) also concluded that the upper part of the Duvanny Yar yedoma was formed mostly by floodplain silt but contained several relatively thin layers of channel alluvium (sands and silts, sometimes with cross-bedding). Rosenbaum and Pirumova (1983) compared the yedoma silt with the sediments of the modern floodplain of the Kolyma River near Alyoshkina Zaimka.

Problems with the alluvial hypothesis were raised by Sher *et al*. (1979). (1) Why were channel facies of minor significance in the upper part of the yedoma? (2) What explained the excessive thickness (>20 m) of floodplain alluvium? (3) The abrupt switch in tectonic movement from continuous subsidence (needed for thick accumulation of alluvium) to uplift (needed for river incision by about 50 m) was unsubstantiated. (4) How wet was the surface beneath which the large syngenetic ice wedges developed in the yedoma? Very dry surface conditions would tend to limit the amount of surface water-derived ice infilling thermal contraction cracks, whereas very wet conditions (e.g. during submergence of the river floodplain) would tend to melt the ice wedges.

A variant on the floodplain hypothesis emphasised lacustrine deposition and invoked deposition under cycles of lacustrine, alluvial and boggy conditions on the palaeo-Kolyma floodplain (Figure 2A), similar to lacustrine and alluvial sedimentation on the modern lake-dotted floodplain (Y. K. Vasil'chuk, 2005, 2006). Deposition alternated between (1) a large shallow-water lake (or lakes) or mixed lake-river basin in which silts accumulated, and (2) a subaerial, boggy floodplain on which peaty lenses accumulated in some locations and almost organic-free sandy loams in others. Such deposition applied to the central and highest part of the 10 km long sections (Figure 3A), while 'wash-out' processes (e.g. slopewash) redeposited silts in depressions around its margin. In the final stages of silt accumulation, an alas-type lake basin developed on the sloping ground around the central dome, partially reworking and redepositing the sediments within a terrace-shaped bench. Further details about this interpretation are given in Appendix S1.

The hypothesis of alternating subaqueous and subaerial deposition, rather than climatic change, is integral to a model of syngenetic ice-wedge growth (Y. K. Vasil'chuk *et al*., 2001a; Y. K. Vasil'chuk, 2006). The model envisages rapid ice-wedge growth during subaerial phases of sedimentation (when peaty layers accumulate) and slow or no growth during subaqueous phases of sedimentation (when loam, sandy loam and sand accumulate). The peat is characterised by abundant allochthonous organic material eroded from river or lake banks by alluvial and lacustrine processes, and resembles peaty layers in oxbow lakes. Winter climatic conditions – interpreted from almost constant δ^{18}O and δD values of syngenetic wedge ice in yedoma (see Appendix S2) – remained stable throughout

the ≥ 30 000-year-long period of ice-wedge formation. As a result, the properties of the wedges and host silts are attributed primarily to changes in the erosion level and sedimentation – arising from events such as floods inundating the palaeofloodplain, damming of small rivers or coastal subsidence – rather than from climatic change (Y. K. Vasil'chuk, 2006).

We discount the alluvial hypothesis at Duvanny Yar for several reasons:

1. If both the Alyoshkin Suite sediments and the Duvanny Yar yedoma silts are alluvial (Sher *et al*., 1979), then they could not have been deposited at the same time on both the terrace surface 15–20 m asl at Alyoshkina Zaimka and the yedoma surface of 50 m arl at Duvanny Yar, rising to above 100 m asl to the south, as these authors pointed out themselves. While Sher *et al*. (1979) suggested that the Duvanny Yar yedoma was older than the Alyoshkin Suite, more recent dating of the Duvanny Yar yedoma, summarised previously, indicates that the deposition of the Alyoshkin Suite at Alyoshkina Zaimka did coincide with the latter stages of deposition of yedoma silt at Duvanny Yar. This coincidence is readily explained if the sandy sediments of the Alyoshkin Suite are aeolian dune sands, as Hopkins (1982) concluded and we agree. Without invoking huge river floods at least tens of metres deep, we cannot envisage how the floodplain deposits at Alyoshkina Zaimka can be contemporaneous with floodplain silts at Duvanny Yar.
2. The water source for such extensive and repeated flooding of the palaeo-Kolyma River for more than 20 000 years during MIS 3 and 2 is enigmatic. Palaeoenvironmental data in the present study support the widespread view that the MIS 2 climate in western Beringia was much drier than that at present (Guthrie, 2001; Sher *et al*., 2005; Elias and Brigham-Grette, 2013), producing desiccating cold-climate conditions (Brigham-Grette *et al*., 2004) and restricting glaciers to isolated mountain ranges (Figure 2A). Such widespread aridity is incompatible with major floodplain aggradation in northeast Eurasia (Tomirdiaro, 1986), particularly in view of widespread aeolian activity and deposition of loess in central Yakutia (Péwé and Journaux, 1983) and of loess and coversands in western Europe, which was less arid than northeast Yakutia because it was closer to moisture sources in the North Atlantic.
3. Thermokarst activity during or after the inferred floods would have been extensive in the thaw-sensitive yedoma. Accumulation of surface or subsurface water – in streams, ponds, lakes or seeping through the active layer – tends to promote thaw of ice-rich permafrost, on account of its high heat capacity and facility for thermal erosion (reviewed in J. B. Murton, 2009a, table 13.1; Kokelj and Jorgenson, 2013). Therefore, repeated flooding of an aggrading floodplain would have resulted in repeated episodes of ice loss, which should be readily apparent in the cryostratigraphy as thaw unconformities, thermokarst-cave ice and irregular bodies of partially thawed ground ice (J. B. Murton, 2013a). Geocryological evidence for extensive thermokarst activity during the moist conditions of the Holocene in the Kolyma Lowland (Sher *et al*., 1979) is widespread and clear, but evidence for thermokarst activity in the yedoma during either MIS 3 or 2 is very limited, based on the preservation of ground ice in section CY and our observations spanning decades at this site.
4. Tectonically, there is no evidence for a Beringian-wide and sudden switch in tectonic movement at the end of the Pleistocene from continuous subsidence (needed for accumulation of tens of metres of silty alluvium) to uplift (needed to explain the deep river incision by about 50 m at Duvanny Yar; Tomirdiaro, 1982). Instead, there is widespread evidence for increased relative humidity and precipitation that contributed to the rapid demise of the very dry steppe-tundra ecosystem in western Beringia (Sher *et al*., 1979, 2005; Rybakova, 1990; Andreev *et al*., 2011), with attendant increase in floodplain alluviation at the start of the Holocene.
5. Geomorphologically, the distribution of yedoma in the Kolyma Lowland along the margins of river floodplains and extending to the front of adjacent uplands is inconsistent with alluvial deposition. If the yedoma silt was alluvial in origin, it should occur wholly within floodplains, not to the south of the Kolyma floodplain at Duvanny Yar. Additionally, an alluvial origin of the yedoma at this site is inconsistent with the occurrence of buried epigenic soils within it. Soils forming on an active floodplain cannot be epigenic because they would be regularly subject to deposition of new soil-forming material and therefore represent synlithogenic soils.
6. Arctic ground squirrels – whose burrow fills are common in the MIS 3 yedoma silt – require well-drained substrates that are suitable for burrowing, nesting and hibernating (Zazula *et al*., 2011). The squirrels would have actively avoided burrowing in floodplains subject to repeated flooding, and so their burrow fills indicate an absence of flooding (Zanina, 2005).
7. Sedimentary structures indicative of flowing water (e.g. ripple cross-lamination, cross-bedding, channel structures, cut-and-fill structures) and 'trash layers' of flood-deposited organic detritus were not observed in the yedoma of unit 4, despite excellent exposures.

We also discount the lacustrine variant on the alluvial hypothesis because:

1. Pervasive fine roots in the yedoma silt indicate prolonged subaerial conditions when herbaceous vegetation with a large subsurface biomass developed (cf. Goetcheus and Birks, 2001). Had the silt been deposited in lakes, we would expect it to contain pollen belonging to aquatic plants. It does not.
2. Lakes, even shallow ones which froze to the bottom in winter, would have caused at least partial melting of underlying ice wedges and development of ice-wedge pseudomorphs above partially thawed ice wedges.

3. Lake sediments in areas of ice-rich permafrost often include well-stratified facies, as characteristic of unit 3 (Figure 6A–C). Such lake sediments are typical of those in alases in the Kolyma Lowland (Figure 28) and the Dmitry Laptev Strait (Kienast *et al*., 2011, Figure 3), and they are similar to shallow-water thaw lake sediments elsewhere in the Arctic (J. B. Murton, 1996a; Hopkins and Kidd, 1988), but they are quite distinct from the homogeneous yedoma silt.
4. Peaty layers within the yedoma do not represent boggy floodplain deposits similar to those in oxbow lakes (Y. K. Vasil'chuk *et al*., 2001a), but are buried palaeosols, as discussed previously. The single example that we observed of a detrital peat layer (unit 2) underlies the yedoma and is interpreted as a trash layer from a thaw lake that probably developed during the LIG period.
5. Boggy lacustrine conditions are unlikely where ground squirrel burrow fills are common.
6. Relict landforms such as shorelines, benches, deltas or overflow channels would be expected if the silt accumulated in lakes, just as they are common around former Pleistocene lakes elsewhere (e.g. D. K. Murton and J. B. Murton, 2012). Relict shoreline features are common around numerous alases in the Kolyma Lowland, but to our knowledge none have been reported in association with the original yedoma surface, although we cannot exclude the possibility that they have been missed.
7. Lacustrine deposition in floodplains generally results in a high percentage of clay within the sediments (J. Vandenberghe, personal communication, 2014). But clay is not abundant in the yedoma silt of unit 4.

Polygenetic Hypotheses.

Several polygenetic hypotheses for the origin of yedoma silt have been proposed in the Russian permafrost literature. Such hypotheses primarily concern the different genesis of yedoma at different locations rather than at one specific site. Konishchev (1973, 1981) has suggested that yedoma sediments can include alluvial, slope and lacustrine-bog (alas) facies. Zhestkova *et al*. (1982, 1986) considered yedoma to be a climatic phenomenon, the main factors of yedoma formation being cold-climate conditions and continuous long-term sedimentation of any nature (e.g. alluvial, aeolian, colluvial). They considered yedoma as a gigantic polypedon whose formation was strongly affected by pedogenic processes. Sher (1997) and Sher *et al*. (2005) supported these ideas. At Duvanny Yar, Konishchev (1983) interpreted the lower part of the yedoma sediments as alluvial, and the upper part as slope sediments.

Another polygenetic hypothesis was developed to explain the source and deposition of yedoma silt in the Laptev Sea region and the New Siberian Archipelago (Figure 1A) through the conceptual model of *nival lithogenesis* (suggested by Kunitskiy, 1989, and reviewed in Schirrmeister *et al*., 2011b). This model envisages accumulation of plant and mineral debris – the latter produced by cryogenic weathering – in perennial snowfields, followed by downslope transfer of this material by meltwater runoff, and subsequent sediment transport by alluvial, colluvial and aeolian processes to sites of yedoma formation. More recently, Strauss *et al*. (2012a) have attributed deposition of the yedoma silt at Duvanny Yar to seasonal submergence of the floodplain by postsnowmelt flooding or other high-discharge events (leading to overbank deposition) interspersed by aeolian deposition during drier seasons, particularly in autumn or winter. Floodplain overbank (or lacustrine) sediments attributed to suspension settling in ponded water were identified as having a particle-size mode of about 3–4 μm or finer, whereas loess was identified by a distinctly coarser mode of about 40–60 μm, and a small peak at about 200 μm was attributed to either flood events or aeolian saltation or rolling of coarser grains. Waterlain and aeolian sediments were inferred in about equal measure. Additional processes that may have contributed sediment to the yedoma are *in-situ* frost weathering and shallow overland flow caused by rain or thaw events.

The polygenetic hypotheses advocated by Konishchev (1983) and Strauss *et al*. (2012a) are unlikely to explain deposition of the bulk of the silt at Duvanny Yar for two main reasons.

1. Sedimentary structures that record repeated switches in deposition between overbank, aeolian and overland flow processes should be apparent in the stratigraphy and sedimentology, as is the case where airfall and retransported loess are distinguished in central Alaska (Péwé, 1955; Muhs *et al*., 2003) and western Europe (Vandenberghe *et al*., 1998; Antoine *et al*., 1999, 2009, Figure 3C). For example, reworked loess – attributed to deposition by overland flow (Vandenberghe *et al*., 1998) – at Kesselt, Belgium, has distinctive undulating parallel to subparallel laminae that are horizontal to gently dipping (Figure 29A, B); this lamination is quite different from (1) massive loess at Kesselt interpreted by these authors as primary (i.e. airfall) loess, and (2) any sedimentary structures in the sections that we examined through the yedoma at Duvanny Yar. Likewise, laminated loesses attributed to niveo-aeolian processes in France and Germany are also quite different (Figure 29C, D) from the yedoma silt at Duvanny Yar, and any such lamination would be readily detected in the thin sections from there. We observed none.
2. The water source for extensive flooding to submerge the whole region of the Omolon-Anyuy yedoma during very dry conditions of MIS 2 is not apparent.

Loessal Hypothesis.

The loessal hypothesis attributes yedoma silt deposition primarily to trapping of windblown sediment (Hopkins, 1982; Smith *et al*., 1995; Dutta *et al*., 2006) on a land surface vegetated by grass-dominated steppe-tundra plants (Yurtsev, 1981; Zimov *et al*., 2006a, 2006b). The loess – which includes buried palaeosols and dominates the sedimentary sequence at Duvanny Yar (grey-brown silts in

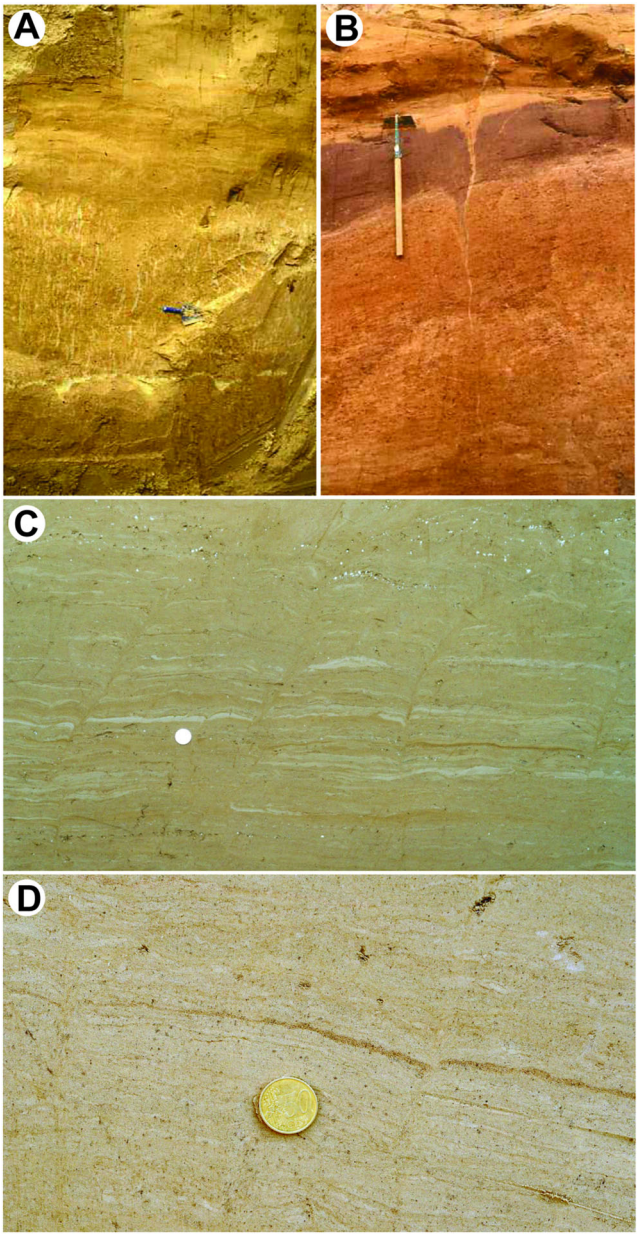

Figure 29 Stratified loess in northwest Europe. (A) and (B) Stratified silt loam of Weichselian age, Kesselt, Belgium. Subhorizontal undulating stratification in upper half of (A) and lower half of (B) is attributed to reworking and redeposition of loess mainly by overland flow. Dark brown layer in (B) is a palaeosol (gleysol) cross-cut by an infilled frost crack. Trowel for scale in (A) and scraper in (B). (C) Laminated loess of Upper Saalian age, Ailly-sur-Somme, northern France. Lamination has been attributed to niveo-aeolian processes, and infilled cracks to cryodesiccation. The white spots are granules of chalk. (D) Laminated loess of Weichselian Upper Pleniglacial age, Nussloch, Germany. Lamination is attributed to *in-situ* aeolian deposition, and not to hillwash processes. Coin for scale in (B) and (C). Photographs in (A) and (B) are by J. Vandenberghe (unpublished), and in (C) and (D) are by P. Antoine. This figure is available in colour online at wileyonlinelibrary.com/journal/ppp

Figure 3A) – is also termed 'cryopedolith', reflecting the co-existence of pedo- and cryogenic processes within the active layer and the regular influx of aeolian silt on the ground surface, leading to accretion of the soil surface and absence of soil profile formation (Gubin and Veremeeva, 2010; Zanina *et al*., 2011).

The aeolian hypothesis for yedoma silt deposition across northeast Asia is set out more fully by Tomirdiaro (1973, 1982, 1986; see also Ryabchun, 1973), the general environmental context by Guthrie (2001, 2006), and the significance of loessal deposition to promoting soil fertility and primary productivity for the Beringian megafauna by Schweger *et al*. (1982) and Schweger (1992, 1997). Geological evidence for the largely aeolian interpretation of yedoma in the northern Russian mainland to the west of western Beringia is summarised by Astakhov (2014). This hypothesis tends to be applied most forcefully to yedoma deposits of MIS 2. For milder conditions of MIS 3, however, some authors have suggested that yedoma may comprise both cryopedoliths and interbedded peats (autochthonous and allochthonous), soils, and alluvial and lacustrine deposits (Gubin and Veremeeva, 2010).

The loessal hypothesis resolves the problems discussed previously and explains some sedimentary properties of the yedoma silt at Duvanny Yar:

1. The absence of primary sedimentary stratification in most of the yedoma silt logged in unit 4 at Duvanny Yar is characteristic of primary (aeolian) loess. Airfall loess accumulates by fallout of dust in suspension and is typically homogeneous and non-stratified (Pye, 1984), properties reproduced experimentally in silt loam deposited from airfall in a vertical sedimentation column (Mücher and De Ploey, 1990). Although faint horizontal lamination or, less commonly, cross-bedding can occur in loess, primary sedimentary structures tend to be subtle and are the exception rather than the rule (Muhs, 2013a, 2013b). Examples of homogeneous loess that generally lacks stratification include the Upper Silt Loam of the southern Netherlands, northeast Belgium (reviewed in Huijzer, 1993), the Brabantian loess of Belgium and northern France (e.g. Antoine *et al*., 1999, 2003), and the uppermost sandy unit of the loess sequence at Nussloch in Germany (units 36–38 in Antoine *et al*., 2009) and Dolní Vestonice in the Czech Republic (unit 1 in Fuchs *et al*., 2013, and Antoine *et al*., 2013). Overall, the homogeneous loess at these European sites is thought to have accumulated during arid and cold periglacial conditions.
2. The occasional faintly stratified layers of yedoma silt at Duvanny Yar resemble secondary (reworked or mixed) loess or the faint stratification in primary loess (Vandenberghe, 2013). Secondary loess is often termed 'laminated loess' in central and northwest Europe (Antoine *et al*., 2009, 2013), where it is more abundant than primary loess. The lamination is attributed to reworking of primary loess by water (and to some extent by mass wasting), as indicated by experimental and

micromorphological investigations of erosion and redeposition of loess by water (Mücher and De Ploey, 1977, 1984; Mücher *et al*., 1981) and comparison of the experimental results with field observations of silt loam deposits (secondary loess) in northwest Europe (Mücher, 1974; Mücher and Vreeken, 1981; Vreeken and Mücher, 1981; Vreeken, 1984; Huijzer, 1993).

i. The experiments indicate that loess is sensitive to redeposition by overland flow (afterflow and meltwater flow) on hillslopes with gradients of less than 2°. Afterflow (i.e. overland flow that occurs briefly after rainfall has ceased) and meltwater flow tend to produce silt loam deposits that are well laminated and well sorted, and include coarse sandy laminae (with grains of 500–1000 μm) covered by clay laminae. Rainwash (i.e. combined rainsplash and flow) deposits are poorly laminated and poorly sorted, whereas raindrop splash alone produces deposits that are neither laminated nor sorted. Mücher and De Ploey's (1990) experiments produced weakly developed lamination during primary aeolian sedimentation by fallout into shallow water and when silt was blown at high velocities (in a wind tunnel) across moist to wet surfaces. In the latter case, the lamination differs from that in afterflow deposits by the absence of sharp contacts between individual laminae and by the limited degree of particle-size sorting.

ii. The field observations of laminated to massive silt loam deposits in northwest Europe suggest that complex interactions occurred between aeolian deposition and reworking by overland flow and rainsplash or mass wasting. At the Weichselian stratigraphic-type locality of Nagelbeek in the Netherlands, a distinct lamination in the Saalian Lower Silt Loam A deposits is thought to indicate that primary loess was cyclically and partially reworked by sheet flow, whereas laminated silt loam of Early Weichselian age was completely reworked and redeposited by sheet flow and shallow channel flow (Mücher and Vreeken, 1981). Subhorizontal lamination also characterises the Middle and Upper Silt Loams deposited at this site during the Weichselian Upper Pleniglacial and has been attributed to redeposition of loess by meltwater flow and mass wasting (Vreeken, 1984). The geomorphic setting of the Nagelbeek silt loams (an upland drainage network of dry valleys spaced up to a few hundred metres apart; Vreeken and Mücher, 1981), however, differs fundamentally from the flattish Omolon-Anyuy yedoma surface at Duvanny Yar, where the loess accumulated on an extensive aggradational plain. Also different are the repeated cycles of erosion inferred from stone lines, truncated weathering zones and erosional unconformities in the Nagelbeek region (Vreeken, 1984), which suggest a much more dynamic erosional environment there than the accumulation plain at Duvanny Yar. Climatically, the laminated Hesbayan (secondary) loess deposits of northwest and central Europe are thought to have accumulated during cold and humid periglacial conditions, probably with more snow cover than the homogeneous Brabantian (primary) loess, which has been attributed to cold and dry conditions (Gullentops, 1957; Huijzer and Vandenberghe, 1998; Antoine *et al*., 2009). The lamination probably resulted from rainwater and snowmelt running downslope, rather than from intercalation of snow during loess deposition (reviewed by Koster and Dijkmans, 1988), because experiments simulating niveo-aeolian sedimentation of loess indicate that intercalation of snow does not leave a laminated structure after the snow has melted out from the loess (Dijkmans and Mücher, 1989).

3. Bimodal to polymodal particle-size distributions are characteristic of many loess deposits and result from mixing of populations of grains derived from different sources and transported by different mechanisms (reviewed in Maher *et al*., 2010, and Vandenberghe, 2013). The main particle-size modes in airborne dust and loess deposits are summarised below in relation to the modes observed at Duvanny Yar and Itkillik (Figure 15).

   i. The coarse silt mode (average = 40.9 μm) in yedoma at Duvanny Yar is similar to the 'coarse' mode of 20–50 μm identified in Chinese loess (e.g. Sun *et al*., 2004) and the medium to coarse silt (sediment type 1b) of Vandenberghe (2013). The latter is thought to be transported by cyclonic near-surface winds that generate dust storms (mainly in spring and early summer). Transport distances of this silt fraction may be limited to between tens of kilometres and about 100 km. Deposition occurs as the silt settles by fallout from low suspension clouds. Source regions include glaciofluvial and alluvial plains and alluvial fans containing sediment eroded from glaciated mountains.

   ii. The fine silt (8–16 μm) and coarse clay to very fine silt (3–5 μm) modes at Duvanny Yar lie within the single 'fine' loess component of Chinese loess (e.g. Sun *et al*., 2002, 2004; Prins *et al*., 2007; Vriend *et al*., 2011) and the fine silt subgroup and clayey to very fine silty subgroup (sediment types 1.c.1 and 1.c.2., respectively) of Vandenberghe (2013). This component has a wide grain-size range of about 2–19 μm and is thought to represent the background dust load that is transported hundreds to thousands of kilometres, mainly by high-altitude westerly airstreams throughout the year. It is deposited continuously as a form of background sedimentation. Source areas include floodplains, alluvial fans, dried lakes and pediments.

   iii. The fine to medium sand mode (150–350 μm) lies within the sand mode of some loess deposits (sediment type 1a of Vandenberghe, 2013). The exact grain size of the sand mode in sandy loess deposits, however, varies substantially. It includes very fine sand in the northern area of the Chinese Loess Plateau (Prins *et al*., 2007) and in loess in southeast Kazakhstan (Machalett *et al*., 2008) and aeolian silt in western Greenland (Dijkmans and Törnqvist, 1991); fine to medium sand in loess above glacial outwash in northeast

Wisconsin, USA (Schaetzl and Luehmann, 2013); and coarse sand in loess near the Danube River in northern Hungary (Novothny *et al.*, 2011). The grain size of the sand fraction is determined more by the size of the available source material than by the wind energy, because storm winds can transport coarse sand, granules or even fine pebbles (e.g. Mountney and Russell, 2004). The source areas include river floodplains, sand dunes and sandy substrates, and the transport distance is usually short (hundreds of metres to a few kilometres). The sand component is largest in dune belts, sandy deserts or marginal loess regions transitional with coversand. Examples include sandy loess interbedded with aeolian sand and sandy loam soils in the Mu Us and Otindag sand fields, representing the sand-loess transition zone of north China (Zhou *et al.*, 2009); and the central region of Argentina, where sandy loess grades proximally to loessal sand and very fine sand (Zárate and Tripaldi, 2012).

iv. The ultrafine mode (0.3–0.7 μm) at Duvanny Yar has a very similar value to the 0.37 μm mode identified in loess from the Chinese Loess Plateau, where it comprises 4–10 per cent of the sediment (Sun *et al.*, 2011). Although an ultrafine fraction is often identified by laser diffraction particle sizers, and may be an expression of a systematic error linked to laser diffraction (J. Vandenberghe, personal communication, 2014), the HORIBA particle sizer used in the present analyses did not identify this fraction in some other silty sediments that we have analysed with it, and so we believe that the ultrafine fraction in the Duvanny Yar yedoma is not an artefact. Additionally, particle-size data that we obtained by pipette analysis confirm the presence of a small but significant < 1 μm fraction, comprising about 10–15 per cent of the yedoma silt plotted in Figure 12. In China, the ultrafine fraction tends to be coarser grained and less abundant in loess layers than that in palaeosols (Sun *et al.*, 2011). Within the loess, the ultrafine fraction is thought to contain considerable amounts of detrital clay minerals derived from aeolian source areas, whereas that in the palaeosols has been altered significantly and pedogenic clay minerals produced by pedogenesis.

v. Mixing of different particle-size modes of windblown dust has been observed in present-day conditions. For example, trimodal aerosol-size distributions recorded during dust events in northwest China had modes of $>$ 11 μm, 4.7–7.0 μm and $<$ 0.43 μm (Wang *et al.*, 2007). Likewise, modern dust deposition in Mali indicates mixing of particles from long-distance sources ($<$5 μm), regional sources (20–40 μm) and local source (50–70 μm) (McTainsh *et al.*, 1997).

4. The sequence of buried soils inferred in Figures 14A and 21A is interpreted as a loess-palaeosol sequence (cf. Zanina *et al.*, 2011). The degree of pedogenesis in yedoma at Duvanny Yar, however, is less than that commonly found in loess-palaeosol sequences developed during cold stages in mid-latitude regions. In northwest Europe, a series of palaeosols (e.g. tundra gleys) is intercalated in laminated (Hesbayan) loess deposits, whereas homogeneous (Brabantian) loess tends either to lack palaeosols or contain only incipient (poorly developed) ones (Huijzer, 1993; Vandenberghe *et al.*, 1998; Antoine *et al.*, 2009). The Duvanny Yar yedoma more closely resembles the Brabantian loess than the Hesbayan loess.

In conclusion, the yedoma silt of unit 4 at Duvanny Yar is, beyond reasonable doubt, mainly of primary loessal origin, as suggested by Hopkins (1982) and Tomirdiaro (1982). We discount an alluvial and lacustrine origin but cannot exclude the possibility that some of the occasional, indistinctly stratified silt has been redeposited on a low-angle slope, particularly in view of annual snowmelt operating on an undulating palaeo-land surface. Overall, however, the bulk of the yedoma represents airfall loess.

Cold-climate Loesses in the Discontinuous Permafrost Zone

In support of a loessal interpretation, we identify similarities between the Duvanny Yar loess-palaeosol sequence and cold-climate loesses in the present-day discontinuous permafrost zone of northwest North America, and in the past permafrost zone of Asia and northwest Europe (Figure 30).

Central Alaska.

Loess is widespread in the Fairbanks area, central Alaska (Figure 31), and much of the loess on north- and northeast-facing slopes has remained continuously frozen since it was deposited in the Pleistocene. The loess comprises both direct airfall silt on uplands and a combination of airfall and colluvially reworked loess in valleys (Péwé, 1975a; Hamilton *et al.*, 1988; Muhs *et al.*, 2003). It resembles the Duvanny Yar loess in terms of its sedimentology, interbedded palaeosols and ground ice (Péwé, 1975b).

Sedimentologically, the central Alaskan loess tends to be massive, with stratification absent to indistinct, not only on uplands (Péwé, 1955) but in many lowlands (Begét, 1988; Hamilton *et al.*, 1988). Although Péwé argued that loess in valley bottoms – where subtle stratification is sometimes apparent – has been retransported from adjacent slopes, the presence of numerous, discrete and continuous tephra layers interbedded in the valley-bottom loess suggests that much of it is also airfall in origin, like that on the uplands, and has experienced only minimal reworking, mostly by wind (Begét, 1988). Airfall deposition is indicated where the tephra beds have not been mixed with loess (which rules out redeposition of the tephra and mixing with loess by hillslope processes) and the horizontality of the tephra deposits. Where redeposition of loess by colluvial processes is likely to have occurred is in valley-bottom and organic-rich 'muck' deposits, which can preserve sedimentary structures attributed to small mudflows, slumps and landslides (Begét, 1988). Unconformities are common in the Fairbanks area loess, and mammal fossils are abundant in retransported silt, and some occur in the upland silt. Carbonate leaching has

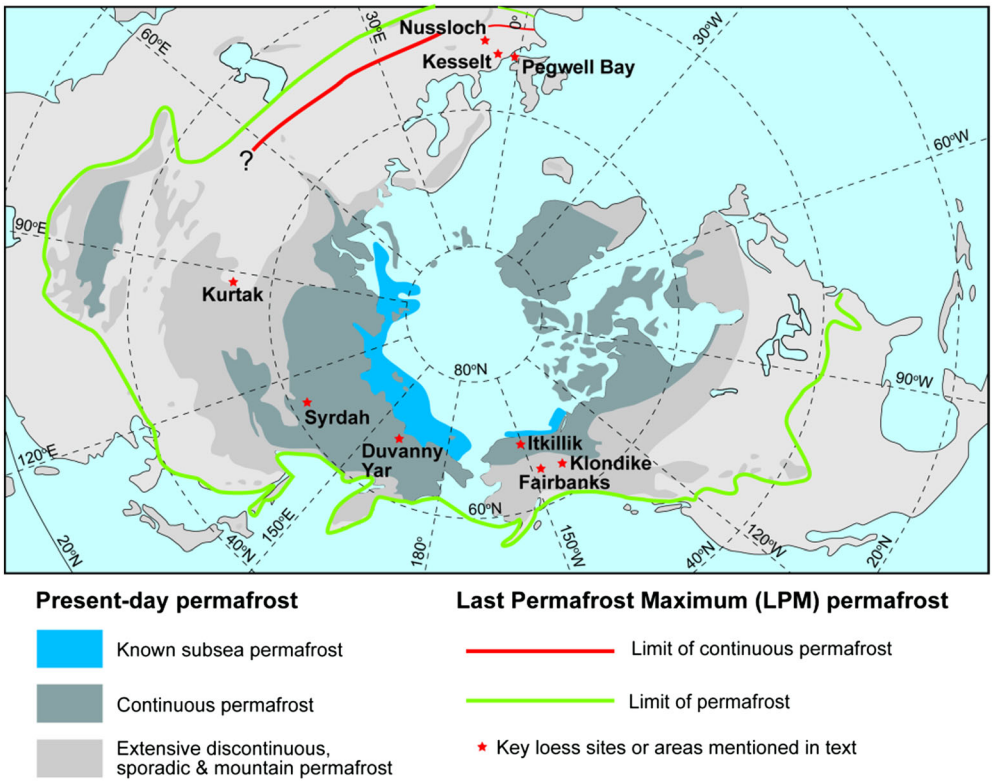

Figure 30 Present-day permafrost zones in the northern hemisphere (modified from the map produced by J. A. Heginbottom in van Everdingen, 1998, Figure 1) and reconstructed limits of permafrost in Eurasia and North America during the Last Permafrost Maximum, a period of maximum cold-climate conditions that occurred towards the end of the last ice age (25 000–17 000 BP; modified from Vandenberghe *et al*., 2014). This figure is available in colour online at wileyonlinelibrary.com/journal/ppp

affected loess in the Fairbanks area, so that the low $CaCO_3$ contents there are not due to low amounts in the potential source sediments (Yukon and Tanana), but due to weathering (Muhs and Budahn, 2006).

The section of the CRREL Permafrost Tunnel is more complicated than many other yedoma sections. Besides the 'original' yedoma, numerous structures reflect thermal erosion, which occurred about 30 ky BP (Hamilton *et al*., 1988): gullies filled with fluvial sediments and underground channels filled with either silt/sand deposits or with thermokarst-cave ice (Shur *et al*., 2004; Bray *et al*., 2006). Most ice wedges in the tunnel were truncated by erosion, though some of them continued growing after erosional events. The 'original' yedoma in the tunnel does not look like typical loess. Massive uniform sediments or sediments with indistinct horizontal stratification are unusual; instead, a very irregular undulating stratification with thin layers of different colours is much more common. Thin sand layers and gravel inclusions are also common. In many cases, it is very hard to distinguish the 'original' yedoma from secondary erosional structures.

Palaeosols are common in the loess of central Alaska. Some near Chena Hot Spring, east of Fairbanks, are discontinuous and vertically welded (cf. palaeosol complex 1 in Figure 5), some terminate abruptly when traced laterally across a section (cf. palaeosol 5 in Figure 5) and some comprise irregular fragments or lens-shaped structures (Muhs *et al*., 2003). Palaeosols dating from the mid-Wisconsin (MIS 3) period in the Fairbanks area are minimally developed, like some of those at Duvanny Yar. Also similar to the latter are the magnetic susceptibility values of the central Alaskan palaeosols, which are characteristically lower than those in the loess. Such low susceptibility is attributed to reduced supply of coarse-grained magnetic minerals during soil-forming episodes that were less windy than loess-forming ones, combined with removal of the fine-grained superparamagnetic component by chemical processes associated with pedogenic gleying (Begét, 2001). Seven organic-rich (peat) horizons a few to several centimetres thick have been identified in part of the CRREL Permafrost Tunnel, and distinctive ice layers (belts) occur about 0.4–0.6 m beneath each of them (Kanevskiy *et al*., 2008). The ice layers are thought to indicate periods of temporary stabilisation of the ground surface during slower sedimentation, allowing ice accumulation in the bottom of the active layer and peat accumulation on the surface. A similar association between an organic layer and underlying ice-rich layer from Duvanny Yar yedoma is shown in Figure 9D and E.

Ground ice in the central Alaskan loess includes cryostructures characteristic of syngenetic permafrost, and yedoma sections up to 30 m thick occur with extremely

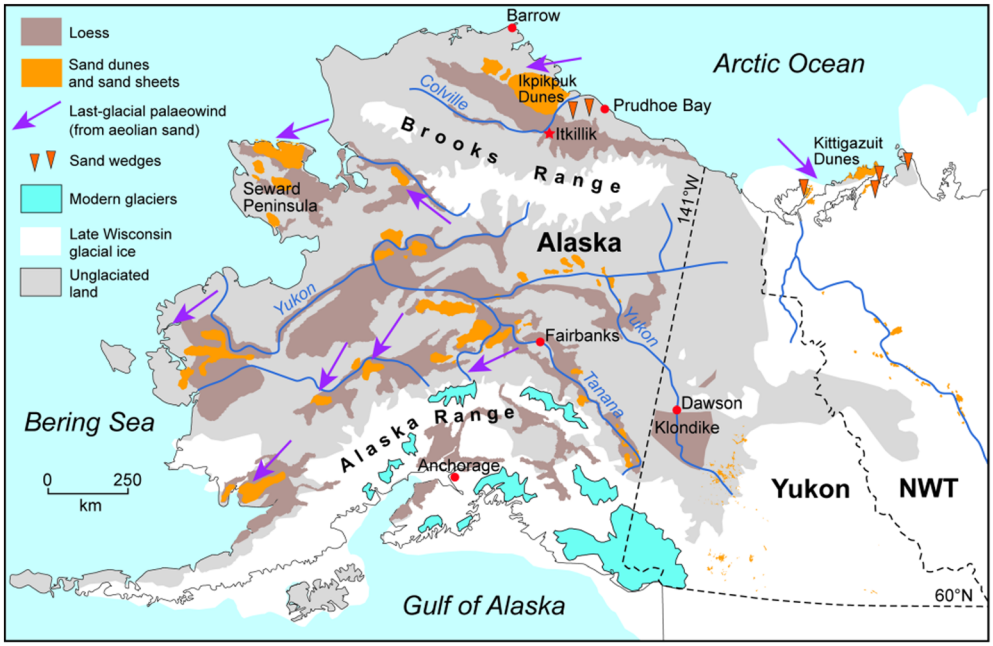

Figure 31 Distribution of aeolian deposits of northwestern North America. Loess in Alaska compiled from Hopkins (1963) and Sainsbury (1972) for the Seward Peninsula, and Péwé (1975a) for all other parts of the region. Aeolian sand distribution in Alaska from Hopkins (1982) and Lea and Waythomas (1990). Palaeowinds are from Hopkins (1982), Lea and Waythomas (1990) and Muhs and Budahn (2006). Loess and aeolian sand in Canada derived from various sources as compiled by Wolfe *et al*. (2009). Palaeowinds in Canada are based on Dallimore *et al*. (1997). This figure is available in colour online at wileyonlinelibrary.com/journal/ppp

highcontents of wedge and segregated ice. Detailed cryostratigraphic studies of ice-rich loess in the CRREL Permafrost Tunnel and along the proposed new alignment to the Dalton Highway between Mile Post 8 and 12 have revealed layered, lenticular-layered and particularly microlenticular cryostructures indicative of syngenetic permafrost, as well as massive and reticulate-chaotic cryostructures in sediments reworked by thermal erosion (Shur *et al*., 2004; Bray *et al*., 2006; Kanevskiy *et al*., 2008, 2012; Fortier *et al*., 2008). Layered (bedded), lenticular-layered and microlenticular cryostructures are also common in the yedoma at Duvanny Yar, consistent with syngenetic permafrost there. Where the ground ice in the permafrost tunnel differs from that at Duvanny Yar is in its smaller syngenetic ice wedges and the abundance of thermokarst-cave ice. Many ice wedges in the tunnel have been partially replaced by thermokarst-cave ice following episodes of underground thermal erosion and refreezing of pooled water in tunnels or cavities (Shur *et al*., 2004; Bray *et al*., 2006; Fortier *et al*., 2008). Many such wedges continued their growth after these erosional events.

Klondike, Yukon.

Although loess deposits are widespread in western Yukon, they are thinner and less continuous than those in Alaska. Loess occurs in most valleys in southwestern and west-central Yukon, though the deposits have no distinctive surficial expression, and thus it is probably underrepresented relative to its true extent (Wolfe *et al*., 2011). The thickest and most extensive loess deposits in Yukon Territory occur in the unglaciated Klondike region of the Yukon River valley (Figure 31). These ice-rich loessal (or 'muck') deposits are also likened to Siberian yedoma (Froese *et al*., 2009).

The stratigraphic unit most similar to the Duvanny Yar yedoma is the Quartz Creek Member of the King Solomon Formation (Kotler and Burn, 2000), or lower part of the Silt unit of Fraser and Burn (1997). Texturally, the latter is dominated by 20–50 μm silt, with smaller amounts of finer silt and some fine to very fine sand. Its organic content (measured by loss on ignition) is generally about 4–6 per cent in the main part of the unit (Fraser and Burn, 1997, Figure 8). Both the texture and organic content are similar to those from Duvanny Yar, as shown in Figure 14A. Although some parts of the Klondike Silt unit up to 3 m thick are massive (interpreted as airfall loess), in other parts stratification appears to be more strongly developed and common than that at Duvanny Yar. Gently inclined planar bedding – with individual beds up to 5 cm thick – in the former is emphasised by ice seams, colour variation, organic laminae and laminae of coarser sediment, with individual strata from $<$ 1 mm up to 5 cm thick (Fraser and Burn, 1997; Sanborn *et al*., 2006, Figure 6C). In addition, some beds (up to 3 cm thick) are convoluted, and a few channel-shaped zones that contain cross-bedding cut across the convolutions. These features suggest that redeposition by colluvial processes was more important in the Klondike valley bottoms than the loess plain at Duvanny Yar. Radiocarbon ages indicate that thick loess deposition occurred in association with the last (McConnell) glaciation (Fraser and

Burn, 1997; Kotler and Burn, 2000; Froese *et al*., 2002), and older tephra beds indicate several intervals of loess accumulation associated with previous glacial intervals (Westgate *et al*., 2001).

Palaeosols of MIS 4 and 2 age interbedded in the Klondike muck deposits resemble palaeosols 2 and 5 at Duvanny Yar in terms of colour, increased clay and organic contents, abundant fine roots and also experienced only limited chemical weathering (Sanborn *et al*., 2006; Zazula *et al*., 2006, Figure 7 b and c). At microscale, similarities include ubiquitous root detritus and dispersed partially humified plant residues, sediment aggregates and platy microstructures within and/or between the palaeosols. Additionally, Sanborn *et al*. (2006) identified within the loess numerous incipient A horizons (<1 cm thick) whose slightly darker colours suggest local enrichment of organic matter, possibly similar to some darker bands in the yedoma at Duvanny Yar. Arctic ground squirrel middens – similar to those at Duvanny Yar – in the Klondike loessal deposits indicate that the squirrels colonised full-glacial active layers thicker than modern ones in this area, and consistent with the re-establishment of steppe-tundra vegetation and well-drained loessal soils during successive cold stages between MIS 4 and 2 in eastern Beringia (Zazula *et al*., 2007, 2011).

Ground ice within the muck deposits includes ice wedges (of syn-, epi- and anti-syngenetic types), thermokarst-cave ice, massive ice, intrusive ice and aggradational ice (Naldrett, 1982, pp. 112–122; French and Pollard, 1986; Kotler and Burn, 2000). Non-visible ice is abundant in the silt of the Quartz Creek Member, with volumetric ice contents averaging 65 per cent (Kotler and Burn, 2000). Such volumetric ice contents, however, more likely correspond to microcryostructures, for they are high for sediments without visible ice. The apparent absence of ice wedges, despite their occurrence in under- and overlying units, is attributed by these authors to very dry full-glacial conditions of MIS 2 that precluded ice-wedge formation because of insufficient snowmelt infiltration.

Cold-climate Loesses in the Past Permafrost Zone

Western and Central Siberia.

Loesses in western and central Siberia – near the upper courses of the rivers Ob, Yenisey, Angara and Lena (Figure 32) – are mostly unfrozen and located near the southern boundary of the present-day permafrost zone (Figure 1A). Such loess deposits often contain evidence of past permafrost, for example, ice-wedge pseudomorphs. They also contain numerous palaeosols that show varying degrees of development (Chlachula, 2003), as at Duvanny Yar. The loess is massive to weakly stratified, and the magnetic susceptibility signal of palaeosols at sites such as Kurtak is the same as palaeosols in central Alaska and Duvanny Yar (i.e. minima in palaeosols and maxima in loess), and opposite to those of the Chinese loess (Chlachula *et al*., 1997), a characteristic that Zhu *et al*. (2003) attributed to short-distance transport of coarse silt or very fine sand magnetite grains by saltation or modified saltation from local river channels. Some palaeosols of MIS 3 age have stratigraphically associated ice-wedge pseudomorphs and involutions and represent periglacially altered soils (Frechen *et al*., 2005; Haesaerts *et al*., 2005). As at Duvanny Yar, some soils are poorly developed (incipient) regosolic soils attributed to development on a cold and arid tundra-steppe. Interestingly, some pure aeolian loess of MIS 2 age at Kurtak is homogeneous and very sandy (the 63–200 μm fraction constituting about 10–20% of the sediment), suggesting a local origin and short-distance transport from the floodplain of the Yenisey River (Frechen *et al*., 2005). Loess-like sediment (reworked loess) at this site shows distinctive wavy bedding with poorly defined erosional boundaries, and is attributed to slopewash and sheet erosion.

Northwest Europe.

Loess-palaeosol sequences in northwest Europe no longer contain permafrost but do contain indications of its former occurrence (Figure 30), notably ice-wedge pseudomorphs (Jahn, 1975, pp. 177–188; Rousseau *et al*., 2007). At Kesselt, Belgium, Vandenberghe *et al*. (1998) have reconstructed a Weichselian environment with discontinuous permafrost in which ice wedges and therefore permafrost developed in silty substrates during the coldest periods, whereas ice-wedge melting, partial thaw of permafrost and development of tundra gleysols occurred during warmer periods.

Weichselian permafrost that developed within loess in northwest Europe differed in several respects to that in the yedoma of northern Yakutia: (1) the former was warmer and thinner; (2) it experienced repeated cold-warm climate cycles that lasted typically 1000–2000 years and caused repeated permafrost growth and thaw (reviewed in J. B. Murton and Kolstrup, 2003; Vandenberghe *et al*., 2004), thereby limiting the time for build-up of substantial ground ice (Vandenberghe *et al*., 1998; Vandenberghe and Nugteren, 2001); and so (3) it probably contained much less ground ice (J. B. Murton and Kolstrup, 2003; cf. Van Vliet-Lanoë, 1996) than the loess at Duvanny Yar. Although well-preserved wedge structures interpreted as ice-wedge pseudomorphs are widely preserved in European loess (Jahn, 1975, p. 75; Vandenberghe *et al*., 1998), they are much smaller than the very large syngenetic ice wedges that characterise the yedoma of continuous permafrost terrain. Syngenetic ice-wedge pseudomorphs whose growth was interrupted episodically by erosion are also well known from sandy Weichselian deposits in western Europe (e.g. Vandeberghe and Kasse, 1993; Kasse *et al*., 1995), but again their maximum heights (about 5 m) are much smaller than many syngenetic ice wedges in yedoma of northern Yakutia. Indeed, large syngenetic ice wedges in very ice-rich yedoma like that at Duvanny Yar are unlikely to produce pseudomorphs, except perhaps in their toes, because the silts become liquid-like on thaw, and so they are prone to

Figure 32 Distribution of aeolian deposits and deserts during the last glacial (MIS 2) in northern Asia. Compiled from Hopkins (1982), Velichko *et al.* (1984, 2006, 2011), Liu (1985), Dodonov (2007), Frechen *et al.* (2009) and Vriend *et al.* (2011). Red stars indicate yedoma sites referred to in the text. Legend as in Figure 32. Areas glaciated during MIS 2 are approximated from Brigham-Grette *et al.* (2004), Elias and Brigham-Grette (2013) and Ehlers *et al.* (2013). MIS = Marine Isotope Stage; BL = Bol'shoy Lyakhovsky. This figure is available in colour online at wileyonlinelibrary.com/journal/ppp

reworking and erosion (J. B. Murton, 2013b). Thus, large syngenetic ice wedges probably never developed in the northwest European loess, and so we disagree with Tomirdiaro (1982) that the European loess was as ice-rich as the Yakutian loess. As the permafrost in the relatively ice-poor European loess degraded, widespread ice-wedge casting was able to take place and organic matter largely degraded. Instead of Pleistocene roots preserved in, for example, the loess at Pegwell Bay, UK, calcareous tubes (rhizoliths) provide casts of former roots (Pitcher *et al.*, 1954), similar in size and abundance to the roots in yedoma at Duvanny Yar (Figure 10C).

At Nussloch, Germany, the type sequence of loess and palaeosols in western Europe (Antoine *et al.*, 2009), magnetic susceptibility maxima occur in the loess and minima occur in interbedded tundra gley soils, similar to our findings at Duvanny Yar. In addition, some of the Nussloch loess is sandy, and attributed to local transport from the dried-out and exposed braidplain of the River Rhine during MIS 2. The soils vary substantially in their degree of development, from incipient to well-developed gley horizons.

Overall, loess deposition in northwest Europe experienced more reworking than that associated with the Chinese loess or the yedoma at Duvanny Yar and Itkillik. In Europe, deposition was more erratic and temporary, subject to repeated cycles of erosion, reworking and redeposition by overland flow and mass wasting (Mücher, 1974; Huijzer, 1993, pp. 159–161; Vandenberghe *et al.*, 1998). This reflects the location of northwest Europe just downwind of a major moisture source (the North Atlantic), the repeated climatic and vegetations shifts associated with Dansgaard-Oeschger cycles during the last cold stage (reviewed in Vandenberghe *et al.*, 2004; J. B. Murton and Kolstrup, 2003) and, locally, geomorphic settings that favoured erosion and redeposition (e.g. growing dry valley networks at Nagelbeek (Vreeken and Mücher, 1981; Vreeken, 1984)) and proximity to a terrace escarpment at Belvédère (Huijzer,

1993, p. 95). Thus, the loess is primarily of secondary (reworked) character. In contrast, the Chinese loess and the yedoma at Duvanny Yar and Itkillik lack the general laminated appearance of the European loess and, for the most part, represent primary (airfall) loess.

Modern Analogues for Yedoma Silt Deposition

Several modern analogues elucidate the processes of yedoma silt deposition on a local scale, based on the observation that

> 'Present-day entrainment and deposition of locally-derived dust in cold, humid environments is restricted mostly to large alluvial river valleys where fine-textured sediment is exposed on channel bars and deltas during low flows…' (Hugenholtz and Wolfe, 2010, p. 274)

One of the closest analogues sedimentologically for development of a loess-palaeosol sequence in the yedoma occurs in the Kluane Lake region of southwest Yukon, Canada. Active loess deposition in summer contributes silt particles to soils that are warm and dry, and supports an *Artemisia-Festuca* grassland whose fertility and biomass increase with silt content, supporting the hypothesis that productivity of grassland increases with deposition of loess (Laxton *et al*., 1996). The diurnal rise and fall of outflows from the nearby Slims River create ideal conditions for deposition of fine glacial silts over the wide delta flats (Nickling, 1978). Dust storms occur throughout the year in the nearby Slims River valley, but are most frequent from May to July. They erode fine sand and silt from the sparsely vegetated surface of the proglacial Slims River delta, particularly when the river is at a low stage and the delta surface is dry. The storms move sediment mainly by saltation and suspension, with a very small proportion moved by creep. They deposit silts downwind of the delta as Neoglacial loess at the surface of grasslands around Kluane Lake (Laxton *et al*., 1996). Beneath the Neoglacial loess is the Slims palaeosol, which developed on the older Kluane loess, which itself accumulated after Late Pleistocene glaciation of the region. Organic contents – measured by loss on ignition – range from 4.5 per cent from Kluane loess and Slims palaeosol to 7.0 per cent for humified loess (Laxton *et al*., 1996, table 3), comparable to those in the yedoma at Duvanny Yar (Figure 14A). Similarly, along other rivers in southwestern Yukon such as the Alsek and White, which today are fed by glacial meltwater, modern aeolian silts are generated and deposited in this region of Yukon (Laxton *et al*., 1996; Sanborn and Jull, 2010) and near the junctions of streams (Kindle, 1952).

Holocene loess deposits in continuous permafrost in lower Adventdalen, Spitsbergen, provide a second, small-scale analogue for yedoma silt accumulation. Sediment deposited by the Adventelva River (a glacial meltwater stream) is deflated during low-stage conditions in summer, with clouds of fine sediment transported several kilometres (Bryant, 1982). The silts are redeposited on both flanks of the valley as proximal loess, on a landsurface covered by a patchy vegetation of willow, sedges and mosses, and with a widespread salt crust. Unusually for loess, the upper 1 m is horizontally laminated, which Bryant attributed to winnowing of primary deposits after partial cementation by salt.

A third partial analogue for yedoma silt deposition presently occurs windward of large braided river floodplains on the Alaskan Arctic Coastal Plain. The silts originated by glacial grinding in the Brooks Range, primarily during times of extensive Late Wisconsin glaciation, and were transported downstream along most major rivers in the central and eastern part of the coastal plain, for example, the Sagavanirktok and Canning rivers near Prudhoe Bay. Silt and fine sand are blown from their gravelly floodplains, mainly by east-northeasterly winds, and accumulate downwind as sand dunes and loess, favouring the development of minerotrophic plant communities (Walker and Everett, 1991). The loess is less than 2 m thick between the Sagavanirktok and Kuparuk rivers, and thins downwind. Although loess deposition has often been regarded as more prevalent during summer, when the braided rivers are snow-free, substantial deposition can also occur during winter, as indicated by snow drifts that contain considerable amounts of dust that becomes evident in spring after snowmelt (D. A. Walker, personal communication, 2014). Walker has observed that the dust moves easily across relatively smooth snow surfaces along with windblown snow in winter. The winter season is long and the autumn and winter winds are stronger than the summer winds. The braided river channels are often blown free of snow in the winter, and so there is a source of silt in the river channels, even during winter.

A fourth partial analogue for yedoma silt deposition is provided by upland loess that has been accumulating for at least 4750 years alongside proglacial valley sandurs in West Greenland (Dijkmans and Törnqvist, 1991; Willemse *et al*., 2003). The silt has a median particle size of about 30–45 μm and forms a mantle up to 1 m thick. In field examination, the silt appears to be mainly unstratified, but micromorphological analysis reveals a microlamination of fine and coarse silt layers (<0.1 mm and 0.2–0.3 mm thick, respectively) broken into fragments 1–2 mm long. The silt is commonly enriched in organic material and shows a gradation between aeolian silt and silty peat. The silt is derived by deflation, mainly during summer, of glacial outwash. Dust clouds that can exceed 100 m in height transport the silt in suspension and deposit it on vegetated surfaces within a few kilometres of its source as proximal loess on uplands that intersperse areas of aeolian dunes and sand sheets. On some mountain ridges, elongate blowouts in the silt have developed by local deflation.

Loess deposition and soil formation have been identified as competing processes that began in the mid-Holocene and have continued to the present day in the Matanuska Valley of southern Alaska (Muhs *et al*., 2004). The silt particles are produced by grinding by the Matanuska and Knik glaciers, deposited as outwash sediments on floodplains, entrained by strong winds and finally redeposited as loess

in boreal forest and coastal forest. The loess thickness, sand content and sand plus coarse silt content decrease over a downwind distance of about 40 km, whereas the fine silt (2–20 μm) content increases. Close to the probable sediment source (Matanuska River valley), the aeolian deposits consist of horizontally interbedded silts and fine sands with a sand content of 33–71 per cent and a silt content of 17–58 per cent, whereas at distances beyond a few kilometres from the source, the sand (>53 μm) content is generally less than about 20–25 per cent. Loess deposition is episodic, as indicated by the presence of palaeosols at distances of > 10 km from the source. Palaeosols show a gradation from Entisols or Inceptisols near the outwash source to Spodosols (or Inceptisols trending towards Spodosols) in distal areas, where the degree of pedogenesis and chemical weathering has been greater and where loess deposition rates have been lower. The number of palaeosols and loess units reached a maximum at distances intermediate (10–25 km) from the sediment source.

A partial analogue for yedoma silt accumulation occurs near Chitina, along the Copper River in southern Alaska. The silt particles are derived from glacial sources in the Wrangell Mountains, the Chugach Mountains and probably the Alaska Range, and entrained by wind from the Copper River floodplain (Muhs *et al*., 2013). Loess deposition has occurred contemporaneously with boreal forest growth during the last 10 000 years. The basal 1 m of aeolian sediments contains about 30–60 per cent sand beds that are intercalated with minimally developed palaeosols. Above this sandy loess are about 8 m of crudely laminated loess with a silt content (2–53 μm) of 50–70 per cent. In recent years, large dust-generating events in the Copper River valley and other sources of glacially derived sediment have occurred mostly between late October and mid-November, lasting from a few days to 2 weeks, and have transported dust several hundred kilometres offshore into the Gulf of Alaska (Crusius *et al*., 2011; Muhs *et al*., 2013). The occurrence of such events in autumn is thought to reflect the time when large areas of outwash sediments are exposed because river discharge is at its annual minimum. In summer, peak discharges largely submerge the potential dust sources, whereas in winter snow tends to cover them, although dust events in this region do sometimes occur in late winter (Crusius *et al*., 2011).

Cold-climate loess also accumulates widely in Iceland (reviewed in Arnalds, 2010). The dust (mostly volcanic glass) is deflated from confined plume areas and extensive sandy deserts, where much of it derives from glacial and glaciofluvial sediments and from volcanic debris. In some localities, loess is thought to have accumulated continuously throughout the Holocene (e.g. Jackson *et al*., 2005) and deposition continues at the present day.

Silts and sands similar to yedoma sediments are deposited on floodplains of some Arctic rivers (Popov, 1952; Katasonov, 1954, published in 2009; Rosenbaum, 1973; Gasanov, 1981; Rosenbaum and Pirumova, 1983). These authors have identified similarities between yedoma and modern floodplain alluvium in terms of sediment texture, ice wedges and cryostructures. For example, silts deposited on the floodplain of the Colville River Delta, northern Alaska, experience syngenetic permafrost aggradation and tend to be rich in ground ice, with lenticular, layered, reticulate and ataxitic cryostructures similar to those at Duvanny Yar (Shur and Jorgenson, 1998). Sedimentologically, however, the sedimentary sequence differs in several respects to that which we have observed in unit 4 at Duvanny Yar: (1) medium to coarse sands, massive or cross-bedded, deposited in river channels; (2) interbedded medium and fine sand, silt and detrital organic material, showing cross-bedding and ripples, deposited by lateral accretion of river bars; and (3) significant amounts of interbedded peat.

In conclusion, we interpret the yedoma silt at Duvanny Yar as cold-climate (permafrost) loess analogous to those loess deposits discussed previously and to modern loess accumulating on a grassland in southwest Yukon and adjacent to braided rivers in Spitsbergen, northern Alaska, southern Alaska and Iceland. What sets it apart from the loess deposits in western and central Siberia and northwest Europe is the persistence of permafrost since silt accumulation began and the abundance of ground ice and rootlets within the yedoma. Significantly, both permafrost and ground ice persist in some central Alaskan loess; indeed, the loess-ice sequence in the CRREL Permafrost Tunnel and along the Dalton Highway has been identified by Kanevskiy *et al*. (2011, 2012) as yedoma. To find very similar ground-ice and permafrost conditions to those of the Duvanny Yar yedoma, we now compare it to yedoma from other regions of continuous permafrost.

Yedoma Deposits in the Continuous Permafrost Zone

Itkillik, Northern Alaska.

The Itkillik yedoma has been mapped as upland loess deposits (Carter, 1988) and occurs within 100–200 km of Holocene and modern loess deposits of the Prudhoe Bay region (Walker and Everett, 1991) and the Colville River Delta (Shur and Jorgenson, 1998). It closely resembles yedoma at Duvanny Yar in several respects: (1) the uniform (massive) appearance of the silt, with occasional indistinct subhorizontal stratification; (2) large syngenetic ice wedges; (3) cryostructures diagnostic of yedoma and typical of syngenetic permafrost, particularly those comprising thin (<1 mm) and densely spaced ice lenses ('microcryostructures'; Kanevskiy *et al*., 2011, figs 4 and 6), often forming bands of centimetre-scale thickness in outcrop; (4) particle-size distributions, mostly with three or four modes (Figure 15); (5) pervasive fine roots throughout the yedoma, contributing to organic contents of typically a few per cent (Figure 14); (6) drops in magnetic susceptibility in the transition zone (Figure 14); and (7) gravimetric ice contents that are characteristically about 40 per cent (Figure 14).

Horizontal stratification in the Itkillik silt is indicated by horizontal partings in thawing silt and by differential erosion attributed to vertical variation in root concentration

(Carter, 1988). We interpret Carter's observations to reflect a mixture of: (1) thawing ice lenses that may or may not reflect primary stratification; (2) bands formed either of almost pure ice or high concentrations of < 1 mm thick ice lenses ('ice belts' in the Russian permafrost literature); (3) bands of differing root density; and (4) true primary horizontal stratification, all features that occur at Duvanny Yar.

Differences between the Itkillik and Duvanny Yar yedoma concern carbonate content and thermokarst-cave ice. Greater carbonate contents at Itkillik (Figure 14B) presumably reflect carbonate source areas of the silt. Limestones occur to the south of Itkillik, in the north-central Brooks Range (Nelson and Csejtey, 1990). Several bodies of thermokarst-cave ice have been observed in the middle and lower parts of the Itkillik bluffs (Table 6), indicating local underground thermal erosion (Kanevskiy *et al*., 2011). In contrast, none have been identified in yedoma of unit 4 at Duvanny Yar, although three possible occurrences were seen in massive silt of unit 1, beneath the yedoma (Figure 6B). We note, however, that the geomorphic context of Itkillik is somewhat different to that of Duvanny Yar: the Itkillik site is closer to foothills (of the Brooks Range), although the surface of the yedoma is completely flat, and its elevation is from 90 to 110 m asl. The nearest outcrop of bedrock is just several kilometres from the site.

Northern Yakutia.

The yedoma elsewhere in the Kolyma, Indigirka and Yana lowlands shares a number of features with that at Duvanny Yar:

1. Silty or sandy-silty deposits poor in clay and enriched with fine, dispersed plant detritus.
2. Homogeneous and monotonous brownish or greyish colour that is determined by the abundance of detritus and expression of gleyic features.
3. Abundant relict organic carbon homogeneously dispersed in the mineral material (0.5–3% by weight).
4. Stratification based on colour or texture change with strata from 0.4 to 4–6 m thick, with no significant changes within them.
5. Blocky structure formed after thawing of deposits.
6. Abundant *in-situ* distal parts of plant roots (0.5–5 cm long).
7. Lenticular microcryostructures or ataxitic cryostructures are common.
8. Thaw consolidation and subsidence of the material.

In the High Arctic of Siberia, the wedge ice content is definitely higher than that in other areas of yedoma. There are many yedoma locations in the river valleys in the mountains of northern Yakutia, for example, along the north part of the Ulakhan-Sis ridge (Figure 2A). We believe that many yedoma sections in such areas are formed by slope sediments (Gravis, 1969; Kanevskiy, 2003), which can consist of retransported aeolian silt or weathering products and that include buried intermediate layers similar to those at Duvanny Yar.

In the Laptev Sea region and the New Siberian Archipelago (Figure 1A), yedoma resembles that at Duvanny Yar in terms of its stratigraphic position, elevation above sea level, silty to sandy texture, carbonate content, radiocarbon age and ground-ice properties (details in Schirrmeister *et al*., 2011b). Comparison of the yedomas in terms of their sedimentary structures and palaeosols, however, is difficult to evaluate without further geological and pedogenetic information. Some of these yedoma deposits differ from that at Duvanny Yar in their geomorphological context, with those from the western Laptev Sea coastlands and Lena Delta region occurring near low-elevation coastal mountains, and those from Bol'shoy Lyakhovsky and Cape Svyatoy Nos related to cryoplanation terraces (Figure 32). But all of these landscapes are alike in comprising extensive and fairly flat surfaces, with very low hydrological gradients (Schirrmeister *et al*., 2011b). Significantly, the heavy-mineral composition of the very fine sand fraction (63–125 μm) varies between different yedoma deposits in the Laptev Sea region and the New Siberian Archipelago, which these authors attribute to local sediment sources from adjacent mountains, in support of a model of nival lithogenesis for the yedoma. However, the local derivation of the very fine sand fraction does not discriminate between waterlain and aeolian deposition. Aeolian sand transport by saltation from local sources is a common feature in cold-climate loesses (Frechen *et al*., 2005), and is observed during summer dust storms near Kluane Lake, southwest Yukon (Nickling, 1978).

Central Yakutia.

In the central Yakutian lowland (Figure 1A) – directly west of western Beringia – silty yedoma deposits occur where continuous permafrost is about 400–700 m thick (Popp, 2006). The yedoma is ice-rich and blankets large parts of the lowland to thicknesses as much as 60 m, near Syrdah, about 70 km northeast of Yakutsk (Figure 32; Are, 1973, Figure 7). The silt has been attributed to a variety of depositional and weathering processes (reviewed by Péwé and Journaux, 1983). Of these, the most popular amongst Russian permafrost scientists is the lacustrine-alluvial hypothesis (e.g. Katasonov and Ivanov, 1973; Konishchev, 1973; Popov, 1953, 1973), in which the silts are thought to have accumulated (1) during great floods on huge floodplains, (2) in extensive shallow lakes and (3) on marshy plains adjacent to rivers such as the palaeo-Lena and palaeo-Aldan. Such conditions with water-saturated sediments were thought to be essential to allow growth of large syngenetic ice wedges. However, a more convincing interpretation of the silt is that of loess, in places retransported by slope processes (Péwé and Journaux, 1983). The source of the loess is attributed to deflation plains of braided river systems such as the palaeo-Lena and palaeo-Aldan, with increasing proportions of sediment derived from the local Verkhoyansk Mountains at sites closer to mountain valleys (Popp *et al*., 2007).

Sedimentologically, the frozen silt of central Yakutia is grey to black, with thin dark carbonaceous layers and

iron-stained bands and mottles. The silt tends to be massive, with little or no stratification, except in valley bottoms, where some has been retransported and is crudely stratified. Texturally, the silt is very uniform spatially throughout the central Yakutian lowland and vertically in stratigraphic sections, comprising 70 per cent silt, 17 per cent sand and 13 per cent clay, with higher percentages of sand (i.e. sandy loess) near the Aldan and Lena river floodplains. The median particle size (determined by sedimentation in water and sieving) of 27 samples of loess, sandy loess and clayey loess averages 21.6 μm (i.e. medium silt) (Péwé and Journaux, 1983, table 3), which is similar to the equivalent value of 28.4 μm from Duvanny Yar (Figure 14A). Carbonate contents tend to be no more than 2–3 per cent (Péwé and Journaux, 1983, Table 7), similar to the average value of 2.1 per cent measured at Duvanny Yar, although some central Yakutian loess have values as high as 7.6 per cent, which is higher than the maximum value of 3.5 per cent from Duvanny Yar (Figure 14A). Major elemental concentrations in the silt are nearly constant over large areas but differ from those at Duvanny Yar (Figure 22), suggesting differences in source mineralogy of the two loess regions. Both the central Siberian and the Duvanny Yar loesses, however, show low degrees of mineralogical maturity as they are close to the typical values of Na_2O/Al_2O_3 versus K_2O/Al_2O_3 present in unaltered igneous rocks (Figure 22E); according to Gallet *et al*. (1998) and Muhs and Budahn (2006), this proximity suggests that both loesses have undergone limited cycles of weathering, erosion and transportation, which is consistent with derivation of at least some of the loess from glaciogenic sediment. Vertebrate bones, sometimes articulated, are common in the yedoma, and include taxa similar to those at Duvanny Yar (e.g. mammoth, horse, bison). Finally, interbedded palaeosols within loess-like sediments have been identified near the Tumara River (Zech *et al*., 2008). Interestingly, these sediments contain no pedogenetically unaltered loess, which is rather different from the yedoma at Duvanny Yar. Ground ice within the silt is dominated by large syngenetic ice wedges and ice lenses, forming an 'ice-complex' (Are, 1973; Katasonov and Ivanov, 1973; Soloviev, 1973). This complex is very similar to that in the Kolyma Lowland in terms of structure, thickness, ice types and contents, syngenetic cryostructures and mantle-like occurrence on the landscape.

Table 7 Deposition rates for yedoma silt at Duvanny Yar calculated from the age model in Figure 23.

Section	Calibrated age (yr BP)	Height (m arl)	Deposition rate (mm yr^{-1})
Top S12	23,600	35.9	0.75
Bottom S13	30,300	30.9	
Top S10	35,100	31.0	2.00
Bottom S10	36,100	29.0	
Top S9	36,800	27.9	0.78
Bottom S9	38,700	26.4	
Top S8	45,400	25.9	?[a]
Bottom S4	>50,000	12.5	

[a]Deposition rate for silt deposited between the bottom of section 4 and the top of section 8 is not calculated because of uncertainty about the age of deposition, which may be substantially older than the radiocarbon ages. arl = Above river level. S = section.

We conclude that the Duvanny Yar yedoma represents the same ice-rich loess or reworked loess facies as that present at Itkillik and in the central Yakutian lowland. The yedoma in these areas is similar to greater or lesser degrees to that of the Laptev Sea region and the New Siberian Archipelago. All studied sections in these areas have both similarities and differences – in ice contents (wedge and segregated), grain size, organic contents and other soil properties, and sedimentation modes at these sites may have differed because of different geomorphological context and climate conditions. We suggest that many lowland yedoma sections are primarily of aeolian origin (or consist of reworked aeolian sediments), but we cannot exclude other depositional processes (e.g. alluvial and slope origin of some yedoma sections in river valleys and mountains, e.g. Kanevskiy, 2003).

Conceptual Model of Yedoma Silt Deposition and Syngenetic Ice-Wedge Growth

We propose a conceptual model of yedoma silt deposition and syngenetic ice-wedge growth (Popov, 1955) for aeolian deposits under cold-climate conditions such as those at Duvanny Yar, distinguishing deposition according to season. The time frame is from about 50 000 to 16 000 cal BP, encompassing most of MIS 3 and 2.

Winter was characterised by limited accumulation of snow, often dusty, and by deep thermal contraction cracking beneath thin snow covers. Loess deposition in winter was more limited than that in summer or autumn. A frozen ground surface overlain with a limited snow cover restricted deflation and silt supply, as observed in the present day in cold-climate loess regions such as western Greenland (Dijkmans and Törnqvist, 1991), in flattish lowland sites in the Canadian Arctic Archipelago (Lewkowicz and Young, 1991) and in inland areas of Iceland (Arnalds, 2010). Limited aeolian transport of sand may have occurred in winter, based on analogy with modern windy Arctic settings close to sandy sources (e.g. McKenna Neuman, 1990). Sediment trapping by dead grasses, often snow covered, diminished substantially in winter. Soil particles within wedge ice at Duvanny Yar (Sher *et al*., 1979), including distinct veins of grey sandy loam (Y. K. Vasil'chuk *et al*., 2001a), indicate that silt was mixed with snow (Y. K. Vasil'chuk *et al*., 2001b), as also observed in some present-day loess environments such as the Prudhoe Bay region of northern Alaska, where many snow drifts contain considerable amounts of windblown dust (D. A. Walker, personal communication, 2014). Pollen, spores and coal particles in syngenetic wedge ice at the Bison section (Figure 2A) provide additional evidence for an aeolian dust input, some reworked from older sediments (Y. K. Vasil'chuk *et al*.,

2003); such organic material was also mixed with snow. The ground surface, after the time of thermal contraction cracking, was typically covered by a thin layer of snow (cf. Hopkins, 1982), otherwise the wedges would contain much more silt or sand than they do, and therefore occur as soil or composite ice-soil wedges rather than ice wedges (J. B. Murton, 2013b), as illustrated by composite ice and silt wedges of primary infilling in the CRREL Permafrost Tunnel, central Alaska (Kanevskiy *et al*., 2008, Figure 3). Thermal contraction cracking was enhanced by the ice-rich substrates, which doubled or more the thermal coefficient of linear expansion (α) compared to dry loess (J. B. Murton and Kolstrup, 2003). High values of α favoured greater thermal contraction as the ground cooled in winter, in turn favouring wider and/or deeper or more closely spaced cracks, and facilitating growth of large syngenetic wedges, much larger than the wedges that developed in the warmer and less icy loesses of northwest Europe.

In spring, meltwater infilled thermal contraction cracks, and rivers experienced limited nival floods. Frost cracks infilled with snow meltwater, supplemented by hoarfrost and melt of ground ice in the active layer (Y. K. Vasil'chuk *et al*., 2001a). Spring snowmelt supplied meltwater to open cracks, infilling them with ice, mineral particles and organic detritus melted out from the snow. Dusty snow promoted earlier snowmelt in spring (due to lowered albedo) and therefore active-layer deepening, as observed near some Arctic roads where road dust is mixed with snow (Everett, 1980; Walker and Everett, 1987; Walker *et al*., 2014); dusty snow hastens snowmelt and promotes greater warming of soil in summer, in turn promoting deeper active layers. Sublimation of hoar ice crystals onto crack walls also occurred in spring, when the air became warmer than the permafrost. Although the contribution of hoarfrost to wedge growth is uncertain, it may have been significant, based on analogy with ice wedges in very arid climatic conditions of northern Victoria Land, Antarctica, whose growth has been attributed to hoarfrost accretion (Vtyurin, 1975; Tomirdiaro, 1980; French and Guglielmin, 2000). In late spring and summer during MIS 2, pulses of meltwater from glaciers of limited extent in some uplands near the Kolyma Lowland (Figure 2A) delivered sediment to the floodplain of the palaeo-Kolyma River.

Summer and/or autumn were the main seasons of loess accumulation. In summer, after snowmelt, the land surface (e.g. floodplains and Khallerchin tundra) was snow-free, unfrozen and relatively dry, making it vulnerable to deflation. The hydrology of the sediment source area was an important control on the timing of dust-generating events, as observed in present-day conditions in river valleys that drain glacierised catchments in southern Alaska, where river discharges are lowest in autumn and winter, and dust events are most frequent in October and November (Crusius *et al*., 2011). By late summer and autumn, rivers crossing the Kolyma Lowland would have been at a relatively low stage. Graminoids, forbs and biological soil crust communities trapped and stabilised windblown sediments, as occurs today in the Kluane grassland of southwest Yukon (Laxton *et al*., 1996; Marsh *et al*., 2006). Aeolian silt deposition in summer presently occurs on the floodplains and adjacent forested terrain of central Alaska (Péwé, 1951; Begét, 2001) and on uplands near proglacial valleys containing braided rivers in western Greenland (Dijkmans and Törnqvist, 1991). Loess accumulation was a mixture of semicontinuous deposition of fine background particles and episodic, discrete dust storms that deposited coarse silt (cf. Begét, 2001; Prins *et al*., 2007).

Reworking of primary loess by hillslope erosion was generally of minor significance and localised in occurrence. The limited elevation ranges of the undulating palaeolandsurface at Duvanny Yar and/or limited surface runoff from snowmelt and summer rain were insufficient to favour widespread and frequent hillslope erosion and reworking of silt, unlike regions with well-developed gulley or valley networks. Had reworking been significant, much of the yedoma silt would be laminated, similar to reworked Hesbayan (secondary) loess in Europe. Instead, most of the yedoma silt is massive, similar to the homogeneous Brabantian (primary) loess.

Rates of loess deposition varied through time, probably in part because source availability of silt varied (discussed below). High rates favoured accumulation of loess and development of cryopedoliths, and slow rates or cessation of deposition favoured soil development. Deposition rates constrained by our age model (Figure 23) are 0.78 mm yr^{-1} between 38 700 and 36 800 cal BP, 2.0 mm yr^{-1} between 36 100 and 35 100 cal BP and 0.75 mm yr^{-1} between 30 300 and 23 600 cal BP (Table 7). A high rate of 2.91 mm yr^{-1} calculated from the lower part of the age model is regarded as less definitive. As these rates do not take into account the ice volume in the silts, which we have calculated to average 58 per cent, the actual deposition rates were somewhat lower than these values. For comparison, loess accumulation rates of 0.02–0.94 mm yr^{-1} are reported for Pleistocene loess in Alaska and northwest Canada (Muhs *et al*., 2003, table 5). In western and central Siberia, loess accumulation rates of 0.13–0.67 mm yr^{-1}, 0.21–1.0 mm yr^{-1} and 0.03–0.26 mm yr^{-1} are reported for MIS 2, the LGM and MIS 3, respectively (Chlachula, 2003, table 3B). These comparisons indicate that loess deposition at Duvanny Yar was relatively rapid.

Permafrost aggraded syngenetically upward through the accumulating loess. As a result, roots and other organic material at the base of the palaeo-active layer were incrementally frozen into the rising permafrost. At the same time, segregated ice accumulating in the transition zone was also incorporated into the stable permafrost, producing a stacking or amalgamation of palaeotransition zones (French and Shur, 2010). Higher deposition rates led to fast vertical growth of syngenetic ice wedges, while slower rates resulted in widening of ice wedges and an increase in the amount of segregated ice in the palaeotransition zones. As a result, even during the periods of very low rates of silt accumulation, the ground surface continued to rise, mostly because of accumulation of ground ice (wedge ice and excess segregated and pore ice).

Potential Sources of Loess

Determining the source of the Duvanny Yar loess requires systematic characterisation of the mineralogy or geochemistry of the loess and potential source sediments and bedrocks, as well as determination of spatial patterns of particle size in the loess, which is beyond the scope of the present study. Nonetheless, some potential sources can be identified, based on understanding of cold-climate loess deposits elsewhere and the regional palaeoenvironmental conditions in and adjacent to the Kolyma Lowland. Such sources included: (1) sediments and weathered bedrock on uplands to the east, south and southwest of the Kolyma Lowland; (2) alluvium deposited by rivers draining these uplands; and (3) sediments exposed in the Khallerchin tundra to the north and on the emergent continental shelf of the East Siberian Sea farther north (Figure 2).

The uplands within the catchment of the palaeo-Kolyma River probably generated large quantities of silt and fine sand as a result of widespread frost weathering and local glacial grinding. Frost weathering by volumetric expansion of water freezing in microcracks or gas-liquid inclusions may break up individual quartz sand grains more readily than feldspar and produce silt-size material (Konishchev and Rogov, 1993; Matsuoka and J. B. Murton, 2008). Such weathering was probably greatest in the active layer, where the highest frequency of freeze-thaw cycles occurred, rather than in the more thermally stable permafrost below. Glacial grinding of bedrock and sediment in the basal layers of glaciers produces silty 'rock flour' and is thought to constitute a major source of loess near glaciated regions (Bullard, 2013; Muhs, 2013a). Upland glaciers in the palaeo-Kolyma catchment are thought to have been significantly more extensive in MIS 4 than in MIS 2 (Figure 2A; Glushkova, 2011). We speculate that this may explain the order-of-magnitude thicker yedoma at Duvanny Yar attributed in our age model (Figure 23) to MIS 3 or before (≥30 m) compared to MIS 2 (3–4 m) as the landscape adjusted to non-glacial conditions during MIS 3. Such *paraglacial* modification includes reworking of glaciogenic sediments on hillslopes by landslips, debris flows and surface runoff, and in valley floors by rivers (Ballantyne, 2002). Some silt and fine sand probably experienced deflation in the uplands, leading directly to loess deposition in the Kolyma Lowland, and much was probably reworked by tributaries of the palaeo-Kolyma River. Deflation was probably facilitated by two-sided freezing of the active layer, which tends to concentrate segregated ice near the top and bottom of the active layer, with the result that thaw of the upper centimetres of the active layer in summer leaves it loose and vulnerable to deflation.

Glacially sourced tributaries of the palaeo-Kolyma River must have contributed glacially ground silt into channel and/or floodplain deposits, and these were probably reworked by wind and deposited as loess in the Kolyma Lowland. A significant number of the palaeo-Kolyma's tributaries contained glacier ice in their catchments during MIS 4, and fewer during MIS 2 (Figure 2A). The map of yedoma deposits in the Kolyma Lowland (Figure 2B; Grosse *et al.*, 2013) clearly shows that their spatial distribution relates to river valleys, either infilling them or extending locally to regionally away from them. A broadly similar spatial association of glacially sourced rivers and loess occurs in central and northern Alaska, where loess tends to be associated with floodplain sources of rivers draining glaciated areas of the Alaska Range and the Brooks Range (Figure 31). Even today where glaciers occupy only small percentages of drainage basin areas, as with the Yukon River (Brabets *et al.*, 2000) and Athabasca River in Canada (Hugenholtz and Wolfe, 2010), they can still generate abundant silt, influence the stream hydrographs and supply loess deposits nearby (see review in Bullard, 2013).

The whole palaeo-Kolyma system can be considered as somewhat analogous to the Slims River delta in the Yukon, taking into account the combined flow contributions from the palaeo-Malyy Anyuy, Bol'shoy Anyuy, Omolon and Kolyma rivers. The southern limits of yedoma extend quite far into the upland ranges (Figure 2B), suggesting the loess is locally derived from each of these stream systems, right up into the valley systems. Katabatic winds from these ranges probably played a part in mobilising local sediment sources as they do today in the Slims River. The confluences of each stream system, particularly the palaeo-Omolon and the palaeo-Kolyma, may have been peak source areas for loess. Spring floods induced by snowmelt in the palaeo-Kolyma catchment were probably much more limited in magnitude than modern nival floods as a result of dry conditions that characterised MIS 2 and parts of MIS 3, as discussed previously. Summer flows in tributaries containing glaciers (Figure 2A) were supplemented by glacial meltwater during MIS 2, dependent on upland weather conditions (precipitation and temperature) that were responsible for summer melt on glacier surfaces. After spring snowmelt had ended and the floodplain of the palaeo-Kolyma and Omolon had dried in summer, silt deflation from this area would have occurred, similar to that observed today on floodplains of central Alaska (Péwé, 1951; Begét, 2001).

The coarser particles (exceeding about 30–40 μm) in the Duvanny Yar loess must have been locally derived from the Kolyma Lowland, because strong winds are needed to suspend such grains. Likely sources include sands deflated from the palaeo-Kolyma floodplain and the Khallerchin tundra to the north, consistent with a prevailing wind direction in summer towards the southeast, as in the present day (Figure 2A). For comparison, coarser particles in the Fairbanks loess (Begét, 1988) probably derive mostly from the floodplain of the Tanana River.

Assuming that synoptic conditions were broadly similar to those at present, we hypothesise that winds during MIS 2 and 3 tended to be strongest in summer and had a prevailing southeastward component near Duvanny Yar, as at present (Figure 2A), whereas winter winds were calmer than summer winds due to the intensification and longer residence time of the Siberian high over central Eurasia. Summer winds deflated sediment exposed on the East Siberian Sea shelf, producing aeolian sands now preserved as

Alyoshkin Suite sands across a dune tract represented by the Khallerchin tundra, which formed on the surface of a braided floodplain of the palaeo-Kolyma River (Hopkins, 1982). Hopkins interpreted the loess at Duvanny Yar as a distal facies of finer windblown sediment derived from the same sediment source. Kolpakov (1982) reported that ventifacts in deflation deserts are rare in the Kolyma Lowland, consistent with loess there being also deflated from floodplains.

Palaeoenvironmental Reconstruction of Duvanny Yar Sedimentary Sequence

Based on our interpretation of the sedimentary sequence comprising units 1 to 5 at Duvanny Yar (Table 4), we reconstruct the palaeoenvironmental conditions as follows:

Cold-stage Deposition (MIS 6).

The taberal sediment in unit 1 yielded pollen spectra typical of cold-stage pollen floras, dominated by Poaceae and forbs. The depositional history of the sediments, however, is not known.

Thermokarst Activity (Kazantsevo Interglacial).

The wood-rich detrital peat of unit 2 is dominated by *Pinus* (haploxylon) pollen, here interpreted as *P. pumila* pollen. The high value (about 75%) of *P. pumila* pollen is atypical of the Holocene, but Lozhkin *et al.* (2006) reported values of 60 per cent from the LIG at Lake El'gygytgyn (Chukotka) from sediments dating to MIS 5. Thus, the high value is compatible with a LIG age for the detrital peat in unit 2 at Duvanny Yar.

The sequence at Duvanny Yar suggests that interglacial-age deposits unconformably overlie cold-stage deposits, as would be the case if interglacial thermokarst activity had occurred. Thermokarst activity was probably expressed by one or more thaw lakes developing at Duvanny Yar during the Kazantsevo interglacial. Lake water resulted in thaw of the massive silt of unit 1, interpreted as taberal sediments (cf. Kaplina *et al.*, 1978), in a talik beneath the lake bottom. Vegetation flanking the lake was redeposited as a result of lake expansion to form a 'trash layer' of detrital plant material on the lake bottom (peat of unit 2). Stratified silt (unit 3) winnowed by lake waves and currents buried the peat, to form the main lacustrine infill of the lake. Lake initiation may have occurred during the Kazantsevo interglacial of MIS 5e. Similar thermokarst-related lake development occurred in the Dmitry Laptev Strait (Kienast *et al.*, 2011), and widespread thermokarst activity in northern Yakutia is consistent with warmer-than-modern conditions during the Kazantsevo interglacial in western Beringia (discussed previously). At Duvanny Yar, thermal erosion and subsequent refreezing of pooled water produced thermokarst-cave ice (Figure 6B).

Lacustrine to Aeolian Transition.

The palaeoenvironmental conditions and exact timing of the transition from lacustrine deposition in unit 3 to aeolian deposition in unit 4 are not known, as we did not observe the contact between these units. The transition post-dates MIS 5e and predates 50 000 cal BP (the oldest yedoma silt according to our age ^{14}C model; Figure 23) and 48.6 ± 2.9 ka (the oldest OSL age from the yedoma). We speculate that it occurred around the early part of the Zyryan glacial (MIS 4) as a result of colder and drier climate conditions commencing then (Elias and Brigham-Grette, 2013).

Loess Accumulation, Pedogenesis and Syngenetic Permafrost (Karginsky Interstadial and Sartan Glacial).

Loess accumulation, pedogenesis and syngenetic permafrost aggradation characterised environmental conditions during yedoma formation at Duvanny Yar in the Karginsky interstadial and Sartan glacial. These processes may have commenced during the Zyryan glacial, given the uncertainties of our ^{14}C age model below elevations of 15–20 m arl in section CY. Pedogenesis formed cryopedoliths as incremental loess deposition continually buried the landsurface. During the Karginsky interstadial, loess deposition episodically slowed significantly or ceased, allowing palaeosols to develop. During the Sartan glacial, loess deposition prevailed, suppressing palaeosol development.

Insight into Beringian MIS 2 soils comes from a land surface buried under tephra on the Seward Peninsula, Alaska, which is underlain by well-preserved palaeosols (Höfle *et al.*, 2000). Soil descriptions (Höfle and Ping, 1996) attest to a thin or discontinuous surface organic layer and ALTs of about 0.5 m. Chemically, the soils conform to Inceptisols, with little evidence of leaching; there is little visual evidence of differentiated horizons, and the soils are nutrient-rich because of continual additions from loess deposition. They are associated with vegetation similar to modern dry, meadow and herb-rich tundra with a continuous moss layer. Snowbeds and hollows provided damper habitats for more moisture-demanding taxa such as *Salix*, and loess continuously accumulated on the land surface (Goetcheus and Birks, 2001). Péwé (1975a) and Hopkins (1982) conjectured that much of lowland Beringia during the LGM was characterised by accumulation of loess, and the Kitluk profiles are consistent with this. With continual loess input and freezing of the silt into permafrost within a few thousand years, soil development of the Kitluk palaeosol was prevented beyond the incipient stage (Höfle *et al.*, 2000), similar to the inferred palaeosols 3 and 4 in unit 4 at Duvanny Yar. Aridity and loess deposition favoured herbaceous species over shrubs (Höfle *et al.*, 2000).

Syngenetic permafrost developed in the accumulating loess at Duvanny Yar. Despite dry conditions prevailing through much of MIS 3 and 2, the permafrost accumulated abundant excess ground ice, mostly as syngenetic ice wedges and segregated ice. The wedges record a snow cover that was thin enough to promote rapid ground cooling and deep thermal contraction cracking in winter, but thick enough to supply meltwater to the cracks in spring. The segregated ice within the loess reflects the highly frost-

susceptible nature of the sediment, as material of this particle size is very efficient at locking up available liquid water as ice in near-surface permafrost. Pollen assemblages do not clearly distinguish between LGM and other periods, although an absence of *Larix* and lower forb diversity aligns with other data from the region that suggest the LGM climate was harsher than that of bracketing periods (e.g. Sher *et al*., 2005; Andreev *et al*., 2011).

Cessation of Yedoma Formation (Lateglacial).

Yedoma formation at Duvanny Yar ceased about 14 000–13 000 ^{14}C BP (17 000–15 500 cal BP), during the transition from the Sartan glacial period to the early part of the Lateglacial (Allerød). This cessation may reflect the onset of warmer and wetter conditions, with abundant willow and graminoids between the very cold and dry mammoth steppe and the rise of mesic-hydric taiga and tundra vegetation (Guthrie, 2006, Figure 2). Alternatively, it might reflect cessation of windy conditions in addition to reduced production and/or deflation of silts from alluvial sources. In step with this transition, synlithogenic soil formation that characterised the Late Pleistocene in the coastal lowlands of northern Yakutia was replaced by epigenic soil formation during the Holocene (Gubin and Lupachev, 2008).

Thermokarst Activity (Early Holocene).

Widespread thermokarst activity occurred during the early Holocene in the Kolyma Lowland, as indicated by the formation of thaw lake basins.

Permafrost Aggradation (Mid to Late Holocene).

Permafrost aggradation has occurred during the mid and late Holocene, leading to refreezing of the lower and central part of the deep early Holocene palaeo-active layer. This produced an ice-rich intermediate layer overlain by a slightly less icy transient layer (Figure 16).

The two Holocene pollen samples have radiocarbon ages that correspond to about 100 years (1900 AD) and about 150 years (1850 AD) years before today. However, the pollen spectra come from 0.5 and 0.7 m below the modern surface, within the transition zone, and thus they are unlikely to be recent. Arboreal taxa and Ericales dominate and abundant *Sphagnum* suggests moist, organic substrates. Although their actual age is uncertain, these samples have similar *Pinus* values to modern samples in the forest-tundra or *Larix* forest zones of the lower Kolyma. The modern and Holocene samples are similar, and they clearly differ from all the other samples compositionally (Appendix S4), confirming the major switch in vegetation that characterised the onset of the Holocene.

Beringian and Eurasian Aeolian Activity

The Duvanny Yar loess is consistent with evidence of widespread aeolian activity in the Late Pleistocene of Beringia and Eurasia. D. M. Hopkins (1982) hypothesised that many areas of Beringia experienced intense aeolian activity during MIS 2 but acknowledged that their deposits of windblown silt and sand are far from completely inventoried and many of their ages are poorly known. Increasing geological evidence to support Hopkins' suggestion has subsequently been presented from North America and Eurasia. In northwestern North America, dunefields, sand sheets, sand wedges and composite wedges, deflation areas and loess characterised much of the unglaciated region, particularly during MIS 2, and extended into deglaciated regions (Figure 31). On the Alaskan Arctic Coastal Plain, a Late Pleistocene sand sea (*Ikpikpuk Dunes*) grades distally into the loess belt along the foothills of the Brooks Range (Carter, 1981, 1988; Hopkins, 1982; Dinter *et al*., 1990) and proximally into a region with large aeolian sand wedges (Carter, 1983). Farther east, on the Canadian Arctic Coastal Plain another Late Pleistocene sand sea (*Kittigazuit Dunes*) developed on the Tuktoyaktuk Coastlands and offshore across the emergent eastern Beaufort Sea Shelf, NWT (Dallimore *et al*., 1997; Bateman and J. B. Murton, 2006; J. B. Murton, 2009b; J. B. Murton *et al*., 2007). Large sand wedges and composite wedges of Late Pleistocene age developed widely in this region, particularly during deglaciation of the Laurentide Ice Sheet (J. B. Murton, 1996b; J. B. Murton *et al*., 1997). Foresets in the Ikpikpuk Dunes indicate a palaeowind direction generally towards the west-southwest (Carter, 1981), similar to modern sediment-transporting wind directions (Muhs and Budahn, 2006), and those in the Kittigazuit Dunes towards the southeast (Dallimore *et al*., 1997) (Figure 31). In Siberia, Kolpakov (1982) reported that deflation deserts covering large regions from Mongolia to the Laptev Sea were associated with intensive release of sand and silt, and subsequent deposition as aeolian sand and thick accumulations of loess (yedoma). Recently, Velichko *et al*. (2011) have reconstructed a vast cold desert that covered the northern half of West Siberia during the Younger Dryas Stadial and probably the LGM, based on surface textures characteristic of aeolian abrasion of quartz sand grains from sands beneath peat. These authors suggested that highly arid conditions and intense aeolian processes there led to widespread reworking of sand deposits and deflation of silt particles that contributed to loess deposition in the southern part of the West Siberian Plain (Figure 32). However, the degree and extent of LGM aeolian activity in this region remains to be determined, because the development of a LGM cold desert over all the west Siberian north is not supported by the evidence of mammoths living there (Astakhov, 2014). Geological evidence for aeolian activity in the form of coversands and dune sands in the Pechora basin area of northern European Russia (Figure 32) and, less commonly, in west Siberia is summarised by this author.

Regarding potential sediment-transporting palaeowinds during MIS 2 and 3 in Arctic and Subarctic regions, Muhs and Budahn (2006) have hypothesised regional-scale pressure gradients and more localised lower-level winds. During the last glacial period, Siberian and Canadian high-pressure cells coupled with a strengthened Aleutian low-pressure cell would have created enhanced pressure

gradient-driven winds sufficient to entrain sand or silt. Whereas today such conditions are restricted to winter, longer residence time of this synoptic pattern may have existed during the last glacial period. In addition to these enhanced regional-scale winds, stronger localised winds created by local downslope gravity flows (katabatic winds) may also have entrained sediment. In central Alaska, stronger lower-level katabatic wind conditions may have resulted from expanded glaciers in the Alaska Range. Similarly, we suggest that local katabatic winds in summer may have transported silt generally northwards towards the Kolyma Lowland, particularly during times of extended upland glaciation during the Zyryan (MIS 4) period, whereas winter winds carried limited amounts of silt generally southwards as a result of pressure gradient forces.

We conclude that the Duvanny Yar loess represents part of an extensive cold-climate loess deposit that stretches westwards from northeast Yakutia through central Yakutia to the loess belt of Europe and eastwards to the loess of eastern Beringia. The loess represents a gradation between two end members. One constitutes very ice-rich loess (yedoma) characteristic of continuous permafrost that existed throughout MIS 4 to 2 in much of Beringia and central Yakutia and persists to the present day within continuous to discontinuous permafrost (Figure 30). The other constitutes ice-poor loess characteristic of permafrost that developed episodically in northwest Europe and in western and central Siberia, where permafrost degraded during the last glacial-interglacial transition. The ice-rich loess at Duvanny Yar was deposited in a 'cold-polar' (rather than seasonally cold) aeolian environment (see Wolfe, 2013), and during the last glacial-interglacial transition, the environment there has changed from what might once have been considered as glacially proximal cold-polar into continental cold-polar. Persistence of cold continuous permafrost conditions during loess deposition at Duvanny Yar led to stacking of ice-rich transition zones and growth of large syngenetic ice wedges characteristic of yedoma. By contrast, episodic permafrost conditions in warmer regions to the south and west led to repeated permafrost thaw and development of small ice wedges now represented by ice-wedge and composite-wedge pseudomorphs.

SUMMARY AND CONCLUSIONS

1. Five litho- and cryostratigraphic units identified in yedoma remnant 7E at Duvanny Yar comprise, in ascending stratigraphic order: (1) massive silt, (2) peat, (3) stratified silt, (4) yedoma silt and (5) near-surface silt (Table 4).
2. The yedoma silt of unit 4 is at least 34 m thick and displays subtle colour bands between 2.5Y 3/1 (very dark grey) and 2.5Y 3/2 (very dark greyish brown). The bands are commonly 1–20 cm thick (maximum 1 m), horizontal to gently undulating, parallel and internally massive. The bands are thought to reflect changes in the quantity and type of plant detritus, humification and mineralisation, and organic coatings on mineral particles. In terms of primary sedimentary structures, the great majority of the yedoma silt is unstratified and very uniform in appearance. Occasionally, faint stratification occurs locally in the form of horizontal, parallel strata a few millimetres to about 10 cm thick.
3. The organic fraction in the yedoma silt is dominated by semidecomposed fine plant material, with pervasive fine *in-situ* roots. Larger woody roots and wood fragments also occur. Two organic layers 0.15–0.20 m thick form stratigraphic marker horizons at 11.7 and 30.2 m arl, the lower of which is involuted. Three root-rich horizons occur between 6.2 and 6.6 m arl. Organic contents average 4.4 per cent (range: 1.9 to 9.5%). Higher-than-average values of about 6–8 per cent occur in organic layers 1 and 2, and in the three root-rich layers. Two additional peaks in organic content (8.0 and 9.5%) occur at heights of 21.3 and 25.4 m arl.
4. Syngenetic ice wedges up to at least 34 m high and up to a few metres wide penetrate the yedoma and contain minor amounts of disseminated silt. Epigenetic ice wedges up to a few metres high and about 1 m wide extend down from the transition zone into the upper several metres of yedoma.
5. Texturally, the yedoma silt of unit 4 has mean values of 65 ± 7 per cent silt, 15 ± 8 per cent sand and 21 ± 4 per cent clay. Particle-size distributions are bi- to polymodal. The primary mode is about 41 μm (coarse silt) and subsidiary modes are 0.3–0.7 μm (very fine clay to fine clay), 3–5 μm (coarse clay to very fine silt), 8–16 μm (fine silt) and 150–350 μm (fine sand to medium sand). Higher-than-average clay contents are associated with organic layers 1 and 2, and some root-rich layers, and also occur at heights of about 23 and 26 m arl. For comparison with the sediment properties of Duvanny Yar yedoma, samples of yedoma silt from Itkillik (northern Alaska) are similarly bi- to polymodal.
6. Pollen spectra in yedoma silt of unit 4 (as opposed to those in interglacial deposits) are characterised by varying concentrations and ratios of arboreal to non-arboreal pollen (pollen zones D to B in Figure 26). The pollen patterns were likely mediated by windiness, which partly controlled the contribution of the long-distance element of the pollen rain. Samples from silt dated to the LGM (pollen zone B in Figure 26) are not readily distinguishable from other MIS 2–3 samples, but they do appear floristically less diverse and they lack *Larix*. All except interglacial samples feature a range of forb taxa and tend to have high values of *S. rupestris*, which is virtually absent in interglacial samples. Holocene samples (pollen zone A in Figure 26) are similar to modern ones from the lower Kolyma region. The sample from peat of unit 2 (Figure 25), attributed to the LIG, stands out as being dominated by *Pinus* (haploxylon), but this is not dissimilar to interglacial spectra from Lake El'gygytgyn in Chukotka.

7. An age model for yedoma silt deposition at Duvanny Yar is based on 47 ^{14}C ages from a composite stratigraphic section through unit 4, supplemented by three OSL ages on quartz grains in the 90–180 μm fraction (Figure 23). Unlike previous ^{14}C dating attempts at Duvanny Yar (Figure 4), ^{14}C ages revealed good stratigraphical order, suggesting continuous silt deposition. Discontinuities in the ^{14}C age-height sequence at heights of 25.9–26.4 m, around 31 m and 35.9–36.2 m coincide with boundaries between constituent stratigraphic sections or with palaeosols. The ^{14}C age model for yedoma deposition extends from 19 000 ± 300 cal BP at 36.7 m arl to around 50 000 cal BP or beyond at 4.3 m arl. ^{14}C ages of yedoma below 24 m arl are close to the limit of ^{14}C dating and beyond the range of the ^{14}C calibration curve, and so are considered to be less definitive than the age model of yedoma above 24 m arl. The three OSL ages range from 21.2 ± 1.9 ka near the top of the yedoma to 48.6 ± 2.9 ka near the bottom, broadly consistent with the ^{14}C age model.
8. Most of the yedoma silt at Duvanny Yar has experienced incipient pedogenesis before syngenetic freezing. Such *cryopedolith* material has properties that reflect pedogenic processes but lacks well-expressed buried soil profiles.
9. Five buried palaeosols and palaeosol 'complexes' are identified between cryopedolith material in the yedoma silt (Figure 5). Three palaeosols correspond with organic layers and root-rich layers identified in field sections, and two are interpreted on the basis of elevated values of organic matter and phosphorus and reduced mobile-to-immobile element ratios (Na_2/TiO_2, SiO_2/TiO_2, MgO/TiO_2, K_2O/TiO_2) (Figure 21A), which are attributed to pedogenic processes and chemical weathering. All five palaeosols, as well as the modern soil, show some elevated Ti/Zr ratios and clay contents.
10. Yedoma silt at Duvanny Yar accumulated on an undulating palaeo-land surface with a relief of several metres or more (indicated by variable elevations of palaeosols) rather than a flat and horizontal plain underlain by a layercake stratigraphy. Substantial deformation and uplift of the ground surface resulted from syngenetic ice-wedge growth adding volume to the permafrost.
11. Syndepositional erosion of yedoma silt is indicated by an angular unconformity (erosion surface) about 13.7 m arl, and may have occurred by running water or wind.
12. The alluvial-lacustrine hypothesis for deposition of yedoma silt at Duvanny Yar is discounted because: (1) alluvial silts cannot have been deposited at the same time at elevations of 15–20 m arl at Alyoshkina Zaimka and 50–100 m arl across the Omolon-Anyuy yedoma (Figure 2B) without invoking unreasonably deep river floods; (2) the water source for such extensive and repeated flooding of the palaeo-Kolyma River for more than 20 000 years during drier-than-present environmental conditions in MIS 3 and 2 is enigmatic; (3) thermokarst activity during or after the inferred floods or lake development would have been extensive in the thaw-sensitive yedoma, but lacks cryostratigraphic evidence; (4) a Beringian-wide and sudden switch in tectonic movement at the end of the Pleistocene from continuous subsidence (needed for accumulation of tens of metres of silty alluvium) to uplift (needed for current deep river incision by about 50 m) is unsubstantiated; (5) the geomorphic location of the yedoma outside of rather than within floodplains, as well as the occurrence within the yedoma of buried epigenic rather than synlithogenic soils are inconsistent with alluvial deposition; (6) Arctic ground squirrels, whose burrows fills are common in MIS 3 cryopedoliths at Duvanny Yar, would have actively avoided burrowing in floodplains subject to repeated flooding; and (7) sedimentary structures indicative of flowing water and lacustrine deposits have not been observed in the well-exposed yedoma.
13. Polygenetic hypotheses for yedoma silt deposition at Duvanny Yar are discounted because: (1) sedimentary structures recording switches in deposition between overbank, aeolian and overland flow processes have not been observed; and (2) the water source for extensive flooding to submerge the whole region of the Omolon-Anyuy yedoma during very dry conditions of MIS 2 is unknown.
14. The loessal hypothesis for deposition of yedoma silt is the only reasonable hypothesis that can account for the bulk of the yedoma silt at Duvanny Yar. It resolves the problems associated with the alluvial-lacustrine and polygenetic hypotheses, and explains: (1) the absence of primary sedimentary stratification in most of the yedoma silt in terms of airfall (primary) loess; (2) the occasional faintly stratified layers of yedoma silt in terms of reworked (secondary) loess; (3) the bi- to polymodal particle-size distributions in terms of mixing of populations of grains derived from different sources and transported by different wind-driven mechanisms; and (4) the buried palaeosols in terms of a loess-palaeosol sequence. Although the bulk of the yedoma silt is interpreted as primary (airfall) loess that settled from suspension, occasional indistinctly stratified silt may have been redeposited on low-angle slopes, particularly in view of annual snowmelt operating on an undulating palaeo-land surface.
15. Supporting the loessal interpretation are sedimentological similarities between the Duvanny Yar loess-palaeosol sequence and cold-climate loess-palaeosol sequences in the past permafrost zone of western and central Siberia and northwest Europe. What sets the Duvanny Yar loess apart from such sequences is the persistence of permafrost and abundance of ground ice and fine *in-situ* roots within the yedoma. The Duvanny Yar yedoma is part of a subcontinental-scale region of Late Pleistocene cold-climate loess. One end member, exemplified by the yedoma silt at Duvanny Yar, was loess rich in syngenetic ground ice (Beringian

yedoma). The other, exemplified by loess in northwest Europe, was ice-poor and subject to complete permafrost degradation at the end of the last ice age. These end members reflect a distinction between enduring cold continuous permafrost conditions that led to stacked transition zones and large syngenetic ice wedges in much of Beringia versus cold-warm oscillating permafrost conditions that led to repeated permafrost thaw and small ice-wedge pseudomorphs in northwest Europe.

16. Modern analogues of cold-climate loess deposition are envisaged at a local scale in cold humid climates where local entrainment and deposition of loess are generally restricted to large alluvial valleys containing rivers that are glacially sourced or drain areas containing Late Pleistocene glacial deposits, and thus glacially ground silts. Examples include the Kluane Lake region of southwest Yukon, Canada; lower Adventdalen, Spitsbergen; large braided river floodplains on the Alaskan Arctic Coastal Plain and in southern Alaska; and alongside proglacial valley sandurs in West Greenland. In each case, much of the silt derives from glacial grinding in adjacent mountains. Potential sources of loess at Duvanny Yar include: (1) sediments and weathered bedrock on uplands to the east, south and southwest of the Kolyma Lowland; (2) alluvium deposited by rivers draining these uplands; and (3) sediments exposed in the Khallerchin tundra to the north and on the emergent continental shelf of the East Siberian Sea. Glacially sourced tributaries of the palaeo-Kolyma River contributed glacially ground silt into channel and/or floodplain deposits, and some of these were probably reworked by wind and deposited as loess in the Kolyma Lowland.
17. The Duvanny Yar yedoma silt shares many sedimentological and geocryological features with yedoma interpreted as ice-rich loess or reworked loess facies at Itkillik (northern Alaska) and in the central Yakutian lowland, and with cold-climate loess-palaeosol sequences in the discontinuous permafrost zone of central Alaska and the Klondike in Yukon, Canada. It is also similar to yedoma in the Laptev Sea region and the New Siberian Archipelago. It is therefore suggested that many lowland yedoma sections across Beringia are primarily of aeolian origin (or consist of reworked aeolian sediments), although other depositional processes (e.g. alluvial and colluvial) may account for some yedoma sequences in river valleys and mountains.
18. A conceptual model of yedoma silt deposition and syngenetic ice-wedge growth at Duvanny Yar in MIS 3 and MIS 2 envisages summer or autumn as the main season of loess deposition. At this time, the land surface was snow-free, unfrozen and relatively dry, and therefore vulnerable to deflation. Graminoids, forbs and biological soil crust communities trapped and stabilised windblown sediments, with the accumulating loess recording a mixture of semicontinuous deposition of fine background particles and episodic, discrete dust storms that deposited coarse silt. Winter was characterised by deep thermal contraction cracking beneath thin and dusty snow covers. Snow and frozen ground restricted deflation and sediment trapping by dead grasses in winter.
19. Loess deposition rates constrained by the age model are 0.78 mm yr^{-1} between 38 700 and 36 800 cal BP, 2.0 mm yr^{-1} between 36 100 and 35 100 cal BP and 0.75 mm yr^{-1} between 30 300 and 23 600 cal BP (Table 7). Such rates are relatively rapid compared with Late Pleistocene loess in Alaska, northwest Canada, and western and central Siberia.
20. The palaeoenvironmental reconstruction of the sedimentary sequence at Duvanny Yar is traced from MIS 6 to the late Holocene (Table 4). It includes thermokarst activity associated with thaw lake development in the Kazantsevo interglacial (MIS 5e), loess accumulation, pedogenesis and syngenetic permafrost development in the Karginsky interstadial and Sartan glacial, cessation of yedoma silt deposition during the Lateglacial, renewed thermokarst activity in the early Holocene and permafrost aggradation in the mid to late Holocene.
21. Beringian coastlands from northeast Yakutia through the north Alaskan Coastal Plain to the Tuktoyaktuk Coastlands (Canada) were characterised by extensive aeolian activity (deflation, loess, sand dunes, sand sheets, sand wedges) during MIS 2. Siberian and Canadian high-pressure cells coupled with a strengthened Aleutian low-pressure cell would have created enhanced pressure gradient-driven winds sufficient to entrain sand or silt on a regional scale. Summer winds probably deflated sediment exposed on the East Siberian Sea shelf and deposited silt as a distal aeolian facies to the south. Additionally, strong localised winds created by local downslope gravity flows (katabatic winds) may also have entrained sediment. Katabatic winds in summer may have transported silt generally northwards towards the Kolyma Lowland, particularly during times of extended upland glaciation during the Zyryan (MIS 4) period, whereas winter winds carried limited amounts of silt generally southwards as a result of pressure gradient forces.
22. High-resolution sampling of drill core from the central, higher part of Duvanny Yar has the potential to provide important palaeoenvironmental data on MIS 3 and LGM atmospheric conditions in northeast Eurasia.

ACKNOWLEDGEMENTS

Funding for the research was supported by the EU ECOCHANGE Programme (to MEE). Fieldwork at Duvanny Yar was supported by Sergey and Nikita Zimov of the North-East Science Station, Cherskii. Research by SVG and AVL was partly supported by funding from the Russian Foundation for Basic Research (RFBR) (grants 11-04-01274a, 12-04-10049k, 13-04-10053k and 13-05-90768mol_rf_nr)

and by the Russian Geographical Society (grant 70/2013-H7). Research by ACV and YKV was partly supported by the RFBR (grants 14-05-00795 and 14-05-00930). Yedoma studies in Alaska were supported by National Science Foundation grants ARC-0454939, ARC-1023623 and ARC-1107798 (to MK and YS). John Fletcher of the British Geological Survey is thanked for making thin sections for micromorphological analysis. Photomicrographs were taken in the Centre of Micromorphology at Queen Mary University of London. Rob Ashurst assisted with the preparation on the OSL dating material. Pierre Antoine and Jef Vandenberghe kindly provided photographs of European loess. We thank Jef Vandenberghe, Dan Muhs and an anonymous referee for their valuable comments on earlier versions of the manuscript.

REFERENCES

Alfimov AV, Berman DI. 2001. Beringian climate during the late Pleistocene and Holocene. *Quaternary Science Reviews* **20**: 127–134. DOI:10.1016/S0277-3791(00)00128-1.

Alfimov AV, Berman DI, Sher AV. 2003. Tundra-steppe insect assemblages and reconstructions of late Pleistocene climate in the lower reaches of the Kolyma River. *Zoologicheskiy Zhurnal* **82**: 281–300 (in Russian).

Anderson PM, Lozhkin AV. 2001. The Stage 3 interstadial complex (Karginskii/middle Wisconsinan interval) of Beringia: variations in paleoenvironments and implications for paleoclimatic interpretations. *Quaternary Science Reviews* **20**: 93–125. DOI:10.1016/S0277-3791(00)00129-3.

Anderson PM, Lozhkin AV (eds). 2002. *Late Quaternary Vegetation and Climate of Siberia and the Russian Far East*. National Oceanic and Atmospheric Administration and Russian Academy of Sciences: Magadan, Russia.

Andreev AA, Schirrmeister L, Tarasov PE, Ganopolski A, Brovkin V, Siegert C, Wetterich S, Hubberten H-W. 2011. Vegetation and climate history in the Laptev Sea region (Arctic Siberia) during Late Quaternary inferred from pollen records. *Quaternary Science Reviews* **30**: 2182–2199. DOI:10.1016/j.quascirev.2010.12.026.

Antoine P, Rousseau D-D, Lautridou JP, Hatté C. 1999. Last interglacial–glacial climatic cycle in loess-palaeosol successions of north-western France. *Boreas* **28**: 551–563.

Antoine P, Catt J, Lautridou J-P, Sommé J. 2003. The loess and coversands of northern France and southern England. *Journal of Quaternary Science* **18**: 309–318. DOI:10.1002/jqs.750.

Antoine P, Rousseau D-D, Moine O, Kunesch S, Hatté C, Lang A, Tissoux H, Zöller L. 2009. Rapid and cyclic aeolian deposition during the Last Glacial in European loess: a high-resolution record from Nussloch, Germany. *Quaternary Science Reviews* **28**: 2955–2973. DOI:10.1016/j.quascirev.2009.08.001.

Antoine P, Rousseau D-D, Degeai J-P, Moine O, Lagroix F, Kreutzer S, Fuchs M, Hatté C, Gauthier C, Svoboda J, Lisá L. 2013. High-resolution record of the environmental response to climatic variations during the Last Interglacial–Glacial cycle in Central Europe: the loess-palaeosol sequence of Dolní Vestonice (Czech Republic). *Quaternary Science Reviews* **67**: 17–38. DOI:10.1016/j.quascirev.2013.01.014.

Are FE. 1973. *Development of thermokarst lakes in central Yakutia. Guidebook*. Second International Conference on Permafrost. USSR Academy of Sciences: Section of Earth Sciences, Siberian Division, Yakutsk.

Arkhangelov AA. 1977. Underground glaciation of the Kolyma Lowland. In *Problems of Cryolithology*, Popov AI (ed). Moscow State University: Moscow, Vol. **VI**: 26–57 (in Russian).

Arkhangelov AA, Rogov VV, Lyanos-Mas AV. 1979. The cryogenic-facies structure of the edoma rock series in the Duvannyi Yar of the Kolyma lowland. In *Problems of Cryolithology*, Popov AI (ed). Moscow State University Press: Moscow, Vol. **VIII**: 145–156 (in Russian).

Arinushkina EV. 1970. *Guidelines for Chemical Analysis of Soils*. Moscow State University Press: Moscow.

Arnalds O. 2010. Dust sources and deposition of aeolian materials in Iceland. *Icelandic Agricultural Sciences* **23**: 3–21.

Astakhov V. 2014. The postglacial Pleistocene of the northern Russian mainland. *Quaternary Science Reviews* **92**: 388–408. DOI:10.1016/j.quascirev.2014.03.009.

Ballantyne CK. 2002. Paraglacial geomorphology. *Quaternary Science Reviews* **21**: 1935–2017. DOI:10.1016/S0277-3791(02)00005-7.

Bateman MD, Catt JA. 1996. An absolute chronology for the raised beach deposits at Sewerby, E. Yorkshire, UK. *Journal of Quaternary Science* **11**: 389–395. DOI:10.1002/(SICI)1099-1417(199609/10)11:5<389::AID-JQS260>3.0.CO;2-K.

Bateman MD, Murton JB. 2006. Late Pleistocene glacial and periglacial aeolian activity in the Tuktoyaktuk Coastlands, NWT, Canada. *Quaternary Science Reviews* **25**: 2552–2568. DOI:10.1016/j.quascirev.2005.07.023.

Bateman MD, Murton JB, Boulter CB. 2010. The source of De variability in periglacial sand wedges: Depositional processes versus measurement issues. *Quaternary Geochronology* **5**: 250–256. DOI:10.1016/j.quageo.2009.03.007.

Begét JE. 1988. Tephras and sedimentology of frozen Alaskan loess. In *Permafrost*, Fifth International Conference, August 2–5, 1988, Senneset K (ed). Tapir: Trondheim, Vol. **1**: 672–677.

Begét JE. 2001. Continuous Late Quaternary proxy climate records from loess in Beringia. *Quaternary Science Reviews* **20**: 499–507. DOI:10.1016/S0277-3791(00)00102-5.

Bigelow NH, Brubaker LB, Edwards ME, Harrison SP, Prentice IC, Anderson PM, Andreev AA, Bartlein PJ, Christiansen TR, Cramer W, Kaplan JO, Lozhkin AV, Matveyeva NV, Murray DF, McGuire AD, Razzhivin VY, Ritchie JC, Smith B, Walker DA, Gajewski K, Wolf V, Holmqvist BH, Igarashi Y, Kremenetskii K, Paus A, Pisaric MFJ, Volkova VS. 2003. Climate change and arctic ecosystems: 1. Vegetation changes north of 55 N between the last glacial maximum, mid-Holocene, and present. *Journal of Geophysical Research* **108**: D19, 8170. DOI: 10.1029/2002JD002558

Binney HA, Willis KJ, Edwards ME, Bhagwat SA, Anderson PM, Andreev AA, Blaauw M, Damblon F, Haesaerts P, Kienast F, Kremenetski KV, Krivonogov SK, Lozhkin AV, MacDonald GM, Novenko PO, Sapelko T, Väliranta M, Vazhenina L. 2009. The distribution of late-Quaternary woody taxa in northern Eurasia: evidence from a new macrofossil database. *Quaternary Science Reviews* **28**: 2445–2464. DOI:10.1016/j.quascirev.2009.04.016.

Black RF. 1974. Ice-wedge polygons of northern Alaska. In *Glacial geomorphology*, Coates DR (ed). State University of New York: Binghamton; 247–275.

Black RF. 1983. Three superposed systems of ice wedges at McLeod Point, northern Alaska, may span most of the Wisconsinan stage and Holocene. In *Permafrost*, Fourth International Conference, Proceedings, July 17–22, 1983. National Academy Press: Washington, DC; 68–73.

Boeskorov GG, Lazarev PA, Sher AV, Davydov SP, Bakulina NT, Shchelchkova MV, Binladen J, Willerslev E, Buigues B,

Tikhonov AN. 2011. Woolly rhino discovery in the lower Kolyma River. *Quaternary Science Reviews* **30**: 2262–2272. DOI:10.1016/j.quascirev.2011.02.010.

Brabets TP, Wang B, Meade RH. 2000. *Environmental and Hydrologic Overview of the Yukon River Basin, Alaska and Canada*. US Geological Survey Water-Resources Investigations Report 99-4204: Anchorage, Alaska.

Braconnot P, Otto-Bliesner B, Harrison S, Joussaume S, Peterchmitt, J-Y, Abe-Ouchi A, Crucifix M, Driesschaert E, Fichefet Th, Hewitt CD, Kageyama M, Kitoh A, Lâıné A, Loutre M-F, Marti O, Merkel U, Ramstein G, Valdes P, Weber SL, Y. Yu Y, Zhao Y. 2007. Results of PMIP2 coupled simulations of the Mid-Holocene and Last Glacial Maximum – Part 1: experiments and large-scale features. *Climate of the Past* **3**: 261–277. DOI: 10.5194/cp-3-261-2007

Bray MT, French HM, Shur Y. 2006. Further cryostratigraphic observations in the CRREL permafrost tunnel, Fox, Alaska. *Permafrost and Periglacial Processes* **17**: 233–243. DOI:10.1002/ppp.558.

Briant RM, Bateman MD. 2009. Luminescence dating indicates radiocarbon age underestimation in late Pleistocene fluvial deposits from eastern England. *Journal of Quaternary Science* **24**: 916–927. DOI:10.1002/jqs.1258.

Brigham-Grette J. 2001. New perspectives on Beringian Quaternary paleogeography, stratigraphy, and glacial history. *Quaternary Science Reviews* **20**: 15–24. DOI:10.1016/S0277-3791(00)00134-7.

Brigham-Grette J, Lozhkin AV, Anderson PM, Glushkova OY. 2004. Paleoenvironmental conditions in Western Beringia before and during the Last Glacial Maximum. In *Entering America. Northeast Asia and Beringia before the Last Glacial Maximum*, Madsen DB (ed). University of Utah Press: Salt Lake City; 29–61.

Brubaker LB, Anderson PM, Edwards ME, Lozhkin AV. 2005. Beringia as a glacial refugium for boreal trees and shrubs: new perspectives from mapped pollen data. *Journal of Biogeography* **32**: 833–848. DOI:10.1111/j.1365-2699.2004.01203.x.

Bryant ID. 1982. Loess deposits in Lower Adventdalen, Spitsbergen. *Polar Research* **2**: 93–103.

Bullard JE. 2013. Contemporary glacigenic inputs to the dust cycle. *Earth Surface Processes and Landforms* **38**: 71–89. DOI:10.1002/esp.3315.

Burn CR, Smith MW. 1990. Development of thermokarst lakes during the Holocene at sites near Mayo, Yukon Territory. *Permafrost and Periglacial Processes* **1**: 161–176. DOI:10.1002/ppp.3430010207.

Carter LD. 1981. A Pleistocene sand sea on the Alaskan Arctic Coastal Plain. *Science* **212**: 381–383. DOI:10.1126/science.211.4480.381.

Carter LD. 1983. Fossil sand wedges on the Alaskan Arctic Coastal Plain and their paleoenvironmental significance. In *Permafrost*, Fourth International Conference, Proceedings, July 17–22, 1983. National Academy Press: Washington, DC; 109–114.

Carter LD. 1988. Loess and deep thermokarst basins in Arctic Alaska. In *Permafrost*, Fifth International Conference, August 2–5, 1988, Senneset K (ed). Tapir: Trondheim, Vol. **1**: 706–711.

CAVM Team. 2003. *Circumpolar Arctic Vegetation Map* (1:7,500,000 scale). Conservation of Arctic Flora and Fauna (CAFF) Map No. 1. US Fish and Wildlife Service: Anchorage, Alaska.

Chlachula J. 2003. The Siberian loess record and its significance for reconstruction of Pleistocene climate change in north-central Asia. *Quaternary Science Reviews* **22**: 1879–1906. DOI:10.1016/S0277-3791(03)00182-3.

Chlachula J, Rutter NW, Evans ME. 1997. A late Quaternary loess-paleosol record at Kurtak, southern Siberia. *Canadian Journal of Earth Sciences* **34**: 679–686. DOI:10.1139/e17-054.

Crusius J, Schroth AW, Gassó S, Moy CM, Levy RC, Gatica M. 2011. Glacial flour dust storms in the Gulf of Alaska: Hydrologic and meteorological controls and their importance as a source of bioavailable iron. *Geophysical Research Letters* **38**: L06602. DOI:10.1029/2010GL046573.

Dallimore SR, Wolfe SA, Matthews JV Jr, Vincent J-S. 1997. Mid-Wisconsinan eolian deposits of the Kittigazuit Formation, Tuktoyaktuk Coastlands, Northwest Territories, Canada. *Canadian Journal of Earth Sciences* **34**: 1421–1441. DOI:10.1139/e17-116.

Davydov SP, Fyodorov-Davydov DG, Neff JC, Shiklomanov NI, Davydova AE. 2008. Changes in active layer thickness and seasonal fluxes of dissolved organic carbon as a possible baseline for permafrost monitoring. In *Proceedings of the Ninth International Conference on Permafrost*, June 29–July 3, 2008, Kane DL, Hinkel KM (eds). Institute of Northern Engineering, University of Alaska Fairbanks: Fairbanks, AK, Vol. **1**: 333–336.

Dijkmans JWA, Mücher HJ. 1989. Niveo-aeolian sedimentation of loess and sand: an experimental and micromorphological approach. *Earth Surface Processes and Landforms* **14**: 303–315. DOI:10.1002/esp.3290140406.

Dijkmans JWA, Törnqvist TE. 1991. Modern periglacial eolian deposits and landforms in the Søndre Strømfjord area, West Greenland and their palaeoenvironmental implications. *Meddelelser om Grønland Geoscience* **25**: 1–39.

Dinter DA, Carter DL, Brigham-Grette J. 1990. Late Cenozoic geological evolution of the Alaskan North Slope and adjacent continental shelves. In *The Arctic Ocean Region. The Geology of North America, Vol. L*, Grantz A, Johnson L, Sweeney JF (eds). Geological Society of America: Boulder, Colorado; 459–490.

Dodonov AE. 2007. Central Asia. In *Encyclopedia of Quaternary Science*, First Edition, Elias SA (ed). Elsevier: Amsterdam; 1418–1429.

Dutta K, Schuur EAG, Neff JC, Zimov SA. 2006. Potential carbon release from permafrost soils of Northeastern Siberia. *Global Change Biology* **12**: 2336–2351. DOI:10.1111/j.1365-2486.2006.01259.x.

Edwards ME. 1997. Pollen analysis of Beringian terrestrial deposits. In *Terrestrial Paleoenvironmental Studies in Beringia: Proceedings of a Joint Russian-American Workshop, Fairbanks, Alaska, 1991*, Edwards ME, Sher AV, Guthrie, RD (eds). Alaska Quaternary Center: Fairbanks; 73–78.

Ehlers J, Astakhov V, Gibbard PL, Mangerud J, Svendsen JI. 2013. Late Pleistocene in Eurasia. In *Encyclopedia of Quaternary Science*, Second Edition, Elias SA, Mock CJ (eds). Elsevier: Amsterdam; *Vol.* **2**, 224–235.

Elias SA, Brigham-Grette J. 2013. Late Pleistocene glacial events in Beringia. In *Encyclopedia of Quaternary Science*, Second Edition, Elias SA, Mock CJ (eds). Elsevier: Amsterdam, Vol. **2**: 191–201.

Everett KR. 1980. Distribution and properties of road dust along the northern portion of the Haul Road. In *Environmental engineering and ecological baseline investigations along the Yukon River-Prudhoe Bay Haul Road*, Brown J, Berg R (eds). US Army Cold Regions Research and Engineering Laboratory, CRREL Report 80-19: 101–128.

Fortier D, Kanevskiy M, Shur Y. 2008. Genesis of reticulate-chaotic cryostructure in permafrost. In *Proceedings of the Ninth International Conference on Permafrost*, June 29–July 3, 2008, Kane DL, Hinkel KM (eds). Institute of Northern Engineering, University of Alaska Fairbanks: Fairbanks, AK, Vol. **1**: 451–456.

Fraser TA, Burn CR. 1997. On the nature and origin of "muck" deposits in the Klondike area, Yukon Territory. *Canadian Journal of Earth Sciences* **34**: 1333–1344. DOI:10.1139/e17-106.

Frechen M, Zander A, Zykina V, Boenigk W. 2005. The loess record from the section at Kurtak in Middle Siberia. *Palaeogeography, Palaeoclimatology, Palaeocology* **228**: 228–244. DOI:10.1016/j.palaeo.2005.06.004.

Frechen M, Kehl M, Rolf C, Sarvati R, Skowronek A. 2009. Loess chronology of the Caspian Lowland in northern Iran. *Quaternary International* **198**: 220–233. DOI: 10.1016/j.quaint.2008.12.012.

French HM, Guglielmin M. 2000. Frozen ground phenomena in the vicinity of Terra Nova Bay, Northern Victoria Land, Antarctica: a preliminary report. *Geografiska Annaler* **82A**: 513–526. DOI:10.1111/j.0435-3676.2000.00138.x.

French HM, Pollard WH. 1986. Ground-ice investigations, Klondike District, Yukon Territory. *Canadian Journal of Earth Sciences* **23**: 550–560. DOI:10.1139/e86-055

French HM, Shur Y. 2010. The principles of cryostratigraphy. *Earth-Science Reviews* **101**: 190–206. DOI:10.1016/j.earscirev.2010.04.002.

Froese DG, Westgate JA, Preece S, Storer J. 2002. Age and significance of the late Pleistocene Dawson tephra in eastern Beringia. *Quaternary Science Reviews* **21**: 2137–2142. DOI:10.1016/S0277-3791(02)00038-0.

Froese DG, Westgate JA, Sanborn PT, Reyes AV, Pearce NJG. 2009. The Klondike goldfields and Pleistocene environments of Beringia. *GSA Today* **19**: 4–10. DOI:10.1130/GSATG54A.1.

Fuchs M, Kreutzer S, Rousseau DD, Antoine P, Hatté C, Lagroix F, Moine O, Gauthier C, Svoboda J, Lisá L. 2013. The loess sequence of Dolní Vestonice, Czech Republic: A new OSL-based chronology of the Last Climatic Cycle. *Boreas* **42**: 664–677. DOI:10.1111/j.1502-3885.2012.00299.x.

Fyodorov-Davydov DG, Sorokovikov VA, Kholodov AL, Ostroumov VE, Gubin SV, Gilichinsky DA, Mergelov NS, Davydov SP, Zimov SA. 2003. Spatial and temporal observations of seasonal thawing in the Northern Kolyma lowlands. In *Permafrost, Extended Abstracts Reporting Current Research and New Information, Eighth International Conference on Permafrost*, 21–25 July 2003, Zurich, Switzerland, Haeberli W, Brandová D (eds). A. A. Balkema: Lisse; 41–42.

Galbraith RF, Green PF. 1990. Estimating the component ages in a finite mixture. *Radiation Measurements* **17**: 197–206. DOI:10.1016/1359-0189(90)90035-V.

Gale SJ, Hoare PG. 1991. *Quaternary Sediments*. Belhaven: New York.

Gallet S, Jahn B, Van Vliet-Lanoë B, Dia A, Rossello EA. 1998. Loess geochemistry and its implications for particle origin and composition of the upper continental crust. *Earth and Planetary Science Letters* **156**: 157–172. DOI:10.1016/S0012-821X(97)00218-5.

Garrels RM, MacKenzie FT. 1971. *Evolution of Sedimentary Rocks*. Norton: New York.

Gasanov SH. 1981. *Cryolithological Analysis*. Nauka: Moscow (in Russian).

Glushkova OY. 2011. Late Pleistocene glaciations in North-East Asia. In *Quaternary Glaciation Extent and Chronology: a Closer Look*, Ehlers J, Gibbard PL, Hughes PD (eds). Developments in Quaternary Science 15. Elsevier: Amsterdam; 865–875.

Goetcheus VG, Birks HH. 2001. Full-glacial upland tundra vegetation preserved under tephra in Beringia National Park, Seward Peninsula, Alaska. *Quaternary Science Reviews* **20**: 135–147. DOI:10.1016/S0277-3791(00)00127-X.

Goslar T, Czernik J, Goslar E. 2004. Low-energy 14C AMS in Poznan radiocarbon Laboratory, Poland. *Nuclear Instruments and Methods in Physics Research B* **223-224**: 5–11.

Goslar T, van der Knaap WO, van Leeuwen J, Kamenik C. 2009. Free-shape ^{14}C age-depth modelling of an intensively dated modern peat profile. *Journal of Quaternary Science* **24**: 481–499. DOI:10.1002/jqs.1283.

Gravis GF. 1969. *Slope Deposits in Yakutia*. Nauka: Moscow, (in Russian).

Griffin CG, Frey KE, Rogan J, Holmes RM. 2011. Spatial and interannual variability of dissolved organic matter in the Kolyma River, East Siberia, observed using satellite imagery. *Journal of Geophysical Research* **116**: G03018. DOI:10.1029/2010JG001634.

Grimm E. 2004. TILIA and TGView Software, Version 2.0.2. Illinois State University.

Grosse G, Robinson JE, Bryant R, Taylor MD, Harper W, DeMasi A, Kyker-Snowman E, Veremeeva A, Schirrmeister L, Harden J. 2013. Distribution of late Pleistocene ice-rich syngenetic permafrost of the Yedoma Suite in east and central Siberia, Russia. US Geological Survey Open File Report 2013-1078.

Gubin SV. 1984. Palaeopedological analysis of Late Pleistocene (Yedoma) deposits of the Duvanny Yar exposure. *Bulletin of Quaternary Commission* **53**: 125–128 (in Russian).

Gubin SV. 1994. Late Pleistocene soil formation in coastal lowlands of northern Yakutia. *Soil Science* **8**: 5–14 (in Russian).

Gubin SV. 1999. Late Pleistocene soil formation on ice-bearing loesses of northeast Eurasia. Summary of Doctoral Science dissertation in biology. Institute of Fundamental Problems of Biology of Russian Academy of Sciences: Pushchino (in Russian).

Gubin SV. 2002. Pedogenesis—the main component of the Late Pleistocene Ice Complex forming. *Earth Cryosphere* **6**: 82–91 (in Russian).

Gubin SV, Lupachev AV. 2008. Soil formation and the underlying permafrost. *Eurasian Soil Science* **41**: 574–585. DOI:10.1134/S1064229308060021.

Gubin SV, Lupachev AV. 2012. Approaches to the distinguishing and investigation of buried soils in frozen deposits of Ice Complex. *Earth Cryosphere* **2**: 79–84 (in Russian).

Gubin SV, Veremeeva AA. 2010. Parent materials enriched in organic matter in the northeast of Russia. *Eurasian Soil Science* **43**: 1238–1243. DOI:10.1134/S1064229310110062.

Gubin SV, Zanina OG. 2013. Variation of soil cover during the Ice Complex deposit formation, Kolyma Lowland (Part 1). *Earth Cryosphere* **XVII**(4): 48–56.

Gubin SV, Zanina OG. 2014. Variation of soil cover during the Ice Complex deposit formation, Kolyma Lowland (Part 2). *Earth Cryosphere* **XVIII**(1): 77–82.

Gubin SV, Maximovich SV, Zanina OG, Stakhov VL. 2011. Morphogenetics of Plant Remains from Palaeosols and Rodent Burrows Buried in Permafrost of the Late Pleistocene (32-28000 BP). In *Plant Archaeogenetics*, Gyulai G (ed). Nova Press: Hauppauge, NY, USA; 11–21.

Gullentops F. 1957. Stratigraphie du Pleistocène supérieur en Belgique. *Geologie en Mijnbouw* **19**: 305.

Guthrie RD. 2001. Origin and causes of the mammoth steppe: A story of cloud cover, woolly mammal tooth pits, buckles, and inside-out Beringia. *Quaternary Science Reviews* **20**: 549–574. DOI:10.1016/S0277-3791(00)00099-8.

Guthrie RD. 2006. New carbon dates link climatic change with human colonization and Pleistocene extinctions. *Nature* **441**: 207–209. DOI:10.1038/nature04604.

Haesaerts P, Chekha VP, Damblon F, Drozdov NI, Orlova LA, Van der Plicht J. 2005. The loess-palaeosol succession of Kurtak (Yenisei basin, Siberia): a reference record from the Karga Stage (MIS 3). *Quaternaire* **16**: 3–24.

Hamilton TD, Craig JL, Sellmann PV. 1988. The Fox permafrost tunnel: A late Quaternary geologic record in central Alaska. *Geological Society of American Bulletin* **100**: 948–969. DOI:10.1130/0016-7606(1988)100<0948:TFPTAL>2.3.CO;2.

Hao Q, Oldfield F, Bloemendal J, Guo Z. 2008. Particle size separation and evidence for pedogenesis in samples from the Chinese Loess Plateau spanning the past 22 m.y. *Geology* **36**: 727–730. DOI:10.1130/G24940A.1.

Höfle C, Ping CL. 1996. Properties and soil development of late-Pleistocene paleosols from Seward Peninsula, northwest Alaska.

Geoderma **71**: 219–243. DOI:10.1016/0016-7061(96)00007-9.

Höfle C, Edwards ME, Hopkins DM, Mann DH, Ping CL. 2000. The full-glacial environment of the northern Seward Peninsula, Alaska, reconstructed from the 21,500-Year-Old Kitluk Paleosol. *Quaternary Research* **53**: 143–153. DOI:10.1006/qres.1999.2097.

Hopkins DM. 1963. Geology of the Imuruk Lake area, Seward Peninsula, Alaska. US Geological Survey, Bulletin 1141-C.

Hopkins DM. 1982. Aspects of the paleogeography of Beringia during the late Pleistocene. In *Paleoecology of Beringia*, Hopkins DM, Matthews JV, Jr, Schweger CE, Young SB (eds). New York: Academic Press; 3–28.

Hopkins DM, Kidd JG. 1988. Thaw lake sediments and sedimentary environments. In *Permafrost*, Fifth International Conference, August 2–5, 1988, Senneset K (ed). Tapir: Trondheim, Vol. **1**: 790–795.

Hopkins DM, Matthews JV, Jr, Schweger CE, Young SB (eds). 1982. *Paleoecology of Beringia*. Academic Press: New York.

Hugenholtz CH, Wolfe SA. 2010. Rates and environmental controls on aeolian dust accumulation, Athabasca Valley, Canadian Rocky Mountains. *Geomorphology* **121**: 274–282. DOI:10.1016/j.geomorph.2010.04.024.

Huijzer AS. 1993. Cryogenic Microfabrics and Macrostructures: Interrelations, Processes and Paleoclimatic Significance. PhD thesis, Vrije Universiteit, Amsterdam.

Huijzer AS, Vandenberghe J. 1998. Climatic reconstruction of the Weichselian Pleniglacial in northwestern and central Europe. *Journal of Quaternary Science* **13**: 391–417. DOI:10.1002/(SICI)1099-1417(1998090)13:5<391::AID-JQS397>3.0.CO;2-6.

IUSS Working Group WRB. 2006. World Reference Base for Soil Resources. World Soil Resources Reports No. 103. Food and Agricultural Organization of the United Nations: Rome.

Jackson MG, Oskarsson N, Trønnes RG, McManus JF, Oppo DW, Grönvold K, Hart SR, Sachs JP. 2005. Holocene loess deposition in Iceland: evidence for millennial-scale atmosphere-ocean coupling in the North Atlantic. *Geology* **33**: 509–512. DOI:10.1130/G21489.1.

Jahn A. 1975. *Problems of the Periglacial Zone* (Zagadnienia strefy peryglacjalnef). Panstwowe wydawnictwo Naukowe: Warsaw.

Jorgenson MT, Yoshikawa K, Kanveskiy M, Shur Y, Romanovsky V, Marchenko S, Grosse G, Brown J, Jones B. 2008. Permafrost characteristics of Alaska. In *Extended Abstracts of the Ninth International Conference on Permafrost*, June 29–July 3, 2008, Kane DL, Hinkel KM (eds). Institute of Northern Engineering, University of Alaska Fairbanks: Fairbanks, AK; 121–122.

Kanevskiy M. 2003. Cryogenic structure of mountain slope deposits, northeast Russia. In *Permafrost, Proceedings of the Eighth International Conference on Permafrost*, 21–25 July 2003, Zurich, Switzerland, Phillips M, Springman SM, Arenson LU (eds). A. A. Balkema: Lisse, Vol. **1**: 513–518.

Kanevskiy M, Fortier D, Shur Y, Bray M, Jorgenson T. 2008. Detailed cryostratigraphic mapping of syngenetic permafrost in the winze of the CRREL Permafrost Tunnel, Fox, Alaska. In *Proceedings of the Ninth International Conference on Permafrost*, June 29–July 3, 2008, Kane DL, Hinkel KM (eds). Institute of Northern Engineering, University of Alaska Fairbanks: Fairbanks, AK, Vol. **1**: 889–894.

Kanevskiy M, Shur Y, Fortier D, Jorgenson MT, Stephani E. 2011. Cryostratigraphy of late Pleistocene syngenetic permafrost (yedoma) in northern Alaska, Itkillik River exposure. *Quaternary Research* **75**: 584–596. DOI:10.1016/j.yqres.2010.12.003.

Kanevskiy M, Shur Y, Connor B, Dillon M, Stephani E, O'Donnell J. 2012. Study of the ice-rich syngenetic permafrost for road design (Interior Alaska). In *Tenth International Conference on Permafrost, June 25–29, 2012, Salekhard, Russia, Vol. 1, International Contributions*, Hinkel KM (ed). The Northern Publisher: Salekhard, Russia; 191–196.

Kaplan JO, Bigelow NH, Prentice IC, Harrison SP, Bartlein PJ, Christensen TR, Cramer W, Matveyeva NV, McGuire AD, Murray DF, Razzhivin VY, Smith B, Walker DA, Anderson PM, Andreev AA, Brubaker LB, Edwards ME, Lozhkin AV. 2003. Climate change and Arctic ecosystems: 2. Modeling, paleodata-model comparisons, and future projections. *Journal of Geophysical Research* **108**: D19, 8171. DOI:10.1029/2002JD002559.

Kaplina TN. 1981. History of permafrost development in late Cenozoic. In *History of Development of Permafrost in Eurasia*, Dubikov GI, Baulin VV (eds). Nauka: Moscow; 153–180 (in Russian).

Kaplina TN. 1986. Regularities of Development of Cryolithogenesis in Late Cenozoic in Accumulation Flood Plain of Northeastern Asia. Summary of Dr Sci dissertation in geology and mineralogy. Permafrost Institute of the Siberian Branch: USSR Academy of Science, Moscow (in Russian).

Kaplina TN, Giterman RYe, Lakhtina OV, Abrashov BA, Sher AV. 1978. Duvanny Yar, a key section of upper Pleistocene sediments of the Kolyma lowland. *Bulletin of the Commission of the USSR Academy of Sciences for Studying the Quaternary* **48**: 49–65 (in Russian). Translation 1863194. Geological Survey of Canada: Ottawa.

Kasse K, Bohncke S, Vandenberghe J. 1995. Fluvial periglacial environments, climate and vegetation during the Middle Weichselian in the northern Netherlands with special reference to the Hengelo Interstadial. *Mededelingen Rijks Geologische Dienst* **52**: 387–414.

Katasonov EM. 1954. Lithology of frozen Quaternary deposits (cryolithology) of the Yana Coastal Plain. PhD thesis, Obruchev Permafrost Institute (published in 2009, Production and Research Institute for Engineering Surveys in Construction: Moscow) (in Russian).

Katasonov EM, Ivanov MS. 1973. Cryolithology of Central Yakutia. Guidebook. Second International Conference on Permafrost. USSR Academy of Sciences: Section of Earth Sciences, Siberian Division, Yakutsk.

Kemp RA. 2001. Pedogenic modification of loess: significance for palaeoclimatic reconstructions. *Earth-Science Reviews* **54**: 145–156. DOI:10.1016/S0012-8252(01)00045-9.

Kienast F, Schirrmeister L, Siegert C. 2005. Palaeobotanical evidence for warm summers in the East Siberian Arctic during the last cold stage. *Quaternary Research* **63**: 283–300. DOI:10.1016/j.yqres.2005.01.003.

Kienast F, Wetterich S, Kuzmina S, Schirrmeister L, Andreev AA, Tarasov P, Nazarova L, Kossler A, Frolova A, Kunitsky VK. 2011. Paleontological records indicate the occurrence of open woodlands in a dry inland climate at the present-day Arctic coast in western Beringia during the Last Interglacial. *Quaternary Science Reviews* **30**: 2134–2159. DOI:10.1016/j.quascirev.2010.11.024.

Kindle ED. 1952. Dezadeash Map-Area, Yukon Territory. Geological Survey of Canada, Memoir 268.

Klute A (ed). 1986. *Methods of Soil Analysis, Part 1, Physical and Mineralogical Methods*, Second Edition. Soil Science Society of America Book Series No. 5 and American Society of Agronomy. Agronomy Monographs 9(1): Madison, Wisconsin.

Kokelj S, Jorgenson MT. 2013. Advances in thermokarst research. *Permafrost and Periglacial Processes* **24**: 108–119. DOI:10.1002/ppp.1779.

Kolpakov VV. 1982. Occurrence and morphology of yedoma suite. In *Permafrost and Geologic Processes and Paleogeography of the Lowlands of North-East Asia*, Shumilov YV (ed). North-East Complex Research Institute Far East Scientific Center USSR Academy of Sciences: Magadan; 22–29 (in Russian).

Konert M, Vandenberghe J. 1997. Comparison of laser grain size analysis with pipette

and sieve analysis: a solution for the underestimation of the clay fraction. *Sedimentology* **44**: 523–535. DOI:10.1046/j.1365-3091.1997.d01-38.x.

Konishchev VN. 1973. Origin of the icy siltstones of northern Yakutia. In *USSR Contribution, Permafrost Second International Conference, 13–28 July 1973, Yakutsk, USSR*, Sanger FJ, Hyde PJ (eds). National Academy of Sciences: Washington, DC; 823–824.

Konishchev VN. 1981. *Formirovanie sostava dispersnykh porod v kriolitosfere*. [*Formation of Soil Composition in Permafrost Regions*.] Nauka: Novosibirsk (in Russian).

Konishchev VN. 1983. Cryolithological evidences for the heterogenic structure of the "ice complex" deposits in the Duvannyi Yar outcrop. In *Problems of Cryolithology*, Konishchev VN, Tumel NV, Arkhangelov AA, Kuznetsova TP, Rosenbaum GE, Spolanskaya NA (eds). Moscow State University: Moscow, Vol. **XI**: 56–64 (in Russian).

Konishchev VN. 2009. Climate warming and permafrost. Moscow State University. *Geography-Environment-Sustainability* **1**: 4–19.

Konishchev VN, Rogov VV. 1993. Investigations of cryogenic weathering in Europe and Northern Asia. *Permafrost and Periglacial Processes* **4**: 49–64. DOI:10.1002/ppp.3430040105.

Koronovsky N. 2002. Tectonics and geology. In *The Physical Geography of Northern Eurasia*, Shahgedanova M (ed). Oxford University Press: Oxford; 1–35.

Koster EA, Dijkmans JWA. 1988. Niveo-aeolian deposits and denivation forms, with special reference to the Great Kobuk Sand Dunes, Northwestern Alaska. *Earth Surface Processes and Landforms* **13**: 153–170. DOI:10.1002/esp.3290130206.

Kotler E, Burn CR. 2000. Cryostratigraphy of the Klondike "muck" deposits west-central Yukon Territory. *Canadian Journal of Earth Sciences* **37**: 849–861. DOI:10.1139/cjes-37-6-849.

Kuhry P, Grosse G, Harden JW, Hugelius G, Koven CD, Ping C-L, Schirrmeister L, Tarnocai C. 2013. Characterisation of the permafrost carbon pool. *Permafrost and Periglacial Processes* **24**: 146–155. DOI:10.1002/ppp.1782.

Kunitskiy VV. 1989. Cryolithology of the Lower Lena River. Permafrost Institute, Academy of Sciences of the USSR: Yakutsk (in Russian).

Laxton NF, Burn CR, Smith CAS. 1996. Productivity of loessal grasslands in the Kluane Lake region, Yukon Territory, and the Beringian "production paradox. *Arctic* **49**: 129–140. DOI: 10.14430/arctic1191

Lea PD, Waythomas CF. 1990. Late-Pleistocene eolian sand sheets in Alaska. *Quaternary Research* **34**: 269–281. DOI:10.1016/0033-5894(90)90040-R.

de Leffingwell EK. 1915. Ground-ice wedges—the dominant form of ground-ice on the north coast of Alaska. *Journal of Geology* **23**: 635–654.

Lewkowicz AG, Young KL. 1991. Observations of aeolian transport and niveo-aeolian deposition at three lowland sites, Canadian Arctic Archipelago. *Permafrost and Periglacial Processes* **2**: 197–210. DOI:10.1002/ppp.3430020304.

Liu T. 1985. *Loess in China*, Second edition. Beijing/Berlin: China Ocean Press/Springer-Verlag.

Lopatina DA, Zanina OG. 2006. Paleobotanical analysis of materials from fossil gopher burrows and Upper Pleistocene host deposits, the Kolyma Lowland lower reaches. *Stratigraphy and Geological Correlation* **14**: 549–560. DOI:10.1134/S0869593806050078.

Lozhkin AV. 1976. Late Pleistocene and Holocene vegetation in Western Beringia. In *The Bering Land Bridge and its role for the History of Holarctic floras and faunas in the Late Cenozoic*, Kontrimavichus VL (ed). Academy of Sciences of USSR, Far-Eastern Scientific Centre, Institute of Biology Problems of North: Vladivostok; 72–77 (in Russian).

Lozhkin AV, Anderson PM. 1995. The last interglaciation in northeast Siberia. *Quaternary Research* **43**: 147–158. DOI:10.1006/qres.1995.1016.

Lozhkin AV, Anderson PM. 2011. Forest or no forest: implications of the vegetation record for climatic stability in Western Beringia during Oxygen Isotope Stage 3. *Quaternary Science Reviews* **30**: 2160–2181. DOI:10.1016/j.quascirev.2010.12.022.

Lozhkin AV, Anderson PM. 2013a. Northern Asia. In *Encyclopedia of Quaternary Science*, Second Edition, Elias SA, Mock CJ (eds). Elsevier: Amsterdam, Vol. **4**: 27–38.

Lozhkin AV, Anderson PM. 2013b. Vegetation responses to interglacial warming in the Arctic, examples from Lake El'gygytgyn, northeast Siberia. *Climate of the Past* **9**: 1211–1219. DOI:10.5194/cp-9-1211-2013.

Lozhkin AV, Anderson PM, Matrosova TV, Minyuk PS. 2006. The pollen record from El'gygytgyn Lake: Implications for vegetation and climate histories of northern Chukotka since the late Middle Pleistocene. *Journal of Paleolimnology* **37**: 135–153. DOI:10.1007/s10933-006-9018-5.

Lupachev AV, Gubin SV. 2008. Pedogenesis and its influence on the upper layer of permafrost. In *Proceedings of the Ninth International Conference on Permafrost, June 29–July 3, 2008*, Kane DL, Hinkel KM (eds). Institute of Northern Engineering, University of Alaska Fairbanks: Fairbanks, AK, Vol. **2**: 1083–1085.

Lupachev AV, Gubin SV. 2012. Suprapermafrost organic-accumulative horizons in the tundra cryozems of northern Yakutia. *Eurasian Soil Science* **45**: 45–55. DOI:10.1134/S1064229312010115.

Machalett B, Oches EA, Frechen M, Zoller L, Hambach U, Mavlyanova NG, Markovic SB, Endlicher W. 2008. Aeolian dust dynamics in central Asia during the Pleistocene: Driven by the long-term migration, seasonality, and permanency of the Asiatic polar front. *Geochemistry Geophysics Geosystems* **9**: Q08Q09. DOI:10.1029/2007GC001938.

Mackay JR. 1963. The Mackenzie Delta area, N.W.T. Geographical Branch, Department of Mines and Technical Surveys, Canada, Memoir 8.

Mackay JR. 1990. Some observations on the growth and deformation of epigenetic, syngenetic and anti-syngenetic ice wedges. *Permafrost and Periglacial Processes* **1**: 15–29. DOI:10.1002/ppp.3430010104.

Maher BA, Prospero JM, Mackie D, Gaiero D, Hesse PP, Balkanski Y. 2010. Global connections between aeolian dust, climate and ocean biogeochemistry at the present day and at the last glacial maximum. *Earth-Science Reviews* **99**: 61–97. DOI:10.1016/j.earscirev.2009.12.001.

Majhi I, Yang D. 2008. Streamflow characteristics and changes in Kolyma Basin in Siberia. *Journal of Hydrometeorology* **9**: 267–279. DOI:10.1175/2007JHM845.1.

Marsh J, Nouvet S, Sanborn P, Coxson D. 2006. Composition and function of biological soil crust communities along topographic gradients in grasslands of central interior British Columbia (Chilcotin) and southwestern Yukon (Kluane). *Canadian Journal of Botany* **84**: 717–736. DOI:10.1139/B06-026.

Matsuoka N, Murton J. 2008. Frost weathering: recent advances and future directions. *Permafrost and Periglacial Processes* **19**: 195–210. DOI:10.1002/ppp.620.

McCave IN, Hall IR. 2006. Size sorting in marine muds: Processes, pitfalls, and prospects for paleoflow-speed proxies. *Geochemistry, Geophysics, Geosystems* **7**: Q10N05. DOI:10.1029/2006GC001284.

McCave IN, Hall IR, Bianchi GG. 2006. Laser vs. settling velocity differences in silt grainsize measurements: estimation of palaeocurrent vigour. *Sedimentology* **53**: 919–928. DOI:10.1111/j.1365-3091.2006.00783.x.

McCulloch DS, Hopkins DM. 1966. Evidence for an early recent warm interval in northwestern Alaska. *Geological Society of America Bulletin* **77**: 1089–1108. DOI:10.1130/0016-7606(1966)77[1089:EFAERW]2.0.CO;2.

McCune B, Mefford MJ. 2011. PC-ORD. Multivariate Analysis of Ecological Data. Version 6. MjM Software, Gleneden Beach, Oregon, USA.

McKenna Neuman C. 1990. Observations of winter aeolian transport and niveo-aeolian deposition at Crater Lake, Pangnirtung Pass, N.W.T., Canada. *Permafrost and Periglacial Processes* **1**: 235–247. DOI:10.1002/ppp.3430010304.

McTainsh GH, Nickling WG, Lynch AW. 1997. Dust deposition and particle size in Mali, West Africa. *Catena* **29**: 307–322. DOI:10.1016/S0341-8162(96)00075-6.

Meyer H, Dereviagrin A, Seigert C, Hubberten H-W. 2002a. Paleoclimate studies on Bykovsky Peninsula, North Siberia—hydrogen and oxygen isotopes in ground ice. *Polarforschung* **70**: 37–51.

Meyer H, Dereviagin A, Siegert C, Schirrmeister L, Hubberten HW. 2002b. Palaeoclimate reconstruction on Big Lyakhovsky Island, North Siberia—hydrogen and oxygen isotopes in ice wedges. *Permafrost and Periglacial Processes* **13**: 91–105. DOI:10.1002/ppp.416.

Mountney NP, Russell AJ. 2004. Sedimentology of cold-climate aeolian sandsheet deposits in the Askja region of northeast Iceland. *Sedimentary Geology* **166**: 223–244. DOI:10.1016/j.sedgeo.2003.12.007.

Mücher HJ, De Ploey J. 1984. Formation of afterflow silt loam deposits and structural modification due to drying under warm conditions: an experimental and micromorphological approach. *Earth Surface Processes and Landforms* **9**: 523–531. DOI:10.1002/esp.3290090606.

Mücher HJ, De Ploey J. 1990. Sedimentary structures formed in eolian-deposited silt loams under simulated conditions on dry, moist and wet surfaces. In *Soil Micromorphology: a Basic and Applied Science. Proceedings of the Eighth International Working Meeting of Soil Micromorphology*, Douglas LA (ed). Elsevier: Amsterdam; Developments in Soil Science 19: 155–160.

Mücher HJ. 1974. Micromophology of slope deposits: the necessity of a classification. In *Soil Microscopy*: *Proceedings of the Fourth International Working-Meeting on Soil Micromorphology*, *Department of Geography*, *Queen's University*, *Kingston*, *Ontario*, *Canada*, *27th–31st August*, *1973*, Rutherford GK (ed). Limestone Press: Kingston, Ontario; 553–566.

Mücher HJ, De Ploey J. 1977. Experimental and micromorphological investigation of erosion and redeposition of loess by water. *Earth Surface Processes and Landforms* **2**: 117–124. DOI:10.1002/esp.3290020204.

Mücher HJ, Vreeken WJ. 1981. (Re)deposition of loess in southern Limbourg, The Netherlands: 2. Micromorphology of the Lower Silt Loam complex and comparison with deposits produced under laboratory conditions. *Earth Surface Processes and Landforms* **6**: 355–363. DOI:10.1002/esp.3290060314.

Mücher HJ, De Ploey J, Savat J. 1981. Response of loess materials to simulated translocation by water: micromorphological observations. *Earth Surface Processes and Landforms* **6**: 331–336. DOI:10.1002/esp.3290060312.

Muhs DR. 2013a. The geologic records of dust in the Quaternary. *Aeolian Research* **9**: 3–48. DOI:10.1016/j.aeolia.2012.08.001.

Muhs DR. 2013b. Loess deposits: origins and properties. In *Encyclopedia of Quaternary Science*, Second Edition, Elias SA, Mock CJ (eds). Elsevier: Amsterdam, Vol. **2**: 573–584.

Muhs DR, Budahn JR. 2006. Geochemical evidence for the origin of late Quaternary loess in central Alaska. *Canadian Journal of Earth Sciences* **43**: 323–337. DOI:10.1139/e05-115.

Muhs DR, Ager TA, Bettis EA III, McGeehin J, Been JM, Begét JE, Pavich MJ, Stafford TW Jr, Stevens De ASP. 2003. Stratigraphy and paleoclimatic significance of late Quaternary loess-paleosol sequences of the last interglacial-glacial cycle in central Alaska. *Quaternary Science Reviews* **22**: 1947–1986. DOI:10.1016/S0277-3791(03)00167-7.

Muhs DR, McGeehin JP, Beann J, Fisher E. 2004. Holocene loess deposition and soil formation as competing processes, Matanuska Valley, southern Alaska. *Quaternary Research* **61**: 265–276. DOI:10.1016/j.yqres.2004.02.003.

Muhs DR, Ager TA, Skipp G, Beann J, Budahn J, McGeehin JP. 2008. Paleoclimatic significance of chemical weathering in loess-derived paleosols of subarctic central Alaska. *Arctic, Antarctic and Alpine Research* **40**: 396–411. DOI:10.1657/1523-0430(07-022)[MUHS]2.0.CO;2.

Muhs DR, Budahn JR, McGeehin JP, Bettis EA III, Skipp G, Paces JB, Wheeler EA. 2013. Loess origin, transport, and deposition over the past 10,000 years, Wrangell-St. Elias National Park, Alaska. *Aeolian Research* **11**: 85–99. DOI:10.1016/j.aeolia.2013.06.001.

Murray AS, Wintle AG. 2003. The single aliquot regenerative dose protocol: potential for improvements in reliability. *Radiation Measurements* **37**: 377–381. DOI:10.1016/S1350-4487(03)00053-2.

Murton DK, Murton JB. 2012. Middle and Late Pleistocene glacial lakes of lowland Britain and the southern North Sea Basin. *Quaternary International* **260**: 115–142. DOI:10.1016/j.quaint.2011.07.034.

Murton JB. 1996a. Thermokarst-lake-basin sediments, Tuktoyaktuk Coastlands, Western Arctic Canada. *Sedimentology* **43**: 737–760. DOI:10.1111/j.1365-3091.1996.tb02023.x.

Murton JB. 1996b. Morphology and paleoenvironmental significance of Quaternary sand veins, sand wedges, and composite wedges, Tuktoyaktuk Coastlands, Western Arctic Canada. *Journal of Sedimentary Research* **66**: 17–25. DOI:10.1306/D4268298-2B26-11D7-8648000102C1865D.

Murton JB. 2009a. Global warming and thermokarst. In *Permafrost Soils, Soil Biology*, Margesin R (ed). Springer-Verlag: Berlin, Heidelberg, Vol. **16**: 185–203. DOI: 10.1007/978-3-540-69371-0_13

Murton JB. 2009b. Stratigraphy and paleoenvironments of Richards Island and the eastern Beaufort Continental Shelf during the last glacial-interglacial cycle. *Permafrost and Periglacial Processes* **20**: 107–125. DOI:10.1002/ppp.647.

Murton JB. 2013a. Ground ice and cryostratigraphy. In *Treatise on Geomorphology, Vol. 8, Glacial and Periglacial Geomorphology*, Shroder JF (editor-in-chief), Giardino R, Harbor J (volume eds). Academic Press: San Diego; 173–201. DOI: 10.1016/B978-0-12-374739-6.00206-2

Murton JB. 2013b. Ice wedges and ice-wedge casts. In *Encyclopedia of Quaternary Science*, Second Edition, Elias SA, Mock CJ (eds). Elsevier: Amsterdam, Vol. **3**: 436–451.

Murton JB, French HM. 1993. Thaw modification of frost-fissure wedges, Richards Island, Pleistocene Mackenzie Delta, western Canadian Arctic. *Journal of Quaternary Science* **8**: 185–196. DOI:10.1002/jqs.3390080302.

Murton JB, Kolstrup E. 2003. Ice-wedge casts as indicators of palaeotemperatures: precise proxy or wishful thinking? *Progress in Physical Geography* **27**: 155–170. DOI:10.1191/0309133303pp365ra.

Murton JB, French HM, Lamothe M. 1997. Late Wisconsinan erosion and aeolian deposition, Summer and Hadwen Islands, Mackenzie Delta area, western Canadian Arctic: optical dating and implications for glacial chronology. *Canadian Journal of Earth Sciences* **34**: 190–199. DOI:10.1139/e17-015.

Murton JB, Worsley P, Gozdzik J. 2000. Sand veins and wedges in cold aeolian environments. *Quaternary Science Reviews* **19**: 899–922. DOI:10.1016/S0277-3791(99)00045-1.

Murton JB, Frechen M, Maddy D. 2007. Luminescence dating of Mid- to Late Wisconsinan aeolian sand as a constraint on the last advance of the Laurentide Ice Sheet across the Tuktoyaktuk Coastlands, western Arctic Canada. *Canadian Journal of Earth Sciences* **44**: 857–869. DOI:10.1139/e07-015.

Murton JB, Edwards ME, Murton DK, Bateman MD, Haile J. 2010. Age and origin of ice-rich Yedoma silts at Duvanny Yar, northeast Siberia: a record of Beringian environmental change since the last interglacial. American Geophysical Union, Fall Meeting 2010, abstract #PP13A-1484.

Murton JB, Edwards ME, Goslar T, Bateman MD, Murton DK. 2013. Aeolian deposition and chronology of Late Pleistocene Yedoma silts (Ice Complex), Duvanny Yar, northeast Siberia. In *Program and Abstracts*, *Canadian Quaternary Association and Canadian Geomorphology Research Group Conference August 2013*. University of Alberta: Edmonton; 180.

Murzaev EM. 1984. *Dictionary of Folk Geographical Terms*. Mysl: Moscow (in Russian).

Naldrett DL. 1982. Aspects of the surficial geology and permafrost conditions, Klondike goldfields and Dawson City, Yukon Territory. Unpublished MSc thesis, University of Ottawa, Ottawa, Ontario.

Nelson WH, Csejtey B, Jr. 1990. Stratigraphy and structure of the Ekokpuk Creek area, north-central Brooks Range, Alaska. US Geological Survey Bulletin 1848.

Nickling WG. 1978. Eolian sediment transport during dust storms: Slims River Valley, Yukon Territory. *Canadian Journal of Earth Sciences* **15**: 1069–1084. DOI:10.1139/e78-114.

Nikolayev VI, Mikhalev DV. 1995. An oxygen-isotope paleothermometer from ice in Siberian permafrost. *Quaternary Research* **43**: 14–21. DOI:10.1006/qres.1995.1002.

Novothny A, Frechen M, Horváth E, Wacha L, Rolf C. 2011. Investigating the penultimate and last glacial cycles of the Süttö loess section (Hungary) using luminescence dating, high-resolution grain size, and magnetic susceptibility data. *Quaternary International* **234**: 75–85. DOI:10.1016/j.quaint.2010.08.002.

PALE Steering Committee. 1994. Research protocols for PALE: paleoclimate of Arctic Lakes and Estuaries, PAGES Workshop Report Series 94-1. PAGES Core Project Office: Bern.

Park H, Yamazaki T, Yamamoto K, Ohta T. 2008. Tempo-spatial characteristics of energy budget and evapotranspiration in the eastern Siberia. *Agricultural and Forest Meteorology* **148**: 1990–2005. DOI:10.1016/j.agrformet.2008.06.018.

Péwé TL. 1951. An observation of wind-blown silt. *Journal of Geology* **59**: 399–401.

Péwé TL. 1955. Origin of the upland silt near Fairbanks, Alaska. *Geological Society of America Bulletin* **66**: 699–724.

Péwé TL. 1975a. Quaternary Geology of Alaska. US Geological Survey Professional Paper 835, Washington, DC.

Péwé TL. 1975b. Quaternary Stratigraphic Nomenclature in Unglaciated Central Alaska. US Geological Survey Professional Paper 862, Washington, DC.

Péwé TL, Journaux A. 1983. Origin and character of loess-like silt in unglaciated south-central Yakutia, Siberia, U.S.S.R.. United States Geological Survey Professional Paper 1262, Washington, DC.

Pigati JS, Quade J, Wilson J, Jull AJT, Lifton NA. 2007. Development of low-background vacuum extraction and graphitization systems for 14C dating of old (40–60 ka) samples. *Quaternary International* **166**: 4–14. DOI:10.1016/j.quaint.2006.12.006.

Pitcher WS, Shearman DJ, Pugh DC. 1954. The loess of Pegwell Bay, Kent, and its associated frost soils. *Geological Magazine* **91**: 308–314.

Popov AI. 1952. Frost contraction cracks and problems of identification of fossil ice. In *Permafrost of different regions of USSR*. Proceedings of the Obruchev Permafrost Institute of the USSR Academy of Science, Publishing House of the USSR Academy of Science: Moscow, Vol. **IX**: 3–18 (in Russian).

Popov AI. 1953. Lithogenesis of alluvial lowlands in the cold climatic conditions. *Izvestiya* (*Transactions*) *of the USSR Academy of Sciences*, *Geography* **2**: 29–41 (in Russian).

Popov AI. 1955. Origin and development of thick fossil ice. In *The Materials for the Fundamentals of the Study on Frozen Zones of the Earth's Crust*, Issue 2, Meister LA (ed). Publishing House of the USSR Academy of Science: Moscow; 5–25 (in Russian).

Popov AI. 1973. Origin of the deposits of the Yedoma Suite on the Primor'ye floodplain of northern Yakutia. In *USSR Contribution, Permafrost Second International Conference, 13–28 July 1973, Yakutsk, USSR*, Sanger FJ, Hyde PJ (eds). National Academy of Sciences: Washington, DC; 824–825.

Popp S. 2006. Late Quaternary Environment of Central Yakutia (NE Siberia): Signals in Frozen Ground and Terrestrial Sediments. Unpublished PhD thesis, Universität Potsdam, Potsdam.

Popp S, Belolyubsky I, Lehmkuhl F, Prokopiev A, Siegert C, Spektor V, Stauch G, Diekmann B. 2007. Sediment provenance of late Quaternary morainic, fluvial and loess-like deposits in the southwestern Verkhoyansk Mountains (eastern Siberia) and implications for regional palaeoenvironmental reconstructions. *Geological Journal* **42**: 477–497. DOI:10.1002/gj.1088.

Prescott JR, Hutton JT. 1994. Cosmic ray contributions to dose rates for luminescence and ESR dating: large depths and long-term variations. *Radiation Measurements* **23**: 497–500. DOI:10.1016/1350-4487(94)90086-8.

Prins MA, Vriend M, Nugteren G, Vandenberghe J, Lu HY, Zheng HB, Weltje GJ. 2007. Late Quaternary aeolian dust input variability on the Chinese Loess Plateau: inferences from unmixing of loess grain-size records. *Quaternary Science Reviews* **26**: 230–242. DOI:10.1016/j.quascirev.2006.07.002.

Pye K. 1984. Loess. *Progress in Physical Geography* **8**: 176–217.

Reimer PJ, Baillie MGL, Bard E, Bayliss A, Beck JW, Blackwell PG, Ramsey CB, Buck CE, Burr GS, Edwards RL, Friedrich M, Grootes PM, Guilderson TP, Hajdas I, Heaton TJ, Hogg AG, Hughen KA, Kaiser KF, Kromer B, McCormac FG, Manning SW, Reimer RW, Richards DA, Southon JR, Talamo S, Turney CSM, van der Plicht J, Weyhenmeyer CE. 2009. IntCal09 and Marine09 radiocarbon age calibration curves, 0–50,000 years cal BP. *Radiocarbon* **51**: 1111–1150.

Roberts RG, Galbraith RF, Yoshidaa H, Laslett GM, Olley JM. 2000. Distinguishing dose populations in sediment mixtures: a test of single-grain optical dating procedures using mixtures of laboratory-dosed quartz. *Radiation Measurements* **32**: 459–465. DOI:10.1016/S1350-4487(00)00104-9.

Romanovskii NN. 1993. *Fundamentals of Cryogenesis of Lithosphere*. Moscow University Press: Moscow (in Russian).

Rosenbaum GE. 1973. Alluvium of rivers of the Eastern Subarctic plains (Yana and Omoloy rivers case study). In *Problems of Cryolithology*, Popov AI (ed). Moscow State University: Moscow, Vol. **III**: 7–62 (in Russian).

Rosenbaum GE, Pirumova LG. 1983. A facies-genetic characteristic of the "ice complex" deposits at the Duvannyi Yar section. In *Problems of Cryolithology*, Konishchev VN, Tumel NV, Arkhangelov AA, Kuznetsova TP, Rosenbaum GE, Spolanskaya NA (eds). Moscow State University: Moscow, Vol. **XI**: 65–80 (in Russian).

Rousseau D-D, Derbyshire E, Antoine P, Hatté C. 2007. Europe [Loess records]. In *Encyclopedia of Quaternary Science*, Second Edition, Elias SA, Mock CJ (eds). Elsevier: Amsterdam, Vol. **2**: 606–619.

Ryabchun VK. 1973. More about the genesis of the yedoma deposit. In *USSR Contribution, Permafrost Second International Conference, 13–28 July 1973, Yakutsk, USSR*, Sanger FJ, Hyde PJ (ed). National Academy of Sciences: Washington, DC; 816–817.

Rybakova NO. 1990. Changes in the vegetation cover and climate in the Kolyma lowlands in late-Quaternary time. *Polar Geography* **14**: 279–286. DOI:10.1080/10889379009377440.

Sainsbury CL. 1972. Geologic Map of the Teller Quadrangle, Western Seward Peninsula, Alaska. US Geological Survey, Miscellaneous Geologic Investigations, Map I-685, scale 1:250 000.

Sanborn PT, Smith CAS, Froese DG, Zazula GD, Westgate JA. 2006. Full-glacial paleosols in perennially frozen loess sequences, Klondike goldfields, Yukon Territory, Canada. *Quaternary Research* **66**: 147–157. DOI:10.1016/j.yqres.2006.02.008.

Sanborn PT, Jull TAJ. 2010. Loess, bioturbation, fire, and pedogenesis in a boreal forest – grassland mosaic, Yukon Territory, Canada. 19th World Congress of Soil Science, Soil Solutions for a Changing World, 1–6 August 2010, Brisbane, Australia. Published on DVD.

Schaetzl RJ, Luehmann MD. 2013. Coarse-textured basal zones in thin loess deposits: products of sediment mixing and/or paleoenvironmental change. *Geoderma* **192**: 277–285. DOI:10.1016/j.geoderma.2012.08.001.

Schirrmeister L, Grosse G, Wetterich S, Overduin PP, Strauss J, Schuur EAG, Hubberten H-W. 2011a. Fossil organic matter characteristics in permafrost deposits of the northeast Siberian Arctic. *Journal of Geophysical Research* **116**: G00M02. DOI:10.1029/2011JG001647.

Schirrmeister L, Kunitsky V, Grosse G, Wetterich S, Meyer H, Schwamborn G, Babiy O, Derevyagin A, Siegert C. 2011b. Sedimentary characteristics and origin of the Late Pleistocene Ice Complex on North-East Siberian Arctic coastal lowlands and islands – A review. *Quaternary International* **241**: 3–25. DOI:10.1016/j.quaint.2010.04.004.

Schirrmeister L, Froese D, Tumskoy V, Grosse G, Wetterich S. 2013. Yedoma: Late Pleistocene ice-rich syngenetic permafrost of Beringia. In *Encyclopedia of Quaternary Science*, Second Edition, Elias SA, Mock CJ (eds). Elsevier: Amsterdam, Vol. **2**: 542–552.

Schweger CE. 1992. The full-glacial ecosystem of Beringia. In *Prehistoric Mongoloid Dispersal Project*. Tokyo: Report 7; 35–51.

Schweger CE. 1997. Late Quaternary palaeoecology of the Yukon: a review. In *Insects of the Yukon*, Danks HV, Downes JA (eds). Biological Survey of Canada (Terrestrial Arthropods): Ottawa; 59–72.

Schweger CE, Matthews JV, Jr, Hopkins DM, Young SB. 1982. Paleoecology of Beringia – a synthesis. In *Paleoecology of Beringia*, Hopkins DM, Matthews JV, Jr, Schweger CE, Young SB (eds). New York: Academic Press; 425–444.

Shahgedanova M, Perov V, Mudrov Y. 2002. The mountains of northern Russia. In *The Physical Geography of Northern Eurasia*, Shahgedanova M (ed). Oxford University Press: Oxford; 284–313.

Sher AV. 1997. Yedoma as a store of paleoenvironmental records in Beringida. In *Beringia Paleoenvironmental Workshop September 1997*, Elias S, Brigham-Grette J (eds). Ohana Productions: Nepean, ON, Canada; 92–94.

Sher AV, Kaplina TN, Giterman RE, Lozhkin AV, Arkhangelov AA, Kiselyov SV, Kouznetsov Yu V, Virina EI, Zazhigin VS. 1979. *Late Cenozoic of the Kolyma Lowland: XIV Pacific Science Congress, Khabarovsk August 1979, Tour Guide XI*. USSR Academy of Sciences: Moscow.

Sher AV, Kuzmina SA, Kuznetsova TV, Sulerzhitsky LD. 2005. New insights into the Weichselian environment and climate of the East Siberian Arctic, derived from fossil insects, plants, and mammals. *Quaternary Science Reviews* **24**: 533–569. DOI:10.1016/j.quascirev.2004.09.007.

Shur YL, Jorgenson MT. 1998. Cryostructure development on the floodplain of Colville River Delta, Northern Alaska. In *Permafrost Seventh International Conference, June 23–27, 1998, Proceedings*, Lewkowicz AG, Allard M (eds). Collection Nordicana 57. Centre d'études Nordiques, Université Laval: Québec; 993–999.

Shur Y, French HM, Bray MT, Anderson DA. 2004. Syngenetic permafrost growth: cryostratigraphic observations from the CRREL Tunnel near Fairbanks, Alaska. *Permafrost and Periglacial Processes* **15**: 339–347. DOI:10.1002/ppp.486.

Shur Y, Hinkel KM, Nelson FE. 2005. The transient layer: implications for geocryology and climate-change science. *Permafrost and Periglacial Processes* **16**: 5–17. DOI:10.1002/ppp.518.

Shur Y, Jorgenson T, Kanevskiy M, Ping C-L. 2008. Formation of frost boils and earth hummocks. In *Proceedings of the Ninth International Conference on Permafrost, June 29–July 3, 2008*, Kane DL, Hinkel KM (eds). Institute of Northern Engineering, University of Alaska Fairbanks: Fairbanks, AK; Extended Abstracts, 287–288.

Shur Y, Jorgenson MT, Kanevskiy MZ. 2011. Permafrost. In *Encyclopedia of Snow, Ice and Glaciers; Encyclopedia of Earth Sciences Series*, Singh VP, Singh P, Haritashya UK (eds). Springer: Dordrecht, The Netherlands; 841–848. DOI: 10.1007/978-90-481-2642-2.

Shur YL. 1988a. *Upper horizon of permafrost and thermokarst*. Nauka: Novosibirsk (in Russian).

Shur YL. 1988b. The upper horizon of permafrost soils. In *Permafrost, Fifth International Conference, August 2–5, 1988*, Senneset K (ed). Tapir: Trondheim, Vol. **1**: 867–871.

Smith CAS, Swanson DK, Moore JP, Ahrens JP, Bockheim JG, Kimble JM, Mazhitova GG, Ping CL, Tarnocai C. 1995. A description and classification of soils and landscapes of the lower Kolyma River, northeastern Russia. *Polar Geography and Geology* **19**: 107–126. DOI:10.1080/10889379509377563.

Soloviev PA. 1973. Alass thermokarst relief of central Yakutia. Guidebook. Second International Conference on Permafrost. USSR Academy of Sciences: Section of Earth Sciences, Siberian Division, Yakutsk.

Stakhov VL, Gubin SV, Maksimovich SV, Rebrikov DV, Savilova AM, Kochkina GA, Ozerskaya SM, Ivanushkina NE, Vorobyova EA. 2008. Microbial communities of ancient seeds derived from permanently frozen Pleistocene deposits. *Microbiology* **77**: 348–355. DOI:10.1134/S0026261708030156.

Strauss J. 2010. Late Quaternary environmental dynamics at the Duvanny Yar key section, Lower Kolyma, East Siberia. Diploma thesis, Universität Potsdam, Potsdam.

Strauss J, Schirrmeister L, Wetterich S, Borchers A, Davydov SP. 2012a. Grain-size properties and organic-carbon stock of Yedoma Ice Complex permafrost from the Kolyma lowland, northeastern Siberia. *Global Biogeochemical Cycles* **26**: GB3003. DOI:10.1029/2011GB004104.

Strauss J, Ulrich M, Buchhorn M (eds). 2012b. Expeditions to Permafrost 2012: Alaskan North Slope/Itkillik, Thermokarst in Central Yakutia, EyeSight-NAAT-Alaska. *Polar and Marine Research Report 655*. Alfred Wegener Institute for Polar and Marine Research: Bremerhaven, Germany. hdl:10013/epic.40371

Sun D, Bloemendal J, Rea DK, Vandenberghe J, Jiang F, An Z, Su R. 2002. Grain-size distribution function of polymodal sediments in hydraulic and aeolian environments, and numerical partitioning of the sedimentary components. *Sedimentary Geology* **152**: 263–277. DOI:10.1016/S0037-0738(02)00082-9.

Sun D, Bloemendal J, Rea DK, An Z, Vandenberghe J, Lu H, Su R, Liu T. 2004. Bimodal grain-size distribution of Chinese loess, and its palaeoclimatic implications. *Catena* **55**: 325–340. DOI:10.1016/S0341-8162(03)00109-7.

Sun D, Su R, Li Z, Lu H. 2011. The ultrafine component in Chinese loess and its variation over the past 7.6 Ma: implications for

the history of pedogenesis. *Sedimentology* **58**: 916–935. DOI:10.1111/j.1365-3091.2010.01189.x.

Suzuki R, Razuvaev VN, Bulygina ON, Ohata T. 2007. Baseline Meteorological Data in Siberia Version 4.1, Institute of Observational Research for Global Change, Japan Agency for Marine-Earth Science and Technology, Yokosuka, Japan. http://www.jamstec.go.jp/iorgc/cgi-bin/database/v01/browse_summary.cgi?program=hcorp&group=CDC&cat=Russia&-id=BMDS_41 [11 June 2015].

Taber S. 1943. Perennially frozen ground in Alaska: its origin and history. *Bulletin of the Geological Society of America* **54**: 1433–1548. DOI:10.1130/GSAB-54-1433.

Tomirdiaro SV. 1973. Cryogenous-eolian genesis of yedoma deposits. In *USSR Contribution, Permafrost Second International Conference, 13–28 July 1973, Yakutsk, USSR*, Sanger FJ, Hyde PJ (eds). National Academy of Sciences: Washington, DC; 817–818.

Tomirdiaro SV. 1980. *Loess-ice Formation of East Siberia in Late Pleistocene and Holocene*. Nauka: Moscow.

Tomirdiaro SV. 1982. Evolution of lowland landscapes in northern Asia during Late Quaternary time. In *Paleoecology of Beringia*, Hopkins DM, Matthews JV, Jr, Schweger CE, Young SB (eds). New York: Academic Press; 29–37.

Tomirdiaro SV. 1986. Arctic loess-ice plain as a bridge between America and Asia and it thermokarstal disintegration in the Holocene. In *Beringia in the Cenozoic Era*, Kontrimavichus VL (editor-in-chief). A. A. Balkema: Rotterdam; 96–110.

Tomirdiaro SV, Chyornen'kiy BI. 1987. *Cryogenic Eolian Deposits of the Eastern Arctic and Subarctic*. Nauka: Moscow (in Russian).

Vadyunina AF, Korchagina ZA. 1986. *Methods of Investigation of Physical Properties of Soils*, Third edition. Agropromizdat: Moscow.

Vandenberghe J. 2013. Grain size of fine-grained windblown sediment: a powerful proxy for process identification. *Earth-Science Reviews* **121**: 18–30. DOI:10.1016/j.earscirev.2013.03.001.

Vandenberghe J, Kasse, K. 1993. Periodic ice-wedge formation and Weichselian cold-climate floodplain sedimentation in the Netherlands. In *Proceedings of the Sixth International Conference on Permafrost*, 5–9 July 1993, Beijing, China. South China University of Technology Press: Wushan Guangzhou; Vol. 1, 643–647.

Vandenberghe J, Nugteren G. 2001. Rapid climatic changes recorded in loess succcessions. *Global and Planetary Change* **28**: 1–9. DOI:10.1016/S0921-8181(00)00060-6.

Vandenberghe J, Mücher H, Roebroeks W, Gemke D. 1985. Lithostratigraphy and palaeoenvironment of the Pleistocene deposits at Maastricht–Belvédère. *Mededelingen Rijks Geologische Dienst* **39-1**: 7–18. hdl: handle.net/1887/28104

Vandenberghe J, Huijzer BS, Mücher H, Laan W. 1998. Short climatic oscillations in a western European loess sequence (Kesselt, Belgium). *Journal of Quaternary Science* **13**: 471–485. DOI:10.1002/(SICI)1099-1417(1998090)13:5<471::AID-JQS401>3.0.CO;2-T.

Vandenberghe J, Lowe JJ, Coope R, Litt T, Zöller L. 2004. Climatic and environmental variability in the mid-latitude Europe sector during the last interglacial–glacial cycle. In *Past Climate Variability through Europe and Africa*, Battarbee RW, Gasse F, Stickley CE (eds). Springer: Dordrecht, The Netherlands; 393–416.

Vandenberghe J, French HM, Gorbunov A, Marchenko S, Velichko AA, Jin H, Cui Z, Zhang T, Wan X. 2014. The Last Permafrost Maximum (LPM) map of the northern hemisphere: permafrost extent and mean annual air temperatures, 25–17 ka BP. *Boreas* **43**: 652–666. DOI:10.1111/bor.12070.

van Everdingen RO (ed). 1998, revised May 2005. *Multi-language Glossary of Permafrost and Related Ground-ice Terms*. National Snow and Ice Data Center/World Data Center for Glaciology: Boulder, Colorado.

Van Vliet-Lanoë B. 1996. Relations entre la contraction thermique des sols en Europe du Nord-Ouest et la dynamiqe de l'inlandsis weichsélien. Comptes Rendus Académie des Sciences, Paris 322, série IIa: 461–468.

Vasil'chuk AC, Vasil'chuk YK. 2008. Appearance of Heinrich Events on Pollen Plots of Late Pleistocene Ice Wedges. In *Proceedings of the Ninth International Conference on Permafrost, June 29–July 3, 2008*, Kane DL, Hinkel KM (eds). Institute of Northern Engineering, University of Alaska Fairbanks: Fairbanks, AK, Vol. **2**: 1803–1808.

Vasil'chuk AC, Kim J-C, Vasil'chuk YK. 2005. AMS ^{14}C dating of pollen concentrate from Late Pleistocene ice wedges from the Bison and Seyaha sites in Siberia. *Radiocarbon* **47**: 243–256.

Vasil'chuk YK. 1992. *Oxygen isotope composition of ground ice (application to paleogeocryological reconstructions)*. Theoretical Problems Department, Russian Academy of Sciences and Geological Faculty of Moscow University, Research Institute of Engineering Site Investigations: Moscow, Vol. **2**: 93–96 (in Russian with English contents section).

Vasil'chuk YK. 2005. Heterochroneity and heterogeneity of the Duvanny Yar Edoma. *Doklady Earth Sciences* **402**: 568–573.

Vasil'chuk YK. 2006. *Ice Wedge: Heterocyclity, Heterogeneity, Heterochroneity*. Moscow University Press: Moscow (in Russian).

Vasil'chuk YK. 2013. Syngenetic ice wedges: cyclical formation, radiocarbon age and stable-isotope records. *Permafrost and Periglacial Processes* **24**: 82–93. DOI:10.1002/ppp.1764.

Vasil'chuk YK, Vasil'chuk AC. 1998. Oxgyen-isotope and C^{14} data associated with Late Pleistocene syngenetic ice-wedges in mountains of Magadan region, Siberia. *Permafrost and Periglacial Processes* **9**: 177–183. DOI:10.1002/(SICI)1099-1530(199804/06)9:23.0.CO;2-T.

Vasil'chuk YK, Vasil'chuk AC, Rank D, Kutschera W, Kim J-C. 2001a. Radiocarbon dating of δ^{18}O - δD plots in Late Pleistocene ice-wedges of the Duvanny Yar (Lower Kolyma River, Northern Yakutia). In *Proceedings of the 17th International ^{14}C Conference*, Carmi I, Boaretto E (eds). *Radiocarbon* **43**(2B): 541–553.

Vasil'chuk YK, Vasil'chuk AC, van der Plicht J, Kucschera V, Rank D. 2001b. Radiocarbon dating of the Late Pleistocene ice wedges in the Bizon Section in the lower reaches of the Kolyma River. *Doklady Earth Sciences* **379**: 589–593.

Vasil'chuk YK, Vasil'chuk AC, Kim J-C. 2003. The AMS radiocarbon dating of pollen concentrate from the Late Pleistocene ice wedge of the Bison Section, Kolyma region. *Doklady Earth Sciences* **393**: 1141–1145.

Velichko A, Spasskaya I. 2002. Climatic change and the development of landscapes. In *The Physical Geography of Northern Eurasia*, Shahgedanova M (ed). Oxford University Press: Oxford; 36–69.

Velichko AA, Bogucki AB, Morozova TD, Udartsev VP, Khalcheva TA, Tsatskin AI. 1984. Periglacial landscapes of the East European Plain. In *Late Quaternary Environments of the Soviet Union*, Velichko AA, Wright HE, Jr, Barnosky CW (eds). University of Minnesota Press: Minneapolis; 94–118.

Velichko AA, Morozova TD, Nechaev VP, Rutter NW, Dlusskii KG, Little EC, Catto NR, Semenov VV, Evans ME. 2006. Loess/paleosol/cryogenic formation and structure near the northern limit of loess deposition, East European Plain, Russia. *Quaternary International* **152–153**: 14–30. DOI:10.1016/j.quaint.2005.12.003.

Velichko AA, Timireva SN, Kremenetski KV, MacDonald GM, Smith LC. 2011. West Siberian Plain as a late glacial desert. *Quaternary International* **237**: 45–53. DOI:10.1016/j.quaint.2011.01.013.

Veremeeva AA, Gubin SV. 2008. Approaches to allocation of terrain complexes

(landscapes) in areas of thermokarst development. In *Proceedings of the Ninth International Conference on Permafrost, June 29–July 3, 2008*, Kane DL, Hinkel KM (eds). Institute of Northern Engineering, University of Alaska Fairbanks: Fairbanks, AK, Vol. **2**: 1827–1832.

Veremeeva AA, Gubin SV. 2009. Modern tundra landscapes of the Kolyma Lowland and their evolution in the Holocene. *Permafrost and Periglacial Processes* **20**: 399–406. DOI:10.1002/ppp.674.

Vincent J-S. 1989. Quaternary geology of the northern Canadian Interior Plains. In *Quaternary Geology of Canada and Greenland*, Fulton RJ (ed). Geological Survey of Canada, Geology of Canada, no. 1, 100–137.

Vorobyov LA. 1998. *Chemical Analysis of Soil*. Moscow State University Press: Moscow.

Vreeken WJ. 1984. (Re)deposition of loess in southern Limbourg, The Netherlands. 3. Field evidence for conditions of deposition of the middle and upper silt loam complexes, and landscape evolution at Nagelbeek. *Earth Surface Processes and Landforms* **9**: 1–18. DOI:10.1002/esp.3290090102.

Vreeken WJ, Mücher HJ. 1981. (Re)deposition of loess in southern Limbourg, The Netherlands: 1. Field evidence for conditions of deposition of the Lower Silt Loam complex. *Earth Surface Processes and Landforms* **6**: 337–354. DOI:10.1002/esp.3290060313.

Vriend M, Prins MA, Buylaert JP, Vandenberghe J, Lu H. 2011. Contrasting dust supply patterns across the northwestern Chinese Loess Plateau during the last glacial–interglacial cycle. *Quaternary International* **240**: 167–180. DOI:10.1016/j.quaint.2010.11.009.

Vtyurin BI. 1975. *Ground Ice in the USSR*. Nauka: Moscow (in Russian).

Walker DA, Everett KR. 1987. Road dust and its environmental impact on Alaskan taiga and tundra. *Arctic and Alpine Research* **19**: 479–489. DOI:10.2307/1551414.

Walker DA, Everett KR. 1991. Loess ecosystems of northern Alaska: regional gradient and toposequence at Prudhoe Bay. *Ecological Monographs* **61**: 437–464. DOI:10.2307/2937050.

Walker DA, Raynolds MK, Buchhorn M, Peirce JL (eds). 2014. Landscape and permafrost change in the Prudhoe Bay Oilfield, Alaska. Alaska Geobotany Center, University of Alaska, AGC Publication 14-01, Fairbanks, AK.

Wang T, Ta WQ, Liu LC. 2007. Dust emission from desertified lands in the Heihe River Basin, Northwest China. *Environmental Geology* **51**: 1341–1347. DOI:10.1007/s00254-006-0432-9.

Werner K, Tarasov PE, Andreev AA, Müller S, Kienast F, Zech M, Zech W, Diekmann B. 2010. A 12.5-ka history of vegetation dynamics and mire development with evidence of the Younger Dryas larch presence in the Verkhoyansk Mountains, East Siberia, Russia. *Boreas* **39**: 56–68. DOI:10.1111/j.1502-3885.2009.00116.x.

Westgate JA, Preece SJ, Froese DG, Walter RC, Sandhu AS, Schweger CE. 2001. Dating Early and Middle (Reid) Pleistocene glaciations in Central Yukon by tephrochronology. *Quaternary Research* **56**: 335–348. DOI:10.1006/qres.2001.2274.

Wetterich S, Schirrmeister L, Kholodov AL. 2011a. The joint Russian-German expedition Beringia/Kolyma 2008 during the International Polar Year (IPY) 2007/2008. *Polar and Marine Research Report 636*. Alfred Wegener Institute for Polar and Marine Research: Bremerhaven, Germany. hdl: 10013/epic.38415

Wetterich S, Rudaya N, Tumskoy V, Andreev AA, Opel T, Schirrmeister L, Meyer L. 2011b. Last Glacial Maximum records in permafrost of the East Siberian Arctic. *Quaternary Science Reviews* **30**: 3139–3151. DOI:10.1016/j.quascirev.2011.07.020.

Willemse NW, Koster EA, Hoogakker B, van Tatenhove FGM. 2003. A continuous record of Holocene eolian activity in West Greenland. *Quaternary Research* **59**: 322–334. DOI:10.1016/S0033-5894(03)00037-1.

Willerslev E, Davison J, Moora M, Zobel M, Coissac E, Edwards ME, Lorenzen ED, Vestergård M, Gussarova G, Haile J, Craine J, Bergmann G, Gielly L, Boessenkool S, Epp LS, Pearman PB, Cheddadi R, Murray D, Bråthen KA, Yoccoz N, Binney H, Cruaud C, Wincker P, Goslar T, Alsos IG, Bellemain E, Brysting AK, Elven R, Sønstebø JH, Murton J, Sher A, Rasmussen M, Rønn R, Mourier T, Cooper A, Austin J, Möller P, Froese D, Zazula G, Pompanon F, Rioux D, Niderkorn V, Tikhonov A, Savvinov G, Roberts RG, MacPhee RDE, Gilbert MPT, Kjær K, Orlando L, Brochmann C, Taberle P. 2014. Fifty thousand years of arctic vegetation and megafauna diet. *Nature* **506**: 47–51. DOI:10.1038/nature12921.

Wolfe SA. 2013. Cold-climate aeolian environments. In *Treatise on Geomorphology, Vol. 11, Aeolian Geomorphology*, Shroder JF (editor-in-chief), Lancaster N, Sherman DJ, Baas ACW (volume eds). Academic Press: San Diego; 375–394. DOI: 10.1016/B978-0-12-374739-6.00312-2

Wolfe SA, Robertson L, Gillis A. 2009. Late Quaternary Eolian Deposits of northern North America: Age and Extent. Geological Survey of Canada, Open File 6006, CD-ROM.

Wolfe SA, Bond J, Lamothe M. 2011. Dune stabilization in central and southern Yukon in relation to early Holocene environmental changes, northwestern North America. *Quaternary Science Reviews* **30**: 324–334. DOI:10.1016/j.quascirev.2010.11.010.

Yashina S, Gubin S, Maksimovich S, Yashina A, Gakhova E, Gilichinsky D. 2012. Regeneration of whole fertile plants from 30,000-y-old fruit tissue buried in Siberian permafrost. *Proceedings of the National Academy of Sciences* **109**: 4008–4013. DOI:10.1073/pnas.1118386109.

Yurtsev BA. 1981. *Relic Steppe Complexes of North-East Asia*. Nauka: Novosibirsk (in Russian).

Zanina OG. 2005. Fossil rodent burrows in frozen Late Pleistocene beds of the Kolyma lowland. *Entomological Review* **85**(Supplement 1): 133–140.

Zanina OG, Gubin SV, Kuzmina SA, Maximovich SV, Lopatina DA. 2011. Late-Pleistocene (MIS 3–2) palaeoenvironments as recorded by sediments, palaeosols, and ground-squirrel nests at Duvanny Yar, Kolyma lowland, northeast Siberia. *Quaternary Science Reviews* **30**: 2107–2123. DOI:10.1016/j.quascirev.2011.01.021.

Zárate MA, Tripaldi A. 2012. The aeolian system of central Argentina. *Aeolian Research* **3**: 401–417. DOI:10.1016/j.aeolia.2011.08.002.

Zazula GD, Froese DG, Elias SA, Kuzmina S, La Farge C, Reyes AV, Sanborn PT, Schweger CE, Smith CAS, Mathewes RW. 2006. Vegetation buried under Dawson tephra (25,300 ^{14}C years BP) and locally diverse late Pleistocene paleoenvironments of Goldbottom Creek, Yukon, Canada. *Palaeogeography, Palaeoclimatology, Palaeoecology* **242**: 253–286. DOI:10.1016/j.palaeo.2006.06.005.

Zazula GD, Froese DG, Elias SA, Kuzmina S, Mathewes RW. 2007. Arctic ground squirrels of the mammoth-steppe: paleoecology of middens from the last glaciation, Yukon Territory, Canada. *Quaternary Science Reviews* **26**: 979–1003. DOI:10.1016/j.quascirev.2006.12.006.

Zazula GD, Froese DG, Elias SA, Kuzmina S, Mathewes RW. 2011. Early Wisconsinan (MIS 4) Arctic ground squirrel middens and a squirrel-eye-view of the mammoth-steppe. *Quaternary Science Reviews* **30**: 2220–2237. DOI:10.1016/j.quascirev.2010.04.019.

Zech M, Zech R, Zech W, Glaser B, Brodowski S, Amelung W. 2008. Characterisation and palaeoclimate of a loess-like permafrost palaeosol sequence in NE

Siberia. *Geoderma* **143**: 281–295. DOI:10.1016/j.geoderma.2007.11.012.

Zhestkova TN, Shvetsov PF, Shur YL. 1982. Yedoma, a climatic formation. In *XI Congress of International Union for Quaternary Research*, *Moscow*, *1982*. Abstracts, Vol. II; 389.

Zhestkova TN, Shvetsov PF, Shur YL. 1986. On genesis of yedoma. In *Geocryology Studies*, Ershov ED (ed). Moscow State University: Moscow; 108–113 (in Russian).

Zhou Y, Lu H, Zhang J, Mason JA, Zhou L. 2009. Luminescence dating of sand–loess sequences and response of Mu Us and Otindag sand fields (north China) to climatic changes. *Journal of Quaternary Science* **24**: 336–344. DOI:10.1002/jqs.1234.

Zhu R, Matasova G, Kazansky A, Zykina V, Sun JM. 2003. Rock magnetic record of the last glacial-interglacial cycle from the Kurtak loess section, southern Siberia. *Geophysical Journal International* **152**: 335–343. DOI:10.1046/j.1365-246X.2003.01829.x.

Zimov SA, Davydov SP, Zimova GM, Davydova AI, Schuur EAG, Dutta K, Chapin FS III. 2006a. Permafrost carbon: Stock and decomposability of a globally significant carbon pool. *Geophysical Research Letters* **33**: L20502. DOI:10.1029/2006GL027484.

Zimov SA, Schuur EAG, Chapin FS III. 2006b. Permafrost and the global carbon budget. *Science* **312**: 1612–1613. DOI:10.1126/science.1128908.

SUPPORTING INFORMATION

Additional supporting information may be found in the online version of this article at the publisher's web site.

Supporting Figures

Figure S1 Ice wedges at Duvanny Yar.

Figure S2 $\delta^{18}O$ plots of syngenetic wedge ice at Duvanny Yar.

Figure S3 Pollen and spores in wedge ice and surrounding yedoma sediments at Duvanny Yar.

Figure S4 Pollen spectra from wedge ice at Duvanny Yar.

Figure S5 Modern surface pollen spectra in the lower Kolyma region.

Figure S6 Bi-plot of fossil and modern pollen samples scores from Duvanny Yar and the lower Kolyma region.

Figure S7 Profiles of palaeosols 3 and 4 in yedoma remnant 6E at Duvanny Yar.

Figure S8 Buried palaeosol profiles in yedoma exposure of Stanchikovsky Yar.

Supporting Tables

Table S1 ^{14}C ages previously obtained from organic material in yedoma at Duvanny Yar.

Table S2 The youngest ^{14}C ages obtained in each horizon of yedoma at Duvanny Yar.

Table S3 Conventional ^{14}C age from a bulk sample of Duvanny Yar yedoma and AMS ^{14}C ages for its different organic fractions.

Table S4 AMS ^{14}C ages of organic material from wedge ice at Duvanny Yar.

Table S5 $\delta^{18}O$ values from wedge ice in 1985 sampling programme at Duvanny Yar.

Table S6 $\delta^{18}O$, $\delta^{2}H$ and d_{exc} values from ice-wedge ice in 1999 sampling programme at Duvanny Yar.

Appendices

Appendix S1 Previous ^{14}C Geochronology of the Yedoma (Ice Complex) at Duvanny Yar.

Appendix S2 Palaeotemperature Significance of Stable-Isotope Records from Syngenetic Ice wedges.

Appendix S3 Pollen Spectra from Ice Wedges at Duvanny Yar.

Appendix S4 Pollen Spectra of the Modern Surface of the Lower Kolyma Region and of Units 1, 4 and 5 at Duvanny Yar.

Appendix S5 Palaeosol Correlations between the 2009 Study and Previous Studies at Duvanny Yar and Stanchikovsky Yar.